FUNGAL PROTEIC BIOSURFACTANTS FOR THE DEVELOPMENT OF BIOSENSING PLATFORMS

Ilaria Stanzione

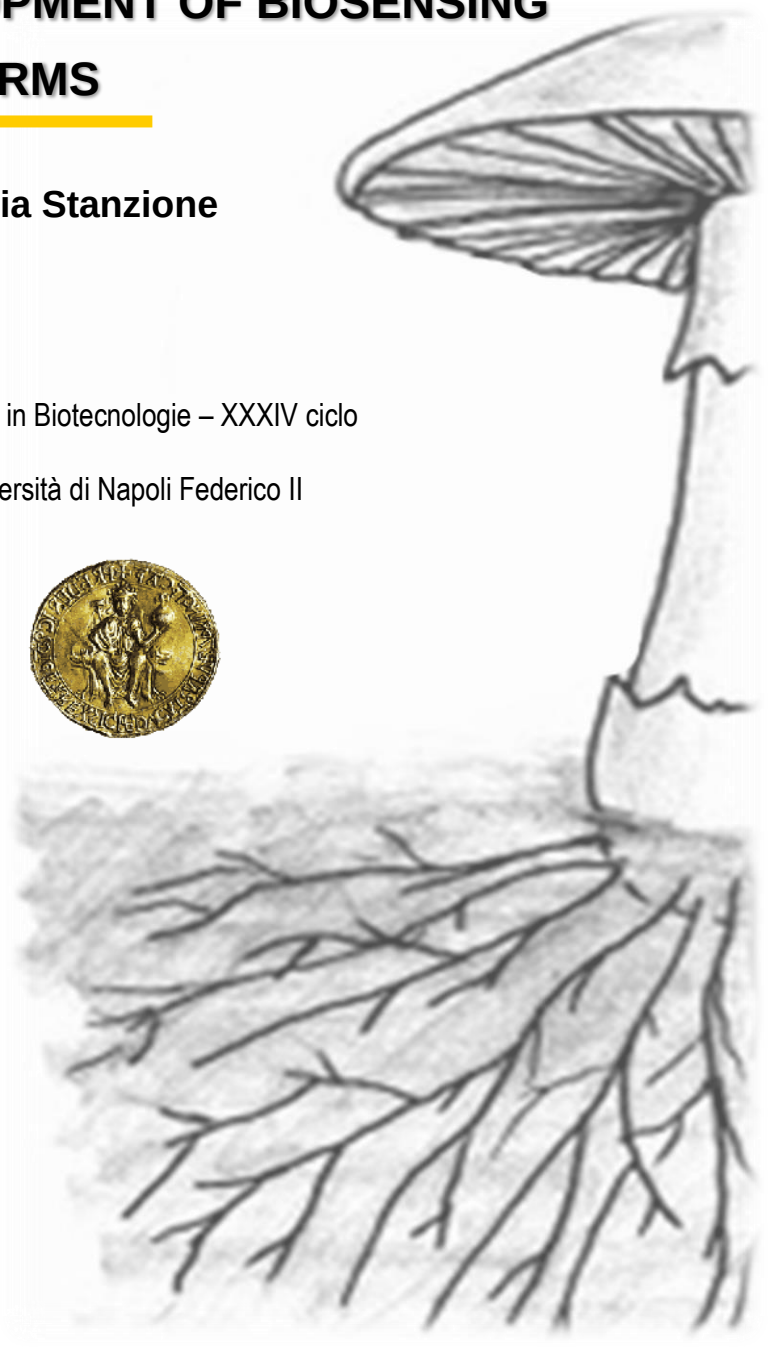

Dottorato in Biotecnologie – XXXIV ciclo

Università di Napoli Federico II

Dottorato in Biotecnologie – XXXIV ciclo

Università di Napoli Federico II

FUNGAL PROTEIC BIOSURFACTANTS FOR THE DEVELOPMENT OF BIOSENSING PLATFORMS

Ilaria Stanzione

Dottorando: Ilaria Stanzione

Relatore: Prof. Paola Giardina

Correlatore: Prof. Alessandra Piscitelli

Coordinatore: Prof. Marco Moracci

Settore Scientifico Disciplinare BIO-10

I am among those who think that science has great beauty. A scientist in his laboratory is not only a technician, he is also a child placed before natural phenomena which impress him like a fairy tale.

Marie Curie

INDEX

Riassunto

A. INTRODUZIONE

Nell'ambito dello sviluppo di una economia sostenibile, i microrganismi, come batteri, funghi e piante, svolgono un ruolo fondamentale come fonte di prodotti naturali. La natura biologica di questi composti li rendono ottimi sostituti delle loro controparti sintetiche. I funghi filamentosi, ad esempio, rappresentano una straordinaria fonte di biomolecole quali enzimi, antibiotici e proteine. Grazie alle loro proprietà intrinseche, tali microrganismi sono estremamente interessanti per una vasta gamma di applicazioni. Prima tra tutte, la loro capacità di degradare materiale organico e sostanze polimeriche, li rende capaci di crescere in diversi ambienti, da quello terrestre a quello marino. Inoltre, grazie al fatto che producono svariati composti tensioattivi, meglio conosciuti come biosurfattanti (BSs), i funghi sono capaci di crescere in liquido, nell'aria e su superfici solide. I biosurfattanti sono composti che, possedendo porzioni idrofobiche ed idrofiliche, hanno la capacità di posizionarsi all'interfaccia tra due fasi con diversa polarità, come ad esempio acqua/olio o aria/acqua. Essi, inoltre, sono capaci di ridurre la tensione superficiale e di formare e stabilizzare emulsioni. Sono generalmente classificati in base al loro peso molecolare, definendo come bioemulsionanti i tensioattivi ad alto peso molecolare che esibiscono un elevato potere emulsionante, e come biosurfattanti quei composti a basso peso molecolare che riducono la tensione superficiale. Tale classificazione, però, non è sempre categorica, infatti è possibile che un bioemulsionante possa abbassare la tensione superficiale e viceversa. La loro natura biologica, la biodegradabilità e la bassa tossicità rendono i BSs utili in svariati campi di applicazione, tra cui l'industria alimentare nella quale vengono utilizzati, ad esempio, come additivi o conservanti, o nel biorisanamento, grazie alla loro capacità di migliorare la solubilità degli idrocarburi. Tra i biosurfattanti ad alto peso molecolare, si possono annoverare alcune proteine fungine, le Idrofobine e le Ceratoplatanine che svolgono un ruolo fondamentale nel ciclo vitale del microorganismo. Le prime, infatti, sono molecole tensioattive prodotte da funghi filamentosi e posseggono la capacità di auto-assemblare alle interfacce idrobofiche/idrofiliche rendendo possibile lo sviluppo delle strutture aree come ife e corpi fruttiferi. Sono costituite da circa 100 amminoacidi, possiedono un motivo conservato di otto cisteine e sono generalmente suddivise in due classi. La differenza sostanziale tra le due classi risiede nella stabilità dei film anfifilici che formano. Le idrofobine di classe I formano film più stabili e hanno delle strutture simili a fibrille amiloidi dissociabili solo in presenza di acidi forti come l'acido formico o l'acido trifluoroacetico (TFA), mentre i film formati da quelle di classe II sono poco stabili e mancano di strutture amiloidi. Quindi le idrofobine di classe II sono più solubili e meno tendenti all'aggregazione,

utilizzabili per scopi diversi rispetto a quelle di classe I. Entrambe le classi, però, hanno la capacità di modificare le caratteristiche chimico-fisiche delle superfici sulle quali vengono immobilizzate. Ad esempio, la funzionalizzazione di una superficie idrofobica, quale il polistirene, permette alle proteine di aderire fortemente tramite la formazione di interazioni idrofobiche, esponendo così la porzione idrofilica e cambiando, di conseguenza, la bagnabilità della superficie. Questa caratteristica potrebbe, talvolta, permettere l'utilizzo delle idrofobine nel campo biomedicale per evitare la formazione di biofilm batterici sui dispositivi medici, o nella nanotecnologia, in quanto la funzionalizzazione dei nanomateriali con queste proteine permette un incremento della solubilità degli stessi e quindi una migliore stabilità. Parimenti, come stabilizzatori di emulsioni, le idrofobine possono essere impiegate nell'industria alimentare o nei processi di biorisanamento. Oltre a creare film proteici sulle superfici, tali tensioattivi hanno anche l'abilità di permettere l'adesione di altre biomolecole nella loro forma attiva, rendendo le idrofobine interessanti anche dal punto di vista biosensoristico. In questo e in altri campi, l'idrofobina di classe I Vmh2, prodotta dal fungo edibile *Pleurotus ostreatus*, è stata ampiamente utilizzata. Questa idrofobina, infatti non solo è stata impiegata per migliorare la solubilità di nanomateriali come il grafene, ma è stata anche utilizzata per funzionalizzare superfici come ferro, polistirene e vetro per permettere una successiva immobilizzazione di enzimi nella loro forma attiva. Soprattutto nel campo della biosensoristica, invece di utilizzare il film proteico come piattaforma di immobilizzazione per altre biomolecole, si è preferito produrre Vmh2 in maniera ricombinante, fusa a livello genico, con proteine di interesse biotecnologico, come la Glutatione-S-transferasi, la Green-Fluolescence Protein, l'enzima laccasi. In tutti i casi, il gruppo di ricerca di cui faccio parte, è stato in grado di sviluppare biosensori ottici ed elettrochimici utili per l'analisi di un'ampia gamma di analiti. Un'altra classe di biosurfattanti proteici prodotti da funghi consiste nelle Ceratoplatanine. Anch'esse sono caratterizzate dalla presenza di cisteine e possono essere secrete dal fungo nel brodo di coltura o trattenute sulle ife e sulle spore. Il ruolo fisiologico delle ceratoplatanine nel fungo non è ancora ben noto, ma esse possono fungere sia da fattori di virulenza che da elicitori. Pur essendo strutturalmente diverse dalle idrofobine, le ceratoplatanine hanno alcune caratteristiche funzionali in comune, anch'esse riescono ad assemblare alle interfacce idrofobiche/idrofiliche attraverso la formazione di film proteici anfipatici. È stato dimostrato, infatti, che queste proteine riescono a stabilizzare emulsioni e ridurre la tensione superficiale. Oltre ad avere proprietà in comune con le idrofobine, le ceratoplatanine presentano strutturalmente il dominio N-terminale simile alle espansine e, come queste, possiedono la capacità di indebolire le maglie di cellulosa senza alcuna attività idrolitica rendendole più disponibili all'azione di enzimi idrolitici. Questa proprietà rende le

ceratoplatanine interessanti nel campo delle biotecnologie per la valorizzazione di materiali di scarto.

B. CARATTERIZZAZIONE DI NUOVI BIOSURFATTANTI PROTEICI

Come precedentemente descritto, i microorganismi, siano essi terrestri o marini, rappresentano una fonte inestimabile di biomolecole. L'ecosistema marino, in generale, gioca un ruolo fondamentale nel mantenimento dell'equilibrio ambientale ed è, contemporaneamente, fonte di una straordinaria biodiversità. Pur avendo sviluppato abilità fisiologiche che li rendono capaci di sopravvivere in un ambiente estremo, i microorganismi marini restano comunque poco caratterizzati. Un esempio è rappresentato dai funghi, il cui termine è erroneamente associato solo a quelli terrestri pur essendo state trovate più di 10.000 specie in ogni tipo di habitat marino, dalle acque superficiali a quelle profonde. In più, come quelli terrestri, i funghi marini sono fonte di composti tensioattivi, tra cui biosurfattanti e bioemulsionanti, largamente impiegati in svariati settori. In questo contesto una parte del presente lavoro di tesi si è focalizzato sull'isolamento e sulla caratterizzazione di nuovi biosurfattanti proteici prodotti da funghi marini. In particolare, la proteina *Sap-Pc,* prodotta dal fungo *Penicillium chrysogenum,* è stata ampiamente caratterizzata in base alla sua capacità emulsionante, all'abilità di abbassare la tensione superficiale e alla sua propensione all'aggregazione. Inoltre, in collaborazione con un gruppo di ricerca sud-americano, abbiamo dimostrato che altri due ceppi fungini, *Paradendryphiela salina* e *Talaromyces pinophilus,* sono capaci di crescere utilizzando come fonte nutrizionale materiali di scarto e producendo, allo stesso tempo, noti biosurfattanti proteici quali le idrofobine e le ceratoplatanine.

C. APPLICAZIONI DELL'IDROFOBINA VMH2 DA *P. ostreatus*

C.1 DIAGNOSI DEI BENI CULTURALI

L'approfondita caratterizzazione dell'idrofobina di classe I Vmh2, ha permesso, come già spiegato, il suo utilizzo in un'ampia gamma di applicazioni. Più recentemente, la sua capacità di formare film proteici stabili sulle superfici per permettere poi l'adesione di enzimi funzionali è stata sfruttata nel campo dei beni culturali. L'analisi proteomica di affreschi, sarcofagi, resti lapidei, non solo permette di capire la composizione naturale dei pigmenti un tempo utilizzati, ma spesso permette anche di datare il bene in questione. Molto spesso però tale analisi risulta essere invasiva e deteriorante, per cui l'utilizzo dell'idrofobina è venuto in aiuto per lo sviluppo un sistema che possa consentire il superamento di tali problematiche. In questo progetto di tesi è riportato, infatti, un kit portatile costituito da un foglietto di acetato di cellulosa, funzionalizzato con la Vmh2, sul quale sono stati immobilizzati due enzimi proteolitici: la tripsina, generalmente utilizzata

per l'identificazione di proteine, e la PNGaseF, utilizzata per migliorare l'identificazione di glicoproteine data la sua capacità di catalizzare la scissione di legami glicosidici. L'azione della PNGase, quindi, permette un miglior accesso alla tripsina che in questo modo riesce ad idrolizzare più facilmente le proteine.

C.2 PROTEINE DI FUSIONE PER LO SVILUPPO DI BIOSENSORI

Per quanto riguarda, invece l'utilizzo della Vmh2 in campo biosensoristico, tecniche di ingegneria genetica hanno permesso la produzione ricombinante di tale idrofobina fusa a proteine di interesse biotecnologico. In particolare, nell'ambito del progetto FlashMob (*Chimera amiloide funzionale per il biosensing marino*), il cui scopo era basato sullo sviluppo di biosensori atti all'analisi di una vasta gamma di analiti utilizzando le proteine di fusione, sono state sviluppate tre diverse chimere. Le prime due sono caratterizzate dalla fusione di Vmh2 con i frammenti variabili a catena singola ScFv (*Single chain Fragment variable*) di due anticorpi capaci di legare due tossine algali, la saxitossina e l'acido domoico. Analizzare tali composti è di notevole importanza dal momento che questi si accumulano generalmente nei molluschi e, arrivando all'uomo attraverso la catena alimentare, provocano importanti malattie neuronali. Quindi, lo sviluppo di un biosensore che sfrutti l'interazione antigene/anticorpo può essere una buona strategia per il loro rilevamento. Le chimere Vmh2-ScFv sono state espresse in maniera ricombinante nel batterio *Escherichia coli* e rinaturate dai corpi di inclusione. Una volta verificata, poi, l'attività di entrambi i partner di fusione, sono stati messi a punto biosensori ottici ed elettrochimici immobilizzando le proteine su nanoparticelle magnetiche. In ambito biosensoristico i nanomateriali sono ampiamente utilizzati grazie alle loro proprietà intrinseche. Questi, infatti, presentano, non solo un elevato rapporto superficie/volume, che permette l'immobilizzazione di una maggiore quantità di biomolecole, ma anche proprietà conduttive che li rendono buoni candidati come trasduttori. Sulla base di queste considerazioni, un'altra proteina chimerica, Vmh2-Laccasi, è stata prodotta in maniera ricombinante nel lievito *Pichia pastoris* e immobilizzata su nanomateriali quali grafene e nanotubi di carbonio. La natura redox dell'enzima laccasi, e quindi la sua capacità di ossidare una vasta gamma di composti aromatici insieme con la riduzione dell'ossigeno molecolare ad acqua, è stata sfruttata per sviluppare diversi biosensori elettrochimici volti all'analisi di contaminanti quali antracene, catecolo e dopammina.

D. CONCLUSIONI

I risultati conseguiti nel presente progetto di tesi sono quelli riportati qui di seguito:

1. Nuovi biosurfattanti proteici, tra cui idrofobine e ceratoplatanine, prodotti da tre ceppi fungini di origine marina sono stati identificati e caratterizzati come tensioattivi e bioemulsionanti.
2. Foglietti di acetato di cellulosa funzionalizzati con l'idrofobina Vmh2 sono stati utilizzati come piattaforma per l'immobilizzazione di enzimi proteolitici, per lo sviluppo di un kit portatile utile nel campo della diagnosi dei beni culturali.
3. Le proteine chimeriche, Vmh2-ScFv, sono state espresse con successo in *E. coli* e correttamente immobilizzate su nanoparticelle magnetiche utilizzate poi per lo sviluppo di biosensori ottici e elettrochimici volti al rilevamento di due neurotossine algali.
4. La proteina di fusione, Vmh2-Laccasi è stata prodotta in maniera ricombinante nel lievito *Pichia pastoris* e successivamente immobilizzata su nanomateriali, come grafene e nanotubi di carbonio, per lo sviluppo di biosensori elettrochimici capaci di rilevare contaminanti aromatici.

SUMMARY

Protein biosurfatants produced by marine and terrestrial filamentous fungi represent the best example of biomolecules that can be widely used as a replacement of their synthetic counterparts, thanks to their low toxicity and biodegradability. Among them, hydrophobins and ceratoplatanins are proteins able to self-assemble at hydrophobic/hydrophilic interfaces forming amphiphilic layers. It is well known that the hydrophobins are involved in the fungal growth thanks to their capability to reduce the surface tension of the air/water interface, instead, while the ceratoplatanins can act both as virulence factor and as elicitors. Moreover, the amphiphilic nature of both classes of proteins makes them of great interest in many fields. For this reason, one of the purposes of the present PhD project is the isolation and characterization of protein biosurfactants from marine fungal strains. The isolated protein from *Penicillium chrysogenum* has been characterized both as biosurfactant and bioemulsifier, indeed its capabilities to stabilize emulsion and to reduce the surface tension have been verified. Moreover, it has been proved that two marine fungi, *Paradendryphiela salina* and *Talaromyces pinophilus* grown on seaweed wastes, are able to produce both cerato-platantins and hydrophobins. Another hydrophobin deeply characterized and exploited in my research group, is Vmh2, produced by the edible fungus *P. ostreatus*. This protein can form protein layers on several surfaces changing their physical-chemical properties and allowing the attachment of other biomolecules in their active form. Thus, the exploitation of Vmh2 in the diagnosis of cultural heritage and in biosensing field has been under investigation in this PhD project. The functionalization of cellulose acetate sheets with Vmh2 has been employed to immobilize proteolytic enzymes, trypsin and PNGaseF, developing a portable, easy-to-use and non-invasive kit for the identification of ancient proteins on cultural heritage objects. Furthermore, in biosensing field the same hydrophobin has been genetically fused to two Single chain Fragment variables of two antibodies able to bind algal marine neurotoxins, and to a laccase enzyme that can oxidize aromatic and phenolic compounds. The recognition ability of chimeric proteins has been coupled with the interesting characteristics of nanomaterials, such as graphene, carbon nanotubes and magnetic beads. The functionalized 2D-materials with both chimeric proteins have been exploited to develop electrochemical and optical biosensors for the detection of the analytes mentioned above.

Chapter 1

1. INTRODUCTION

In the current century, research is facing several challenges for the development of a sustainable bioeconomy and for the exploration of natural sources that can support a cleaner environment. Thus, the investigation of biobased solutions is becoming progressively more important. In this context, nature offers amazing biological products that are similar, or often better, than their synthetic counterparts. Over the last decades, the natural products produced by a plethora of microorganisms, such as bacteria, fungi and plants, have been used as a replacement of the chemical compounds for several applications. Filamentous fungi, for example, represent an extraordinary source of organic acids, enzymes, drugs, antibiotics, proteins, vitamins that are fundamental in our daily life.
The capabilities of filamentous fungi to feed on and break down organic matter and polymeric substances are of great interest allowing the fungal growth in several environments [1], from the terrestrial to the marine one. Moreover, these microorganisms efficiently degrade lignocellulosic biomass and convert the sugars into energy-rich molecules, these features ensure their exploitation in biorefinery applications towards second generation biofuels or chemicals [2]. The amazing ability of filamentous fungi to growth in liquid, semiliquid or into the air and onto solid surfaces is aided by a variety of surface-active compounds, also known as biosurfactants (BSs), that fungi produce during their life cycle [3] through fermentative processes using sugars, oils, hydrocarbons and residues as substrates [4].

1.1 BIOSURFACTANTS

The uniqueness of these compounds resides in their structural characteristics; indeed, they possess both hydrophobic and hydrophilic moieties that allow their position at the interface between two phases with different degrees of polarity (*i.e.* oil/water or air/water interfaces). These structural features make the BSs able to reduce surface tension and to form emulsions solubilizing hydrophobic compounds in hydrophilic environments. Therefore, BSs exhibit interesting ability such as detergency, emulsification and foaming that make them versatile and useful in several applications [5,6]. Thanks to their biological nature, biosurfactants are less toxic than their synthetic counterparts [7] and, moreover, they can provide more advantages, such as pH, temperature and salinity resistance, exploitable in bioremediation processes or in medical, pharmaceutical, textile and food industry. Only in the last decades, it has been discovered that BSs are produced also by filamentous fungi because, until now, their production was associated to other microorganisms such as bacteria and yeasts. Nonetheless, one of the drawbacks of BSs exploitation is represented by their low production yield and the high cost of the processes. For this reason,

to overcome these disadvantages some strategies have been adopted, such as the usage of genetic modified microorganisms or the employment of agricultural waste material as carbon source [8,9]. Based on their molecular weight, the surface-active compounds are often classified as biosurfactants (BS) or bioemulsifiers (BE) [10]. Lipoproteins, proteins and lipopolysaccharides belong to the class of the high molecular mass molecules, better defined as BE, and they exhibit a higher emulsification ability respect to that one displayed by the low molecular mass biosurfactants. These last compounds consist of amino acid, fatty acids, glycolipids, lipopeptides and are often recognized thanks to their capability to decrease the interfacial tension (**Fig.1)**. However, it cannot be ruled out that a bioemulsifier can reduce the surface tension and viceversa.

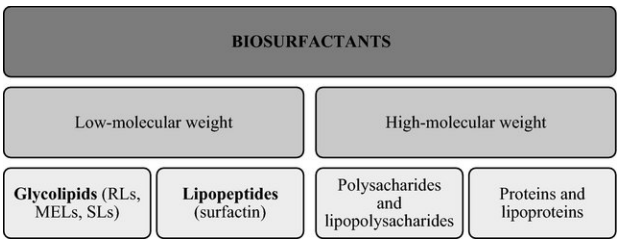

***Figure 1**: Classification of Biosurfactants according to their molecular weight* [11]

Mainly due to their low toxicity, biodegradability and sustainable production, BSs are of great interest in many applications [12]. In food industry, for instance, they are exploitable as food additives or preservatives [13], due to their effectiveness in emulsion formation and stabilization. Furthermore, thanks to the surface-active compounds ability to alter the hydrophobicity of the surfaces, the BS functionalized area can show anti-adhesive activity affecting the microbial adhesion and making BS useful in biomedical application. Moreover, in environmental and agriculture fields, the structural properties of the BS have been exploited for enhancing the oil recovery and for stimulating the hydrocarbons biodegradation due to the BS capabilities to reduce hydrophobic compounds viscosity and to enhance the hydrocarbons solubility [14].

As regard the protein biosurfactants, proteins are intrinsically amphipatic molecules, even if their amphiphilic nature is affected by several factors such as the protein folding or posttranslational modifications. However, the production of these surface-active compounds is essential for many microorganisms whose abilities are actually due to an array of protein biosurfactants expressed during their life. Among them, hydrophobins (HFBs) and ceratoplatanins (CPs), small proteins mainly produced by terrestrial and marine fungi, deserve attention as surface-active molecules.

1.2 FUNGAL PROTEIC BIOSURFACTANTS: THE HYDROPHOBINS

1.2.1 Biological role

To grow into the air, filamentous fungi, both ascomycetes and basidiomycetes, produce a particular class of surface-active proteins, the HFBs, able to self-assemble at hydrophobic/hydrophilic interfaces allowing the development of fungal structures such as aerial hyphae and fruiting bodies [15]. These proteins are secreted as monomers, then their polymerization process, called interfacial self-assembly [16], starts when they find an interface between air and water, or a hydrophobic surface (**Fig 2**).

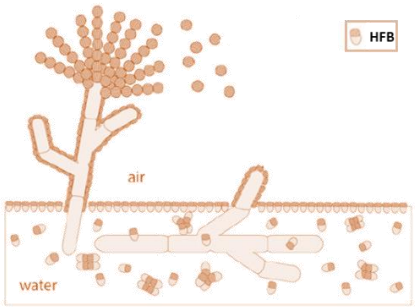

***Figure 2**: Biological role of hydrophobin in the fungal growth* [17].

Hydrophobins were discovered by Wessel and co-authors [18] during their studies on the fruiting bodies of *Schizophyllum commune*. They understood that during a particular growth phase of the fungus, an interesting gene was abundantly expressed. This gene encodes for a small protein characterized by a large amount of hydrophobic amino acids, for this reason they attributed to it the name hydrophobin. SC3 hydrophobin was the first studied hydrophobin and its involvement in the fungal aerial growth has been clarified [19]. Once the mycelium has been formed, the basidiomycete *S. commune* secretes into the medium the SC3 protein. As the majority of the hydrophobins, SC3 decreases the surface tension of aqueous environment allowing the growth of hyphae. Then, SC3 proteins self-assemble at the interface between hydrophobic air and the hydrophilic cell wall, forming an amphipathic layer in which all the proteins are held together by hydrophobic interactions. In this way they expose hydrophobic side, characterized by a mosaic of rodlets.

Moreover, by using the same process, HFB layer enables the aerial growth of the fungus coating the spores, improving their dispersion in the air and preventing their recognition by immune cells in the initial step of infections [20]. Likewise, HFBs play an essential role in the symbiosis process [21], indeed they are able to mediate the attachment of the fungus to the surface

of the host, if it is hydrophobic. Each of these roles is due to the structural characteristics of HFBs that make them a very versatile class of protein biosurfactants.

1.2.2 Structural features

HFBs are composed by about 100 aa and one of their main features is represented by the presence of eight conserved cysteine residues [22]. The eight cysteines form four disulfide bridges, connecting C1-C6, C2-C5, C3-C4 and C7-C8, that are fundamental to keep the protein in solution, as confirmed by the study on the SC3 hydrophobin [23]. Except for these conserved residues, the amino acid sequences of the proteins show a low identity, even if the relative positions of non-polar and polar amino acid seem to be quite preserved. However, the alignment of the amino acid sequences suggested that HFBs can be divided in two main classes based on the length of the inter-cysteine spaces (**Fig.3**).

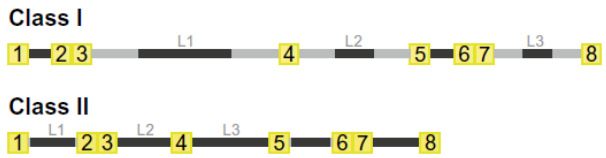

Figure 3: *Schematic representation of the differences and variations in inter-cysteine length that underlie the classification of HFBs. The eight conserved cysteine residues are highlighted in yellow. The lengths of the N- and C-terminal regions have been omitted for clarity. The lengths of the polypeptide chains between the cysteine residues vary from that shown in black (shortest) to the combined length illustrated in black and grey (longest). The positions of the loops 1, 2 and 3 are indicated by L1, L2 and L3.*

Naturally, these differences give to the proteins belonging to the two classes different structural and functional characteristics. Indeed, Class I HFBs assemble into polymeric layer composed of fibrillar structures that can be disassembled only by the usage of strong acid treatment (such as Trifluoroacetic or formic acids) [24]. On the contrary, Class II HFBs form protein layers that can be dissociated in organic solvents or detergents [25]. Recently this classification has been questioned, indeed an intermediate third class has been proposed based on the hydrophobicity profiles and protein properties [26]. In the case of the *Aspergillus* species, for example, several hydrophobins, with inter-cysteine spaces different from class I and II, have been identified [27]. As shown in **Fig.4**, the 3D structures of some soluble class I and II hydrophobins have been solved. In particular, EAS (*Neurospora crassa*), DewA (*Aspergillus nidulans*), MPG1 (*Magnaporthe grisea*), RodA (*Aspergillus fumigatus*) and SC16 (*S. commune*) for class I hydrophobins [22,28–31] and HFBI, HFBII (*Trichoderma reesei*), and NC2 (*N. crassa*) for class II hydrophobins [32,33]. All of them are characterized by

the presence of a four-stranded β-barrel core, while the main differences regard the length of the loops and the position of α-helical structures. Indeed, Class I hydrophobins show a variation not only in length but also in structure of the loops. The loop L1 of SC16 contains a α-helical structure while that of EAS is unstructured; L3 loops are unstructured, while L2 contains β-sheet structure. On the contrary, Class II hydrophobins are composed by two short loops (L1 and L3) and another one that contains an α-helical structure (L2).

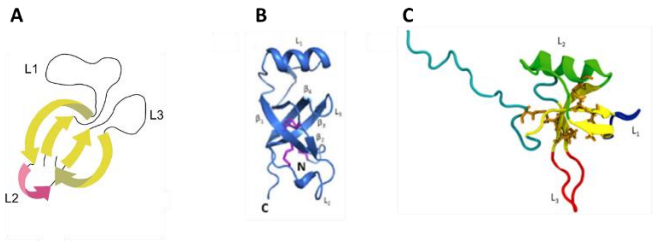

Figure 4: *Representation of the 3D structures of Class I hydrophobin (A)EAS* [34]*, (B) SC16* [22] *and class II hydrophobin (C) NC2* [33]

These structural characteristics entail the diverse ability of the two classes of HFBs to form fibrillar structures. For example, in SC16 the α-helix structure is associated with the β-barrel and a hydrophobic interface is formed between them. This α-helix is in the loop L1, while it is present in L2 in the class II hydrophobins where it is linked to the core β-barrel by a disulfide bridge. Thus, the different degree of conformational flexibility of the α-helix structure allows a higher propensity to the fibrils formation for SC16 than the class II HFB. Recently, to clarify the molecular determinants that play a key role in the self-assembly process, five mutants of the class I hydrophobin, Vmh2 from *P. ostreatus,* have been produced by site-directed mutagenesis. Then, starting from a reliable 3D model built using the structure of the class I hydrophobin SC16 from *S. commune* as a template, a possible mechanism of formation of amyloids has been proposed. As shown, (**Fig.5**) part of the loop L1 of Vmh2 changes conformation forming a β-hairpin, which represents the β-spine of the fibrils, whereas the bulk of the protein is accommodated externally [35].

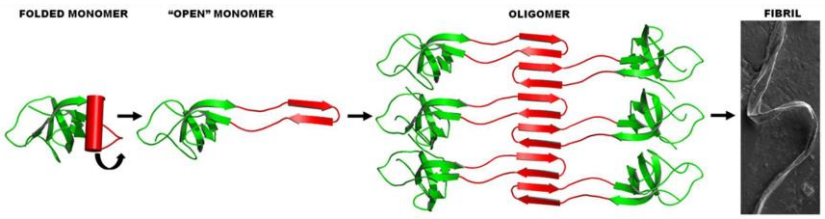

Figure 5: *A model for the formation of fibrils proposed after site-directed mutagenesis studies*

1.2.3 Applications

The exploitation of the HFBs in several application fields is mainly due to their capability to change the physical-chemical properties of a wide range of surfaces and to stabilize emulsions (**Fig.6**).

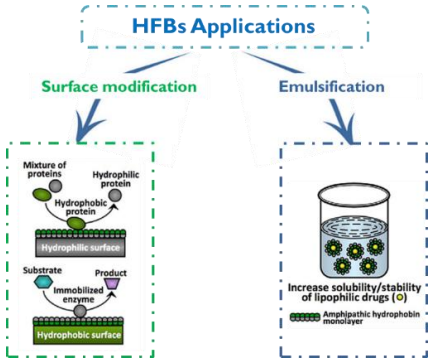

Figure 6: *Schematic representation of possible HFBs applications*

In cosmetic, pharmaceutical and food applications [36,37], the HFBs emulsifying capability have been investigated as a replacement of the typical synthetic emulsifiers, and it has been demonstrated that Class II HFBs show a higher emulsifying activity and longer stabilizing period of oil droplets than class I HFBs [38]. Moreover, this capability can be exploited in bioremediation processes of soil and water. in fact, they can promote water solubility of hydrophobic pollutants, which facilitates their removal [39].

Both classes of HFBs have been largely employed to solubilize hydrophobic solids in water, as occurred for nanomaterials dispersions that are often affected by the aggregation processes. Different nanomaterials such as two-dimensional graphene, carbon nanotubes (CNT) or multi-walled carbon nanotubes (MWCNT) have been coated by HFBs. Indeed, these proteins are able to create hydrophobic interactions with nanomaterials and, at the same time, to expose their hydrophilic sites keeping the materials in solution. HFBs capability to form protein layers on several surfaces by non-covalent bonds [40] represents a valid alternative for conventional surface modification methods that are more complicated and time consuming. Moreover, the HFB protein layers can be also used as a platform to immobilize a wide range of proteins exploitable, for example, in the biosensing field [41–47]. However, the use of HFBs can be affected by their low production and purification yields, even if a high grade of purity can be necessary when the protein is employed, for example, in foodstuff or medicines [48], while a low purified sample can be sufficient as foaming agent. However, these issues have been often overcome by the recombinant production of these fungal proteins in microorganisms such as bacteria and yeasts [49,50].

Among the Class I HFBs deeply characterized by our research group and used in a very wide range of applications, Vmh2, secreted by the fungus *P. ostreatus*, can be counted.

1.3 VMH2: A CLASS I HYDROPHOBIN

The family of genes coding for *P. ostreatus* hydrophobins is large and complex and the function of the encoded proteins is regulated by different developmental stages. Vmh2 is secreted by the fungus basidiomycete *P. ostreatus*, an important edible mushroom used as a source of proteins and other chemicals, containing also seven genes encoding cerato-platanins. Belonging to the Class I HFBs, Vmh2 can form amyloid-like structures that can be disassembled only using strong acid treatments. Structural and functional properties of the protein as a function of the environmental conditions have been also determined. Indeed, solvent polarity, pH, temperature, and the presence of calcium ions trigger the protein transition towards amyloid structural states [51]. Vmh2 is soluble in alkaline aqueous buffer and, thanks to the alcohols ability to mask the exposed hydrophobic areas avoiding the interactions between the proteins, its solubility increases in less polar solvents (e.g., 60% ethanol). The Vmh2 natural capability to form protein layers has been largely exploited in the modification of several surfaces (**Fig. 7)** both to change their wettability and to immobilize biomolecules in their active form.

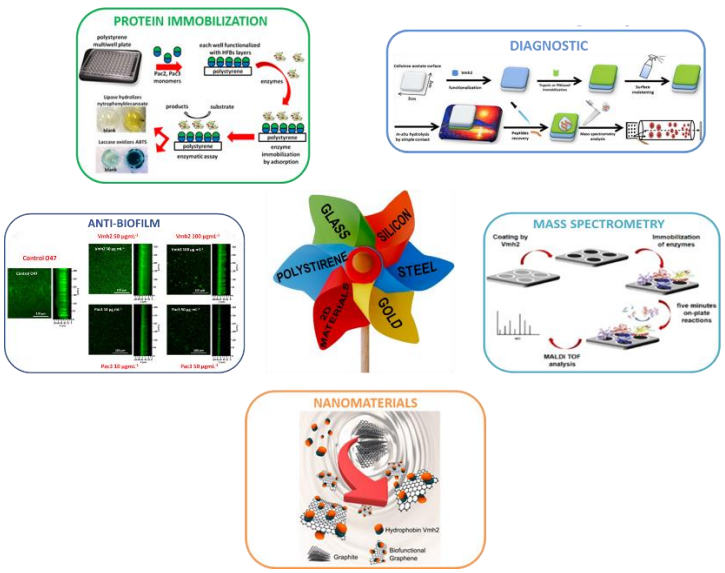

Figure 7: *Examples of Vmh2 modified surfaces used to develop several systems suitable for different applications*

The amphiphilic nature of the hydrophobin has been used, for example, to biofunctionalize silicon surface allowing the adhesion of two different proteins: the bovine serum albumin and a laccase enzyme [52]. Furthermore, in proteomic and diagnostic fields, the Vmh2 layer has been employed to improve the MS analysis through the adhesion of hydrolyzed peptides or proteolytic enzymes [41,53]. To avoid the sampling invasiveness of cultural heritage objects, a similar proteomic approach has been used in the development of a minimally invasive and portable method. In fact, the Vmh2 functionalized cellulose acetate sheets have been used to easily immobilize proteolytic enzymes. Then, only by a fast contact with the ancient object, the proteomic analysis has been possible[54]. Instead, in nanobiotechnology field, the same HFB has been used to obtain functionalized graphene through exfoliation process of low-cost graphite performed in presence of the protein solution in ethanol-water mixture [55]. Likewise, the Vmh2 functionalization of gold-nanoparticles has been performed by one-step synthesis obtaining a modified surface able to interact with protein and antibodies and to recognize and monitor glucose in aqueous solutions [56,57]. If on one hand the coating capability of the Vmh2 allows the protein adhesion, on the other hand, hydrophobin layer can avoid the attachment of microorganisms on the biofunctionalized surfaces. In fact, it has been demonstrated that the Vmh2 functionalized polystyrene is able to prevent the *Staphylococcus epidermidis* biofilm formation [58]. Furthermore, the genetic fusion of the Vmh2 and the human antimicrobial peptide LL37 has allowed the development of antibacterial surfaces against a wider spectrum of bacteria [59].

In biosensing field the Vmh2 has been used to overcome some issues related to the immobilization of bioreceptors on the transducer elements. Indeed, the adhesion of biomolecules, such as enzymes, antibodies, peptides is often mediated by chemical linkers whose preparation can be expensive and time-consuming. The employment of Vmh2 layers represents a valid alternative to tightly bind the biomolecules in an easy, rapid, and reliable way, within very short times, without resorting to covalent chemistry. As reported by Della Ventura et al [60], exploiting the natural ability of Vmh2 to bind glucose, gold nanoparticles functionalized with the hydrophobin have been used to quantitatively analyze the sugar. More recently, a homogeneous biocatalytic layer has been formed using Vmh2 fusion proteins. Indeed, the HFB has been genetically fused to different biomolecules of biotechnological interest. In this way, the obtained chimeric protein is endowed with both the adhesive capability of Vmh2 and the specific function of the target protein. Therefore, the enzyme glutathione-S-transferase (GST) fused to Vmh2 has been immobilized on polystyrene surface to develop an optical biosensor to quantify pesticides in aqueous environmental samples [61]. Likewise, the chimeric protein GreenFluorescentProtein (GFP)-Vmh2 has been used to develop an optical biosensor to detect and quantify thrombin in real plasma, thanks to the presence of a thrombin cleavage site between the two fusion

partners [62]. Moreover, another optical biosensor to detect caffeic acid (3-(3,4-dihydroxyphenyl)-2-propenoic acid) and L-DOPA ((S)-2-amino-3-(3,4-dihydroxyphenyl) propanoic acid), has been developed immobilizing the chimera PoxA1b laccase-Vmh2 on the same surface [63]. For the detection of As (III), an innovative electrochemical biosensor has been developed immobilizing the chimera Arsenate reductase-Vmh2 on gold-coated piezoelectric quartz crystals, exploiting the ability of the target protein to reduce As(V) to As(III) [64]. Then, the fusion protein Vmh2-H3w peptide (a heavy metal binding peptide) has been immobilized on a polystyrene surface to develop an easy and portable biosensor to detect mercury (II) in sea water [65]. The achieved results open a very interesting scenario, exploiting both the protein layer formation and the design and the production of new fusion proteins.

1.4 FUNGAL PROTEIC BIOSURFACTANTS: THE CERATOPLATANINS

Another class of fungal biosurfactant proteins, even if very poorly studied from this point of view, consists of the small cysteine-containing proteins named CP. They can be released into the culture filtrate by the filamentous fungi, but they can also be found in the cell wall of the hyphae and spores. Even though the biological role of CPs in fungi is not still clear, these proteins can act both as virulence factor and as elicitors. Indeed, it is reported that some CPs from plant pathogenic fungi act as phytotoxins inducing the cell necrosis. On the contrary, some beneficial fungi produce the CPs proteins to induce plant defence responses, thus showing an eliciting activity [66]. These proteins, structurally different from HFBs, show some similarity concerning their functional characteristics. Indeed, ceratoplatanins can self-assemble at hydrophobic-hydrophilic interfaces into ordered amphipatic layers as the HFBs [67]. However, some studies indicated that the CPs behavior is opposite to that of HFBs, for example, the ceratoplatanin EPL1 from *Trichoderma atroviride* increases the polarity of solutions and surfaces [68]. Moreover, as demonstrated by Pitocchi et al [69], CPs can stabilize emulsion and reduce the surface tension. Furthermore, while the self-assembling mechanisms of HFBs has been widely studied, the study on the cerato-platanin assembly is still limited, even if it has been confirmed that this process is linked to the protein concentration and to the interaction with a hydrophobic material [70]. The importance to study this mechanism is mainly due to the potential use of CPs in the fabrication of new biofunctionalized materials and in the field of nano-biotechnology. Additionally, CPs are homologous to the N-terminal domain of expansins, which are proteins associated with carbohydrate binding and loosening of the cellulose scaffolds in plant cell walls [71]. Indeed, ceratoplatanins are also able to weaken cellulose substrate disrupting its non-covalent bonds without any hydrolytic activity [69,72]. This ability has been exploited, for example, in

biotechnological applications contributing to the valorization of lignocellulosic waste materials using the *Th*CP protein from *Trichoderma harzianum.* Indeed, this CP has been recently used in a pretreatment process of apple pomace, coffee silverskin and potato peel to enhance the cellulases activity obtaining a high sugar conversion [73].

WORK DESCRIPTION

The main purposes of this PhD project are related to both the identification and characterization of novel protein biosurfactants produced by marine fungal strains and the exploitation of the hydrophobin Vmh2 in different application fields (**Fig. 8**). In particular:

- The isolated surface-active proteins have been characterized both as biosurfactants and bioemulsifiers through several specific techniques.
- The wild type Vmh2 has been employed in the development of a portable kit exploitable in the cultural heritage field.
- By engineering genetic techniques, the same hydrophobin has been fused two Single chain Fragment variable (ScFv) of antibodies to detect two algal neurotoxins and to a laccase enzyme (PoxA1b) for the detection of aromatic compounds. In both cases, optical and electrochemical biosensors have been developed to detect different contaminants.

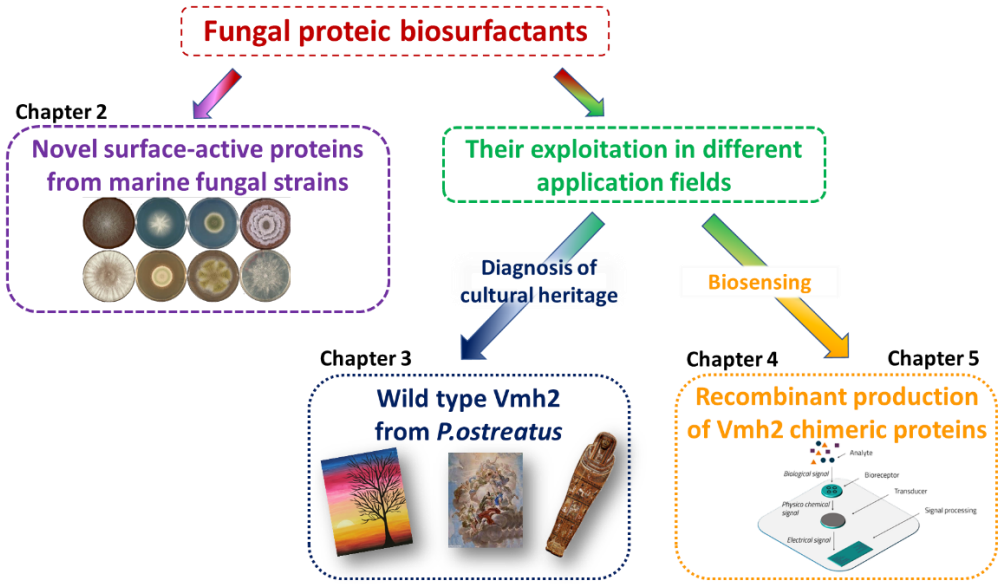

Figure 8: *Schematic flow of this PhD project*

Chapter 2

2. Characterization of novel protein biosurfactants from marine fungal strains

Marine ecosystems perform several key environmental functions, and it represents the greatest source of biodiversity. Indeed, the marine microorganisms have developed physiological abilities to survive in extreme habitats, among their physiological adaptation the production of new metabolites that are often absent in the terrestrial ones. Nonetheless, due to the enormity of the marine ecosystem, most of the marine microbial world is still unexplored. The word fungus, for example, is wrongly synonymous of the terrestrial microorganism, while in nature there are more than 10.000 marine species found inhabiting several marine habitats, ranging from surface seawater to the sea depths [74].

More generally, the filamentous fungi can be classified into three groups namely *Ascomycetes, Basidiomycetes and Zygomycete* [75]. They are ubiquitous and very relevant in the maintenance of the environmental equilibrium thanks to their ability to recycle nutrient, to form symbiotic interactions and to decompose organic matter [76]. Exploiting these skills, fungi are studied, for example, as a valid alternative to physicochemical processes to remove micropollutants [77,78] and the production of extracellular enzymes makes them useful in the valorisation of substrate nutritional value [79] and as a pre-treatment step of lignocellulosic materials [80].

Among the interesting biomolecules produced by fungal microorganisms, the surface-active proteins are studied due to their usage as biosurfactants and/or bioemulsifiers. Recent studies carried out in our laboratory and in collaboration with other national and south-American research groups gave the possibility to isolate two kinds of surface-active proteins from some marine fungal strains: the hydrophobins and the ceratoplatanins [69,81].

In this context, the section 2.1 is focused on the characterization of a new surface-active protein, named *Sap-Pc,* produced by a marine strain of *Penicillium chrysogenum* and my contribute was mainly related to the isolation of the protein and its characterization by Surface tension and Dynamic Light Scattering measurements. Moreover, the section 2.2 is focused on the growth of two marine fungi on seaweed polysaccharides and their production of cerato-platantins and hydrophobins. Considering my skills about the manipulation of fungal strains, my contribution was related to set up and optimize the protein purification process from the fungal culture broths.

2.1 Characterization of surface-active protein extracted from a marine strain of *Penicillium chrysogenum*

International Journal of *Molecular Sciences*

MDPI

Article

Characterization of a Surface-Active Protein Extracted from a Marine Strain of *Penicillium chrysogenum*

Paola Cicatiello [1], Ilaria Stanzione [1], Principia Dardano [2], Luca De Stefano [2], Leila Birolo [1], Addolorata De Chiaro [1], Daria Maria Monti [1], Ganna Petruk [1], Gerardino D'Errico [1] and Paola Giardina [1,*]

1 Department of Chemical Sciences, University of Naples (Federico II), Via Cinthia, 80126 Naples, Italy
2 Institute for Microelectronics and Microsystems, Unit of Naples-National Research Council, Via P. Castellino 111, 80127 Naples, Italy
* Correspondence: giardina@unina.it; Tel.: +39-081-674319

Received: 5 June 2019; Accepted: 27 June 2019; Published: 2 July 2019

check for updates

Abstract: Marine microorganisms represent a reservoir of new promising secondary metabolites. Surface-active proteins with good emulsification activity can be isolated from fungal species that inhabit the marine environment and can be promising candidates for different biotechnological applications. In this study a novel surface-active protein, named Sap-*Pc*, was purified from a marine strain of *Penicillium chrysogenum*. The effect of salt concentration and temperature on protein production was analyzed, and a purification method was set up. The purified protein, identified as Pc13g06930, was annotated as a hypothetical protein. It was able to form emulsions, which were stable for at least one month, with an emulsification index comparable to that of other known surface-active proteins. The surface tension reduction was analyzed as function of protein concentration and a critical micellar concentration of 2 μM was determined. At neutral or alkaline pH, secondary structure changes were monitored over time, concurrently with the appearance of protein precipitation. Formation of amyloid-like fibrils of SAP-*Pc* was demonstrated by spectroscopic and microscopic analyses. Moreover, the effect of protein concentration, a parameter affecting kinetics of fibril formation, was investigated and an on-pathway involvement of micellar aggregates during the fibril formation process was suggested.

Keywords: marine fungi; biosurfactant proteins; amyloid fibrils; emulsions

1. Introduction

Most of the emulsifiers currently used are synthetic; however, in the era of green technology, great interest is being given to surface-active biomolecules [1]. These compounds offer many advantages over their synthetic counterparts thanks to their biodegradable and environmentally friendly nature [2,3]. The constant research of efficient surface-active compounds, biosurfactants (BSs), and bioemulsifiers (BEs), with improved thermo-physical properties could make several industrial processes more sustainable. Indeed, these molecules find applications in cosmetics, pharmaceutics, food processes, and bioremediation [4–6]. In an oil polluted environment, these molecules play a specific role of binding to dispersed hydrocarbons and oils, preventing them from merging together, thus increasing their access and availability for biodegradation. These amphiphilic molecules mainly produced by microorganisms occur in nature as different kinds of compounds characterized by low molecular weight, i.e., glycolipids, lipopeptides, phospholipids, and fatty acids, or high molecular weight, i.e., amphipathic polysaccharides, proteins, lipopolysaccharides, lipoproteins or complex mixtures of these biopolymers [7].

According to Uzoigwe et al. [8], the terms BE and BS are not interchangeable, because they differ for physico–chemical properties and physiological roles. The low molecular weight compounds, known as BSs, have excellent surface activity, reduce the surface and interfacial tension between different phases, possess a low critical micelle concentration (cmc), and form stable emulsions. On the other hand, BEs are the high molecular weight compounds, which can efficiently emulsify two immiscible liquids even at low concentrations but are less effective at surface tension reduction. Therefore, they possess emulsifying activity, but not high surface activity.

In this last decade, different habitats have been explored to isolate BE and BS compounds resistant to extreme conditions to replace their synthetic counterparts. Since marine microorganisms live in a stressful habitat, under cold, lightless, and high-pressure conditions or in association with other organisms, they represent a reservoir of promising secondary metabolites. Indeed, a wide variety of genera producing diverse types of surface-active compounds are associated with the marine environment [9–11]. Adaptive changes in secondary metabolite production by facultative marine microorganisms with respect to their terrestrial counterparts have been observed in response to environmental variations in pressure, temperature, and salinity [12]. Among the marine microorganisms, production of surface-active compounds from bacterial species are well explored, whereas little is known about their production from fungi [13,14]. In most of the studies, these biomolecules were only partially characterized, and their activities analyzed using the crude extracts rather than purified molecules [15,16]. Among them, few proteins were isolated and classified as BE. To date, most surface-active proteins known to be produced by fungi are the hydrophobins (HPBs) [17,18]. The intriguing features of these proteins rely on their amphiphilic nature, intrinsically related to their 3D structure. They self-assemble at the hydrophilic/hydrophobic interface, stabilizing air bubbles and water/oil emulsions [19–21]. The HPB family can be divided into two distinct classes: Class I HPBs self-assemble into very stable layers, forming amyloid-like fibrils, resistant to very harsh conditions (hot 2% sodium dodecyl sulphate); and Class II HPB aggregates are nonfibrillar and less stable, and can be more easily dissolved in detergent or organic solvents.

A screening of marine fungi was previously carried out to isolate new HPBs or other surface-active proteins [22,23]. Twenty-three fungi were selected for their ability to produce foam during their growth in shaking culture. Extraction methods were set up to isolate secreted or cell wall associated HPBs, allowing the identification of six new putative HPBs. The protein produced by *Penicillium chrysogenum* MUT 5039 was endowed with the best emulsification capacity tested on a mixture of water and olive oil. Actually, marine isolates of *P. chrysogenum* were already proven to be good sources of new and interesting bioactive compounds [13]. Based on the stability of the amphiphilic layer it formed, the protein was predicted to be a member of the Class II HPB family [22]. This proteic BE was very promising from a biotechnological point of view and was herein characterized. At first, the attention was focused on the protein production yield and on its purification, then the protein was characterized and its surface activity analyzed. Unexpectedly, it was not an HPB but a previously unknown proteic BE, which forms amyloid-like fibrils.

2. Results

2.1. Purification and Identification of the Penicillium chrysogenum BE Protein

The strain *P. chrysogenum* MUT 5039 was previously selected as a good BE producer from a pool of marine fungi [22]. This is a facultative marine fungus, able to grow in the presence or absence of NaCl, suggesting that it may have been spilled into the sea and then adapted to the new salty environment [24,25]. In the previous work [22], the sodium dodecyl sulphate polyacrylamide gel electrophoresis (SDS–PAGE) analysis of the proteins extracted from the culture broth of this fungus after bubbling, showed only one main protein band.

Herein, to select the optimal fungal growth conditions to obtain the protein, the strain was grown in liquid medium in the presence of 0%, 1.5%, and 3% NaCl at 20 °C and 28°C. The fungal growth was

not significantly affected by salt concentrations or temperature; indeed, the same amount of mycelium was produced in all conditions (about 10 g of dry mycelia per liter of culture). On the other hand, the highest protein yield was obtained at 20°C supplying the medium with 1.5% NaCl, obtaining about 30 mg of protein per liter of culture (Figure S1).

After air-bubbling of the culture broth, 80% of the initial protein amount was recovered in half of the original volume. However, samples before and after bubbling, analyzed by SDS–PAGE, showed smeared bands (Figure S2). Similar results were obtained even after trichloroacetic acid (TCA) precipitation and dissolution of the concentrated sample in 60% ethanol. The presence of lipid contaminants proven by Fourier-transform infrared spectroscopy (FTIR) and thin-layer chromatography (TLC) analysis, was significantly reduced after methanol chloroform extraction (Figure S3). Then a sharp SDS–PAGE band of the protein, dissolved in 60% ethanol, was obtained (Figure 1a, lane 1). This band was analyzed by a proteomic approach with LC–MSMS analysis, leading to the identification of the protein Pc13g06930 (ID NCBIr 255936199), with five peptides, for a total sequence coverage of 31% (Figure 1c, Table S1). The molecular mass of the protein, named SAP-Pc, was 13,213 m/z, as estimated by MALDI-TOF (Figure 1b), whereas the expected mass of Pc13g06930, without the putative signal peptide, was 13,313 m/z. This 100 Da difference could be due to aminoacidic substitutions or post-translational modifications occurring in this strain.

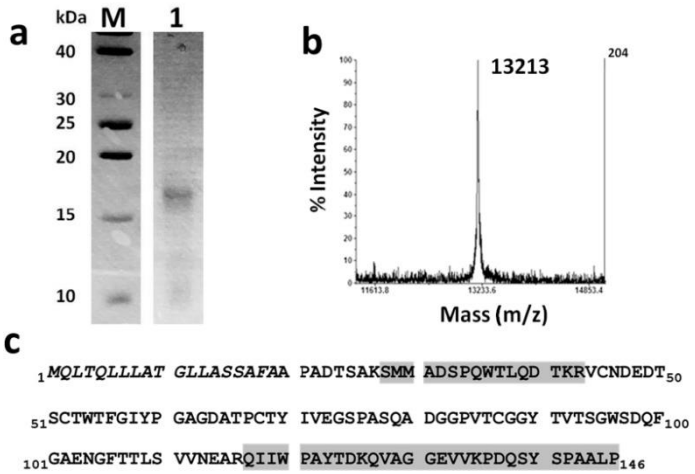

Figure 1. (**a**) SDS analysis of SAP-*Pc* in 60% ethanol solution after methanol chloroform treatment; (**b**) MALDI-TOF spectrum of SAP-*Pc* in 60% ethanol solution in linear mode; (**c**) sequence coverage of the primary structure of identified SAP-*Pc* highlighted in grey.

Pc13g06930, annotated as hypothetical protein, is similar to many other uncharacterized proteins found in different fungal species, whose genomes are known. The hydrophobicity plot in Figure S4 shows that the first half of the sequence is more hydrophilic than the second half.

2.2. Protein Characterization as Biosurfactant

At first, the concentration of SAP-*Pc* in aqueous buffers at three different pHs (4, 7, and 9) was verified to be the same as in 60% ethanol solution (100 µg/mL).

The SAP-*Pc* emulsification ability was tested in the presence of a "model oil", Dectol [26]. The emulsification index E_{24} of samples dissolved at 100 µg/mL at different pHs (4, 7, and 9) was

measured, as reported in Figure 2a. The best performance as emulsifier was obtained at both neutral and alkaline conditions, showing an E_{24} of about 70%. These emulsions remained stable for at least one month. On the contrary, the E_{24} in acidic conditions was lower (50%) and the emulsion less stable during the time. The E_{24} at different SAP-*Pc* concentrations was evaluated at pH 7 (Figure 2b). Doubling the protein concentration from 50 to 100 µg/mL, the E_{24} increased from 30 to 70%. After that, the E_{24} value was almost constant up to the maximum concentration used (400 µg/mL).

a

Sap-*Pc* (100 µg/mL)	E_{24} (%)
pH 4	50
pH 7	70
pH 9	70

b

Sap-*Pc* pH 7 (µg/mL)	E_{24} (%)
50	30
100	70
200	70
400	70

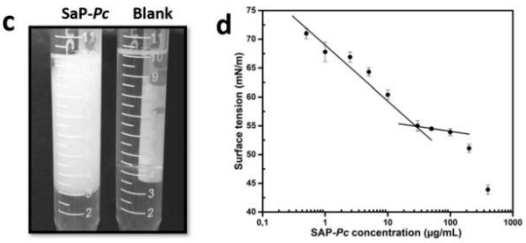

Figure 2. (**a**) Table of E_{24} values of 100 µg/mL of SAP-*Pc* at different pHs in the presence of Dectol; (**b**) table of E_{24} values of SAP-*Pc* dissolved at pH 7 at different concentrations in the presence of Dectol. All results are averages from three replicate experiments and the standard deviation is less than 10%. (**c**) Emulsion of 100 µg/mL SAP-*Pc* in 10 mM phosphate buffer at pH 7 (4 mL) mixed to 6 mL of Dectol after 24 h, in comparison to the mixture of buffer and Dectol, in the absence of the protein. (**d**) graph of surface tension of SAP-*Pc* in 10 mM phosphate buffer at pH 7 as function of protein concentration.

Surface tension of solutions of SAP-*Pc* dissolved at different concentrations in phosphate buffer with pH 7, was measured (Figure 2d). It must be noted that the lowest value at each protein concentration was reached slowly, as is typical for proteins [27,28], and at least one hour was needed to reach the final equilibrium value. When SAP-*Pc* concentration increased from 0.5 to 30 µg/mL, the surface tension was gradually reduced from 72 mN/m of the aqueous buffer to 55 mN/m; then the value remained almost constant from 30 to 100 µg/mL. Therefore, a cmc of 28 µg/mL (2 µM) was calculated as the point of intersection between two trend lines. At protein concentrations higher than about 100 µg/mL, a steep decline of the surface tension indicated the occurrence of another aggregation phenomenon.

2.3. SAP-Pc Aggregation

The solution of SAP-*Pc* in 60% ethanol remained stable for several months at room temperature. On the other hand, when the protein was stored at 100 µg/mL in aqueous buffers at different pHs, a concentration reduction (60–70%) was observed after about four days at pH 7 and 9, while no variation was detected at acidic pH. Hence further analyses were performed to investigate SAP-*Pc* aggregation processes.

The protein dissolved in the aqueous buffers showed a random coil structure when analyzed by far UV-circular dichroism (CD), with a minimum at 200 nm at all pHs used (4, 7, and 9), whereas it

was more structured in 60% ethanol solution, as expected (Figure 3). The CD spectra of the protein incubated at room temperature in the three buffers were recorded. At neutral and alkaline conditions, the protein showed significant conformational changes during that time (Figure 3a,b). On the contrary, the spectra of SAP-*Pc* in acidic conditions, or in 60% EtOH, appeared unchanged over time (Figure 3c).

Taking into consideration that these structural changes led to a higher contribution of β structures (e.g., see the spectrum after 4 days at pH 7), the formation of amyloid-like fibrils can be envisaged. The fluorescent dye thioflavin-T (ThT), typically used to detect the presence of amyloid fibrils, was used to verify their formation. A significant increase of the ThT fluorescence intensity was observed at neutral and alkaline pHs during a period of one week (Figure 3d). To confirm the formation of amyloid-like structures, atomic force microscopy (AFM) analysis of SAP-*Pc* was performed, just after dissolution in aqueous buffer at pH7 (t0), and after 4 days (Figure 4). At t0, ellipsoidal protein aggregates were observed (54 ± 30 nm), whereas fibrils were detected in samples 4 days after dissolution. Their length was more than 1 μm, the medium width was 30nm, and their shape looked like an alignment of aggregates.

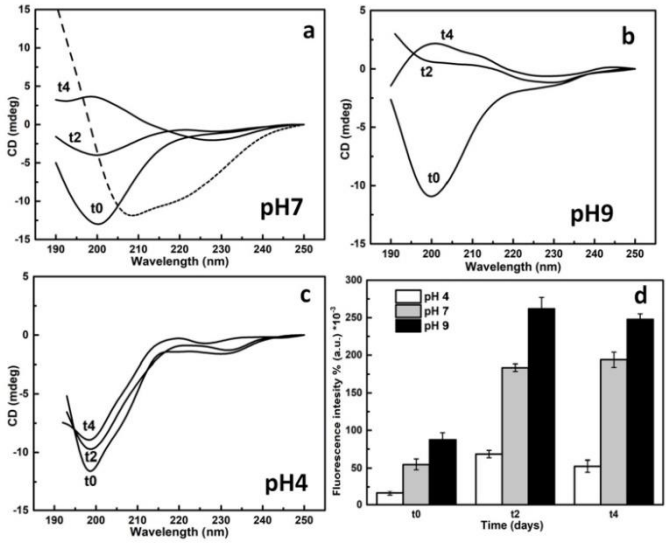

Figure 3. Circular dichroism (CD) spectra of SAP-*Pc* (100 μg/mL) dissolved in aqueous buffers at pH 7 (**a**), pH 9 (**b**), and pH 4 (**c**), just after dissolution (t0) and after 2 and 4 days. The dotted line in panel a corresponds to the spectrum of the protein in 60% ethanol; (**d**) ThT assay: fluorescence intensity of the same samples in the presence of 30 μM ThT.

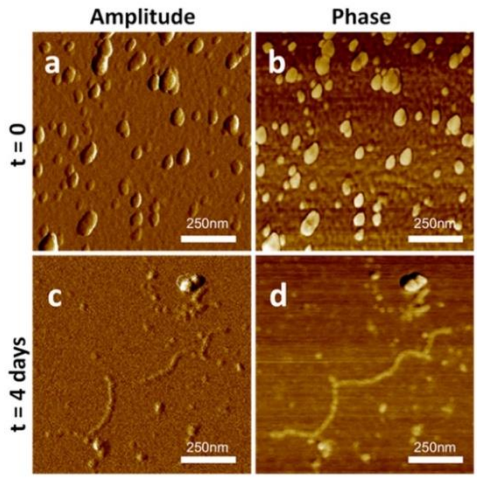

Figure 4. AFM imaging of 100 μg/mL SAP-*Pc* in 10 mM phosphate buffer pH 7 after washing: Non-contact mode (NCM) amplitude (left column) and phase (right column) at t_0 (**a**,**b**) and after 4 days (**c**,**d**).

2.4. Effect of Protein Concentration on SAP-Pc Aggregation

Protein concentration is an important parameter affecting self-assembling processes [29,30]. Indeed, the ThT fluorescence intensity remarkably increased at SAP-*Pc* concentrations ranging from 200 to 600 μg/mL at pH 7 (Figure 5a), while its decrease at higher concentrations was probably due to protein precipitation. Therefore, a concentration parameter based on ThT assays can be established and can be named critical aggregation concentration (cac), according to other authors [31,32]. Its value was 191 μg/mL (14 μM), calculated as the point of intersection between two trend lines.

Formation of SAP-*Pc* aggregates at different protein concentrations (pH 7) was also analyzed by dynamic light scattering (DLS). At protein concentrations ranging from 5 to 10 μg/mL, a population with a hydrodynamic radius of about 20 ± 9 nm was observed together to a population of 140 ± 20 nm, which is very large for a 13 kDa protein, (i.e., lysozyme: M_W = 14.5 kDa, R_H = 1.9 nm [33]) thus demonstrating the presence of aggregates even at these low concentrations. The population of smaller aggregates appeared more evident in the graph of volume-averaged size distribution (Figure S5). From 10 to 100 μg/mL the main peak remained centered at 140 ± 20 nm, while at 250 μg/mL a R_H value of 830 ± 30 nm was reached (Figure 5b,c). At 400 μg/mL the sample appeared too heterogeneous and poly-dispersed to obtain reliable measurements.

AFM analysis of samples at 10, 100, and 200 μg/mL were in line with these results. Statistics, as shown in Figure 5d,e,g, gave an average radius of 50 ± 30 nm, 110 ± 70 nm, and 150 ± 90 nm, for 10, 100, and 200 μg/mL concentrations, respectively. Furthermore, very long alignments of aggregates forming fibrils were detected in the more concentrated sample. However, these long fibrils tended to leave the mica surface when washed.

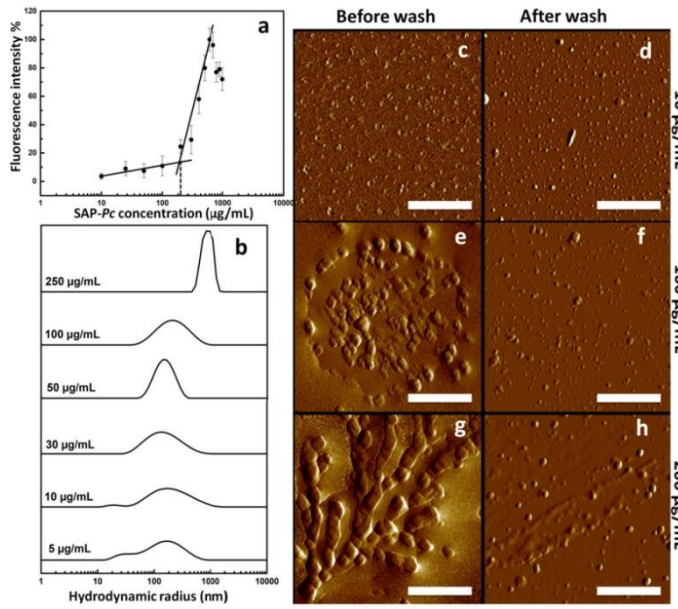

Figure 5. (**a**) Fluorescence intensity of SAP-*Pc* dissolved in 10 mM phosphate buffer at pH 7 at different concentrations in the presence of 30 µM ThT; (**b**) the averaged-intensity of hydrodynamic size distribution of SAP-*Pc* dissolved in 10 mM phosphate buffer at pH 7 at different concentrations. (**c**–**g**) AFM imaging of 10 (**c**,**d**), 100 (**e**,**f**), and 200 (**g**,**h**) µg/mL, respectively from top to bottom, SAP-*Pc* in 10 mM phosphate buffer at pH 7. Non-contact mode (NCM) amplitude images of casted samples before (left column) and after washing (right column) (scale bar is 1 µm).

2.5. Toxicity Analysis

As a preliminary approach in view of a potential use in the cosmetics or medical field, SAP-*Pc* biocompatibility was investigated on human immortalized keratinocytes, which represent the outer part of the skin and are considered as guard cells for the human body. Cells were incubated in the presence of increasing amounts of SAP-*Pc* for 24 and 48 h and cell viability was determined. As shown in Figure S6, SAP-*Pc* induced 20–25% of toxicity after 24 h incubation at 50 and 100 µg/mL, and 20–30% of toxicity after 48 h incubation.

3. Discussion

The protein SAP-*Pc* was purified from the culture broth of a facultative marine strain of *P. chrysogenum*, whose selection was based on its ability to form foam during growth. The purification procedure used was set up to isolate Class II HPBs, known fungal surface-active proteins, secreted in culture media [22]. Nevertheless, the principal protein secreted by this fungus, under the stressful conditions of the marine habitat, was not HPB but an unknown protein, which we named SAP-*Pc*. The emulsification ability of SAP-*Pc* is similar to that reported for HFBII, a Class II HPB [26] in the same conditions and the emulsions obtained in the presence of SAP-*Pc* are very stable [22]. Moreover, its low toxicity suggests potential applications in the cosmetics and biomedical fields, considering also its low cost in terms of culture broth and purification procedure.

Oligomeric assemblies formed by amphiphilic proteins can be considered as "micelle(s)", with properties consistent with those of well characterized micelle-forming substances [34]. Taking into consideration the first two regions of the plot of surface tension vs. log of surfactant concentration, a cmc can be determined, like that of any surfactant. The surface tension decreased when the cmc was small, as for other BEs [8]. However, it was clear from the same plot that other aggregation phenomena occurred at higher concentrations (more than 200 μg/mL).

Indeed, formation of amyloid like fibrils of SAP-*Pc* was demonstrated at neutral and alkaline pHs, and as a function of time and protein concentration, parameters that generally affect protein aggregation phenomena. On the other hand, the protein remains soluble at pH 4, adopting random coil conformations. Aggregates of ellipsoidal shapes were observed by AFM and detected by DLS already at 10 μg/mL. Four days after dissolution, or at a protein concentration of 200 μg/mL, fibrils were observed by AFM and a precipitate was perceptible to the naked eye. Formation of amyloid-like fibrils at pH 7 was observed by all the techniques used. It is worth noting the typical morphology of these fibrils: they look like a "pearl neck-lace", which can be originated by an array of interacting aggregates. According to the graph of the ThT fluorescence assays vs log of protein concentration, and DLS analysis, a cac can be determined. Hence, the notable decrease of the surface tension observed at concentrations higher than cac can be related to the fibril formation and to their tendency to reside at the interface. Indeed, the behavior of amyloid peptides has often been compared to that of surfactants [31,35]. The concentration dependence of the degree of aggregation is typical for spontaneous cooperative aggregation processes, such as the self-assembly of surfactants into micelles. Usually in these processes, monomers are present in solution at low concentrations, while aggregates form when the concentration exceeds a fixed value.

In the case of SAP-*Pc*, two different phenomena have to be considered, being that the cmc and cac parameters were noticeably different (28 μg/mL cmc,191 μg/mL cac). The presence of aggregates in the concentration range between 30 and 200 μg/mL, with hydrodynamic radius centered at 140 nm, was shown. Much larger aggregates, at and above 200 μg/mL, should correspond to amyloid-like fibril formation, as verified by AFM analysis.

According to Dear et al. [36], proteins can form globular oligomers, micelle-like structures, under appropriate conditions through hydrophobic bonding, because of their amphiphilic character. These morphologies can play the role of intermediates on the way to form the more structured β-sheet-containing species, the amyloid fibrils.

Even in the case of SAP-*Pc*, micelles should be on-pathway with respect to fibril formation and evolve towards fibrillar aggregates, which are formed overtime or more quickly at higher protein concentration. Indeed, DLS analysis in Figure S7 showed the dependence of the lag time to aggregation upon the protein concentration. A higher SAP-*Pc* concentration results in more rapid nucleus formation and reduction of the lag-phase of amyloid fibril formation, thus again indicating that the micelle-like aggregates are intermediates of the fibrillization process.

4. Materials and Methods

4.1. Culture Conditions and Protein Extraction

The fungal strain *Penicillium chrysogenum* MUT 5039 was provided by the Mycotheca Universitatis Taurinensis. The mycelium was maintained at 4 °C through periodic transfer on XNST30 (malt extract 3 g/L; yeast extract 3 g/L; NaCl 30 g/L; 10 g/L glucose; and 5 g/L peptone) agar plates. Mycelia were inoculated in 1 L flasks containing 500 mL of WM (10 g/L glucose; 2 g/L peptone; 1 g/L $(NH_4)_2SO_4$; 0.5 g/L $MgSO_4 \cdot 7H_2O$; 0.875 g/L KH_2PO_4; 0.125 g/L K_2HPO_4; 0.1 g/L $CaCl_2 \cdot 2H_2O$; 0.05 g/L $MnCl_2$; 0.001 g/L $FeSO_4$; different amounts of NaCl, 0 or 15 or 30 g/L), grown at 20 or 28 °C in shaken mode (180 rpm). After 5 days of fungal growth, the culture broth was separated from the mycelium by filtration through Whatman paper and agitated in a Waring blender to produce foam. Next, the foam was recovered and treated with 20% trichloroacetic acid (TCA), incubated overnight at 4 °C, and

centrifuged for 1h at 3300× *g*. The precipitate was collected, dissolved in 60% ethanol aqueous solution, sonicated in Elmasonic S30 water bath sonicator (Elma Schmidbauer GmbH, Singen, Germany) for 20 min, and again centrifuged. The ethanol solution was used because HPBs are usually more soluble and stable in this condition. The raw extract was dried, and lipids were extracted in a mixture of methanol–chloroform 2:1 *v/v* (5 min in bath sonicator). After centrifugation, the protein pellet was dried and dissolved again in 60% ethanol. The protein concentration was evaluated using the PIERCE 660 nm protein assay (ThermoFischer Scientific, Waltham, MA, USA), with bovine serum albumin as the standard. The purity and the molecular weight of the extracted sample was evaluated by SDS–PAGE (15% acrylamide), stained by Coomassie brilliant blue.

4.2. Mass Spectrometry

MALDI mass spectra were recorded on a Sciex 5800 MALDI–TOF–TOF mass spectrometer (AB Sciex, Foster City, CA, USA). The analyte solutions were mixed with sinapinic acid (20 mg/mL in 70%acetonitrile, TFA 0.1% *v/v*) as the matrix, applied to the sample plate, and air dried. The spectrometer was used in the linear mode. The spectrum was calibrated externally.

SDS–PAGE analysis was performed to select the band of interest, which was then cut from the gel, destained by washes with 0.1 M NH_4HCO_3 pH 7.5 and acetonitrile, reduced for 45 min in 100 µL of 10 mM dithiothreitol, 0.1 M NH_4HCO_3, pH 7.5, and carboxyamidomethylated for 30 min in the dark by the addition of 100 µL of 55 mM iodoacetamide dissolved in the same buffer. Enzymatic digestion was performed and analyzed by LC–MSMS on a 6520 Accurate-Mass Q-TOF LC/MS system (Agilent Technologies, Palo Alto, CA, USA) equipped with a 1200 HPLC system and a chip cube (Agilent Technologies) as previously reported [37]. Peptide analysis was performed using data-dependent acquisition of one MS scan (mass range from 300 to 1800 m/z) followed by MS/MS scans of the five most abundant ions in each MS scan. The acquired MS/MS spectra were transformed in Mascot generic format (mgf) and used for protein identification in the unreviewed set of protein entries that are present in the NCBInr database for all fungi, with a licensed version of MASCOT software (http://www.matrixscience.com) version 2.4.0, with additional search parameters. Ion score was −10 log(P), where P is the probability that the observed match is a random event. Individual ion scores >45 indicated identity or extensive homology ($p < 0.05$). Protein scores were derived from ion scores as a non-probabilistic basis for ranking protein hits (http://www.matrixscience.com/help/interpretation_help.html).

4.3. Emulsification Index

The protein in 60% ethanol was dried and re-dissolved in 10 mM phosphate buffer (pH 7), or 10 mM sodium acetate (pH 4), or 10 mM Tris HCl (pH 9). Then, it was mixed with Dectol (decane and toluene in 65:35 volume ratio), which was used as a 'model oil' [26]. In a typical experiment, Dectol (6 mL) was added to the biosurfactant solution (4 mL) in a graduated tube. Then, the mixture was homogenized in a vortex for 2 min at maximum speed at room temperature. After 24 h the emulsification index, E_{24}, was determined, calculating the ratio between the height of emulsifying layer and the total height, multiplied by 100.

4.4. Spectroscopy Techniques

CD spectra were recorded on a Jasco J715 spectropolarimeter (Jasco Corporation, Cremella (LC), Italy) equipped with a Peltier thermostatic cell holder in a quartz cell (0.1 cm light path) from 190 to 250 nm. The temperature was kept at 20 °C, and the sample compartment was continuously flushed with nitrogen gas. The final spectra were obtained by averaging three scans, using a bandwidth of 1 nm, a step width of 0.5 nm, and a 4 s averaging per point.

Fluorescence spectra were recorded at 25 °C with a HORIBA Scientific Fluoromax-4 spectrofluorometer (Horiba Italia, Rome, Italy). Slits were set to 3 and 6 nm spectral band-passes in

excitation and emission monochromators, respectively. ThT, to 30 μM final concentration, was added, the samples were excited at 435 nm, and the emission was monitored from 460 to 560 nm.

4.5. AFM

An XE-100 atomic force microscope (Park Systems, Suwon, Korea) was used for the imaging of fibrils. Surface imaging was obtained in non-contact mode using silicon/aluminum coated cantilevers (SSS-NCHR 10M; Park Systems) 125 μm long with a resonance frequency of 204 to 397 kHz nominal force constant of 42 N/m and a typical tip radius 2 nm (<5 nm max). Here we used a low tip radius probe to improve measurements of fibril widths. The scan frequency was typically 0.5 Hz per line. When necessary, the AFM images were processed by flattening, in order to remove the background slope, and the contrast and brightness were adjusted. As done in [38], for sample preparation, muscovite mica with a surface area of ~1 cm^2 was used as the substratum. The mica was freshly cleaved using adhesive tape prior to each deposition in order to ensure its cleanliness. The dried samples were dissolved in 10 mM phosphate buffer, pH7. 2 μL aliquots of protein were deposited on the substrates and the samples were dried by evaporation at room temperature under a ventilated fume hood. For washed samples, two min after deposition, the surfaces were gently washed with deionized water. Finally, the samples were dried as described above.

4.6. Surface Tension Measurements

Measurements were performed by using the De Nouy ring method with a KSV Sigma 70 digital tensiometer (Dyne Testing Ltd., Newton House, Lichfield, UK). An automatic device was used to select the rising velocity of the platinum ring and to set the time between two consecutive measurements. Thorough attention must be paid in using the De Nouy ring method to deduce bulk properties, because the surfactant adsorption kinetics can influence the results [39]. In our experiments, we set the ring rising velocity low enough to reach the equilibrium between the air–solution interface and the bulk solution. Instrument accuracy was checked to be better than 0.10 $mN{\cdot}m^{-1}$ by measuring γ for 10 mM phosphate buffer, pH 7, before each session of measurements. At least two independent replicates of each sample at different protein concentrations were measured.

4.7. Dynamic Light Scattering

The size evaluation of each sample was performed by dynamic light scattering (DLS). A Zetasizer Nano ZSP instrument (Malvern Instruments, Malvern, UK) equipped with a He–Ne laser (633 nm, fixed scattering angle of 173°, room temperature 25 °C) was used. The protein samples were dissolved in 10 mM phosphate buffer pH 7 and filtered (0.22 μm) before each analysis.

4.8. Cytotoxicity Assay

Immortalized human keratinocyte cells (HaCaT) were from Innoprot (Derio, Bizkaia, Spain), and were cultured in Dulbecco's modified eagle's medium (Sigma-Aldrich, Milan, Italy), supplemented with 10% fetal bovine serum (HyClone, Logan, UT, USA), 2 mM L-glutamine, and antibiotics. Cells were grown in a 5% CO_2 humidified atmosphere at 37 °C. To test the biocompatibility of the molecule, cells were seeded in 96-well plates at a density of 2.5×10^3/well. Then, 24 h after seeding, cells were incubated with increasing amount of the molecule under test (from 10 to 100 μg/mL) for 24, 48, and 72 h. At the end of incubation, cell viability was assessed by the MTT assay as previously described [40]. Cell survival was expressed as a percentage of viable cells in the presence of the analyzed molecule, with respect to control cells. Control cells were represented by cells grown in the absence of the molecule and by cells supplemented with identical volumes of buffer (10 mM sodium phosphate, pH 7.4). Two-way ANOVA was performed as a statistical analysis.

5. Conclusions

The Sap-*Pc* is a proteic BE, herein identified, homologous to many other unidentified ascomycete proteins from *Fusarium*, *Gibberella*, *Aspergillus*, and *Thricoderma sp*. The surface activity and the emulsification ability of these fungal proteins should be analyzed to confirm the existence or otherwise of a new family of proteic BEs.

It is worth noting the high stability of the emulsions obtained in the presence of Sap-*Pc*, which remained unaltered even after one month. These results, together with the low toxicity and the good productivity of the protein, could predict its exploitation as a sustainable BE.

The aggregation process of Sap-*Pc* was also studied and the formation of amyloid-like fibrils in suitable conditions was observed, varying protein concentrations and time. Formation of micelles should be on-pathway with respect to fibril formation, which seems originated by an array of interacting aggregates.

Supplementary Materials: Supplementary materials can be found at http://www.mdpi.com/1422-0067/20/13/3242/s1.

Author Contributions: Investigation, P.C., I.S., G.P., P.D., and A.D.C.; validation, L.B., L.D.S., and D.M.M; writing—original draft preparation, P.C.; writing—review and editing, P.G.; supervision, P.G. and G.D.

Funding: This work was supported by a grant from the University Federico II "Progetto di Ateneo IENA (Immobilization of ENzymes on hydrophobin-functionalized NAnomaterials)".

Acknowledgments: The authors thank Eugenio Notomista at the Department of Biology, University of Naples, Federico II, for helpful discussion, and Giovanna Cristina Varese, Department of Life Sciences and Systems Biology, University of Turin, Italy, for selecting and supplying the *P. chrysogenum* strain.

Conflicts of Interest: The authors declare no conflict of interest.

Abbreviations

AFM	Atomic force microscopy
BE	Bioemulsifier
BS	Biosurfactant
cac	Critical aggregation concentration
CD	Circular dichroism
cmc	Critical micellar concentration
DLS	Dynamic light scattering
E24	Emulsification index
FTIR	Fourier transform infrared spectroscopy
HPB	Hydrophobin
LC–MSMS	Liquid chromatography tandem mass spectrometry
MALDI–TOF	Matrix assisted laser desorption ionization–time of flight
SDS–PAGE	Sodium dodecyl sulphate polyacrylamide gel electrophoresis
TCA	Trichloroacetic acid
ThT	Thioflavin T
TLC	Thin layer chromatography

References

1. McClements, D.J.; Gumus, C.E. Natural emulsifiers—Biosurfactants, phospholipids, biopolymers, and colloidal particles: Molecular and physicochemical basis of functional performance. *Adv. Colloid Interface Sci.* **2016**, *234*, 3–26. [CrossRef] [PubMed]
2. Shete, A.M.; Wadhawa, G.; Banat, I.M.; Chopade, B.A. Mapping of patents on bioemulsifier and biosurfactant: A review. *J. Sci. Ind. Res.* **2006**, *65*, 91–115.
3. Araújo, H.W.C.; Andrade, R.F.S.; Montero-Rodríguez, D.; Rubio-Ribeaux, D.; Alves da Silva, C.A.; Campos-Takaki, G.M. Sustainable biosurfactant produced by Serratia marcescens UCP 1549 and its suitability for agricultural and marine bioremediation applications. *Microb. Cell Fact.* **2019**, *18*, 2. [CrossRef] [PubMed]

4. Santos, D.; Rufino, R.; Luna, J.; Santos, V.; Sarubbo, L. Biosurfactants: Multifunctional Biomolecules of the 21st Century. *Int. J. Mol. Sci.* **2016**, *17*, 401. [CrossRef] [PubMed]
5. Pacwa-Plociniczak, M.; Plaza, G.A.; Piotrowska-Seget, Z.; Cameotra, S.S. Environmental Applications of Biosurfactants: Recent Advances. *Int. J. Mol. Sci.* **2011**, *12*, 633–654. [CrossRef] [PubMed]
6. Vecino, X.; Cruz, J.M.; Moldes, A.B.; Rodrigues, L.R. Biosurfactants in cosmetic formulations: trends and challenges. *Crit. Rev. Biotechnol.* **2017**, *37*, 911–923. [CrossRef]
7. Satpute, S.K.; Banpurkar, A.G.; Dhakephalkar, P.K.; Banat, I.M.; Chopade, B.A. Methods for investigating biosurfactants and bioemulsifiers: A review. *Crit. Rev. Biotechnol.* **2010**, *30*, 127–144. [CrossRef]
8. Uzoigwe, C.; Burgess, J.G.; Ennis, C.J.; Rahman, P.K.S.M. Bioemulsifiers are not biosurfactants and require different screening approaches. *Front. Microbiol.* **2015**, *6*, 245. [CrossRef]
9. Satpute, S.K.; Banat, I.M.; Dhakephalkar, P.K.; Banpurkar, A.G.; Chopade, B.A. Biosurfactants, bioemulsifiers and exopolysaccharides from marine microorganisms. *Biotechnol. Adv.* **2010**, *28*, 436–450. [CrossRef]
10. Harayama, S.; Kishira, H.; Kasai, Y.; Shutsubo, K. Petroleum biodegradation in marine environments. *J. Mol. Microbiol. Biotechnol.* **1999**, *1*, 63–70.
11. Michel, J.P.; Rosales, A. Marine Bioremediation—A Sustainable Biotechnology of Petroleum Hydrocarbons Biodegradation in Coastal and Marine Environments. *J. Bioremediation Biodegrad.* **2015**, *6*, 1–6. [CrossRef]
12. Raghukumar, C. Marine fungal biotechnology: An ecological perspective. *Fungal Divers.* **2008**, *31*, 19–35.
13. Imhoff, J.; Imhoff, F.J. Natural Products from Marine Fungi—Still an Underrepresented Resource. *Mar. Drugs* **2016**, *14*, 19. [CrossRef] [PubMed]
14. Bhardwaj, G.; Cameotra, S.S.; Chopra, H.K. Biosurfactants from Fungi: A Review. *J. Pet. Environ. Biotechnol.* **2013**, *4*, 1–6. [CrossRef]
15. Bovio, E.; Gnavi, G.; Prigione, V.; Spina, F.; Denaro, R.; Yakimov, M.; Calogero, R.; Crisafi, F.; Varese, G.C. The culturable mycobiota of a Mediterranean marine site after an oil spill: Isolation, identification and potential application in bioremediation. *Sci. Total Environ.* **2017**, *576*, 310–318. [CrossRef] [PubMed]
16. Gudiña, E.; Teixeira, J.; Rodrigues, L.; Gudiña, E.J.; Teixeira, J.A.; Rodrigues, L.R. Biosurfactants Produced by Marine Microorganisms with Therapeutic Applications. *Mar. Drugs* **2016**, *14*, 38. [CrossRef]
17. Bayry, J.; Aimanianda, V.; Guijarro, J.I.; Sunde, M.; Latgé, J.P. Hydrophobins-unique fungal proteins. *PLoS Pathog.* **2012**, *8*, e1002700. [CrossRef]
18. Berger, B.W.; Sallada, N.D. Hydrophobins: Multifunctional biosurfactants for interface engineering. *J. Biol. Eng.* **2019**, *13*, 10. [CrossRef]
19. Cox, P.W.; Hooley, P. Hydrophobins: New prospects for biotechnology. *Fungal Biol. Rev.* **2009**, *23*, 40–47. [CrossRef]
20. Khalesi, M.; Gebruers, K.; Derdelinckx, G. Recent Advances in Fungal Hydrophobin Towards Using in Industry. *Protein J.* **2015**, *34*, 243–255. [CrossRef]
21. Ren, Q.; Kwan, A.H.; Sunde, M. Two forms and two faces, multiple states and multiple uses: Properties and applications of the self-assembling fungal hydrophobins. *Biopolymers* **2013**, *100*, 601–612. [CrossRef] [PubMed]
22. Cicatiello, P.; Gravagnuolo, A.M.; Gnavi, G.; Varese, G.C.; Giardina, P. Marine fungi as source of new hydrophobins. *Int. J. Biol. Macromol.* **2016**, *92*, 1229–1233. [CrossRef] [PubMed]
23. Cicatiello, P.; Dardano, P.; Pirozzi, M.; Gravagnuolo, A.M.; De Stefano, L.; Giardina, P. Self-assembly of two hydrophobins from marine fungi affected by interaction with surfaces. *Biotechnol. Bioeng.* **2017**, *10*, 2173–2186. [CrossRef] [PubMed]
24. Kohlmeyer, J.; Kohlmeyer, E. *Marine Mycology: The Higher Fungi*; Academic Press: New York, NY, USA, 1979.
25. Huang, J.; Lu, C.; Qian, X.; Huang, Y.; Zheng, Z.; Shen, Y. Effect of salinity on the growth, biological activity and secondary metabolites of some marine fungi. *Acta Oceanol. Sin.* **2011**, *30*, 118–123. [CrossRef]
26. Blesic, M.; Dichiarante, V.; Milani, R.; Linder, M.; Metrangolo, P. Conference paper Evaluating the potential of natural surfactants in the petroleum industry: The case of hydrophobins. *Pure Appl. Chem.* **2018**, *90*, 305–314. [CrossRef]
27. Askolin, S.; Linder, M.; Scholtmeijer, K.; Tenkanen, M.; Penttilä, M.; de Vocht, M.L.A.; Wösten, H.A.B. Interaction and Comparison of a Class I Hydrophobin from Schizophyllum commune and Class II Hydrophobins from Trichoderma reesei. *Biomacromolecules* **2006**, *7*, 1295–1301. [CrossRef] [PubMed]
28. Szilvay, G.R.; Kisko, K.; Serimaa, R.; Linder, M.B. The relation between solution association and surface activity of the hydrophobin HFBI from *Trichoderma reesei*. *FEBS Lett.* **2007**, *581*, 2721–2726. [CrossRef]

29. Arosio, P.; Knowles, T.P.J.; Linse, S. On the lag phase in amyloid fibril formation. *Phys. Chem. Chem. Phys.* **2015**, *17*, 7606–7618. [CrossRef]
30. Fung, S.Y.; Keyes, C.; Duhamel, J.; Chen, P. Concentration effect on the aggregation of a self-assembling oligopeptide. *Biophys. J.* **2003**, *85*, 537–548. [CrossRef]
31. Novo, M.; Freire, S.; Al-Soufi, W. Critical aggregation concentration for the formation of early Amyloid-β (1–42) oligomers. *Sci. Rep.* **2018**, *8*, 1783. [CrossRef]
32. Kroes-Nijboer, A.; Venema, P.; Bouman, J.; van der Linden, E. The Critical Aggregation Concentration of β-Lactoglobulin-Based Fibril Formation. *Food Biophys.* **2009**, *4*, 59–63. [CrossRef]
33. Parmar, A.S.; Muschol, M. Hydration and hydrodynamic interactions of lysozyme: effects of chaotropic versus kosmotropic ions. *Biophys. J.* **2009**, *97*, 590–598. [CrossRef] [PubMed]
34. Menger, F.M.; Rizvi, S.A.A. Relationship between Surface Tension and Surface Coverage. *Langmuir* **2011**, *27*, 13975–13977. [CrossRef] [PubMed]
35. Yong, W.; Lomakin, A.; Kirkitadze, M.D.; Teplow, D.B.; Chen, S.-H.; Benedek, G.B. Structure determination of micelle-like intermediates in amyloid beta -protein fibril assembly by using small angle neutron scattering. *Proc. Natl. Acad. Sci. USA* **2002**, *99*, 150–154. [CrossRef] [PubMed]
36. Dear, A.J.; Šarić, A.; Michaels, T.C.T.; Dobson, C.M.; Knowles, T.P.J. Statistical Mechanics of Globular Oligomer Formation by Protein Molecules. *J. Phys. Chem. B* **2018**, *122*, 11721–11730. [CrossRef] [PubMed]
37. Itri, F.; Monti, D.M.; Della Ventura, B.; Vinciguerra, R.; Chino, M.; Gesuele, F.; Lombardi, A.; Velotta, R.; Altucci, C.; Birolo, L.; et al. Femtosecond UV-laser pulses to unveil protein–protein interactions in living cells. *Cell. Mol. Life Sci.* **2016**, *73*, 637–648. [CrossRef]
38. Oliviero, G.; D'Errico, S.; Pinto, B.; Nici, F.; Dardano, P.; Rea, I.; De Stefano, L.; Mayol, L.; Piccialli, G.; Borbone, N. Self-Assembly of G-Rich Oligonucleotides Incorporating a 3′-3′ Inversion of Polarity Site: A New Route Towards G-Wire DNA Nanostructures. *ChemistryOpen* **2017**, *6*, 599–605. [CrossRef]
39. Russo Krauss, I.; Imperatore, R.; De Santis, A.; Luchini, A.; Paduano, L.; D'Errico, G. Structure and dynamics of cetyltrimethylammonium chloride-sodium dodecylsulfate (CTAC-SDS) catanionic vesicles: High-value nano-vehicles from low-cost surfactants. *J. Colloid Interface Sci.* **2017**, *501*, 112–122. [CrossRef]
40. Arciello, A.; De Marco, N.; Del Giudice, R.; Guglielmi, F.; Pucci, P.; Relini, A.; Monti, D.M.; Piccoli, R. Insights into the fate of the N-terminal amyloidogenic polypeptide of ApoA-I in cultured target cells. *J. Cell. Mol. Med.* **2011**, *15*, 2652–2663. [CrossRef]

2.2 The growth of marine fungi on seaweed polysaccharides produces cerato-platanin and hydrophobin self-assembling proteins

Microbiological Research 251 (2021) 126835

Contents lists available at ScienceDirect

Microbiological Research

journal homepage: www.elsevier.com/locate/micres

The growth of marine fungi on seaweed polysaccharides produces cerato-platanin and hydrophobin self-assembling proteins

Catalina Landeta-Salgado [a,b], Paola Cicatiello [c], Ilaria Stanzione [c], David Medina [a,b], Isadora Berlanga Mora [a], Carlos Gomez [d], María Elena Lienqueo [a,b,*]

[a] Department of Chemical Engineering, Biotechnology, and Materials, Faculty of Physical and Mathematical Sciences, University of Chile, Santiago, Beauchef 851, 8370456, Chile
[b] Center for Biotechnology and Bioengineering (CeBiB), Santiago, Beauchef 851, 8370456, Chile
[c] Department of Chemical Sciences, University of Naples Federico II, via Cintia 4, I-80126 Naples, Italy
[d] Chemistry Department, University of Valle-Yumbo, Valle del Cauca, 760501, Colombia

ARTICLE INFO

Keywords:
Cerato-platanin
Hydrophobin
Protein aggregation
Self-assembly
Seaweed

ABSTRACT

The marine fungi *Paradendryphiela salina* and *Talaromyces pinophilus* degrade and assimilate complex substrates from plants and seaweed. Additionally, these fungi secrete surface-active proteins, identified as cerato-platanins and hydrophobins. These hydrophobic proteins have the ability to self-assemble forming amyloid-like aggregates and play an essential role in the growth and development of the filamentous fungi. It is the first time that one cerato-platanin (CP) is identified and isolated from *P. salina* (PsCP) and two Class I hydrophobins (HFBs) from *T. pinophilus* (TpHYD1 and TpHYD2). Furthermore, it is possible to extract cerato-platanins and hydrophobins using marine fungi that can feed on seaweed biomass, and through a submerged liquid fermentation process. The propensity to aggregate of these proteins has been analyzed using different techniques such as Thioflavin T fluorescence assay, Fourier-transform Infrared Spectroscopy, and Atomic Force Microscopy. Here, we show that the formation of aggregates of PsCP and TpHYD, was influenced by the carbon source from seaweed. This study highlighted the potential of these self-assembling proteins generated from a fermentation process with marine fungi and with promising properties such as conformational plasticity with extensive applications in biotechnology, pharmacy, nanotechnology, and biomedicine.

1. Introduction

Marine fungus associated with macroalgae is an ecologically important group (Patyshakuliyeva et al., 2020; Yanming Wang et al., 2016), that has a significant potential for different applications, such as antifouling and antibacterial (Bao et al., 2013), anticancer (Arumugam et al., 2015; Bao et al., 2013; He et al., 2016), antioxidant (El-Hady et al., 2015), and lipid-lowering (Wu et al., 2014) activities. The marine macroalgae or seaweed are eukaryotic and photosynthetic organisms, which are distributed worldwide in the coasts and oceans (Charoensiddhi et al., 2017; Rindi et al., 2012). The use of marine fungi for plant and algae biotransformation has been successfully exploited in several fields, such as for the production of low-cost edible proteins, enzymes, biochemical, wastewater treatments, among others (Balabanova et al., 2018; Beena et al., 2011; Harms et al., 2011; Van et al., 2011).

Several studies (Landeta-Salgado et al., 2021; Landeta et al., 2021; Pilgaard et al., 2019; Wang et al., 2016) have been carried out in *Paradendryphiella salina* and *Talaromyces pinophilus* like marine fungi with the capacity to assimilate complex carbohydrates of seaweed. *Dendryphiella salina* is placed in the new genus *Paradendryphiella* (Woudenberg et al., 2013). It belongs to the ascomycete group of filamentous types isolated from marine environments (Woudenberg et al., 2013). *P. salina* has shown high efficiency for the production of an

Abbreviations: CPs, cerato-platanins; HFBs, hydrophobins; PsCP, cerato-platanin of *Paradendryphiella salina*; TpHYD1 and TpHYD2, hydrophobins of *Talaromyces pinophilus*; CMSWA, Cornmeal Seawater Agar; TFA, trifluoroacetic acid; FT-IR, Fourier transform infrared spectroscopy; ThT, Thioflavin T; AFM, atomic force microscopy; SLF, submerged liquid fermentation; PETase, polyethylene terephthalate hydrolase; PET, polyethylene terephthalate.

* Corresponding author at: Department of Chemical Engineering, Biotechnology, and Materials, Faculty of Physical and Mathematical Sciences, University of Chile, Santiago, Beauchef 851, 8370456, Chile.
E-mail addresses: mlienque@uchile.cl, mlienque@cebib.cl (M.E. Lienqueo).

https://doi.org/10.1016/j.micres.2021.126835
Received 2 February 2021; Received in revised form 8 July 2021; Accepted 28 July 2021
Available online 5 August 2021

alginate and brown seaweed degrading enzyme system (Dela Cruz et al., 2006; Edwards et al., 1998; Galpin and Jennings, 1975; Wainwright and Sherbrock-Cox, 1981; Pilgaard et al., 2019; Schaumann and Weide, 1995). The filamentous fungus *Talaromyces pinophilus*, previously known as *Penicilium pinophilum* (Benjiamin, 1955; Houbraken and Samson, 2017) is a fungus with potential to produce high activity enzymes (chitinase, lipase, protease, cellulase and β-glucosidase) (Abdel-Rahim and Abo-Elyousr, 2018; Liu et al., 2020) to transform and degrade the polymeric compounds of green algae.

There are filamentous fungi, regardless of lifestyle, that can secrete surface-active proteins such as hydrophobins (HFBs), along with the carbohydrate-binding proteins known as cerato-platanin (CPs). They are secreted by fungi to control surface activity and substrate: air interface properties. In addition, HFBs have been shown to coat air structures as they emerge from the mycelium and confer water resistance (Sunde et al., 2017). HFB protein sequences are characterized by eight cysteine residues that form four disulfide bonds, beyond which there is a low degree of sequence conservation. The members are further classified as Class I or Class II based on the space between the cysteines, the hydrophobic plots and physical characteristics such as the stability of the assembled layers (Sunde et al., 2017, 2008). HFBs have ability to self-assemble into biocompatible amphipathic and robust layers or films that play different roles in the stages of the life cycle in fungal. These layers can reversibly disassemble and reverse the wettability of a surface (Linder et al., 2005; Sunde et al., 2008; Wösten and De Vocht, 2000; Wösten and Scholtmeijer, 2015), making them available for various applications such as nanodevices, biosensors, materials surface modification (Bleem and Daggett, 2017; Scholtmeijer et al., 2002) immobilization of proteins (Corvis et al., 2005) polymer surface modification (Misra et al., 2006) formulation of water-insoluble drugs, stabilization of emulsions for encapsulation (Haas Jimoh Akanbi et al., 2010; Singh et al., 2018), and can help to increase the biocompatibility of medical implants (Scholtmeijer et al., 2004).

The CP family consists of small, surface-active proteins that possess the ability to bind carbohydrates such as cellulose and promote the activity of fungal cellulase in a similar way to expansin proteins, they are able to weaken cellulose substrates, disrupting its non-covalent bonds without any hydrolytic activity (De Oliveira et al., 2011; Gaderer et al., 2014; Quarantin et al., 2019; Yiming Wang et al., 2016). CPs are not related to HFBs with respect to their sequence, but share some structural and functional characteristics: hydrophobicity, low molecular mass, secreted proteins that are released into the culture filtrate, and have been found within the cell wall of fungal hyphae and spores, stabilize emulsions and forms ordered aggregated layers at hydrophobic/hydrophilic interfaces (Boddi et al., 2004; Bonazza et al., 2015; Pazzagli et al., 2009; Pitocchi et al., 2020). Additionally, other studies have been carried out that revealed that a CP from *Trichoderma* spp. could form aggregates from dimers (Seidl et al., 2006; Vargas et al., 2008), EPL1 forms protein biofilms at air/water interfaces (Frischmann et al., 2013), and other CPs from *Aspergillus terreus* and *Trichoderma harzianum* have been evaluated as biosurfactants and emulsifiers (Pitocchi et al., 2020).

There are several studies on the self-assembly mechanism and morphology of Class I hydrophobin assemblies. Studies of SC3 from *Schizophyllum* showed that the C_3-C_4 loop is involved in the formation of an α-helical structure that drives the formation of rod structures, and the presence of hydrophilic/hydrophobic interfaces influences the self-assembly of SC3 (Wang et al., 2005). Other studies on EAS from *Neurospora crassa* showed that the C_7-C_8 loop of EAS was involved in rod formation, studies of Vmh2 from *Pleurotus ostreatus* showed that assembly was regulated by protein concentration, pH, temperature and ionic strength of the medium (Gravagnuolo et al., 2016). Differences in the self-assembly mechanism exist between different Class I hydrophobins and are dependent on the microorganism and on the specific interface that interacts with the proteins. It is therefore proposed that the self-assembly mechanism is not regulated by a single component (Wang et al., 2017; Berger and Sallada, 2019). In the case of cerato-platanin assembly, studies are scarce. According to Pazzagli et al. (2009), CPs of *Ceratocystis platani* have a peculiar mechanism of aggregation different from HFBs. Soluble prefibrillar structures are formed that do not evolve into insoluble fibrils and assembly is influenced by protein concentration and interaction with a hydrophobic material. The importance of the study of protein assembly and formation of amyloid-type fibrils is linked to their potential use in the fabrication of films for the production of new biomaterials in the field of nanobiotechnology (Wetzel et al., 2007; Macindoe et al., 2011; Gravagnuolo et al., 2016). Therefore, discovering new hydrophobins and cerato-platanins from unstudied microorganisms and understanding the mechanism of self-assembly of these proteins is essential to realize the full potential of these proteins.

In this study, we isolated and identified for the first time the cerato-platanins from *P. salina* (named PsCP) and Class I hydrophobins from *T. pinophilus* (named TpHYD1 and TpHYD2). Moreover, this study is the first to report the production of hydrophobins and cerato-platanins through submerged liquid fermentation and using as a sole carbon source *Ulva* spp., seaweed wastes from brown algae or algae's polysaccharides. We partially characterized the capacity to form PsCP and TpHYD aggregates, underlining the similarities and differences of these proteins concerning their self-assembly and promoted by the carbon source from seaweed.

2. Materials and methods

2.1. Raw material

Ulva spp. was harvested on the coast from submerged marine rocks located in the city of Puerto Montt in the South of Chile. The algae were pulverized by a knife mill basic analytical mill A11 (IKA, USA). The seaweed waste was donated by an industry that produces biostimulants and biofertilizers. It uses brown seaweed as raw material. The pH of this waste is 3.71, and it is necessary to pretreat it. This pretreatment consists of ultrasound, followed by thermo-alkaline pretreatment, according to previously reported methodology (Karray et al., 2015). Briefly, wastes were added to a NaOH solution (5 N) at a concentration of 18 % wt. (wet weight). This solution with wastes was subject to mechanical disruption using ultrasound by sonication with sonicator Q500 (QSONICA, USA), duty cycle 40 %, a constant frequency of 40 kHz in the cold (4 C) for 10 min. This homogenized material was then treated at 121 C for 20 min.

2.2. Marine fungus

The marine fungi *Paradendryphiela salina* 100654 belonging to the collection of fungi of the Biological Resources Center of the National Institute of Evaluation and Technology (NBRC Japan; https://www.nite.go.jp/en/nbrc/index.html), and *Talaromyces pinophilus LF458* belonging to the culture collection of the Kiel Center for marine natural products at GEOMAR, were used. They were propagated on plates of Cornmeal Seawater Agar (CMSWA)[1] medium at 28 °C and maintained at 4 °C. The pre-inoculum was obtained for submerged fermentation by transferring 1 cm^2 of mycelium from Petri dishes (200 mm diameter) to sterile medium minimal (50 mL), supplemented with Yeast extract (5 g/L), and alginate (2 g/L Alginic acid sodium salt from brown algae, Sigma-Aldrich) as sole carbon source (Yanming Wang et al., 2016), and incubation at 25 ± 1 °C for 4 days, and with agitation (200 rpm).

2.3. Fungal growth

P. salina and *T. pinophilus* were maintained through periodic transfer

[1] https://www.nite.go.jp/nbrc/catalogue/NBRCMediumDetailServlet?NO=16

on CMSWA plate at 25 °C. The pre-inoculum was obtained for submerged fermentation by transferring 1 cm^2 of mycelium from Petri dishes (200 mm diameter) to sterile medium minimal base (50 mL) (Yanming Wang et al., 2016), using alginate (2 g/L Alginic acid sodium salt from brown algae, Sigma-Aldrich) as carbon source, supplemented with yeast nitrogen base (5 g/L), and incubated at 25 ± 1 °C for 4 days. The pH of the process was 5.5. Pre-inoculum (50 mL) of *P. salina* and *T. pinophilus* was inoculated in different 1 L flask containing sterile minimal medium base (500 mL) with alginate (2 g/L Alginic acid sodium salt from brown algae, Sigma-Aldrich) as carbon source. Additionally, the pre-inoculum of *P. salina* was inoculated in 1 L flasks containing sterile minimal medium (500 mL) with the seaweed waste as carbon source (Landeta et al., 2021). Also, the pre-inoculum (50 mL) of T. *pinophilus was* inoculated in a 1 L flask containing a different medium minimal (500 mL) (Penttilä et al., 1987) using *Ulva* spp. (25 g/L) as carbon source. Flask was incubated in the dark at 25 °C in an orbital shaker at 250 rpm for 8 days.

2.4. Purification of proteins

After fermentation, it is necessary to separate the mycelium from culture broth by filtration through Miracloth (Millipore Sigma, USA), to remove spores and mycelial residues prior to further purification steps. Proteins were extracted from culture broth according to the previously reported methodology (Cicatiello et al., 2017). Proteins were aggregated by air bubbling, using an Oster blender. The foam was collected and was centrifuged for 1 h at 3.300 *g* at 4 °C. In order to extract Class I HFBs, the precipitate was treated with 100 % Trifluoroacetic acid (TFA) in a bath sonicator, dried using a stream of nitrogen, and then dissolved in a 60 % ethanol solution. The raw extract in 60 % ethanol solution was dried and the lipids were extracted in a mixture of methanol–chloroform 2:1 v/v (30 min 60 °C). After centrifugation, the protein appeared as a solid aggregate at the bottom. It was recovered by removal of the liquid phase. The aggregated protein was dried, treated with TFA for 5 min in a bath sonicator, dried again, dissolved in 60 % ethanol, and centrifuged (90 min at 12,000 *g*). The supernatant was dried, treated with TFA, as described above, and dissolved in the appropriate solutions (Cicatiello et al., 2017). On the other hand, CP was extracted as described elsewhere (Seidl et al., 2006). The precipitate containing the CP was processed in an Amicon Ultra 2 mL 30 K (Millipore, USA) Centrifugal Filter Units with a 3 kDa cut-off disc and dialyzed with distilled water. The ultrafiltrate with low molecular weight proteins (>30 kDa), was concentrated according to the manufacturer's instructions.

Protein concentration was estimated by measuring absorbance at 280 nm using Nano-drop Spectrophotometer (MaestroNaNo, USA) (Desjardins et al., 2010). Then, these proteins were freeze-dried by lyophilization with MicroModulyo 230 (Thermo Savant, USA). Protein extracted and purified from culture broth was analyzed by SDS-PAGE (15 % acrylamide) (Laemmli, 1970). Proteins were stained using a silver staining method (Heukeshoven and Dernick, 1985).

2.5. Protein Identification by bioinformatics analysis

Paradendryphiella salina 100654 genome and transcriptome sequencing and assembly were made by the research group of Microbiology at Utrecht University. The *Talaromyces pinophilus* genome was downloaded from NCBI (Pruitt et al., 2007). For both genomes, protein sequences were extracted using AUGUSTUS (2.7) software (Stanke et al., 2004). Hydrophobin proteins were identified using the conserved cysteine motifs previously reported (Littlejohn et al., 2012). On the other hand, recognition of the cerato-platanin proteins was carried out through sequence alignments using the Protein Blast tool and psi-Blast algorithm with default configuration parameters (Altschul et al., 1997), and employing the Non-redundant database (NR). The candidate sequences were selected considering a conservation percentage higher than 60 % and an e-value less than 0.01. Finally, all candidates were evaluated using the Protein Families Pfam database (Bateman, 2004). Phylogenetic analyzes were developed using the identified sequences, and the different proteins previously reported to exist in other organisms and presenting similar characteristics according to the sequence alignments created formerly. First, multiple sequence alignments were generated using the Muscle algorithm. After that, Maximum likelihood analyzes were used to construct phylogenetic trees, considering the Bootstrap method with 10,000 replications for test the phylogeny, the WAG model as substitution model strategy, and the rest of the parameters with the default configuration. All phylogenetic analyzes were performed using MegaX software (Kumar et al., 2018).

From these sequences, secondary structure content of PsCP, TpHYD1 and TpHYD2 was estimated using the RaptorX program (Torchala and Bates, 2014). The secondary structure of TPHYD1 was estimated using as template the structure with ID PDB 6GCJ, and for the sequence TPHYD2 and PsCP the program used as a template the structure identified as ID PDB 2NBH and ID PDB 3SUK respectively. For the prediction of regions capable of forming aggregations, several algorithms are available. These algorithms allow prediction from the primary sequence and suggest which areas have a high tendency to form amyloid-type and beta-sheet structures (Bemporad and Ramazzotti, 2017). The sequences were analyzed using the ZipperDB algorithm (Goldschmidt et al., 2010; Stanislawski et al., 2013) which has the advantage of using structural information to assess the probability that the primary sequence analyzed can form these aggregations.

2.6. Protein characterization

2.6.1. Fourier transform infrared spectroscopy – FTIR – analysis

Lyophilized proteins were dissolved in 50 mM Tris HCl buffer pH 7 at concentrations of 20 μg/mL. FT-IR spectra of protein solutions were recorded using a FTIR spectrometer Nicolet iS50 (Thermo Scientific, USA) equipped with a Mercuric Cadmium Telluride detector (MCT) and a Thermo Scientific OMNI-Transmission cell. The FTIR spectra were measured at room temperature, and the spectra were acquired at wavenumbers of 400–4000 cm^{-1} in 32 scans with a resolution of 4 cm^{-1}. For FT-IR measurements, 20 μL samples were placed on the surface of the aluminium foil discs, which have a radius of 5 mm (previously dried by evaporation at room temperature overnight) and then placed on the sample chamber.

2.6.2. Thioflavin T (ThT) staining

The self-aggregation of extracted proteins was followed by fluorescence spectroscopy using Thioflavin T (ThT) according to literature (LeVine, 1999). ThT assays were performed with 50 μg/mL cerato-platanin (PsCP) and 40 μM ThT in aqueous buffers at pH 7.0 (50 mM Tris HCL). ThT assays were performed in the same way for hydrophobins (TpHYD1, TpHYD2), with 50 μg/mL at pH 7.0 (Cicatiello et al., 2017; Lo et al., 2014). The assay was performed at room temperature on a fluorescence spectrophotometer Infinite 200 PRO (TECAN, USA) with a 440−10 nm excitation filter and a wavelength range 450–600 nm filter for emission detection (with slit widths set at 10 nm). ThT assays were performed on samples vortexed for 2 min and orbital stirred for 5 min.

2.6.3. Atomic force microscopy (AFM) measurements

Freeze-dried CPs and HFBs were suspending in aqueous buffer 50 mM Tris HCl (pH 7) or ethanol at a concentration of 20–200 μg/mL. This solution was agitated using a vortex set on high for 5 min. Two microliters of the samples dissolved in the buffer solutions (agitated by vortex 30 s) were: i) directly deposited on freshly cleaved mica or (ii) diluted 1:10 1:100 or 1:1000 in water and 20 μL deposited by casting onto a freshly cleaved mica. All the samples were dried by evaporation at room temperature overnight with protection from dust and allowed to dry completely in the static state before imaging. For each sample we prepared control samples with protein-free solutions according to the following procedure: aqueous buffer (pH 7) or ethanol were agitated

using a vortex set on high for 5 min. The samples were diluted 1:10, 1:100 and 1:1000 in Milli-Q water or ethanol. The diluted solutions were agitated by vortex for 30 s and immediately a drop of 20 µL was deposited by casting onto a freshly cleaved mica. All control samples were dried by evaporation at room temperature with protection from dust and allowed to dry completely. In these experiments, the surface roughness height was registered below 0.9 nm.

The morphology of the CPs and HFBs films was characterized with a WITec Alpha 300 RA (WITec, Germany) in AC mode at ambient conditions. The cantilever used was WITec AFM arrow cantilever reflex-coated with a FM, 2.8 N/m spring constant, 75 kHz frequency tip. AFM images were also performed using NT-MDT NTEGRA PRIMA SPM, in semi-contact mode using a FMG01 NT-MDT cantilever. Analysis of the AFM images was performed using the WSxM program (Horcas et al., 2007).

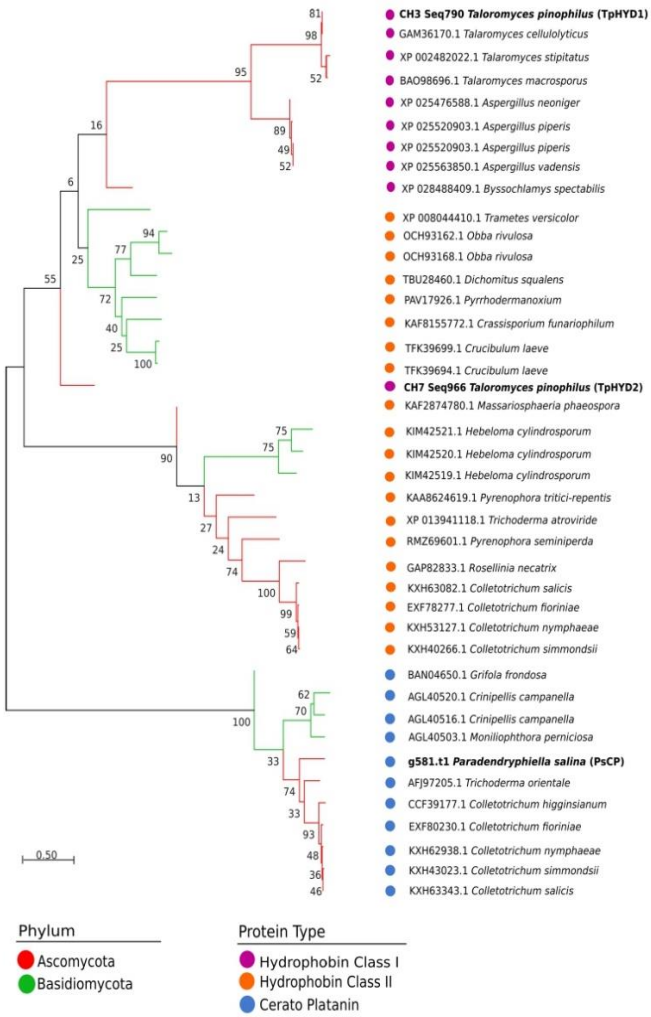

Fig. 1. Phylogenetic analysis of Class I hydrophobin and cerato-platanin proteins. The proposed sequences are highlighted in bold, and the phylum and protein types are divided by colours. Conservation levels based on bootstrap processing are expressed in percentages, where 90 % indicates that of the 10,000 iterations, 9000 of them, the cluster was maintained.

3. Results and discussion

3.1. Protein Identification

Two protein sequences in *T. pinophilus* were successfully identified as putative Class I hydrophobins (named TpHYD1 and TpHYD2), whereas in *P. salina* one sequence was classified as putative cerato-platanin (named PsCP) (Table S1).

Phylogenetic analysis of the protein sequences identified in the organisms of interest presents phylogenetically significant differences between them (Fig. 1). An important point to highlight is the division generated from the analyzed phylum. Both proteins belonging to Ascomycota are in different clusters from the proteins belonging to the Basidiomycota phylum. In other words, not only are proteins clustered by type but also by phylum. In this way, it is possible to infer that they present different behaviors or properties, which causes a divergence between them and gives common ancestors, which can be seen in the processing via Bootstrap. It is important to note that the TpHYD2 sequence classified as Class I hydrophobin has a close evolutionary relationship with Class II hydrophobins. This turns out to be quite interesting because it is correlated with previous reports showing the existence of mixed behaviors of proteins with intermediate characteristics between Class I and Class II. Thus, it is considered necessary to develop clustering and pattern identification systems through data mining or natural language processing techniques for all the hydrophobin sequences reported in the literature to recognize the characteristics that present an evolutionary relationship and correlate them with both linear and structural patterns and estimate the functional relevance of these differences.

Proteins classified as putative hydrophobins show significant differences concerning cerato-platanin, which is demonstrated in a clear subdivision of the sets of sequences in the phylogenetic tree and in the secondary structure estimate (Figs. 1 and 2). In turn, despite the existence of the conserved cysteine motif, that is characteristic of this kind of protein, a division between hydrophobin Class I and Class II sequences is generated, highlighting that the inter-cysteine space is different (Littlejohn et al., 2012). This is consistent with the cysteine spacing pattern of Class I HFBs that is CX(6)CCX(9–39)CX(5–25)CX(5)CCX(8–17)C (Seidl-Seiboth et al., 2011; Wösten and Wessels, 1997). Fig. 2B shows the disulfide bridges characteristic of putative hydrophobins Class I TpHYD1 and TpHYD2 from *T. pinophilus*. These disulfide bridges are connecting these cysteines and span C1–C6, C2–C5, C3–C4, and C7–C8 (Linder et al., 2005). In contrast, the analysis of the amino acid sequences of the putative cerato-platanin of *P. salina* (PsCP) shows that, in this protein family, the general cysteine spacing pattern is C(38)CXXC (54)C (Fig. 2B). Indeed, the CXXC motif in this pattern contains C–G–S/T–C. The disulfide bridges that connect the cysteines in CPs are shown in Fig. 2B (C1-C2 and C3-C4). This is in complete agreement with the literature (Barsottini et al., 2013; De Oliveira et al., 2011). The secondary structures estimated for TpHYD1 and TpHYD2 (Fig. 2A) are consistent with the shared HFB fold in all hydrophobins, which comprises a small β-barrel core structure decorated by ordered and disordered loop regions (Ren et al., 2013) while the structure of PsCP (Fig. 2A) reveals a globular fold containing two α-helices and six β-strands that form a six-stranded double ψβ-barrel characteristic of CPs (De Oliveira et al., 2011).

3.2. Fungal Growth and isolation of secreted proteins

This study was performed to exploit the capability of marine fungi, using seaweed biomass as carbon of source, to produce surface-active proteins (Fig. 3). Recent studies have highlighted the capability of some fungi to grow on complex media also producing interesting proteins. In particular, Pilgaard and co-authors showed the ability of *Paradendryphiella salina* to assimilate alginate from brown algae (Pilgaard et al., 2019) whilst Liu and co-authors focused their attention on the production of cellulase, with a high β-glucosidase activity, from *Talaromyces pinophilus* suggesting its ability to assimilate the

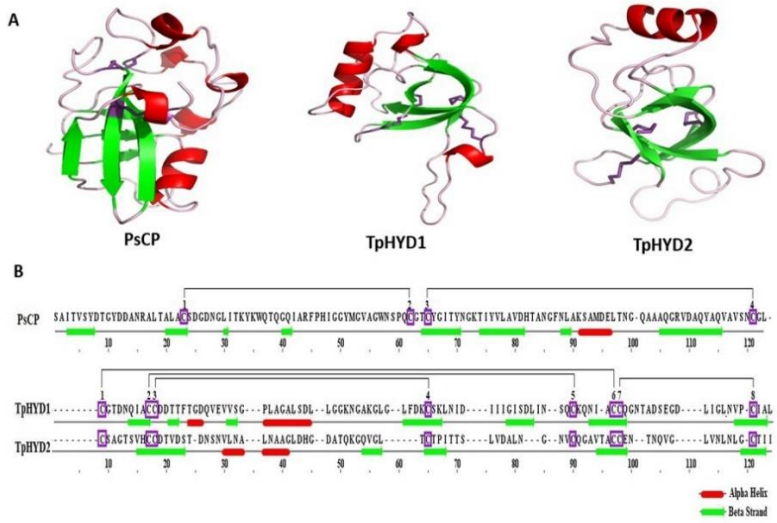

Fig. 2. (A) Modelled 3D structure of PsCP (cerato-platanin of *P. salina*), TpHYD1 and TpHYD2 (Class I hydrophobins of *T. pinophilus*) (cartoon representation with S—S bonds displayed in purple produced using Phyre2 software (Kelley et al., 2015). (B) Secondary structures of monomeric forms of the proteins studied, with alignment on cysteine residues. Cysteine residues position and disulfide bridges are displayed. β-Sheets are shown as green arrows and α-helices as red helix.

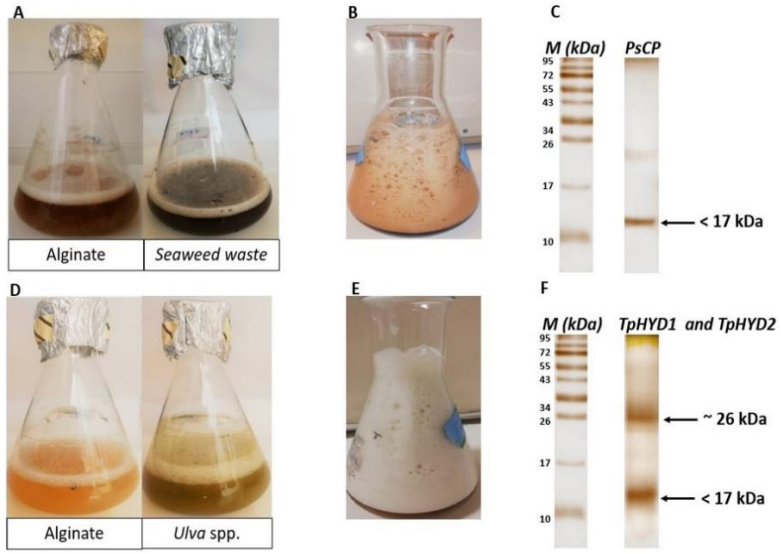

Fig. 3. (A) *Paradendryphiella salina* grown in the presence of alginate and seaweed waste as the sole carbon source. (B) Formation of strong foam in culture broth of *P. salina* with seaweed waste upon filtration and air bubbling. (C) SDS-PAGE of PsCP (cerato-platanin) isolated from foam with alginate of *P. salina*, M is the molecular weight marker (D) *Talaromyces pinophilus* grown in the presence of alginate and *Ulva* spp. as the sole carbon source. (E) Formation of strong foam in culture broth of *T. pinophilus* with *Ulva* spp. upon filtration and air bubbling. (F) SDS-PAGE of TpHYD1 and TpHYD2 (hydrophobins) isolated from foam with alginate of *T. pinophilus*, M is the molecular weight marker.

polysaccharide from green algae (Liu et al., 2020). Against this background, in this study we aimed to exploit the capability of *P. salina* and *T. pinophilus* to grow on seaweed biomasses and analyze their capacity to produce protein biosurfactants. In particular, *P. salina* and *T. pinophilus* were grown in submerged liquid fermentation (SLF) using as carbon source seaweed wastes (SW) and *Ulva* spp., respectively and alginate in both cases (Fig. 3A and D).

The biosurfactants proteins, exploiting their capacity to self-assemble at air water interfaces producing stable bubbles, were isolated via bubbling from culture broth. (Fig. 3B and E).

The amount of secreted proteins was evaluated. The PsCP production yield from the culture broth of *P. salina* with seaweed waste and alginate was of 18.44 ± 1.4 and 2.08 ± 0.4 mg/L, respectively. In the case of *T. pinophilus*, before proceeding with the analysis, a treatment with pure trifluoroacetic acid was necessary to solubilize the sample of isolated hydrophobins TpHYD1 and TpHYD2. The protein production yield from the culture broth of *T. pinophilus* with *Ulva* spp. and alginate was of 40.29 ± 2.3 and 27.68 ± 3.2 mg/L, respectively. At least three biological replicated were analyzed in each condition.

There are no studies analyzing the influence of the culture medium on the yield of hydrophobins and cerato-platanins. Nevertheless, studies on the analysis of the secretome of terrestrial fungi with lignocellulose degradation capacity have shown that in *P. ostreatus* cultures, hydrophobins and cerato-platanins are the most expressed proteins in the category of other proteins, after the main secreted protein families (redox enzymes, proteases, and glycoside hydrolases) (Alfaro et al., 2016, 2020). According to Alfaro et al. (2020), the secretion of enzymes involved in cellulose and hemicellulose degradation in *P. ostreatus* are induced by wood. Some hydrophobins are known to be related to fungal development (Wessels, 1992) and are also involved in hydrophobicity, and adhesion of hyphae on substrates on which endophytic (Kim et al., 2005) and entomopathogenic fungi feed (Aimanianda et al., 2009; Dagenais et al., 2010). According to Gao et al. (2020), cerato-platanins of *Trichoderma* contribute to the ability of fungi to modify the substrates on which they feed by making the surfaces more hydrophilic and more accessible for enzymes and subsequent nutrient acquisition. This function could be complementary to the function of hydrophobins. Thus, if fungal secretomes cluster according to fungal lifestyles, it could be hypothesized that secretion of hydrophobins and cerato-platanins in marine fungi is induced by the substrate they feed on in their marine environment. These proteins would encourage the binding of the fungus to the substrate and enhance the absorptive nutrition of the substrate, which in this case is seaweed. This phenomenon would explain our results on the higher yield of these surface-active proteins when seaweed is used as a carbon source. It is important to carry out secretome studies that can support this information.

Extracted HFBs and CPs proteins were analyzed with SDS-PAGE. (Fig. 3). The molecular weight of the extracted PsCP protein ranged between 10 and 17 kDa (Fig. 3C). Unfortunately, it was not possible to investigates these proteins from culture bubbling with seaweed waste by SDS-PAGE because of some compounds that interfere with the analysis. The extracted HFBs showed a molecular weight that ranged between 10 and 26 kDa (Fig. 3F). Similarly, the SDS-PAGE analysis of the extracted proteins from a culture medium with *Ulva* spp. was not possible.

These studies showed the capacity to extract self-assembling surface-active proteins from a co-product (culture broth) of naturally foaming marine fungi. This fungi *P. salina* and *T. pinophilus* are able to produce mycoprotein (biomass of fungi) from the SLF process and using seaweed biomass as carbon source (Landeta-Salgado et al., 2021; Landeta et al., 2021; Yanming Wang et al., 2016). These results suggest that it is possible to extract the proteins CPs and HFBs from the foam of culture broth. Thus, it is possible to take advantage of the properties that these

proteins have to self-assemble at the air/water interface and produce stable foams due to the concentration of these proteins (Frischmann et al., 2013; Linder et al., 2005; Lohrasbi-Nejad et al., 2016; Lonchamp et al., 2019).

3.3. Protein characterization

Fourier transform infrared spectroscopy – FTIR – analysis (Fig. 4A and B) shows the secondary structure of PsCP and TpHYD due to the shape and frequency of the amide I band. The structural transitions of these proteins induced by the growth of the fungi in seaweed biomass as sole carbon source was also investigated by FT-IR. We observed differences in the intensity and the shape of the bands (1625–1685 cm^{-1}) between PsCP and TpHYD, and between each protein from the different media (Fig. 4). This result showed that these proteins contained mainly β-sheet (1630–1640 cm^{-1}) and α-helical or random coil (~1660–1680 cm^{-1}) structures (Zandomeneghi et al., 2009). The self-assembly of a hydrophobin in *Schizophyllum commune* (SC3) has been studied, during the assembly of this protein a state has been identified that gives rise to the assembly that is a previous α-helical state, and that is induced by the interaction of the protein with a hydrophobic solid support, and finally to β-sheet state, which is induced by the air-water interface (De Vocht et al., 2002).

In PsCP from a medium with seaweed waste a shift of the position of the peak to < 1685 cm^{-1} and a decrease in signal intensity in the peak at ~ 1633 cm^{-1}, was seen compared with PsCP from alginate medium (Fig. 4A). Currently, there are few studies that describe the mechanism of assembly in CP, but it has been seen that its self-assembly is similar to hydrophobins. These proteins self-assemble from a partially unfolded monomeric intermediate that finally form polymeric and amphipathic monolayers similar to amyloid fibrils with a high content of β-sheet, higher than those found in the monomeric form (Carresi et al., 2006; Pazzagli et al., 2009). The secondary structures of TpHYD have also been studied (Fig. 4B). A small change of position of the main peak has been observed in TpHYD from different carbon sources resulting in a shift of the position of the main peak to ~1630 cm^{-1} and a higher decrease in signal intensity in the shoulder at ~ 1660–1680 cm^{-1} in the TpHYD from *Ulva* spp. compared with TpHYD from alginate (Fig. 4B). The presence of the main peak at ~1630 cm^{-1} is consistent with amyloid β-sheet structural content and is suggestive of rodlet assembly (Pham et al. 2016). The change of the profile obtained from TpHYD (alginate), a broader peak at ~1680 cm^{-1} suggests contributions of α-helix and random coils (Fig. 4B). Thus, these results provide evidence of the presence of assembling intermediates or native β-sheet structures (Sunde et al., 2008; Zandomeneghi et al., 2009). Thus, it can be inferred that the combination of the carbon source and the interaction of the protein with a hydrophobic solid led to conformational changes in PsCP and TpHYD, indicated by alterations in the spectra. However, further work will be required to identify the nature of biologically relevant interfaces that activate assembly in these proteins.

The aggregation of PsCP and TpHYD was studied using ThT assays, which greatly enhances the fluorescence upon the binding to amyloid fibrils (Lindgren et al., 2005; Wösten and De Vocht, 2000). The analysis was performed on both proteins isolated from each cultural broth at pH 7. ThT positive aggregates were detected in both PsCP and TpHYD (Fig. 5). The adequate concentration of protein to form ThT positive aggregates (50 μg/mL) was evaluated. Additionally, ThT assay was measured also after agitation (2 and 12 h) not showing any difference (data not shown).

A fluorescence intensity increase was observed for PsCP extracted from both cultural broths compared with blank (ThT in 25 mM Tris HCl pH7). The analysis showed an increase of up to 1.2-fold and 1.4-fold, for PsCP (SW) pH7 and PsCP (alginate), respectively (Fig. 5A).

PsCP from SW showed an increase of intensity, but also the shape of the peak changed and moved to the right; this could be due to SW compounds that are present in the protein and cause interference. Similar results were obtained for TpHYD with the difference that a 4-fold increase in fluorescence intensity of ThT was observed in TpHYD from alginate at pH 7 compared to blank and 2-fold compared with TpHYD from *Ulva* spp. at pH 7 (Fig. 5B). This result is consistent with previous

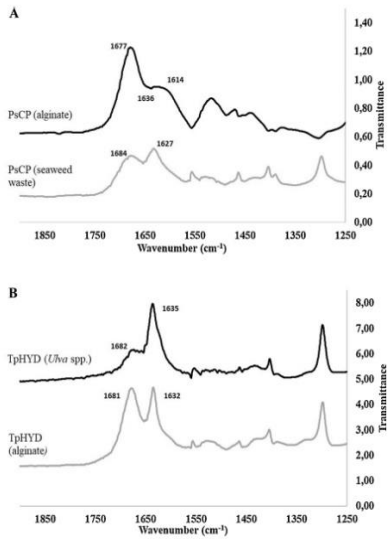

Fig. 4. Fourier-transform infra-red spectra of (A) PsCP obtained under different conditions or carbon sources (alginate and seaweed waste) (B) TpHYD obtained under different conditions or carbon sources (alginate and *Ulva* spp.).

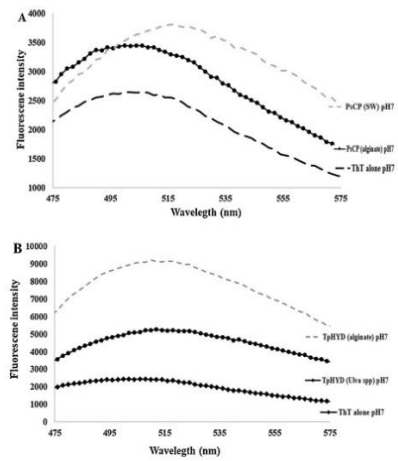

Fig. 5. ThT assays. (A) ThT fluorescence spectra of PsCP (50 μg/mL) obtained under different conditions or carbon sources (alginate and seaweed waste). (B) ThT fluorescence spectra of TpHYD (50 μg/mL) obtained under different conditions or carbon sources (alginate and *Ulva* spp.). Buffer 50 mM Tris HCL pH = 7.0 in the presence of 40 mM ThT.

work that shows that proteins exhibit a selective and preferential binding of anions on their surface and improved protein assembly (Chi et al., 2003; Zykwinska et al., 2014). Prior research has thoroughly investigated in some HFBs the conditions that could induce the formation of amyloid aggregates such as the influence of pH and ionic strength (Cicatiello et al., 2017; Gravagnuolo et al., 2016; Meister et al., 2017; Zykwinska et al., 2014). Thus, to provide further evidence, we partially analyzed conditions of pH that could induce the formation of amyloid aggregates (data no shown). Thus, the amyloid formation of PsCP and TpHYD is not only promoted by the pH but also by polysaccharides components of the algal biomass used as carbon source. A study showed that complex polysaccharides like Schizophyllan, Paramylon and Scleroglucan with high molecular mass and high degree of branching promoted amyloid formation of SC3 hydrophobin (Scholtmeijer et al., 2009). Thus, we can infer that the complex polysaccharides of brown algae such as alginate, fucoidan and laminarin with high molecular weight and a high degree of branching (Garcia-Vaquero et al., 2017) could promote the formation of amyloid-type assemblages. *Ulva* spp. also has complex polysaccharides such as ulvan, rhamnose, glucuronic and iduronic acids and xylose but with a lower degree of branching (Pezoa-Conte et al., 2015), which promote assembly in TpHYD, but to a lesser degree than with alginate. Studies of RolA hydrophobin from *Aspergillus oryzae* show that the assembly of this protein promotes and enhances the polyethylene terephthalate hydrolase (PETase) enzyme to improve the enzymatic hydrolysis of polyethylene terephthalate (PET). The self-assembled RolA protein forms an amphipathic multilayer on the PET surface and increases the binding surface of PETase enzyme to PET (Puspitasari et al., 2021). Therefore, the importance of the assembly of these surfactant proteins to enhance the enzymes responsible for hydrolyzing complex substrates that are subsequently used as nutrients for fungal growth could be demonstrated.

The results of microscopy analysis (AFM) of PsCP from SW in buffer solution pH 7 (50 mM Tris HCl), showed the presence of fibrillary structures about 20 nm with ovoidal shape (Fig. 6A–C), and many small oligomers with heights of 11.8 ± 1.3 nm (Fig. S2). It can be hypothesized that these ovoidal shapes resulted from a complex hierarchical aggregation mechanism driven by hydrophobic forces, in agreement with previous CPs reported in the literature (Pazzagli et al., 2009). In contrast, no fibrils of PsCP from alginate and two contributions by AFM were observed (Figs. 6D, E, and S2). In the histogram distribution of the height of PsCP, we could observe the presence of oligomers with heights about 3.7 ± 0.6 nm and 17.8 ± 2.1 nm, respectively (Fig. S2). Additionally, right-skewed histogram distributions indicate that PsCP tends to form aggregates with maximal height 40 nm (Fig. 6). However, when PsCP from SW were prepared in 60 % ethanol solution, the protein forms long fibrils with different height variation along the fibril length. The height profiles along the fibril axis are in the range of 2–7 nm with a branched structure (Fig. S3). The control experiments of the protein free samples are shown in Fig. S1. In comparison, PsCP from SW observed in ethanol are considerably smaller than in buffer pH 7 solution.

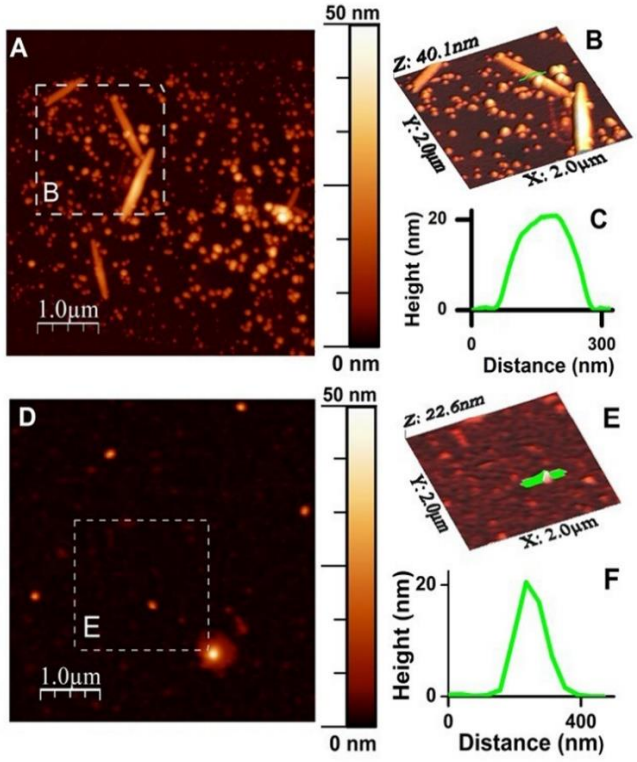

Fig. 6. AFM analysis of PsCP (200 µg/mL, buffer 50 mM Tris HCl pH7) on cleaved mica. (A) from medium with SW as sole carbon source (sample dilution 1:100) fibrillar structures with ovoid aggregates are clearly displayed. The scale indicates the height at each point. (B) zoom of image A, showing elements with height of about 20 nm. (C) profile of section outlined in B. (D) from medium with alginate as sole carbon source (sample dilution 1:100) ovoidal aggregates and small elements is clearly displayed. The scale indicates the height at each point. (E) zoom of image D, showing elements with height of about 20 nm. (F) profile of section outlined in E.

Differences in height and morphology can be attributed to the presence of small proportions of a highly disaggregating solvent in the samples used in those experiments that could be expected to have an influence on the aggregation process. It must be noted that differences in the sample preparation protocols or in the conditions used for the aggregation study (especially temperature and salt concentration) can lead to disparate types of oligomers and fibrils.

On the other hand, AFM images of TpHYD from *Ulva* spp., and from SW in 50 mM Tris HCl pH 7 solution, showed irregular oligomers with height of 1.9 ± 1 nm and fibril formation (Figs. 7A–C and S4A). The aggregation of oligomers has much higher height than those of the fibrils, thus complicating the imaging of the fibrils when both are present. However, AFM images revealed the tendency of the globule-shape oligomers to queue and assemble into fibrillar structures with a length of few micrometers and a height of 1.6 ± 0.3 nm (examples are marked in Fig S5 with arrows and green line). In this way, it was demonstrated that the use of seaweed biomass or algal polysaccharides as carbon source could promote aggregation. Thus, the presence of small oligomers in the samples of TpHYD (*Ulva* spp.) in the solution is reported, while the existence of AFM images of TpHYD from alginate showed branched larger non-fibrillar structures in a large agglomerate being characterized by a disordered assembly of protruding segments aggregates in the samples of TpHYD (alginate) (Fig. 7D). Enlarging the Fig. 7D, one can resolve the details of the fibrillar structures and appreciate its roughness with a height of 6 nm (Fig. 7E and F). In addition, large aggregates containing smaller oligomers with height of 1.7 ± 0.3 nm were observed (Fig. S4). This result confirms previous findings in the literature where the presence of these oligomers by Class I HFBs gives rise to larger assemblies with a height of 7–8 nm (Scholtmeijer et al., 2002; Sunde et al., 2008; Zykwinska et al., 2014). Furthermore, these results also confirm that CP and Class I HFB have unique features (Pazzagli et al., 2009).

4. Conclusion

In this work, for the first time the identification, production and characterization of cerato-platanin isolated from *Paradendryphiella salina* and two Class I hydrophobins from *Talaromyces pinophilus*, has been reported. These are marine fungi with the capacity to assimilate seaweed biomass or algal polysaccharide through submerged liquid fermentation. Furthermore, the impact of complex substrate (sodium alginate, seaweed waste from brown algae and *Ulva* spp.) from seaweed was studied on the production yield and on the propensity to aggregate. The fungi *P. salina* and *T. pinophilus* showed the ability to produce adequate yields of cerato-platanins (PsCP) and hydrophobins (TpHYD), respectively, using algal substrates as carbon source. Characterization of the capacity to form aggregates of these proteins was observed by Thioflavin T fluorescence assay, Fourier-transform infrared spectroscopy, and

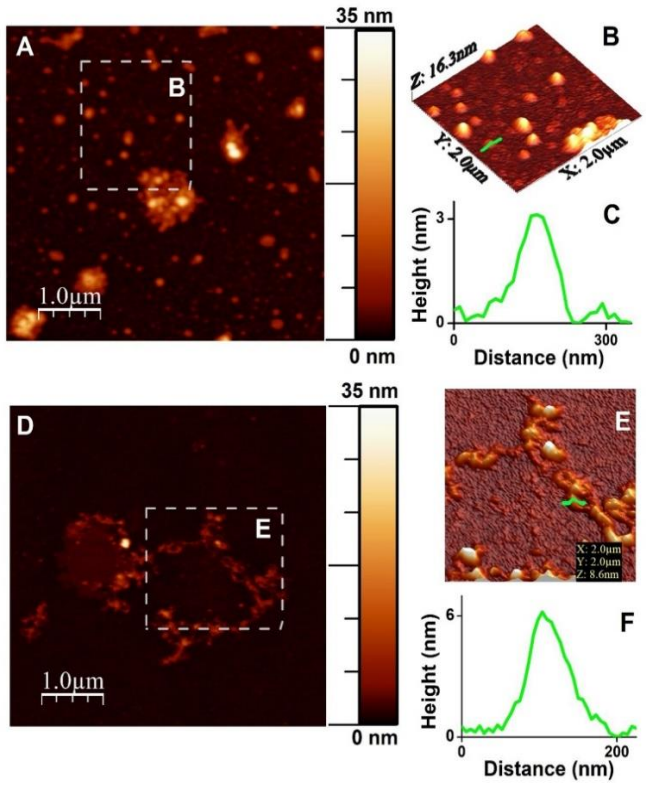

Fig. 7. AFM analysis of TpHYD (200 µg/mL, buffer 50 mM Tris HCl pH7) on cleaved mica. (A) from a medium with *Ulva spp* as sole carbon source (sample dilution 1:100 H_2O) irregular oligomers are displayed. (B) Zoom of image A, showing elements with a height of 1.9 ± 1 nm. (C) profile of section outlined in B. (D) from a medium with alginate as sole carbon source (300 µg/mL sample dilution 1:1000 H_2O) aggregation, is displayed. (E) Zoom of image D showing elements with a height of about 6 nm. (F) profile of section outlined in E.

atomic force microscopy. These analyses helped to partially characterize the aggregates of these proteins with the finality to demonstrate that the formation of aggregates and/or fibrils of PsCP and TpHYD, was influenced by the polysaccharide components of the algal biomass used as carbon source. Therefore, this preliminary study of surface-active proteins from marine fungi demonstrates that the production and assembly of these proteins depends on the fungal lifestyle and are particularly induced by the substrate on which they feed. These proteins could be involved in the potentiation of enzymes responsible for hydrolyzing complex carbohydrates in marine algae. Further studies are important to confirm this hypothesis. These studies could make it possible to achieve higher concentrations and improve the assembly mechanisms of these proteins when using algae or algal waste as a carbon source and could provide new sustainable alternatives to the various chemical-based products with the ability to reverse the polarity of surfaces. In such a way, these proteins can be exploited for different biotechnological, medical and nanotechnology applications.

Funding

This research was supported by the National Commission for Scientific and Technologic Research of the Government of Chile – CONICYT – (Grant number 21161794) and the Centre for Biotechnology and Bioengineering – CeBiB – (Project FB-0001).

CRediT authorship contribution statement

Catalina Landeta-Salgado: Conceptualization, Methodology, Investigation, Formal analysis, Writing - original draft. **Paola Cicatiello:** Investigation, Writing - review & editing. **Ilaria Stanzione:** Investigation, Writing - review & editing. **David Medina:** Investigation, Writing - review & editing. **Isadora Berlanga Mora:** Investigation, Writing - review & editing. **Carlos Gomez:** Investigation, Writing - review & editing. **María Elena Lienqueo:** Conceptualization, Supervision, Writing - review & editing.

Declaration of Competing Interest

The authors report no declarations of interest.

Acknowledgments

The authors thank Prof. Carolina Camus from Center for Research and Development of Resources and Coastal Environments – i~mar – Los Lagos University, Puerto Montt, Chile. The authors thank Prof. Francisco Gracia from the Department of Chemical, Biotechnology and Materials Engineering – DIQBM – Chile University, for his help with the Fourier transform infrared spectroscopy (FT- IR) equipment (FONDECYT 1171193). The authors thank FONDEQUIP (EQM 140142). Prof. Berlanga gratefully acknowledges the financial support given by ANID-Chile (FONDECYT 11190841) as well as the VID of the Universidad de Chile in the framework of "U-Inicia UI003/2018". The authors would like to thank the research group led by Prof. Paola Giardina of Department of Chemical Sciences, Universtiy of Naples, Federico II, for your helpful. The authors would like to thank the research group led by Prof. Han Wösten of Department of Microbiology, Utrecht University, for your helpful.

Appendix A. Supplementary data

Supplementary material related to this article can be found, in the online version, at doi:https://doi.org/10.1016/j.micres.2021.126835.

References

Abdel-Rahim, I.R., Abo-Elyousr, K.A.M., 2018. *Talaromyces pinophilus* strain AUN-1 as a novel mycoparasite of *Botrytis cinerea*, the pathogen of onion scape and umbel blights. Microbiol. Res. 212–213, 1–9. https://doi.org/10.1016/j.micres.2018.04.004.

Aimanianda, V., Bayry, J., Bozza, S., Kniemeyer, O., Perruccio, K., Elluru, S.R., Clavaud, C., Paris, S., Brakhage, A.A., Kaveri, S.V., Romani, L., Latgé, J.P., 2009. Surface hydrophobin prevents immune recognition of airborne fungal spores. Nature 460, 1117–1121.

Alfaro, M., Castanera, R., Lavín, J.L., Grigoriev, I.V., Oguiza, J.A., Ramírez, L., Pisabarro, A.G., 2016. Comparative and transcriptional analysis of the predicted secretome in the lignocellulose-degrading basidiomycete fungus *Pleurotus ostreatus*. Environ. Microbiol. 18, 4710–4726. https://doi.org/10.1111/1462-2920.13360.

Alfaro, M., Majcherczyk, A., Kües, U., Ramírez, L., Pisabarro, A.G., 2020. Glucose counteracts wood-dependent induction of lignocellulolytic enzyme secretion in monokaryon and dikaryon submerged cultures of the white-rot basidiomycete *Pleurotus ostreatus*. Sci. Rep. 10, 1–10. https://doi.org/10.1038/s41598-020-68969-1.

Altschul, S., Madden, T., Schäfferr, A., Zhang, J., Zhang, Z., Miller, W., Lipman, D., 1997. Gapped BLAST and PSI-BLAST: a new generation of protein database search programs. Nucleic Acids Res. 25, 3389–3402. https://doi.org/10.1002/ejlt.200700105.

Arumugam, G.K., Srinivasan, S.K., Joshi, G., Gopal, D., Ramalingam, K., 2015. Production and characterization of bioactive metabolites from piezotolerant deep sea fungus *Nigrospora* spp. in submerged fermentation. J. Appl. Microbiol. 118, 99–111. https://doi.org/10.1111/jam.12693.

Balabanova, L., Slepchenko, L., Son, O., Tekutyeva, L., 2018. Biotechnology potential of marine fungi degrading plant and algae polymeric substrates. Front. Microbiol. 9, 1–15. https://doi.org/10.3389/fmicb.2018.01527.

Bao, J., Sun, Y.L., Zhang, X.Y., Han, Z., Gao, H.C., He, F., Qian, P.Y., Qi, S.H., 2013. Antifouling and antibacterial polyketides from marine gorgonian coral-associated fungus *Penicillium* spp. SCSGAF 0023. J. Antibiot. 66, 219–223. https://doi.org/10.1038/ja.2012.110.

Barsottini, M.R.de O., de Oliveira, J., Adamoski, D., Teixeira, P.J.P.L., Tiezzi, H.O., Sforça, M.L., Cassago, A., Portugal, R.V., de Oliveira, P.S.L., Zeri, A.C.M., Dias, S.M. G., Pereira, G.A.G., Ambrosio, A.L.B., 2013. Functional diversification of Cerato-Platanins in *Moniliophthora perniciosa* as seen by differential expression and protein function specialization. Mol. Plant-Microbe Interact. 26, 1281–1293.

Bateman, A., 2004. The Pfam protein families database. Nucleic Acids Res. 32, 138–141. https://doi.org/10.1093/nar/gkh121.

Beena, P.S., Basheer, S.M., Bhat, S.G., Bahkali, A.H., Chandrasekaran, M., 2011. Propyl gallate synthesis using acidophilic tannase and simultaneous production of tannase and gallic acid by marine *Aspergillus awamori* BTMFW032. Appl. Biochem. Biotechnol. 164, 612–628. https://doi.org/10.1007/s12010-011-9162-x.

Bemporad, F., Ramazzotti, M., 2017. From the evolution of protein sequences able to resist self-assembly to the prediction of aggregation propensity. International Review of Cell and Molecular Biology. Elsevier Inc., pp. 1–47. https://doi.org/10.1016/bs.ircmb.2016.08.008

Benjiamin, C., 1955. Ascocarpos de Aspergillus y Penicillium. Micologia 47, 669–687. https://doi.org/10.2307/3755578.

Berger, B.W., Sallada, N.D., 2019. Hydrophobins: multifunctional biosurfactants for interface engineering. J. Biol. Eng. 13, 1–8. https://doi.org/10.1186/s13036-018-0136-1.

Bleem, A., Daggett, V., 2017. Structural and functional diversity among amyloid proteins: agents of disease, building blocks of biology, and implications for molecular engineering. Biotechnol. Bioeng. 114, 7–20. https://doi.org/10.1002/bit.26059.

Boddi, S., Comparini, C., Calamassi, R., Pazzagli, L., Cappugi, G., Scala, A., 2004. Cerato-platanin protein is located in the cell walls of ascospores, conidia and hyphae of *Ceratocystis fimbriata*f. sp. *platani*. FEMS Microbiol. Lett. 233, 341–346. https://doi.org/10.1016/j.femsle.2004.03.001.

Bonazza, K., Gaderer, R., Neudl, S., Przylucka, A., Allmaier, G., Druzhinina, I.S., Grothe, H., Friedbacher, G., Seidl-Seiboth, V., 2015. The fungal cerato-platanin protein EPL1 forms highly ordered layers at hydrophobic/hydrophilic interfaces. Soft Matter 11, 1723–1732. https://doi.org/10.1039/c4sm02389g.

Carresi, L., Pantera, B., Zoppi, C., Cappugi, G., Oliveira, A.L., Pertinhez, T.A., Spisni, A., Scala, A., Pazzagli, L., 2006. Cerato-platanin, a phytotoxic protein from *Ceratocystis fimbriata*: expression in Pichia pastoris, purification and characterization. Protein Expr. Purif. 49, 159–167. https://doi.org/10.1016/j.pep.2006.07.006.

Charoensiddhi, S., Conlon, M.A., Franco, C.M.M., Zhang, W., 2017. The development of seaweed-derived bioactive compounds for use as prebiotics and nutraceuticals using enzyme technologies. Trends Food Sci. Technol. 70, 20–33. https://doi.org/10.1016/j.tifs.2017.10.002.

Chi, E.Y., Krishnan, S., Randolph, T.W., Carpenter, J.F., 2003. Physical stability of proteins in aqueous solution: mechanism and driving forces in nonnative protein aggregation. Pharm. Res. 20, 1325–1336. https://doi.org/10.1023/A:1025771421906.

Cicatiello, P., Dardano, P., Pirozzi, M., Gravagnuolo, A.M., De Stefano, L., Giardina, P., 2017. Self-assembly of two hydrophobins from marine fungi affected by interaction with surfaces. Biotechnol. Bioeng. 114, 2173–2186. https://doi.org/10.1002/bit.26344.

Corvis, Y., Walcarius, A., Rink, R., Mrabet, N.T., Rogalska, E., 2005. Preparing catalytic surfaces for sensing applications by immobilizing enzymes via hydrophobin layers. Anal. Chem. 77, 1622–1630. https://doi.org/10.1021/ac048897w.

Dagenais, T.R.T., Giles, S.S., Aimanianda, V., Latge, J.P., Hull, C.M., Keller, N.P., 2010. *Aspergillus fumigatus* LaeA-mediated phagocytosis is associated with a decreased hydrophobin layer. Infect. Immun. 78, 823–829.

De Oliveira, A.L., Gallo, M., Pazzagli, L., Benedetti, C.E., Cappugi, G., Scala, A., Pantera, B., Spisni, A., Pertinhez, T.A., Cicero, D.O., 2011. The structure of the elicitor cerato-platanin (CP), the first member of the CP fungal protein family, reveals a double ψβ-barrel fold and carbohydrate binding. J. Biol. Chem. 286, 17560–17568. https://doi.org/10.1074/jbc.M111.223644.

De Vocht, M.L., Reviakine, I., Ulrich, W.-P., Bergsma-Schutter, W., Wösten, H.A.B., Vogel, H., Brisson, A., Wessels, J.G.H., Robillard, G.T., 2002. Self-assembly of the hydrophobin SC3 proceeds via two structural intermediates. Protein Sci. 11, 1199–1205. https://doi.org/10.1110/ps.4540102.

Dela Cruz, T.E., Schulz, B.E., Kubicek, C.P., Druzhinina, I.S., 2006. Carbon source utilization by the marine *Dendryphiella* species *D. arenaria* and *D. salina*. FEMS Microbiol. Ecol. 58, 343–353. https://doi.org/10.1111/j.1574-6941.2006.00184.x.

Desjardins, P., Hansen, J.B., Allen, M., 2010. Microvolume protein concentration determination using the NanoDrop 2000c Spectrophotometer. J. Vis. Exp. 1–4. https://doi.org/10.3791/1610.

Edwards, J., Chamberlain, D., Brosnan, G., West, D., Stanley, M.S., Clipson, N.J.W., Hooley, P., 1998. A comparative physiological and morphological study of *Dendryphiella salina* and *D. arenaria* in relation to adaptation to life in the sea. Mycol. Res. 102, 1198–1202. https://doi.org/10.1017/S0953756298006224.

El-Hady, F.K.A., Abdel-aziz, M.S., Shaker, K.H., El-shahid, Z.A., Ibrahim, L.S., 2015. Antioxidant, acetylcholinesterase and α -glucosidase potentials of metabolites from the marine fungus. Int. J. Pharm. Sci. Rev. Res. 30, 272–278.

Frischmann, A., Neudl, S., Gaderer, R., Bonazza, K., Zach, S., Gruber, S., Spadiut, O., Friedbacher, G., Grothe, H., Seidl-Seiboth, V., 2013. Self-assembly at air/water interfaces and carbohydrate binding properties of the small secreted protein EPL1 from the fungus *Trichoderma atroviride*. J. Biol. Chem. 288, 4278–4287. https://doi.org/10.1074/jbc.M112.427633.

Gaderer, R., Bonazza, K., Seidl-Seiboth, V., 2014. Cerato-platanins: a fungal protein family with intriguing properties and application potential. Appl. Microbiol. Biotechnol. 98, 4795–4803. https://doi.org/10.1007/s00253-014-5690-y.

Galpin, M.F.J., Jennings, D., 1975. Histochemical study of the hyphae and the distribution of adenosine triphosphatase in *Dendryphiella salina*. Trans. Br. Mycol. Soc. 65, 477–483. https://doi.org/10.1016/S0007-1536(75)80045-3. IN6.

Gao, R., Ding, M., Jiang, S., Zhao, Z., Chenthamara, K., Shen, Q., Cai, F., Druzhinina, I.S., 2020. The evolutionary and functional paradox of cerato-platanins in fungi. Appl. Environ. Microbiol. 86 https://doi.org/10.1128/AEM.00696-20.

Garcia-Vaquero, M., Rajauria, G., O'Doherty, J.V., Sweeney, T., 2017. Polysaccharides from macroalgae: recent advances, innovative technologies and challenges in extraction and purification. Food Res. Int. 99, 1011–1020. https://doi.org/10.1016/j.foodres.2016.11.016.

Goldschmidt, L., Teng, P.K., Riek, R., Eisenberg, D., 2010. Identifying the amylome, proteins capable of forming amyloid-like fibrils. Proc. Natl. Acad. Sci. U. S. A. 107, 3487–3492. https://doi.org/10.1073/pnas.0915166107.

Gravagnuolo, A.M., Longobardi, S., Luchini, A., Appavou, M.S., De Stefano, L., Notomista, E., Paduano, L., Giardina, P., 2016. Class I Hydrophobin Vmh2 adopts atypical mechanisms to self-assemble into functional amyloid fibrils. Biomacromolecules 17, 954–964. https://doi.org/10.1021/acs.biomac.5b01632.

Haas Jimoh Akanbi, M., Post, E., Meter-Arkema, A., Rink, R., Robillard, G.T., Wang, X., Wösten, H.A.B., Scholtmeijer, K., 2010. Use of hydrophobins in formulation of water insoluble drugs for oral administration. Colloids Surf. B Biointerfaces 75, 526–531. https://doi.org/10.1016/j.colsurfb.2009.09.030.

Harms, H., Schlosser, D., Wick, L.Y., 2011. Untapped potential: exploiting fungi in bioremediation of hazardous chemicals. Nat. Rev. Microbiol. 9, 177–192. https://doi.org/10.1038/nrmicro2519.

He, P., Li, F., Huang, L., Xue, D., Liu, W., Xu, C., 2016. Chemical characterization and antioxidant activity of polysaccharide extract from spent mushroom substrate of Pleurotus eryngii. J. Taiwan Inst. Chem. Eng. 69, 48–53. https://doi.org/10.1016/j.jtice.2016.10.017.

Heukeshoven, J., Dernick, R., 1985. Simplified method for silver staining of proteins in polyacrylamide gels and the mechanism of silver staining. Electrophoresis 6, 103–112. https://doi.org/10.1002/elps.1150060302.

Horcas, I., Fernandez, J.M., Colchero, J., Gomez-Herrero, J., Baro, A., 2007. WSXM: a software for scanning probe microscopy and a tool for nanotechnology. Rev. Sci. Instrum. 78 https://doi.org/10.1063/1.2432410.

Houbraken, J., Samson, R.A., 2017. Current taxonomy and identification of foodborne fungi. Curr. Opin. Food Sci. 17, 84–88. https://doi.org/10.1016/j.cofs.2017.10.010.

Karray, R., Hamza, M., Sayadi, S., 2015. Evaluation of ultrasonic, acid, thermo-alkaline and enzymatic pre-treatments on anaerobic digestion of *Ulva rigida* for biogas production. Bioresour. Technol. 187, 205–213.

Kelley, L.A., Mezulis, S., Yates, C.M., Wass, M.N., Sternberg, M.J.E., 2015. The Phyre2 web portal for protein modeling, prediction and analysis. Nat. Protoc. 10, 845–858. https://doi.org/10.1038/nprot.2015.053.

Kim, S., Ahn, I.P., Rho, H.S., Lee, Y.H., 2005. MHP1, a *Magnaporthe grisea* hydrophobin gene, is required for fungal development and plant colonization. Mol. Microbiol. 57, 1224–1237.

Kumar, S., Stecher, G., Li, M., Knyaz, C., Tamura, K., 2018. MEGA X: Molecular evolutionary genetics analysis across computing platforms. Mol. Biol. Evol. 35, 1547–1549. https://doi.org/10.1093/molbev/msy096.

Laemmli, U., 1970. Cleavage of Structural Proteins during the Assembly of the Head of Bacteriophage T4, vol. 227. Nature Publishing Group, pp. 680–685.

Landeta, C., Muñoz, R., Blanco, A., Lienqueo, M.E., 2021. Valorization and upgrading of the nutritional value of seaweed and seaweed waste using the marine fungi *Paradendryphiella salina* to produce mycoprotein. Algal Res. 53, 102135 https://doi.org/10.1016/j.algal.2020.102135.

Landeta-Salgado, C., Cicatiello, P., Lienqueo, M.E., 2021. Mycoprotein and hydrophobin like protein produced from marine fungi *Paradendryphiella salina* in submerged fermentation with green seaweed *Ulva* spp. Algal Res. 56, 102314 https://doi.org/10.1016/j.algal.2021.102314.

LeVine, H., 1999. Quantification of β-sheet amyloid fibril structures with thioflavin T. Meth. Enzymol. 309, 274–284. https://doi.org/10.1016/S0076-6879(99)09020-5.

Linder, M., Szilvay, G., Nakari-Setälä, T., Penttilä, M.E., 2005. Hydrophobins: the protein-amphiphiles of filamentous fungi. FEMS Microbiol. Rev. 29, 877–896. https://doi.org/10.1016/j.femsre.2005.01.004.

Lindgren, M., Sörgjerd, K., Hammarström, P., 2005. Detection and characterization of aggregates, prefibrillar amyloidogenic oligomers, and protofibrils using fluorescence spectroscopy. Biophys. J. 88, 4200–4212. https://doi.org/10.1529/biophysj.104.049700.

Littlejohn, K., Hooley, P., Cox, P., 2012. Bioinformatics predicts diverse *Aspergillus* hydrophobins with novel properties. Food Hydrocoll. 27 https://doi.org/10.1016/j.foodhyd.2011.08.018.

Liu, F., Wang, Z., Manglekar, R.R., Geng, A., 2020. Enhanced cellulase production through random mutagenesis of *Talaromyces pinophilus* OPC4-1 and fermentation optimization. Process. Biochem. 90, 12–22. https://doi.org/10.1016/j.procbio.2019.11.025.

Lo, V., Ren, Q., Pham, C., Morris, V., Kwan, A., Sunde, M., 2014. Fungal hydrophobin proteins produce self-assembling protein films with diverse structure and chemical stability. Nanomaterials 4, 827–843. https://doi.org/10.3390/nano4030827.

Lohrasbi-Nejad, A., Torkzadeh-Mahani, M., Hosseinkhani, S., 2016. Heterologous expression of a hydrophobin HFB1 and evaluation of its contribution to producing stable foam. Protein Expr. Purif. 118, 25–30. https://doi.org/10.1016/j.pep.2015.09.025.

Lonchamp, J., Clegg, P.S., Euston, S.R., 2019. Foaming, emulsifying and rheological properties of extracts from a co-product of the Quorn fermentation process. Eur. Food Res. Technol. 245, 1825–1839. https://doi.org/10.1007/s00217-019-03287-z.

Macindoe, I., Kwan, A.H., Ren, Q., Morris, V.K., Yang, W., Mackay, J.P., 2011. Self-assembly of functional, amphipathic amyloid monolayers by the fungal hydrophobin EAS. PNAS 109, 804–811. https://doi.org/10.1073/pnas.1114052109/-/DCSupplemental.www.pnas.org/cgi/doi/10.1073/pnas.1114052109.

Meister, K., Roeters, S.J., Paananen, A., Woutersen, S., Versluis, J., Szilvay, G.R., Bakker, H.J., 2017. Observation of pH-induced protein reorientation at the water surface. J. Phys. Chem. Lett. 8 https://doi.org/10.1021/acs.jpclett.7b00394.

Misra, R., Li, J., Cannon, G.C., Morgan, S.E., 2006. Nanoscale reduction in surface friction of polymer surfaces modified with Sc3 hydrophobin from *Schizophyllum commune*. Biomacromolecules 7, 1463–1470. https://doi.org/10.1021/bm050983y.

Patyshakuliyeva, A., Falkoski, D.L., Wiebenga, A., Timmermans, K., de Vries, R.P., 2020. Macroalgae derived fungi have high abilities to degrade algal polymers. Microorganisms 8, 1–16. https://doi.org/10.3390/microorganisms8010052.

Pazzagli, L., Zoppi, C., Carresi, L., Tiribilli, B., Sbrana, F., Schiff, S., Pertinhez, T.A., Scala, A., Cappugi, G., 2009. Characterization of ordered aggregates of cerato-platanin and their involvement in fungus-host interactions. Biochim. Biophys. Acta - Gen. Subj. 1790, 1334–1344. https://doi.org/10.1016/j.bbagen.2009.07.014.

Penttilä, M., Nevalainen, H., Rättö, M., Salminen, E., Knowles, J., 1987. A versatile transformation system for the cellulolytic filamentous fungus *Trichoderma reesei*. Gene 61, 155–164. https://doi.org/10.1016/0378-1119(87)90110-7.

Pezoa-Conte, R., Leyton, A., Anugwom, I., Schoultz, S. Von, Paranko, J., Mäki-arvela, P., Willför, S., 2015. Deconstruction of the green alga *Ulva rigida* in ionic liquids: closing the mass balance. Algal Res. 12, 262–273. https://doi.org/10.1016/j.algal.2015.09.011.

Pilgaard, B., Wilkens, C., Herbst, F., Vuillemin, M., Rhein-knudsen, N., Meyer, A.S., Lange, L., 2019. Proteomic enzyme analysis of the marine fungus Paradendryphiella salina reveals alginate lyase as a minimal adaptation strategy for brown algae degradation. Nature 9, 1–13. https://doi.org/10.1038/s41598-019-48823-9.

Pitocchi, R., Cicatiello, P., Birolo, L., Piscitelli, A., Bovio, E., Cristina Varese, G., Giardina, P., 2020. Cerato-platanins from marine fungi as effective protein biosurfactants and bioemulsifiers. Int. J. Mol. Sci. 21 https://doi.org/10.3390/ijms21082913.

Pruitt, K.D., Tatusova, T., Maglott, D.R., 2007. NCBI reference sequences (RefSeq): a curated non-redundant sequence database of genomes, transcripts and proteins. Nucleic Acids Res. 35, 61–65. https://doi.org/10.1093/nar/gkl842.

Puspitasari, N., Tsai, S.L., Lee, C.K., 2021. Fungal hydrophobin RolA enhanced PETase hydrolysis of polyethylene terephthalate. Appl. Biochem. Biotechnol. 193, 1284–1295. https://doi.org/10.1007/s12010-020-03358-y.

Quarantin, A., Castiglioni, C., Schäfer, W., Favaron, F., Sella, L., 2019. The Fusarium graminearum cerato-platanins loosen cellulose substrates enhancing fungal cellulase activity as expansin-like proteins. Plant Physiol. Biochem. 139, 229–238. https://doi.org/10.1016/j.plaphy.2019.03.025.

Ren, Q., Kwan, A.H., Sunde, M., 2013. Two forms and two faces, multiple states and multiple uses: properties and applications of the self-assembling fungal hydrophobins. Biopolymers 100, 601–612. https://doi.org/10.1002/bip.22259.

Rindi, F., Soler-Vila, A., Guiry, M.D., Hayes, M., 2012. Taxonomy of marine macroalgae used as sources of bioactive compounds. Marine Bioactive Compounds. Springer, Boston, pp. 1–53.

Schaumann, K., Weide, G., 1995. Efficiency of uronic acid uptake in marine alginate-degrading fungi. Helgoländer Meeresuntersuchungen 49, 159–167. https://doi.org/10.1007/BF02368346.

Scholtmeijer, K., Janssen, M.I., Gerssen, B., De Vocht, M.L., Van Leeuwen, B.M., Van Kooten, T.G., Wösten, H.A.B., Wessels, J.G.H., 2002. Surface modifications created

by using engineered hydrophobins. Appl. Environ. Microbiol. 68, 1367–1373. https://doi.org/10.1128/AEM.68.3.1367-1373.2002.
Scholtmeijer, K., Janssen, M., Leeuwen, V., Van Kooten, T., Hektor, H., Wösten, H.A.B., 2004. The use of hydrophobins to functionalize surfaces. Biomed. Mater. Eng. 14, 447–454.
Scholtmeijer, K., de Vocht, M.L., Rink, R., Robillard, G.T., Wösten, H.A.B., 2009. Assembly of the fungal SC3 hydrophobin into functional amyloid fibrils depends on its concentration and is promoted by cell wall polysaccharides. J. Biol. Chem. 284, 26309–26314. https://doi.org/10.1074/jbc.M109.005553.
Seidl, V., Marchetti, M., Schandl, R., Allmaier, G., Kubicek, C.P., 2006. Epl1, the major secreted protein of Hypocrea atroviridis on glucose, is a member of a strongly conserved protein family comprising plant defense response elicitors. FEBS J. 273, 4346–4359. https://doi.org/10.1111/j.1742-4658.2006.05435.x.
Seidl-Seiboth, V., Gruber, S., Sezerman, U., Schwecke, T., Albayrak, A., Neuhof, T., Von Döhren, H., Baker, S.E., Kubicek, C.P., 2011. Novel hydrophobins from trichoderma define a new hydrophobin subclass: protein properties, evolution, regulation and processing. J. Mol. Evol. 72, 339–351. https://doi.org/10.1007/s00239-011-9438-3.
Singh, B.N., Singh, B.R., Gupta, V.K., Kharwar, R.N., Pecoraro, L., 2018. Coating with microbial hydrophobins: a novel approach to develop smart drug nanoparticles. Trends Biotechnol. 36, 1103–1106. https://doi.org/10.1016/j.tibtech.2018.03.006.
Stanislawski, J., Kotulska, M., Unold, O., 2013. Machine learning methods can replace 3D profile method in classification of amyloidogenic hexapeptides. BMC Bioinformatics 14, 1–9. https://doi.org/10.1186/1471-2105-14-21.
Stanke, M., Steinkamp, R., Waack, S., Morgenstern, B., 2004. AUGUSTUS: a web server for gene finding in eukaryotes. Nucleic Acids Res. 32, 309–312. https://doi.org/10.1093/nar/gkh379.
Sunde, M., Kwan, A.H.Y., Templeton, M.D., Beever, R.E., Mackay, J.P., 2008. Structural analysis of hydrophobins. Micron 39, 773–784. https://doi.org/10.1016/j.micron.2007.08.003.
Sunde, M., Pham, C.L.L., Kwan, A.H., 2017. Molecular characteristics and biological functions of surface-active and surfactant proteins. Annu. Rev. Biochem. 86, 585–608. https://doi.org/10.1146/annurev-biochem-061516-044847.
Torchala, M., Bates, P.A., 2014. RaptorX server: a resource for template-based protein structure modeling. In: Kihara, D. (Ed.), Protein Structure Prediction. Springer protocols, pp. 17–27. https://doi.org/10.1007/978-1-4939-0366-5_13.
Van, H., Rasmussen, M., Sankaran, S., Koza, C., Erickson, D., Mitra, D., Jin, B., 2011. Fungal treatment of crop processing wastewaters with value-added co-products. Sustainable Bioenergy and Bioproducts. Green Energy and Technology 13–44.
Vargas, W.A., Djonović, S., Sukno, S.A., Kenerley, C.M., 2008. Dimerization controls the activity of fungal elicitors that trigger systemic resistance in plants. J. Biol. Chem. 283, 19804–19815. https://doi.org/10.1074/jbc.M802724200.
Wang, X., Shi, F., Wösten, H.A.B., Hektor, H., Poolman, B., Robillard, G.T., 2005. The SC3 hydrophobin self-assembles into a membrane with distinct mass transfer properties. Biophys. J. 88, 3434–3443. https://doi.org/10.1529/biophysj.104.057794.
Wainwright, M., Sherbrock-Cox, V., 1981. Factors influencing alginate degradation by the marine fungi: *Dendryphiella salina* and *D. arenaria*. Bot. Mar. 24, 489–491.
Wang, Yanming, Barth, D., Tamminen, A., Wiebe, M.G., 2016. Growth of marine fungi on polymeric substrates. BMC Biotechnol. 16, 3. https://doi.org/10.1186/s12896-016-0233-5.
Wang, Yiming, Wu, J., Kim, S.G., Tsuda, K., Gupta, R., Park, S.Y., Kim, S.T., Kang, K.Y., 2016. *Magnaporthe oryzae* secreted protein MSP1 induces cell death and elicits defense responses in rice. Mol. Plant-Microbe Interact. 29, 299–312. https://doi.org/10.1094/MPMI-12-15-0266-R.
Wang, X., Song, D., Wang, B., Yang, J., Ge, L., Zhao, L., Xu, H., Qiao, M., 2017. A mutant of hydrophobin HGFI tuning the self-assembly behaviour and biosurfactant activity. Appl. Microbiol. Biotechnol. 101, 8419–8430. https://doi.org/10.1007/s00253-017-8577-x.
Wessels, J., 1992. Gene expression during fruiting in *Schizophyllum commune*. Mycol. Res. 96, 609–620. https://doi.org/10.1016/S0953-7562(09)80485-1.
Wetzel, R., Shivaprasad, S., Williams, A.D., 2007. Plasticity of Amyloid Fibrils. Biochemistry 46.
Wösten, H.A.B., De Vocht, M.L., 2000. Hydrophobins, the fungal coat unravelled. Biochim. Biophys. Acta 1469, 79–86. https://doi.org/10.1016/S0304-4157(00)00002-2.
Wösten, H.A.B., Scholtmeijer, K., 2015. Applications of hydrophobins: current state and perspectives. Appl. Microbiol. Biotechnol. 99, 1587–1597. https://doi.org/10.1007/s00253-014-6319-x.
Wösten, H.A.B., Wessels, J.G.H., 1997. Hydrophobins, from molecular structure to multiple functions in fungal development. Mycoscience 38, 363–374. https://doi.org/10.1007/bf02464099.
Woudenberg, J.H.C., Groenewald, J.Z., Binder, M., Crous, P.W., 2013. Alternaria redefined. Stud. Mycol. 75, 171–212. https://doi.org/10.3114/sim0015.
Wu, Z., Liu, D., Proksch, P., Guo, P., Lin, W., 2014. Punctaporonins H-M: caryophyllene-type sesquiterpenoids from the sponge-associated fungus *Hansfordia sinuosae*. Mar. Drugs 12, 3904–3916. https://doi.org/10.3390/md12073904.
Zandomeneghi, G., Krebs, M.R.H., McCammon, M.G., Fändrich, M., 2009. FTIR reveals structural differences between native β-sheet proteins and amyloid fibrils. Protein Sci. 13, 3314–3321. https://doi.org/10.1110/ps.041024904.
Zykwinska, A., Guillemette, T., Bouchara, J.P., Cuenot, S., 2014. Spontaneous self-assembly of SC3 hydrophobins into nanorods in aqueous solution. Biochim. Biophys. Acta 1844, 1231–1237. https://doi.org/10.1016/j.bbapap.2014.04.003.

Chapter 3

3. Novel application of the Class I hydrophobin of *P. ostreatus* in cultural heritage

In the world of cultural heritage, the main challenges to overcome are represented by the conservation and the diagnosis of the ancient archeological samples. The cultural heritage objects are constantly subjected to degradation agents ranging from the combination of water and air contaminants to the increasing air pollution with aggressive gases. In this context, the amphipathic nature of the hydrophobins and their capability to modify physical-chemical properties of the surfaces have been exploited as protective agents. In particular, the class I hydrophobin DewA from *Aspergillus nidulans* and the class II hydrophobin HFBI from *Trichoderma reesei* have been used to render stones impermeable to water but permeable to vapor [82]. Furthermore, the use of these biomolecules is completely in line with the concept that the protective agents must be removable from the surface without damaging the substrate.

As far as the diagnosis of the archeological objects, the proteins and the proteinaceous binder identification is usually performed by proteomic analysis based on the proteolytic activity of enzymes such as trypsin, chymotrypsin, PNGaseF. The class I hydrophobin Vmh2 from *P. ostreatus* had been employed to improve proteomic analysis. Indeed, its ability to form amphiphilic layer on surfaces and to adsorb proteins in their active form had been used for the development of new diagnosis methods. As demonstrated by Longobardi et al, the hydrophobin Vmh2 can be used as coating of MALDI steel sample-loading plate to allow the immobilization of some proteolytic enzymes [41]. Among them, it has been proved that the immobilization of the trypsin on the Vmh2 layer also provides an enhancement of the enzyme activity. Starting from this assessment and considering that in the cultural heritage the invasiveness of the sampling is often underestimated, a minimally invasive portable kit has been developed by our research group immobilizing the trypsin on a Vmh2 functionalized sheet of cellulose acetate to digest ancient proteins directly on painted surfaces and to later identify the proteinaceous binder through a proteomic analysis [54].

More recently, I was involved in the preparation of cellulose acetate sheets functionalized with Vmh2 and then with enzymes and their application on different real samples. Indeed, in the paper reported in the section 3.1, the identification of glycosylated proteins was improved by adding a new step using PNGaseF immobilized on Vmh2 functionalized acetate sheets.

3.1 A versatile and user-friendly approach for the analysis of proteins in ancient and historical objects

Journal of Proteomics 231 (2021) 104039

Contents lists available at ScienceDirect

Journal of Proteomics

journal homepage: www.elsevier.com/locate/jprot

A versatile and user-friendly approach for the analysis of proteins in ancient and historical objects

Georgia Ntasi [a], Daniel P. Kirby [b], Ilaria Stanzione [a], Andrea Carpentieri [a,c], Patrizia Somma [c], Paola Cicatiello [a], Gennaro Marino [a,c], Paola Giardina [a], Leila Birolo [a,*]

[a] Department of Chemical Sciences, University of Naples Federico II, Naples, Italy
[b] Private Practice, Milton, MA, USA
[c] Department of Humanities, University Suor Orsola Benincasa, Naples, Italy

A B S T R A C T

Identification and characterization of ancient proteins still require technical developments towards non-invasiveness, sensitivity, versatility and ease of use of the analyses. We report that the enzyme functionalized films, described in Cicatiello et al. (2018), can be used efficiently on the surface of different objects ranging from fixative-coated paper to canvas to the coating on an albumen photograph, as well as the much harder surfaces of ivory objects and the proteinaceous binders in the decoration of a wooden Egyptian coffin. The mixture of digested peptides that are efficiently captured on the functionalized surface are also amenable to LC-MS/MS analysis, which is necessary to confidently identify chemical modifications induced upon degradation, in order to characterize the conservation state of proteins. Moreover, in a two-step procedure, we have combined the trypsin functionalized film with a PNGaseF functionalized film, which adds a deglycosylation pretreatment allowing improved detection of glycosylated proteins.

Significance: User friendly trypsin functionalized films were implemented to expand their potential as versatile, modular tools that can be widely exploited in the world of diagnosis of cultural heritage objects, ancient proteins, and palaeoproteomics: a procedure that could be carried out by conservators or archaeologists first *on-site* and later analysed with standard MS techniques.

1. Introduction

Any new information on the chemical composition of artistic objects or archaeological remains provides keys to decipher ancient and historic materials revealing new insights and/or serving cultural heritage conservation.

Recent technical advances in analytical chemistry and, in particular, the astonishing improvements in mass spectrometry (MS), have allowed adaptation of methods for the study of ancient proteins in artworks and objects of cultural heritage [1]. It is now possible to detect proteins with extreme sensitivity (below femtomoles) and characterize them in detail [2–4]. However, most classical procedures and strategies are considered to be invasive even when only micro sampling is required. In this respect, the technical and methodological challenges are still huge considering the complexity of the artwork samples and the microscopic amount often allowed for analyses. A novel method towards the non-invasive analysis of proteinaceous materials from artworks was recently developed, based on a protease functionalized sheet of cellulose acetate to directly digest proteins *in-situ* on painted surfaces without sample removal from the artefact [5]. This work demonstrated that, at least on a short term, temporary scale, the painted surfaces were not altered. Trypsin was readily immobilized on the sheet, taking advantage of the adhesive properties of the previously formed layer of a self-assembling protein, the class I hydrophobin Vmh2 from the fungus *Pleurotus ostreatus* [5]. The *in-situ* digested peptides can then be remotely analysed by standard mass spectrometric approaches to identify the proteins from which they arise, and a number of peptides sufficient for a confident identification of the proteins was obtained. The benefit of this functionalized film is that, unlike similar, existing film/resins [6–9], this is the only one, to the best of our knowledge, that directly allows the digestion of proteins and, due to the adhesive properties of Vmh2, extracts the peptides from the object. In contrast, other film/resin techniques remove intact proteins from the artefacts, but the proteins have to be digested afterwards before MS analysis and identification. Major advantages of the present bioactive films are: i) they can be used without the need to transport the works of art; ii) there is no need for specific technical skills to collect the sample since functionalized sheets can be provided as dried films and moistened just before use and then simply put in contact with the work of art. The bioactive film was developed as a user-friendly device, since sampling could eventually be carried out by

* Corresponding author.
E-mail address: leila.birolo@unina.it (L. Birolo).

https://doi.org/10.1016/j.jprot.2020.104039
Received 8 April 2020; Received in revised form 15 September 2020; Accepted 29 October 2020
Available online 2 November 2020

conservators; after use, the sheet can be stored, and peptides recovered just before mass spectrometric analysis.

The proof of concept was shown with paint replicas and ancient paintings [5]. We herein demonstrate: i) the effectiveness of the functionalized film approach for identifying proteins on a wider range of historical objects and supports; ii) the possibility of using these films for characterizing their conservation state since this experimental protocol is amenable to the analysis by liquid chromatography coupled to tandem mass spectrometry (LC-MS/MS) that is routinely used to confidently identify and localize chemical modifications in proteins; iii) that the use of trypsin functionalized films can be integrated with sheets that have been functionalized with other auxiliary enzymes, such as glycosidases.

Although intrinsically limited to the analysis of the top or immediately next layers, since immobilized trypsin will likely not migrate into the lower layers, the use of functionalized films can be a method of choice whenever physical sampling is not allowed or where information on the lower layers is not needed.

Thus, the overall goal of the present work is to determine i) if relevant analytical information can be obtained and whether the obtained data is comparable to data obtained with other sampling methods, and ii) what, if any, surface alteration occurs to provide guidelines to users as to the suitability of the method in a particular circumstance.

2. Materials and methods

2.1. Samples

A list of the samples herein analysed, with the details of the scope of the specific analysis and the technique is given in Table 1.

Paper samples (Barcham & Green Langley Handmade paper) were brush coated with isinglass, albumen and casein fixatives prepared according to historical methods. The albumen photograph was from a study collection and known to have an albumen coating. Ivory samples from walrus, mammoth and elephant were obtained commercially (Boone Trading Company, Brinnon, WA) and were not prepared in any way except to clean the surface with an alcohol swab prior to analysis. Pictures of the sampled objects are shown in the supplementary materials Figs. S1–S5.

A sample of the lining of historical canvas was taken from the back of an oil painting of "The Virgin and Child, Saints and Cherubins" (an artwork confiscated from Neapolitan mafia) stored in the storehouse of the Cultural Heritage Superintendence of Naples. The painting is attributed to the school of Solimena and can be dated back to 1700. A picture of the sample is reported in the supplementary materials Fig. S6.

A fragment was collected from the painted external layers of a yellow coffin that belonged to the Drosso-Picchianti Collection, at Museo Archeologico Nazionale di Napoli (MANN) [10]. The artefact is an inner anthropoid coffin and belongs to a specific type known as a "yellow coffin" because of a rich decoration painted on a yellow priming layer. A picture of the coffin can be found in [10]. The realization technique of the yellow coffin under study involves different layers; starting from the internal wooden parts there is a first layer (called *mouna*) essentially made of vegetable fibres, then the white preparative layer (made of anhydrite mixed with arabic gum), and finally the yellow background and the external layers of polychromies (analysed in the present study). Coating were probably made of natural (non colored) varnishes [10]. According to its iconography and inscriptions, the coffin is datable by the end of the XXIst and the beginning of the XXIInd Dynasty. (Niwiński, Nicola, and Egizio 2004; *AA.VV. Guida alla collezione egizia del MANN* 2016; Cantilena and Rubino 1989). We analysed a fragment from the surface layer of the yellow coffin (sample A from [10]) to simulate the possibility of *in situ* analysis of the surface of the coffin without removing the pieces from the coffin itself.

3. Procedures

3.1. Hydrophobin production

The protein Vmh2 was extracted from the mycelium of *Pleurotus ostreatus* as reported by Gravagnuolo et al. [11].

3.2. Enzyme immobilization

Trypsin was immobilized on Vmh2 coated cellulose acetate surface as previously reported [5]. Peptide:N-glycosidase F (PNGaseF) was immobilized on Vmh2 coated cellulose acetate surface following a very similar procedure. Briefly, 200 μl of 500 U/ml of PNGaseF solution in 10 mM of sodium phosphate pH 7.5 were deposited for 5 min on the Vmh2 coated surface (0.5 × 0.5 cm). After incubation, the surface was washed with 500 μl of 10 mM of sodium phosphate and left to dry at room temperature. As for trypsin activation, a solution of 50 mM of ammonium bicarbonate pH 7.8 (AMBIC) was sprayed on the PNGaseF biofunctionalized surface to restore the optimal environment for the enzymatic activity.

Table 1
Summary of samples, type of functionalized films, their dimension, the mass spectrometric analysis and its scope.

Samples	Dimension of functionalized surface	Type of functionalized film	Analysis	Scope of the analysis
Casein fixed paper	1st set: 400mm^2 2nd set: 100 and 25mm^2	Trypsin functionalized film	MALDI-TOF	Protein identification
Isinglass fixed paper	1st set: 400mm^2 2nd set: 100 and 25mm^2	Trypsin functionalized film	MALDI-TOF	Protein identification
Mammoth, ivory samples	1st set: 400mm^2 2nd set: 100 and 25mm^2	Trypsin functionalized film	MALDI-TOF	Protein identification
Walrus ivory samples	1st set: 400mm^2 2nd set: 100 and 25mm^2	Trypsin functionalized film	MALDI-TOF	Protein identification
Elephant ivory samples	1st set: 400mm^2 2nd set: 100 and 25mm^2	Trypsin functionalized film	MALDI-TOF	Protein identification
Lining of Canvas "The Virgin and Child, Saints and Cherubins"	400mm^2	Trypsin functionalized film	LC-MS/MS GC–MS	Protein identification Chemical modifications identification Glycation products
Fragment A of a yellow coffin [10]	400mm^2 (trypsin), 400mm^2 (PNGaseF)	Trypsin and PNGaseF functionalized films	LC-MS/MS	Protein identification Chemical modifications identification Test of the PNGaseF functionalized film for the removal of glycosilation
Egg based painting mock-up with azurite [5]	400mm^2 (trypsin), 400mm^2 (PNGaseF)	Trypsin and PNGaseF functionalized films	MALDI-TOF	Test of the PNGaseF functionalized film for the removal of glycosilation

3.3. In situ trypsin hydrolyses on fixative-coated paper, the albumen photograph, and ivory samples

First set: Large film pieces, ~400mm^2 (20x20mm), were spray-moistened with 50 mM AMBIC and applied to the surface being analysed for 10 min. For irregular surfaces, the films were held in place with tweezers to maintain as much surface contact as possible. Films were removed and air dried, and peptides were solubilized from the surface with 25 μl 50 mM AMBIC. Second set: Smaller film pieces were cut from the original 400mm^2 pieces into ~100mm^2 and ~ 25 mm^2 pieces. Rather than spray moistening the films, 5 μl AMBIC (100 mm^2 films) or 2 μl AMBIC (25 mm^2 films) was pipetted onto the surface being sampled, and the film were placed on top for 10 min. Films were then placed into Eppendorf tubes with 25 μl AMBIC, vortexed to extract peptides, dried under air and the films removed. The solubilized peptides in Eppendorf tubes were taken to dryness under a stream of air and resolubilized with 10 μl 0.1% TFA (trifluoroacetic acid). For both sets, MALDI samples were prepared by the addition of 3 μl of the peptides in 0.1% TFA to 20 μl of matrix solution (40% acetonitrile, 0.1% TFA, saturated alpha-Cyano-4-hydroxycinnamic acid) and then spotted onto the MALDI plate.

3.4. In situ hydrolyses on paint replica, historical canvas and fragments from the surface of yellow coffin

When requested, pretreatment of samples with PNGaseF functionalized surface was carried out, similarly to the procedure for tryptic digestion, by putting the sample in direct contact with the PNGaseF functionalized surface for 10 min at room temperature. Then, samples underwent tryptic digestion with the trypsin functionalized film. Digestion was carried out as reported in [5] and peptides recovered in 25–50 μl of AMBIC. For irregular surfaces, the films were held in place with tweezers to maintain as much surface contact as possible. PNGaseF and trypsin hydrolyses in heterogeneous phase (enzyme solution in AMBIC on solid samples) were carried out as reported in [12] on 10 μg of scraping of the lining of the canvas.

3.5. Polysaccharides analysis

The lining of historical canvas was subjected to ammonia extraction following the protocol by [13] with slight changes. Briefly, 400 μl of 2.5 M NH_3 were added to 1 mg of scraping of the lining of the canvas and incubated in an ultrasonic bath at RT for 30 min and afterwards in a water bath for 120 min. This step was repeated twice, and the supernatants combined. The extract is evaporated to dryness under vacuum and a further liquid-liquid extraction is carried out by the addition of 100 μl 1% TFA and 200 μl of diethyl ether (three times). The acid solution (containing proteins, polysaccharides, and free organic salts) is combined with the insoluble extract from the first step. Subsequently, proteins are separated from polysaccharides with MeOH precipitation by the addition of 200 μl MeOH at −20 °C for 120 min. 100 μl of the polysaccharides containing fraction were dried under vacuum and submitted to methanolysis. The reaction was performed by combining the samples with 500 μl of methanolic HCl (125 μl of acetyl chloride in 2.5 ml of anhydrous methyl alcohol); the re-*N*-acetylation of the monosaccharides mixture was performed by adding 500 μl of methanol, 10 μl of pyridine and 50 μl of acetic anhydride at room temperature for 15 min. Sugars were finally trimethylsilylated in 200 μl of *N,O*-bis-(trimethylsilyl)-acetamide (TMSA) at 70 °C for 15 min. The sample was dried under nitrogen, dissolved in 50 μl of hexane and centrifuged to remove the excess of solid reagents. The hexane supernatant (1/60) was used for the GC–MS analysis.

4. Mass spectrometric analyses

4.1. Gas chromatography-mass spectrometry (GC–MS)

GC–MS analyses were performed on an ISQ-QD quadrupole mass spectrometer (Thermo Fisher scientific) equipped with a TRACE™ 1300 Gas Chromatograph using a Zebron ZB-5HT Inferno (5%-Phenyl-95%-Dimethylpolysiloxane) fused silica capillary column (Column 30 m × 0.32 mm × 0.10 μm) from Phenomenex.

The injection temperature was 250 °C, the oven temperature was held at 70 °C for 2 min and then increased to 230 °C at 20 °C/min, increasing to 240 °C at 20 °C/min and finally to 270 °C at 20 °C/min and held for 3 min. Electron Ionization mass spectra were recorded by continuous quadrupole scanning at 70 eV ionization energy, in the mass range of m/z 30–800. Mass spectra assignment was generally based on the direct match with the spectra of NIST library. If the correlation match index was higher than 95%, the identification was considered reliable.

MALDI-TOF analyses were carried out on a 5800 MALDI TOF/TOF instrument (Sciex, Framingham, MA) as reported in [5]. Data analysis was done using the mMass freeware program [14]. Marker ions used for material identification are collected and validated from several sources including published research data and protein sequences, liquid chromatography coupled to tandem mass spectrometry (LC-MS/MS) data from known samples, and analysis of known reference samples. See Supplementary Material Table S-1 for reference details.

4.2. Peptide mass fingerprint (PMF) analysis

PMF is used to identify proteins and simple protein mixtures through the use of marker ions produced by peptides, which are validated indicators for specific proteins. Markers for common proteinaceous materials found in artworks, such egg tempera, casein and animal glues, have been published [5,15] and are shown in Table S-1. These have been used in several recent applications [15–17] as well as in the first development of this functionalized film methodology [5]. PMF is also used routinely in archaeology and cultural heritage to identify mammalian sources of collagen-based [18] materials, wherein marker ion can identify to the family level, in some cases, and to species level in others.

In case of the egg based painting mock-up sample, PMF was carried out with a licensed version of Mascot software (www.matrixscience.com) version 2.4.0. Proteins were identified using a `Gallus gallus` database (29,476 sequences; 15,469,207 residues). Mascot search parameters were: peptide mass tolerance 100 ppm, allowed trypsin missed cleavages up to 3. No fixed chemical modification was inserted, but possible oxidation of methionine residues and deamidation of asparagine and glutamine were considered as variable modifications.

4.3. Liquid chromatography coupled to tandem mass spectrometry (LC-MS/MS)

For LC-MS/MS analysis, the recovered peptides were filtered on 0.22 μm PVDF membrane (Millipore), and peptides were desalted and concentrated on in-house made C18 extraction stage tips [19]. To increase peptides recovery, the unbound fraction from the stage tips was loaded on a reverse-phase C18 Zip Tip pipet tip (Millipore). Peptides were eluted with 20 μL of a solution made of 50% acetonitrile, 50% formic acid 0.1% in Milli-Q water and combined with the eluted fraction from stage tips, dried under vacuum, and finally dissolved in 0.1% of formic acid.

LC – MS/MS analyses were carried out on a 6520 Accurate-Mass Q-TOF LC/MS System (Agilent Technologies, Palo Alto, CA) equipped with a 1200 HPLC system and a chip cube (Agilent *Technologies*) and on a LTQ Orbitrap-XL (ThermoScientific, Bremen, Germany) as reported in [20], and raw data analyses as reported in [12]. Each LC – MS/MS analysis

was preceded and followed by blank runs to avoid carryover contamination. MS/MS spectra were transformed in Mascot Generic files (.mgf) format and routinely used to query the SwissProt database 2015_04 (548,208 sequences; 195,282,524 residues), with Chordata as the taxonomy restriction for protein identification. A licensed version of Mascot software (www.matrixscience.com) version 2.4.0 was used. Standard parameters in the searches were trypsin as the enzyme; 3, as allowed number of missed cleavages; 10 ppm MS tolerance and 0.6 Da MS/MS tolerance; peptide charge from 2+ to 3+. In all the database searches, no fixed chemical modification was inserted, but possible oxidation of methionine residues and deamidation at asparagines and glutamines were considered as variable modifications. When collagen proteins were identified, further identification runs were carried out with the insertion of hydroxylation on lysine and proline as variable modifications, since more confident identifications are commonly obtained for these proteins by taking into consideration their extensive posttranslational modifications. Moreover, to reduce the search space, these runs were carried out using a homemade database, which we named COLLE (60 sequences; 88,859 residues), that collects all the common domesticates used for animal glue. When egg proteins were detected, identification was carried out using a *Gallus gallus* database (29,476 sequences; 15,469,207 residues) with sequences provided from the UniProtKB/Swiss-Prot protein database (www.uniprot.org).

Other parameter changes for the specific database searches are indicated in the Table captions. Only proteins presenting two or more peptides were considered as positively identified. Protein scores are derived from ions scores as a non- probabilistic basis for ranking protein hits. (http://www.matrixscience.com/help/interpretation_help.html). Ions score is −10*Log(P), where P is the probability that the observed peptide match is a random event. Individual ion score threshold provided by Mascot software to evaluate the quality of matches in MS/MS data was used for confidence threshold in protein identification.

Deamidation rates for Asparagine (N) and Glutamine (Q) for individual samples was semi-quantitatively evaluated as variable modifications from MaxQuant's "evidence.txt" file with a code that is freely available on GitHub (https://github.com/dblyon/deamidation). Semi quantitative evaluation is based on calculation of all modification states of all identified peptides that contain N and Q [21].

5. Results and discussion

5.1. Use of trypsin-functionalized films for protein identification of different types of samples

The trypsin functionalized films were evaluated for their ability to detect and identify proteinaceous materials on objects from cultural heritage, including fixative-coated paper (albumen, casein and isinglass), an albumen photograph, and ivory from elephant, mammoth and walrus. These samples were chosen because they are sample types of interest and importance in art and cultural heritage where minimal sampling is usually a necessity. Moreover, species identification of elephantid ivory and their products is still a challenging question and is essential to combat illegal ivory trade [22]. Molecular approaches as simple as the functionalized film combined with PMF are very attractive. Also, the same samples have been used previously to evaluate other minimally invasive techniques, so there was a basis for evaluating the results with the functionalized films. For these initial evaluations, alteration of the sampled surface was observed without magnification: paper and photograph with raking light, polished ivory surfaces with strong reflected light. Ultimately, more stringent observation will be necessary to accurately inform users of any consequences of this minimally invasive procedure.

A first set of specimens (photograph, fixed paper and ivory) was analysed by PMF using 400 mm^2 (20 x 20 mm) film pieces, and proteins were identified by visual inspection of MALDI spectra for marker ions.

Intense spectra were obtained for all the objects and surfaces tested, and all spectra were comparable to those obtained with other sampling methods on the same specimen. No visible alteration of the surfaces of the ivory objects was observed. With the fixative coated papers, the area under the film became slightly swollen, and this mitigates as the paper dries. For the albumen photograph, the surface under the film was heavily distorted, as anticipated, because albumen coatings on prints are known to be very moisture sensitive. Subsequent analyses with small film pieces lessened the effect on paper and the photograph.

The spectrum reported in Fig. 1, which is from the casein-fixed paper with casein markers indicated [15,18], is an example of the high quality of the MALDI data obtained with the first set of samples. The other samples gave results of similar quality. Keratin was noted in some of the samples. This contaminant largely originates from dust/dirt accumulation, typically epithelial keratin, and does not interfere with data interpretation.

Given the high detection sensitivity observed with the first set of samples, a second set was analysed with smaller film pieces (100mm^2 or 25mm^2) and reduced quantities of AMBIC (5 μl for 100 mm^2 films and 2 μl for 25 mm^2 films, respectively). The AMBIC solution was pipetted directly onto the surface/object being sampled, and the film was placed on top for 10 min. As noted above, with the smaller film formats the film was then placed directly into the Eppendorf tube thus improving the overall recovery of produced peptides. The results for 100mm^2 and 25mm^2 films were very similar, and the high quality of the spectra at these reduced film sizes indicates that further size reduction will be possible, further minimizing alteration of the surfaces being sampled. Again, spectra from the second set were comparable with spectra from the same specimen with other sampling methods (see Fig. 2).

With this second set using smaller film pieces, there was no visible alteration of the ivory surfaces, very slight "pillowing" of the paper surfaces at the point of contact that quickly disappeared, and moderate swelling of the albumen photograph at the point of contact that persisted. With even smaller film pieces as a possibility, the effect on the paper and photograph would be expected to diminish further. Although surface alteration might not disappear completely with these specimens, there may be situations where sampling could still be an option. Fig. 2 compares the results from 100mm^2 and 25mm^2 film samples of the casein-fixed paper surface. The inset compares the relative signal-to-noise ratio (S/N) calculated by the mMass program observed for two of the weaker ions with the different film sizes.

Figs. S7–S9 are MALDI spectra from ivory, the albumen photograph, and the isinglass-fixed paper, respectively, obtained using the smallest (25mm^2) film pieces. Albumen and isinglass are identified with markers from Table S1. Elephant ivory is identified with marker ions from a published reference [23].

It is worth noting the high quality of the spectra obtained, considering that no sample cleanup or concentration, for example using Zip Tips, was done before analyzing the analysis. The peptide mixtures were simply collected from the trypsin functionalized film, dried, resolubilized, mixed with matrix and spotted on the MALDI plate. Given the high sensitivity observed with the smallest film pieces (25mm^2), it seems very likely that even smaller formats will be possible, further limiting the impact on sensitive surfaces and allowing analysis of smaller features.

5.2. The trypsin-functionalized film can be used for the characterization of ancient proteins

The trypsin functionalized film has been shown to be amenable for protein identification in several artistic objects, even by a simple MALDI-TOF analysis, without requiring fragmentation spectra, thus showing up as an extremely interesting and powerful tool for all stakeholders in cultural heritage interested in understanding the composition of works of art.

However, the story and the interest in ancient proteins might not stop at the identification level. It is now more and more common that, beside understanding the composing material, chemical analyses must

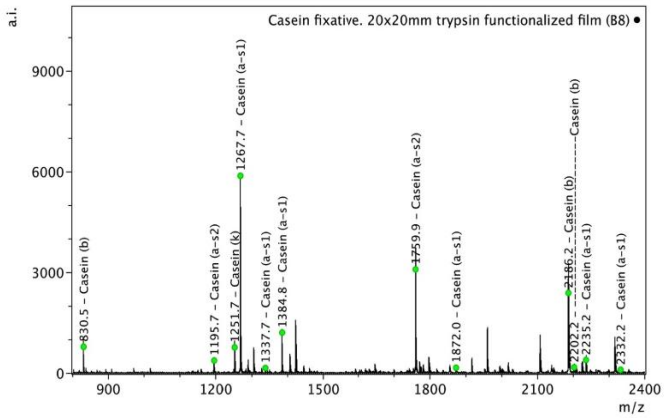

Fig. 1. MALDI spectrum from casein-fixed paper sampled with a 400mm^2 trypsin functionalized film. Major casein marker ions derived from published sequences (see Table S1) are indicated: a-S1: alpha casein S1 (P02662), a-s2: alpha casein S2 (P02663), b: beta casein (P02666) and k: kappa casein (P02668).

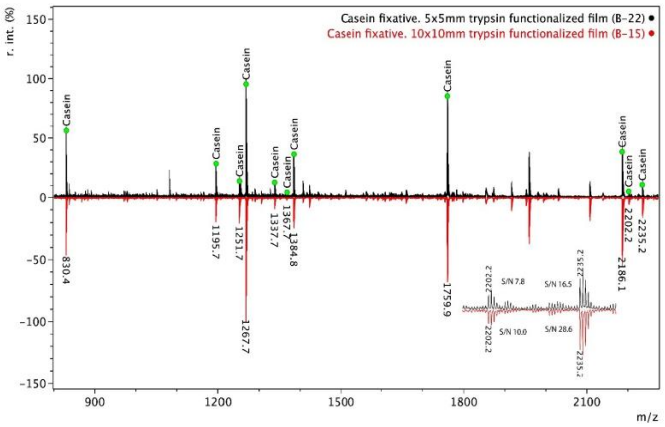

Fig. 2. MALDI spectrum from the casein-fixed paper. Upper, black, 25mm^2 film. Lower, red, 100mm^2 film. The inset shows the 2202 Da and 2235 Da ions to compare the relative S/N observed with the larger (lower) and smaller (upper) film sizes. Casein markers are the same as noted in Fig. 1. (For interpretation of the references to colour in this figure legend, the reader is referred to the web version of this article.)

face the challenge of understanding at the molecular level the conservation state of the work of art [2]. This is at the basis of a wide range of questions, from authentication to restoration interventions. To face this challenging issue, the peptide mixtures recovered from the film are usually analysed by LC-MS/MS, since unambiguous identification and localization in the peptide sequence of chemical modifications that can be considered as markers of degradations, such as oxidations, deamidations or spontaneous hydrolysis, strongly benefit from the analysis of fragmentation spectra [2]. Moreover, LC-MS/MS analysis is crucial in providing unambiguous identifications of complex samples with proteins in mixture, where MS analysis without MSMS, and thereof sequence information, can fail [2]. Therefore, to verify whether the peptide mixtures recovered from the trypsin functionalized films are amenable to LC-MS/MS analysis, a sample from a lining material of the historical canvas "The Virgin and Child, Saints and Cherubins", that dates back to 1700, that was under investigation for the presence of proteinaceous binder, was digested with the trypsin functionalized flexible sheet and the recovered supernatant analysed by LC-MS/MS. The results were compared to those obtained with a parallel experiment where an aqueous trypsin solution was directly added to an aliquot of the same solid sample in a conventional digestion procedure in heterogeneous phase [24], that requires microinvasive sampling of the object. A summary of the identification results is shown in Table 2, and the details of the identifications are reported in the supplementary results (Table S2-S3).

Hide glue from sheep was unambiguously identified since type I and type III collagens from *Ovis aries* were detected. Good confidence was obtained in both cases, although, not unexpectedly, identification was

Table 2
Identification of proteins in the lining of the historical canvas "The Virgin and Child, Saints and Cherubins" by LC-MS/MS.

Sample	Protein (Uniprot entry)	Digestion with the Trypsin functionalized film				Overnight digestion in heterogenous phase			
		Score	Sequence coverage (PSC) (%)	No. of peptides	No. of unique peptides	Score	Protein coverage (PSC) (%)	No. of peptides	No. of unique peptides
Lining of the canvas "The Virgin and Child, Saints and Cherubins"	Collagen 1(I) (W5P481)	1223	27	26	4	2621	53	53	2
	Collagen 2(I) (W5NTT7)	757	22	19	4	2847	43	36	5
	Collagen 1(III) (W5Q4S0)	597	15	14	5	1212	29	30	5

Comparison of results by LC-MS/MS of digestion with the trypsin functionalized film and standard digestion in heterogeneous phase. Raw data were searched by Mascot MS/MS Ion search using the homemade COLLE database. Identification details are reported in Table S2–S3.

on average better with the digestion in heterogeneous phase, possibly also because of the much longer incubation time (o/n digestion *versus* 10 min, roughly ground samples to expose larger surface, constant 37 °C incubation, *etc.*).

Despite the lower yield in peptides, we demonstrated that data collected from LC-MS/MS analysis of the samples recovered from the trypsin- functionalized film are able to be used for characterizing the degradation state of the proteins inside the samples. MS/MS data were indeed used to search for common chemical modifications that are classically linked to molecular damage patterns, such as deamidation at asparagine (N) and glutamine (Q) residues [21,25], spontaneous hydrolysis [26,27], and glycation at lysine (Lys) and arginine (Arg) [21,26].

As it can be seen from Fig. 3, the levels of collagen deamidation that can be calculated are comparable between the two protocols, meaning that, despite the lower yield in peptides with the film, there is no bias in extracting deamidated rather than unmodified peptides in the samples. Interestingly, both protocols demonstrate a remarkably high level of deamidation both for N and Q. Glue preparation frequently involves prolonged boiling of animal connective tissue that would significantly increase the rate of deamidation [28]. The observed deamidation level is therefore the sum of heating during animal glue preparation and aging.

This result is extremely important since deamidation is actually considered an indicator of "authentical age" [2,25] of the sample, although we embrace the sense by Schroeter and colleagues [29] that deamidation should be rather viewed as a global indicator of their preservational quality, since deamidation rates and levels are greatly affected by numerous chemical and environmental factors.

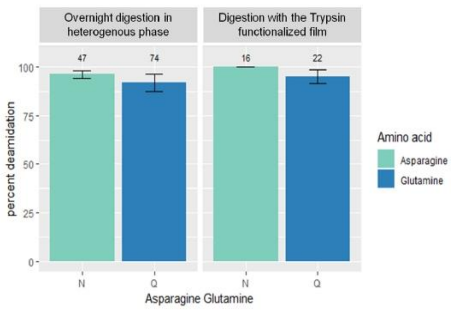

Fig. 3. Overall percentage of deamidation for asparagine (N) and Glutamine (Q) residues for the proteins identified on the surface of the lining material of the historical canvas "The Virgin and Child, Saints and Cherubins". Comparison of deamidation level between the peptide mixtures obtained with the trypsin functionalized film in comparison and a standard digestion in heterogeneous phase. Error bars represent standard deviation and numbers above the bars represent the number of peptides containing N and Q on which the data was based on [21].

We also searched for spontaneous hydrolysis and modifications such as glycation, both non-enzymatic modifications well known to occur upon aging/deterioration. Table 3 reports the results of the search for semitryptic peptides, which are the hallmark for partially hydrolyzed proteins [26,27].

It is worth mentioning that, when semitryptic peptides are considered for protein score computation, the results became almost comparable. However, if we go into the details, the trypsin functionalized film seems to extract a larger number of "damaged" peptides, since semitryptic peptides exceed 80% of the detected peptides with the film *versus* the 50% of the peptides observed with the standard protocol in heterogeneous phase. A plausible explanation might lie in the fact that, during the digestion in heterogeneous phase, trypsin in solution is likely to penetrate more deeply into the layer, whereas when immobilized on the film it might attack only the external, and therefore possibly more degraded, surface of the object. This aspect is beyond the scope of the present paper and deserves further investigation, both to understand how deep the trypsin can go and to explore the possibility of discriminating the protein content and degradation state among different layers.

Even more interesting is the observation that almost all the glycation products, arising from exposure of proteins to sugars, were detected on semitryptic peptides. Tables S6-S7 illustrate the peptides where advanced glycation end-products (AGEs) of lysine and arginine were found. A wide set of AGEs was detected in the sample from trypsin functionalized film: glycation of arginine with the formation of glyoxal and methylglyoxal adduct (mass shift of +39.99 and + 54.01 Da respectively), as well as formation of carboxymethyl and carboxyethyl lysine (with mass shift of +72.01 and + 58.01 Da, respectively). As an example, the fragmentation spectra of a glyoxal and methylglyoxal modified peptide is reported in Fig. S10.

Glycation products are consistent with the presence of sugars as identified by GC–MS analysis (Fig. 4). In particular, arabinose, xylose, mannose and glucose were detected, that, according to the literature [30], might be interpreted as the presence of some plant gum in the binding media of the historical canvas. We suggest that some protein glycation might arise from the binding of reducing sugars from gum to proteins in the complex mixture of the painting media.

Conclusively, we suggest that the trypsin functionalized film can be used to gain information on chemical modifications of proteins on the surface of an artistic object and therefore on its degradation state and not only to merely identify the protein component.

5.3. Development and implementation of the approach

The success of proteomics experiments in cultural heritage objects lies in the efficiency of either protein extraction from solid matrixes or direct digestion of proteins still incorporated inside the matrix itself. In this respect, we already observed that glycosylation of egg proteins created a significant molecular hindrance which hampered proteases to

Table 3
Comparison of spontaneous hydrolysis in proteins in a lining of the historical canvas "The Virgin and Child, Saints and Cherubins" by LC-MS/MS.

		Digestion with the Trypsin functionalized film				Overnight digestion in heterogenous phase			
Sample	Protein (Uniprot entry)	Score	PSC (%)	No. of peptides	No. of semitryptic peptides	Score	PSC (%)	No. of peptides	No. of semitryptic peptides
Lining of the canvas "The Virgin and Child, Saints and Cherubins"	Collagen 1(I) (W5P481)	3970	48	113	90	3852	55	120	55
	Collagen 2(I) (W5NTT7)	2326	43	75	57	2507	52	74	34
	Collagen 1(III) (W5Q4S0)	1286	40	55	35	1468	35	51	18

LC-MS/MS raw data were searched by Mascot MS/MS Ion search using the homemade COLLE database and considering semitrypsin as the enzyme. Identification details are reported in Table S4–S5.

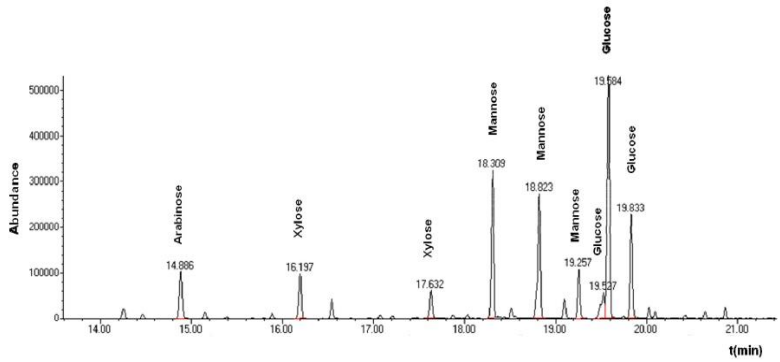

Fig. 4. Sugar analysis of the sample from the lining of the historical canvas "The Virgin and Child, Saints and Cherubins" by GC–MS. GC-TIC chromatogram of TMS sugars identified in the historical canvas. Annotation of the sugars was performed by comparing both the retention times and the fragmentation spectra of the sugars with analytical standards.

efficiently interact with the proteinaceous substrates, thus greatly decreasing proteolytic efficiency and therefore reducing the confidence of protein identification [12]. In these cases, in the standard solution approach, we bypassed the problem of obtaining a reliable identification by introducing a deglycosylation step before treatment with trypsin. We explored the possibility of introducing similarly a treatment with PNGaseF to get rid of the sugar coating that, as we suggested, seems to prevent the accessibility of proteases. We adopted a similar strategy by immobilizing PNGaseF on a separate cellulose acetate sheet to trim out the glycosidic decoration before proceeding with the trypsin functionalized film in a two-step procedure.

The PNGaseF functionalized film was first tested on an egg-based painting mock-up that contained azurite as pigment. Briefly, the sample was placed in contact with the PNGaseF functionalized film for ten minutes and subsequently in contact with the trypsin functionalized film for 10 min. As a control, the same sample was also analysed with only the trypsin functionalized film. MALDI-TOF analysis of the recovered supernatants was then recorded as a pre-screening, and Fig. S11 demonstrates a richer spectrum, in terms of number of ions and identified peptides, in the case where the PNGaseF functionalized film was used. The peptides in table S8 confirmed the presence of several proteins of *Gallus gallus* in the sample, digested with trypsin functionalized films

Table 4
Proteins identified in the painting egg-based painting mock-up sample by LC − MS/MS.

		PNGaseF functionalized film + Trypsin functionalized film				Trypsin functionalized film			
Sample	Protein (Uniprot entry)	Score	PSC (%)	No. of peptides	No. of unique peptides	Score	PSC (%)	No. of peptides	No. of unique peptides
Egg based painting mock-up with azurite	Ovalbumin (P01012)	446	47	15	9	252	30	9	8
	Ovotransferrin (P02789)	186	13	9	8	117	7	6	5
	Ovalbumin-related protein Y (P01014)	168	13	7	6	ND	ND	ND	ND
	Elongation factor 1-alpha 1 (Q90895)	74	7	4	4	57	4	2	2
	Ubiquitin (P79781)	49	19	2	2	ND	ND	ND	ND
	Ovalbumin (P01012)	446	47	15	9	252	30	9	8

Comparison of LC-MS/MS analyses with the trypsin functionalized film with or without pretreatment with immobilized PNGaseF. Raw data were searched by Mascot MS/MS Ion search using Chordata as the taxonomic restriction in the SwissProt protein database. ND: not detected. Details of the identification are given in Table S9 and S10.

after the treatment with immobilized PNGaseF. Therefore, even in this more elaborated configuration, it is possible to successfully analyze samples with a simple, rapid, sensitive and specific approach such as Peptide Mass Fingerprinting, amenable to a museum laboratory, and that can be practiced successfully even by non-specialists.

LC-MS/MS analysis (Table 4) confirmed the effectiveness of the deglycosylation pretreatment step with immobilized PNGaseF on functionalized films, since more proteins were identified when the sample was pretreated with PNGaseF and all more confidently. Details are reported in Table S9-10.

The combination of PNGaseF and trypsin immobilized on cellulose acetate sheets was explored on the decoration of a micro-sample collected from of XXII dynasty wooden coffin (yellow coffin), where egg proteins had been recently identified with the standard protocol in heterogeneous phase, and GCMS analysis had also detected the copresence of rabic gum (reference: sample Sarcofago A in the paper by Melchiorre *et al* [10]). As a further control, the same sample was also digested only with the trypsin functionalized film. The recovered peptides were subjected to LC-MS/MS analysis, since preliminary PMF analysis did not provide satisfactory results, as could be expected from the complex mixture of proteins that LC-MS/MS analysis revealed (Table 5 and details reported in Tables S11-12). Identifications are in agreement with the already published data [10] where trypsin digestion was carried out in heterogeneous phase. We can say that the trypsin functionalized film, (even in the absence of the pretreatment with PNGaseF), is also effective on proteins in the decoration of a wooden surface, since the physical support of the coffin is wood, thus demonstrating again its versatility of use. However, most importantly, it is worth mentioning that trypsin functionalized films and, even more, the combination of PNGaseF plus trypsin functionalized films, produced more confident identifications compared to what we previously reported [10], since numerous proteins from *Gallus gallus* were identified, assessing an unambiguous chicken origin, while in previous experiments lysozyme was the only egg protein detected. Moreover, a clear identification of several collagen chains confirms that a mixture of egg and animal glue was present, accordingly to what had already been observed [10].

6. Conclusion

Trypsin very efficiently works when immobilized on a cellulose acetate sheet with the further benefit that digested peptides are thoroughly captured on the functionalized surface. These are the major advantages of the functionalized films, which we have demonstrated can work on the surfaces of different objects such as albumen, isinglass and casein used as fixatives on paper, the much harder surface of ivory objects, or the proteinaceous binders on a wooden Egyptian coffin. We simulated analyses that can now confidently be carried out directly on the surfaces of the objects in their actual location (namely museums or archaeological sites) and without sample removal from the artefact.

The obtained hydrolysate is definitely comparable to that which is obtained from a standard proteomic approach and is amenable to Peptide Mass Fingerprinting by simple MALDI-TOF analysis as well as to LC-MS/MS analysis of the same peptide mixture. PMF, one of the modern techniques for protein analysis recently introduced into conservation science, is advantageous because of its sensitivity and specificity, speed of analysis, and relatively low cost. However, for more challenging questions, such as the identification of chemical modifications, useful for characterizing the conservation state of proteins or the analysis of more complex protein mixtures, LC-MS/MS is required. We have demonstrated that protein digestion with the functionalized films is fully adequate to both mass spectrometric techniques. Moreover, the functionalized film is amenable to further implementation and modularity: herein we have combined the trypsin functionalized film with a PNGaseF functionalized film thus integrating the deglycosylation pretreatment to improve detection of glycosylated coated proteins. The impact of sampling on sensitive surfaces is extremely relevant in the field of cultural heritage. The minimal sample requirements for current methods of analysis are making it possible to study art and objects where the consequences of removing even micro-amounts of material can be prohibitive. Thus, developing methods for sampling sensitive objects is still an important issue for conservation, and the results from the use of trypsin-functionalized films show great promise. Further development of the present version will focus on further reduction of film dimensions to minimize surface contact and make the technique usable for smaller objects and features. Concomitant with smaller films, smaller volumes of liquid will be used, minimizing effects on sensitive surfaces such as paper and photographs.

In conclusion, we have demonstrated that the enzyme functionalized film is a versatile, user-friendly and modular tool that can be widely exploited in the world of diagnosis of cultural heritage objects. We have shown that relevant analytical information can be obtained, and we have indicated what the consequences of using the films on a variety of different surfaces may be.

Author contributions

G.N, L.B., P.G., D.K. G.M. Conceptualization; G.N., D.K., I.S., P.C. Investigation and Data curation; G.N., D.K., I.S., A.C., P.S., P.C., P.G., L. B. Formal analysis; G.N., D.K., I.S., A.C., P.C., P.G., G.M., L.B Writing - review & editing; L.B. Funding acquisition and Project administration.

Table 5
Proteins identified in the fragments of the painted surface of yellow coffin collected from the decoration of a XXII dynasty wood Sarcophagus (yellow coffin) with the combination of PNGaseF and trypsin functionalized films in comparison with the use of trypsin functionalized film alone.

Fragments of the painted surface of yellow coffin	Protein (Uniprot entry)	Score	Sequences	Unique sequences	Protein sequence coverage (PSC) (%)
PNGAseF + Trypsin functionalized films	Ovalbumin (P01012)	26	4	2	15
	Ubiquitin (P79781)	45	2	2	20
	ATP synthase subunit beta (Q5ZLC5)	34	2	2	5
	Vitellogenin 2 (P02845)	20	4	4	2
	Collagen 1(I) (*Bos taurus*) (P02453)	101	5	0	9
	Collagen 2 (I) (*Bos taurus*) (P02465)	78	5	0	9
	Collagen 2 (I) (*Gallus gallus*) (P02460)	37	2	1	2
	Collagen 1 (III) (*Gallus gallus*) (P12105)	32	2	1	3
	Collagen 1 (I) (*Gallus gallus*) (P02457)	15	2	2	4
Trypsin functionalized films	Ovalbumin (P01012)	69	3	3	6
	Collagen 2 (I) (*Bos taurus*) (P02465)	63	4	0	7

Sample fragments were digested *in situ* with the trypsin functionalized film with or without pretreatment with PNGaseF functionalized film and peptide mixtures were analysed by LC – MS/MS. Raw data were searched by Mascot MS/MS Ion search using Chordata as the taxonomic restriction in the SwissProt protein database. Since collagen was detected, further searches were carried out using the homemade COLLE database considering also hydroxylation at Pro and Lys as variable modifications. Collagen results therefore refer to the homemade COLLE database analysis. Identification details are reported in Table S11 and S12.

Declaration of competing interest

The authors declare to have no conflict of interest.

Acknowledgments

This project has received funding from the European Union's Horizon 2020 Research and Innovation Program under the Marie Sklodowska- Curie Grant Agreement No. 722606, TEMPERA (Teaching Emerging Methods in Palaeoproteomics for the European Research Area), and by POR, Parco Archeologico Urbano di Napoli (PAUN). The authors want to thank Prof. Giancarlo Fatigati, Department of Humanities, University Suor Orsola Benincasa, for providing the case study sample from the yellow coffin.

LC-MS/MS data and COLLE database have been deposited to *Mendeley Data* (https://data.mendeley.com/datasets/nskhk333zp/1) with the dataset identifier 10.17632/nskhk333zp.1.

Appendix A. Supplementary data

Supplementary data to this article can be found online at https://doi.org/10.1016/j.jprot.2020.104039.

References

[1] M.P. Colombini, F. Modugno, Organic Mass Spectrometry in Art and Archeology, John Wiley & Sons, 2009, https://doi.org/10.1007/s00216-009-3185-y.
[2] S. Dallongeville, N. Garnier, C. Rolando, C. Tokarski, Proteins in art, archaeology, and paleontology: from detection to identification, Chem. Rev. 116 (2015) 2–79, https://doi.org/10.1021/acs.chemrev.5b00037.
[3] J. Hendy, F. Welker, B. Demarchi, C. Speller, C. Warinner, M.J. Collins, A guide to ancient protein studies, Nat. Ecol. Evol. 2 (2018) 791–799, https://doi.org/10.1038/s41559-018-0510-x.
[4] T.P. Cleland, E.R. Schroeter, A comparison of common mass spectrometry approaches for Paleoproteomics, J. Proteome Res. 17 (2018) 936–945, https://doi.org/10.1021/acs.jproteome.7b00703.
[5] P. Cicatiello, G. Ntasi, M. Rossi, G. Marino, P. Giardina, L. Birolo, Minimally invasive and portable method for the identification of proteins in ancient paintings, Anal. Chem. 90 (2018) 10128–10133, https://doi.org/10.1021/acs.analchem.8b01718.
[6] S. Fiddyment, B. Holsinger, C. Ruzzier, A. Devine, A. Binois, U. Albarella, R. Fischer, E. Nichols, A. Curtis, E. Cheese, M.D. Teasdale, C. Checkley-Scott, S. J. Milner, K.M. Rudy, E.J. Johnson, J. Vnouček, M. Garrison, S. McGrory, D. G. Bradley, M.J. Collins, Animal origin of 13th-century uterine vellum revealed using noninvasive peptide fingerprinting, Proc. Natl. Acad. Sci. U. S. A. 112 (2015) 15066–15071, https://doi.org/10.1073/pnas.1512264112.
[7] M. Manfredi, E. Barberis, F. Gosetti, E. Conte, G. Gatti, C. Mattu, E. Robotti, G. Zilberstein, I. Koman, S. Zilberstein, E. Marengo, P.G. Righetti, Method for noninvasive analysis of proteins and small molecules from ancient objects, Anal. Chem. 89 (2017) 3310–3317, https://doi.org/10.1021/acs.analchem.6b03722.
[8] G. Zilberstein, U. Maor, E. Baskin, A. D'Amato, P.G. Righetti, Unearthing Bulgakov's trace proteome from the master i Margarita manuscript, J. Proteome 152 (2017) 102–108, https://doi.org/10.1016/j.jprot.2016.10.019.
[9] E. Barberis, S. Baiocco, E. Conte, F. Gosetti, A. Rava, G. Zilberstein, P.G. Righetti, E. Marengo, M. Manfredi, Towards the non-invasive proteomic analysis of cultural heritage objects, Microchem. J. 139 (2018) 450–457, https://doi.org/10.1016/j.microc.2018.03.033.
[10] C. Melchiorre, L. Dello Ioio, G. Ntasi, L. Birolo, G. Trojsi, P. Cennamo, M.R. Barone Lumaga, G. Fatigati, A. Amoresano, A. Carpentieri, A multidisciplinary assessment to investigate a XXII dynasty wooden coffin, Int. J. Conserv. Sci. 11 (2020) 25–38.
[11] A.M. Gravagnuolo, S. Longobardi, A. Luchini, M.S. Appavou, L. De Stefano, E. Notomista, L. Paduano, P. Giardina, Class i hydrophobin Vmh2 adopts atypical mechanisms to self-assemble into functional amyloid fibrils, Biomacromolecules. 17 (2016) 954–964, https://doi.org/10.1021/acs.biomac.5b01632.
[12] R. Vinciguerra, E. Galano, F. Vallone, G. Greco, A. Vergara, I. Bonaduce, G. Marino, P. Pucci, A. Amoresano, L. Birolo, Deglycosylation step to improve the identification of egg proteins in art samples, Anal. Chem. 87 (2015) 10178–10182, https://doi.org/10.1021/acs.analchem.5b02423.
[13] A. Lluveras, I. Bonaduce, A. Andreotti, M.P. Colombini, GC/MS analytical procedure for the characterization of glycerolipids, natural waxes, terpenoid resins, proteinaceous and polysaccharide materials in the same paint microsample avoiding interferences from inorganic media, Anal. Chem. 82 (2010) 376–386, https://doi.org/10.1021/ac902141m.
[14] M. Strohalm, M. Hassman, B. Kosata, M. Kodicek, mMass data miner: an open source alternative for mass spectrometric data analysis, Rapid Commun. Mass Spectrom. 22 (2008) 905–908, https://doi.org/10.1002/rcm.3444.
[15] D.P. Kirby, N. Khandekar, J. Arslanoglu, K. Sutherland, Protein identification in artworks by peptide mass fingerprinting, in: Prepr. ICOM Comm. Conserv. 16th Trienn. Conf. Lisbon, 2011.
[16] D.P. Kirby, M. Buckley, E. Promise, S.A. Trauger, T.R. Holdcraft, Identification of collagen-based materials in cultural heritage, Analyst. 138 (2013) 4849–4858, https://doi.org/10.1039/c3an00925d.
[17] S. Kuckova, R. Hynek, M. Kodicek, MALDI-MS applied to the analysis of protein paint binders, in: F. Colombini, Maria Perla, Modugno (Eds.), Org. Mass Spectrom. Art Archeol., John Wiley & Sons, 2009, pp. 181–203, https://doi.org/10.1002/9780470741917.
[18] M. Buckley, M. Collins, J. Thomas-Oates, J.C. Wilson, Species identification by analysis of bone collagen using matrix-assisted laser desorption/ionisation time-of-flight mass spectrometry, Rapid Commun. Mass Spectrom. 23 (2009) 3843–3854, https://doi.org/10.1002/rcm.4316.
[19] E. Cappellini, L.J. Jensen, D. Szklarczyk, A. Ginolhac, R.A.R. Da Fonseca, T. W. Stafford, S.R. Holen, M.J. Collins, L. Orlando, E. Willerslev, M.T.P. Gilbert, J. V. Olsen, Proteomic analysis of a pleistocene mammoth femur reveals more than one hundred ancient bone proteins, J. Proteome Res. 11 (2012) 917–926, https://doi.org/10.1021/pr200721u.
[20] R. Linn, I. Bonaduce, G. Ntasi, L. Birolo, A. Yasur-Landau, E.H. Cline, A. Nevin, A. Lluveras-Tenorio, Evolved gas analysis-mass spectrometry to identify the earliest organic binder in Aegean style wall paintings, Angew. Chem. Int. Ed. 57 (2018) 13257–13260, https://doi.org/10.1002/anie.201806520.
[21] M. Mackie, P. Rüther, D. Samodova, F. Di Gianvincenzo, C. Granzotto, D. Lyon, D. A. Peggie, H. Howard, L. Harrison, L.J. Jensen, J.V. Olsen, E. Cappellini, Palaeoproteomic profiling of conservation layers on a 14th century Italian wall painting, Angew. Chem. Int. Ed. 57 (2018) 7369–7374, https://doi.org/10.1002/anie.201713020.
[22] J.N. Ngatia, T.M. Lan, Y. Ma, T.D. Dinh, Z. Wang, T.D. Dahmer, Y.C. Xu, Distinguishing extant elephants ivory from mammoth ivory using a short sequence of cytochrome b gene, Sci. Rep. (2019) 1–12, https://doi.org/10.1038/s41598-019-55094-x.
[23] M. Buckley, M.J. Collins, M.I. Biocentre, Collagen survival and its use for species identification in Holocene-lower Pleistocene bone fragments from British archaeological and paleontological sites, Antiqua. 1 (2011) 1–7, https://doi.org/10.4081/antiqua.2011.e1.
[24] G. Leo, L. Cartechini, P. Pucci, A. Sgamellotti, G. Marino, L. Birolo, Proteomic strategies for the identification of proteinaceous binders in paintings, Anal. Bioanal. Chem. 395 (2009) 2269–2280, https://doi.org/10.1007/s00216-009-3185-y.
[25] G. Leo, I. Bonaduce, A. Andreotti, G. Marino, P. Pucci, M.P. Colombini, L. Birolo, Deamidation at asparagine and glutamine as a major modification upon deterioration/aging of proteinaceous binders in mural paintings, Anal. Chem. 83 (2011) 2056–2064, https://doi.org/10.1021/ac1027275.
[26] S. Orsini, A. Yadav, M. Dilillo, L.A. McDonnell, I. Bonaduce, Characterization of degraded proteins in paintings using bottom-up proteomic approaches: new strategies for protein digestion and analysis of data, Anal. Chem. 90 (2018) 6403–6408, https://doi.org/10.1021/acs.analchem.8b00281.
[27] R. Vinciguerra, A. De Chiaro, P. Pucci, G. Marino, L. Birolo, Proteomic strategies for cultural heritage: form bones to paintings, Microchem. J. 126 (2016) 341–348, https://doi.org/10.1016/j.microc.2015.12.024.
[28] A.C.T. Van Duin, M.J. Collins, The effects of conformational constraints on aspartic acid racemization, Org. Geochem. 29 (1998) 1227–1232, https://doi.org/10.1016/S0146-6380(98)00098-9.
[29] E.R. Schroeter, T.P. Cleland, Glutamine deamidation: an indicator of antiquity, or preservational quality? Rapid Commun. Mass Spectrom. 30 (2016) 251–255, https://doi.org/10.1002/rcm.7445.
[30] A. Lluveras-Tenorio, J. Mazurek, A. Restivo, M.P. Colombini, I. Bonaduce, Analysis of plant gums and saccharide materials in paint samples: comparison of GC-MS analytical procedures and databases, Chem. Cent. J. 6 (2012) 1, https://doi.org/10.1186/1752-153X-6-115.

Chapter 4

4. Development of biosensing platforms based on ScFv chimera proteins

The marine environment, which includes the waters of seas and estuaries, the seabed and its subsoils, and all marine wildlife and its sea and coastal habitats, represents a great contributor to economic prosperity and social well-being. Nonetheless, it is extremely vulnerable to the environmental changes due to the human action for the urban and industrial development. Thus, the conservation and sustainable use of the oceans, seas and marine resources for sustainable development is the focus of the 14th Sustainable Development Goal (SDG) of the 2030 Agenda for Sustainable Development. During years, these activities contributed to marine pollution through the discharge of industrial wastewater, agricultural waste, domestic sewage and excessive fertilizer use [83]. Thus, the monitoring of contaminants in the marine environment started to be necessary, even if it is affected by some issues such as the high surface covered by the oceans, the high salinity and the extremely low concentrations of the pollutants. In addition, the delay between sampling and analysis often affects the integrity of the water samples [84]. For these reasons, the research is making efforts to develop portable systems with a high sensitivity. Among them, the biosensors could represent an *ad hoc* solution for the detection of marine pollutants. Thus, our research is involved in this field under the framework of ERA-NET Cofund MarTERA (Maritime and Marine Technologies for a new Era), with the FLAshMoB project (*Functional Amyloid chimera for Marine Biosensing)*, whose aim was the development of small, portable, easy to use, environmentally compatible, robust, and inexpensive sensing platforms to monitor marine contaminants. The innovation of the developed biosensors is based on the use of fusion proteins composed by the class I hydrophobin Vmh2 and target sensing proteins. The genetic fusion of both proteins allows the exploitation of both the adhesive capability of the hydrophobin and the specific recognition ability of the target protein, obtaining very versatile biosensors by changing the target protein. Indeed, the idea was to develop electrochemical and optical biosensors to detect Polycyclic aromatic hydrocarbons (PAHs) and Endocrine Disrupting Chemicals (EDC), arsenic, algal toxins and heavy metals using, respectively, laccase and arsenate reductase enzymes, antibodies and Glutathione-S-Transferase as fusion partners. Moreover, a further development of these biosensors was also possible exploiting the Vmh2 capability to interact, by non-covalent binding, with several nanomaterials used as transducing elements to the recognition events of these original proteins. In particular, the chosen nanomaterials were 2D-nanomaterials, such as graphene, and 3D materials, such as carbon nanotubes and magnetic nanoparticles that can enhance number of immobilized proteins per surface unit thanks to their high surface to volume ratio. Furthermore, the carbon nanomaterials-based show unique structural

features as well as exceptional chemical, electrical, mechanical and optical properties that can trigger direct electron transfers with redox enzymes.
Hence, in the following section my work related to the development of optical and electrochemical biosensors for the detection of two algal toxins is reported. These systems exploit the own characteristics of two new chimeric proteins composed by the hydrophobin Vmh2 and two Single chain Fragment Variables (ScFvs).

4.1 Immobilization of antibodies by genetic fusion to a fungal self-assembling adhesive protein

frontiers in Molecular Biosciences

ORIGINAL RESEARCH
published: 19 October 2021
doi: 10.3389/fmolb.2021.725697

Immobilization of Antibodies by Genetic Fusion to a Fungal Self-Assembling Adhesive Protein

Ilaria Stanzione[1], Daniel Izquierdo-Bote[2], María Begoña González García[2], Paola Giardina[1] and Alessandra Piscitelli[1]*

[1]Dipartimento di Scienze Chimiche, Naples, Italy, [2]Metrohm DropSens, Oviedo, Spain

Although antibody immobilization on solid surfaces is extensively used in several applications, including immunoassays, biosensors, and affinity chromatography, some issues are still challenging. Self-assembling protein layers can be used to coat easily different surfaces by direct deposition. A specific biofunctional layer can be formed using genetic engineering techniques to express fused proteins acting as self-immobilizing antibodies. In this study, fusion proteins combining the self-assembling adhesive properties of a fungal hydrophobin and the functionality of the single chain fragment variables (ScFvs) of two antibodies were produced. The chosen ScFvs are able to recognize marine toxins associated with algal blooms, saxitoxin, and domoic acid, which can bioaccumulate in shellfish and herbivorous fish causing food poisoning. ScFvs fused to hydrophobin Vmh2 from *Pleurotus ostreatus* were produced in *Escherichia coli* and recovered from the inclusion bodies. The two fusion proteins retained the functionality of both moieties, being able to adhere on magnetic beads and to recognize and bind the two neurotoxins, even with different performances. Our immobilization procedure is innovative and very easy to implement because it allows the direct functionalization of magnetic beads with ScFvs, without any surface modification. Two different detection principles, electrochemical and optical, were adopted, thus achieving a versatile platform suitable for different antigen detection methods. The sensitivity of the saxitoxin optical biosensor [limit of detection (LOD) 1.7 pg/ml] is comparable to the most sensitive saxitoxin immunosensors developed until now.

Keywords: biosensors, algal toxins, hydrophobin, ScFv, optical detection, electrochemical detection

OPEN ACCESS

Edited by:
Greta Faccio, Independent researcher, Sankt Gallen, Switzerland

Reviewed by:
Michael Lienemann, VTT Technical Research Centre of Finland Ltd., Finland
Luca De Stefano, Institute of Applied Sciences and Intelligent Systems (ISASI), Italy

****Correspondence:***
Paola Giardina
giardina@unina.it

Specialty section:
This article was submitted to Biophysics, a section of the journal Frontiers in Molecular Biosciences

Received: *15 June 2021*
Accepted: *14 September 2021*
Published: *19 October 2021*

Citation:
Stanzione I, Izquierdo-Bote D, González García MB, Giardina P and Piscitelli A (2021) Immobilization of Antibodies by Genetic Fusion to a Fungal Self-Assembling Adhesive Protein. Front. Mol. Biosci. 8:725697. doi: 10.3389/fmolb.2021.725697

INTRODUCTION

Harmful algal blooms produce a vast quantity of marine toxins, endangering not only the marine world but also human life. These toxins can be accumulated in fish or shellfish (Vilariño et al., 2009), and are often classified according to the human disease for which they are responsible. Saxitoxin (STX) and its derivates, for instance, are classified as paralytic shellfish toxins and can interact with the voltage-gated sodium channels of nerves and muscle cells (Cusick and Sayler, 2013). Moreover, domoic acid (DA) stimulates the glutamate receptors causing amnesic shellfish poisoning (Berman et al., 2002). Therefore, to decrease concerns in terms of human health, environmental preservation, and economic challenges, the detection of algal toxins has drawn attention. To achieve this aim, one of the first methods approved for the study of these toxins was the use of a mouse bioassay. However, due to the unethical nature of animal testing, this technique has been replaced by other analytical techniques, such as HPLC and UPLC-MS/MS

(Greer et al., 2016). Nevertheless, these analyses are expensive and sometimes time-consuming, and thus the development of a rapid and specific assay has become necessary. Thanks to antibody/antigen recognition, the use of immunosensors has enabled the design of specific, faster, and cheaper analytical methods for toxin detection. Moreover, the availability of very sensitive biosensors can allow the on-site detection of neurotoxin traces avoiding demanding pretreatments, thus enabling seafood poisoning prevention. Nonetheless, the development of this kind of biosensor is subject to certain critical issues, such as the stability or immobilization of the antibody onto the surface and the right orientation of the antigen-binding site. Considering that the nature and the length of the linker, responsible for the antibody immobilization, affect the antigen recognition, several adhesion methods have been optimized (Jung et al., 2008). Chemical derivatization of the surfaces, followed by covalent attachment, together with the chemical modification of the antibodies by oxidation of the oligosaccharide moiety of the Fc region has been utilized. Likewise, a more biocompatible strategy to obtain a good steric accessibility of the binding site consists of antibody immobilization on a preformed layer of proteins, such as Protein A and Protein G, and able to interact specifically with the Fc region (Pulido-Tofiño et al., 2000). Most of the issues related to the whole antibody can be overcome using only the active moiety, for example, exploiting antigen-binding fragments (Fab) and single chain fragment variable (ScFv), thanks to their easier structure. In particular, ScFvs consist of small sections of heavy chain (VH) and light chain (VL) joined together by a flexible peptide linker. This simple configuration allows an easier recombinant expression than the full-length immunoglobulin, which is limited by the formation of disulfide bonds in the Fc region (Yusakul et al., 2017). This feature often allows their production in fusion with chemical linkers which improve the immobilization process. The chemical linkers could be replaced by self-assembling proteins, thereby obtaining an innovative immobilization method which does not require a surface modification or covalent bond formation.

Hydrophobins are small proteins typical of filamentous fungi and are described as the most powerful surface-active proteins known due to their self-assembling capability at the hydrophobic–hydrophilic interfaces. Their activity is similar to that of the traditional biosurfactants, but the surface activity of hydrophobins depends only on their characteristic amino acid sequence and the 3D structure (Wösten and de Vocht, 2000). The relative positions of the polar and non-polar amino acids seem quite preserved, determining a hydrophobicity pattern typical of these proteins. Furthermore, eight cysteine residues, which form four disulfide bridges, are well conserved. Hydrophobins can be divided into two main classes based on the different lengths of the inter-cysteine spaces and on the clustering of hydrophobic and hydrophilic groups. Class I hydrophobins assemble into polymeric layers composed of fibrillar structures (Kwan et al., 2006) and are only soluble with strong acid treatments. Furthermore, the soluble forms can polymerize back into rodlets under appropriate conditions. In contrast, class II hydrophobins form layers that can be easily solubilized by organic solvents and detergents (Bayry et al., 2012). Their amphipathic nature makes hydrophobins able to change the physicochemical properties of surfaces, for example, rendering hydrophobic surfaces hydrophilic (Wösten et al., 1994). The formed layer can adhere to different surfaces (polystyrene, silicon, glass, and 2D nanomaterials) by direct deposition, allowing the attachment of biomolecules in their active form on these surfaces (Laaksonen et al., 2010; Gravagnuolo et al., 2015; Longobardi et al., 2015; Piscitelli et al., 2017a). A homogeneous biocatalytic layer can also be formed using genetic engineering techniques to produce fused proteins for the development of self-immobilizing chimerae. The class I hydrophobin Vmh2, produced by the fungus *Pleurotus ostreatus*, has been recombinantly expressed fused to a wide range of proteins of biotechnological interest such as the glutathione-S-transferase (Piscitelli et al., 2017c), a multicopper oxidase (Sorrentino et al., 2019), the green fluorescent protein (Piscitelli et al., 2017b), and the human antimicrobial peptide LL-37 (Sorrentino et al., 2020).

Therefore, in this study, fusion proteins have been produced by combining the self-assembling adhesive properties of the Class I hydrophobin Vmh2 and the functionality of the ScFvs of two antibodies against the two marine neurotoxins, STX and DA. Once the refolding procedure had been optimized, the functionality of both fusion partners was verified by immobilizing them on magnetic beads (MBs), without any kind of derivatization, and testing the antigen-binding capability.

MATERIALS AND METHODS

All the chemicals used in this study were of analytical grade. All the solutions were prepared using ultrapure water of 18 MΩ cm resistivity (Milli-Q purification system Millipore, Merck, Darmstadt, Germany). Sodium chloride, the NaCl Trizma base, EDTA, urea, Triton X, DTT, isopropyl-β-D-thiogalacto-pyranoside, L-Arginine, and bovine serum albumin (BSA) were purchased from Sigma-Aldrich (Saint Louis, Missouri, United States). Tetramethylbenzidine (TMB), H_2O_2, H_2SO_4, HRP-DA, and HRP-STX were provided by the ELISA kit Saxitest and Domotest (Zeulab, S.L., Zaragoza, Spain). 2,2′-azino-bis (3-ethylbenzothiazoline-6-sulfonic acid (ABTS) and NaH_2PO_4 were purchased from Merck (Darmstadt, Germany).

Vector Construction

Four synthetic genes encoding for the hydrophobin Vmh2 from *P. ostreatus*, ScFv against STX or DA, a linker $(Gly_4Ser)_3$, and an His-tag were designed, as shown in **Figure 1A** , and optimized according to the *Escherichia coli* codon usage. The genes obtained were restricted with NcoI and BamHI and ligated into the corresponding sites of the pET22b (+) vector. *E. coli* BL21 (DE3) cells were transformed with the recombinant plasmids pET22b_Vmh2-$ScFv_{STX}$, pET22b_$ScFv_{STX}$-Vmh2, pET22b_Vmh2-$ScFv_{DA}$, and pET22b_$ScFv_{DA}$-Vmh2.

Expression and Isolation of Chimeric Proteins

For each plasmid transformed, a recombinant colony was transferred from the agar plate to 20 ml of LB medium (1% tryptone, 0.5% yeast extract, 1% NaCl) completed with 100 μg/ml of ampicillin and incubated overnight at 37°C, 180 rpm. The

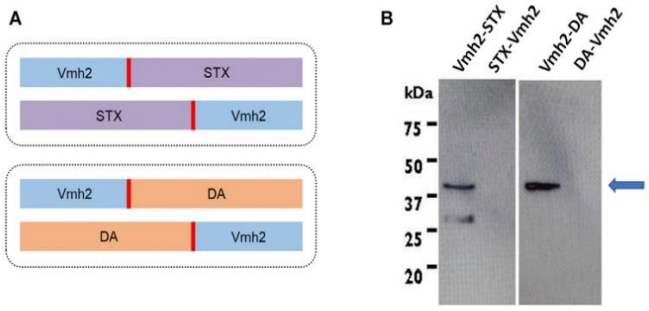

FIGURE 1 | (A) Schematic representation of gene constructs [in blue, the hydrophobin; in red, the $(Gly_4Ser)_3$ linker; in violet, the ScFv against saxitoxin; and in orange, that ScFv against domoic acid]; **(B)** Western blotting analysis of the *E. coli* inclusion bodies. The arrow indicates the expected molecular weight of the chimeras produced.

culture was diluted at an OD_{600} value of 0.08 with 200 ml of LB, supplemented with the same antibiotic, and further incubated at 37°C. To induce the recombinant protein expression, 1 mM IPTG (isopropyl-β-D-thiogalacto-pyranoside) was added when the culture reached an OD_{600} value of 0.5. After 3 h of induction, cells were collected by centrifugation at 3,300 × *g* at 4°C for 15 min. The obtained pellet was resuspended in a lysis buffer (100 mM Tris HCl, 10 mM EDTA, 2 M urea, and 2% Triton X-100 pH 8.0), at a final concentration of 20 OD/ml, and subjected to a sonication process (Bandelin, HD3200, MS 72 probe, running at 40% amplitude) for 30 min (30″ ON and 30″ OFF) in an ice bath. The inclusion bodies were collected by a centrifugation step at 3,300 × g for 15 min and then washed three times with the lysis buffer to remove contaminants. Next, the pellets of the inclusion bodies were dissolved in a denaturing buffer (100 mM Tris HCl, 10 mM EDTA, 8 M urea, and 10 mM DTT, pH 8) and incubated for 1 h at 37°C under stirring. The supernatants were collected after centrifugation at 3,300 × *g* at 4°C for 15 min.

Western blot Analysis

To localize the recombinant proteins, a Western blot analysis was carried out by exploiting the presence of the His-tag at the C-terminus of each chimera. Protein samples were loaded on SDS-PAGE (12.5%) and transferred to a PVDF membrane using an electroblotting transfer apparatus [Trans-Blot Semi-Dry Transfer Cell, Bio-Rad, Segrate (MI), Italy]. The protein detection was carried out by using a monoclonal peroxidase–conjugated anti-polyHistidine antibody at a 1:2,500 ratio (Sigma-Aldrich, Saint Louis, Missouri, United States). The membranes were developed by using a chemiluminescent substrate WESTAR ηC 2.0 (Cyanagen).

Refolding of Recombinant Vmh2-ScFv$_{STX}$ and Vmh2-ScFv$_{DA}$

The refolding protocol of the inclusion bodies was divided into two main steps: i) ultrafiltration and dialysis against the refolding buffer (50 mM Tris HCl pH 8, 1 mM EDTA, 150 mM sodium chloride, 500 mM L arginine, and 2 mM of DTT) to dilute the urea up to a concentration of 0.8 M using a Centricon centrifugal filter unit with a polyethersulfone (PES) membrane (cutoff of 10 kDa); and ii) after an overnight storage at 4°C, dilution of L-Arginine up to a concentration of 50 mM through ultrafiltration and dialysis against 50 mM Tris HCl pH8 + 0.8 M urea. The protein concentration was evaluated using the Pierce 660 nm Protein Assay Kit (Thermo Scientific, Waltham, MA) using bovine serum albumin (BSA) as standard protein.

Chimera Immobilization on Magnetic Beads

10 mg of pristine MBs (Absolute Mag™ Magnetic Particles, 3.0–3.9 μm, Creative Diagnostics, paramagnetic particles prepared by coating a layer of iron oxide and polystyrene over polystyrene core particles) were washed once with 1 ml of water and three times with 1 ml of 50 mM Tris HCl pH8 + 0.8 M urea. Next, the MBs were incubated with 50 μg of Vmh2-ScFv$_{STX}$ or Vmh2-ScFv$_{DA}$ on a rotary tube mixer for three days at 4°C. The functionalized MBs were collected by using a magnet and after three washes with buffer, the immobilization yields were calculated as a difference between the incubated protein amount and that measured in the supernatant and in the washes.

Vmh2-ScFv$_{STX}$ and Vmh2-ScFv$_{DA}$ were also incubated as previously described, but in the absence of the MBs, to rule out protein adhesion on the walls of the reaction vials.

Antibody/Vmh2-ScFv$_{STX}$ Competition

A competitive assay between the anti-STX antibodies of the STX ELISA kit and the chimera Vmh2-ScFv$_{STX}$ was carried out. To achieve this aim, the ELISA test kit for STX detection (SAXITEST) was used in accordance with the manufacturer's instructions (Zeulab, S.L., Zaragoza, Spain), adding the Vmh2-ScFv$_{STX}$ instead of the antigen standard solution. Thus, 100 μL of the kit dilution buffer, 25 μL of anti-STX antibody solution, 50 μL of STX antigen labeled with horseradish peroxidase (HRP-STX) solution, and 25 μL of different concentrations (0, 20, 40, 50, 60,

80, and 100 ng/ml) of Vmh2-ScFv$_{STX}$ were incubated for 30 min at room temperature in each well (containing immobilized sheep anti-rabbit IgG antibodies). After incubation, the plate was emptied and washed three times with the washing buffer and then dried. Subsequently, 100 µL of the substrate mixture 3,3′,5,5′-tetramethylbenzidine (TMB) and hydrogen peroxide were integrated in each well. The enzymatic reaction was carried out for 15 min at room temperature in darkness and then was terminated by adding100 µL of a 0.5 M H_2SO_4 solution. This solution stopped the reaction by decreasing the pH until the HRP lost its activity. Moreover, at this acidic pH, the charge transfer of the complex generated by the oxidation of the TMB yielded to a stable diamine, changing the color of the solution from blue to yellow. Finally, 50 µL of this solution was dropped on the electrode's surface and a potential of + 0.10 V was applied on the Ag pseudo reference electrode for 60 s.

Optical Determination of ScFv Functionality

The capability of the ScFvs to bind the corresponding antigen was tested using some elements of two commercial ELISA kits (Saxitest and Domotest, Zeulab S.L., Zaragoza, Spain) and optimizing different parameters, such as volume, time, and temperature of incubation. In detail, 200 µL of functionalized MBs (10 µg of the Scfv chimera and 2 mg of MBs) were precipitated by using a magnetic field, and the supernatant was removed. Next, 200 µL of a labeled toxin, either HRP-STX or HRP-DA at different dilution rates (1:4, 1:10, 1:20), were added to the MBs and incubated for 3 h at 4°C under stirring. As a control, the non-functionalized MBs were subjected to the same treatment, thereby verifying that no toxin was bound to the surface. After incubation, 50 µL of each supernatant sample was assayed in a multiwell plate with 250 µL of 9.1 mM ABTS (2,2′-azino-bis 3-ethylbenzothiazoline-6-sulfonic acid) dissolved into 100 mM NaH_2PO_4, pH 5, and 10 µL of 0.3% hydrogen peroxide at 420 nm. Thus, the ScFv-binding capability was calculated as a difference between the activity (mU) in the supernatant of each sample and in the corresponding control. Moreover, a competitive assay was performed on Vmh2-ScFv$_{STX}$ functionalized MBs using the labeled STX (diluted 1–20) and the standard toxin at different concentrations (from 5 to 100 pg/ml).

Electrochemical Detection of ScFv Functionality

Electrochemical assay conditions were set up, optimizing different parameters, such as volume, time, and temperature of incubation. Aliquots of 100 µL of functionalized MBs (5 µg of ScFv chimera and 1 mg of MBs) were incubated in the presence of 50 µL of DA-HRP/STX-HRP and 50 µL of DA/STX standard solutions at different concentrations under stirring for 45 min at room temperature. Furthermore, an aliquot of 100 µL of functionalized MBs (5 µg of ScFv chimera and 1 mg of MBs) was incubated in the absence of both a labeled and standard toxin to obtain a blank signal. After the incubation reaction, in order to remove all the unbound antigens, the dispersions were subjected to a magnetic separation and washing steps by using 50 mM Tris-HCl buffer solution pH 8 + 0.8 M urea. A screen-printed carbon electrode (SPCE) (DRP-110, Metrohm DropSens, S.L) was positioned onto the magnetic support, and then an aliquot of 25 µL of MB dispersion was deposited onto the electrode surface. After 2 min, all the MBs had been attracted to the working electrode surface. Next, the drop was carefully removed. Subsequently, 20 µL of TMB/H_2O_2 stock solution were added and incubated on the electrode in darkness at room temperature for 15 min. Hence, the enzymatic reaction produced the oxidation of TMB by HRP in the presence of H_2O_2 generating a blue-colored complex product. Thereafter, the detection took place by the electrochemical reduction of the oxidized TMB applying a potential of −0.20 V vs. the Ag pseudo-reference electrode for 60 s. The reduction current was related to the labeled antigen concentration and inversely related to that of the standard solutions.

RESULTS

Production of Vmh2-ScFv$_{STX}$ and Vmh2-ScFv$_{DA}$

Chimeric proteins were designed with the Vmh2 moiety at the N- or C-terminus and linked to the ScFvs through a sequence of 15 aa $(Gly_4Ser)_3$ (**Figure 1A**). Their production was induced by adding 1 mM IPTG to the culture during the exponential phase. Next, taking advantage of the His-tag at the C-terminus of each chimera, a Western blot analysis using a monoclonal anti-polyHistidine antibody was performed (**Figure 1B**), showing that only chimeric proteins carrying the Vmh2 at the N-terminus (Vmh2-ScFv$_{STX}$ and Vmh2-ScFv$_{DA}$) were detectable and localized in the inclusion bodies.

After solubilization of the inclusion bodies in 8 M urea, an *in vitro* refolding procedure was set up. The optimized protocol consisted of two ultrafiltration steps in which the presence of L-Arginine (Lange and Rudolph, 2009) and 0.8 M urea prevented the chimera aggregation. Nonetheless, the L-Arginine was then removed by dialysis to avoid its interference with the following characterizations. The production yield of both the refolded Vmh2-ScFv$_{STX}$ and Vmh2-ScFv$_{DA}$ was about 5 mg per liter of culture broth. However, other strategies could be adopted to improve the amount of the recombinant protein produced, as suggested by Kirkland et al. (Kirkland and Keyhani, 2011). The refolding procedure was tested, verifying both the adhesive capability of the hydrophobin Vmh2 and the antigen-binding ability of both ScFvs, as described below.

Characterization of Fusion Proteins

Vmh2-ScFv$_{DA}$

The functionality of the adhesive moiety of Vmh2-ScFv$_{DA}$ was verified by incubating 50 µg of the chimera with 10 mg of pristine MBs. No protein adhesion on the walls of the reaction vials and no protein in the solution were detected, thus indicating successful protein immobilization on the beads. On the other hand, when BSA was used as the control, 38 µg of the protein were still present in the solution. Furthermore, Vmh2-ScFv$_{DA}$ was tightly bound to the magnetic surface even after at least three washes with the buffer. Additionally, the capability of Vmh2-

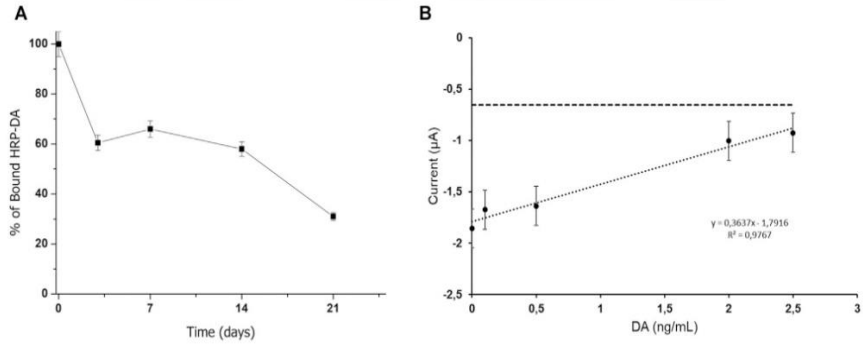

FIGURE 2 | (A) Stability of the Vmh2-ScFv$_{DA}$–functionalized MBs, **(B)** electrochemical detection of the competitive assay using Vmh2-ScFv$_{DA}$–functionalized MBs with the DA concentration in the range from 0 to 2.5 ng/ml. The horizontal line indicates the electrochemical background signal.

ScFv$_{DA}$ to bind the toxin was verified using a colorimetric method based on DA labeled with peroxidase. In the optimized conditions (chimera/MB ratio 0.005 w/w and HRP-DA solution diluted 1: 20), the amount of captured HRP-DA was 0.20 ± 0.05 mU/mg MBs, as calculated by the difference between the peroxidase activity measured in the sample supernatant before (0.9 mU/mg MBs) and after incubation. This value represents a clear indication of a successful chimera/toxin interaction. Nonetheless, a decrease in this binding capacity was observed over time, reducing to a quarter of the initial-binding capacity after 21 days at 4°C (**Figure 2A**).

Since the amount of the bound HRP-DA was too low to perform a colorimetric competitive assay with the DA standard solutions, amperometric analyses were carried out tracking the HRP activity electrochemically. **Figure 2B** shows the current intensity obtained for the calibration curve using DA at concentrations in the range from 0 to 2.5 ng/ml. The electrochemical signal was inversely proportional to the DA concentration, and a linear fitting with a correlation coefficient of 0.9767 was achieved with a calculated limit of detection (LOD) of 0.35 ng/ml, according to 3σ/m (where σ is the standard deviation of the estimated intercept and m is the slope of the calibration curves). This trend highlights the competitive reaction between HRP-DA and DA for the binding domain of the ScFv moiety of the chimera and confirms the successful interaction between the Vmh2-ScFv$_{DA}$ fusion protein and the antigen.

Vmh2-ScFv$_{STX}$

In the case of the chimera Vmh2-ScFv$_{STX}$, an electrochemical analysis aimed at evaluating the competition between the free Vmh2-ScFv$_{STX}$ chimera and the commercial antibody against STX was successfully performed.

The ELISA SAXITEST was performed by adding Vmh2-ScFv$_{STX}$ at different concentrations to a constant amount of the HRP-STX and anti-STX antibodies. In this way, the anti-STX antibodies bound to the wells were modified with the secondary antibodies, while Vmh2-ScFv$_{STX}$ was removed during washing. Therefore, an increasing concentration of the free chimera would produce a decrease in the anti-STX/HRP-STX complex with a consequent decrease of the electrochemical signal. **Figure 3** shows the currents obtained for each concentration of free Vmh2-ScFv$_{STX}$, indicating that the chimera really competes with the commercial antibody and a 50% inhibition was achieved at a concentration value of 60 ng/ml.

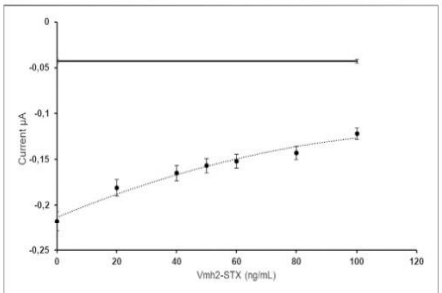

FIGURE 3 | Electrochemical measurements of the free Vmh2-ScFv$_{STX}$/anti-STX competitive assay with the dashed line as an eye-guide. The horizontal line indicates the electrochemical background signal.

As already observed for Vmh2-ScFv$_{DA}$, the immobilization of Vmh2-ScFv$_{STX}$ on pristine MBs was successful, indicating the proper functionality of the hydrophobin moiety. To verify the functionality of the ScFv moiety upon immobilization, the MBs functionalized with the chimera were incubated with labeled STX (HRP-STX, diluted 1:20, 3.6 mU/mg MBs) and analyzed by the HRP colorimetric test. The amount of captured HRP-STX was 0.50 ± 0.05 mU/mg MBs, confirming the efficient antigen/

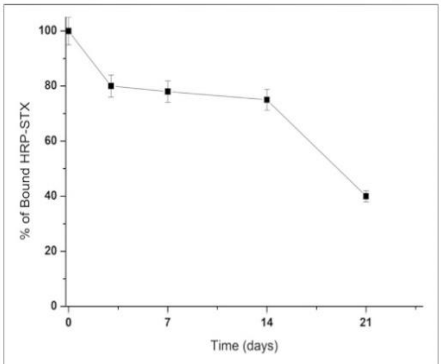

FIGURE 4 | Stability of the Vmh2-ScFv$_{STX}$-functionalized MBs.

antibody interaction. Moreover, 40% of its functionality was retained after 21 days at 4°C (**Figure 4**).

The functionalized MBs were exploited to perform competitive assays between STX at different concentrations and HRP-STX, using both optical and electrochemical measurements.

As can be seen in **Figure 5A**, which reports the electrochemical measurements, a linear trend (correlation coefficient of 0.9845) was observed in the concentration range from 0 to 300 pg/ml, obtaining an LOD of 52 pg/ml and RSD (relative standard deviation) (n = 3) = 9.57%.

In the optical platform, a linear trend (correlation coefficient of 0.9879) (**Figure 5B**) of the HRP activity as a function of the logarithm of STX concentration was observed in the concentration range from 0 to 100 pg/ml, obtaining an LOD of 1.7 pg/ml.

DISCUSSION

Although surface modifications are often the best way to immobilize antibodies, this process can be expensive in terms of both time and reagents. A stable protein coating can be formed using a self-assembling protein layer and/or its engineered variants. Indeed, chimeric proteins formed by adhesive and recognition moieties may represent a breakthrough in the field of surfaces functionalization. Herein, with the aim of enabling antibody immobilization without any chemical derivatization, we have developed for the first time a device based on the fusion of a class I hydrophobin with proteins able to bind antigens, ScFvs. In particular, the adhesive capability of the hydrophobin Vmh2 fused to the two ScFvs against the marine toxins STX and DA was exploited to produce adhesive antibodies. Two different combinations of each chimera were designed, with the hydrophobin at the N- or C-terminus of the constructs (Vmh2-ScFv$_{STX}$, Vmh2-ScFv$_{DA}$, ScFv$_{STX}$-Vmh2, and ScFv$_{DA}$-Vmh2, respectively) (**Figure 1A**). All the fusion proteins were cloned and produced in *E. coli*, but only the Vmh2-ScFv$_{STX}$ and Vmh2-ScFvDA chimeras were detected. This result could be explained in terms of a different stability at the transcript levels or a different propensity to aggregation of the proteins. Indeed, Vmh2-ScFv$_{STX}$ and Vmh2-ScFv$_{DA}$ were found localized in the inclusion bodies, as that occurred in the case of the other Vmh2 chimeras previously produced in *E. coli* (Piscitelli et al., 2017c; Puopolo et al., 2021), with harsh conditions being necessary to solubilize them. According to the TANGO algorithm (tango.crg.es), ScFv$_{DA}$-Vmh2 and ScFv$_{STX}$-Vmh2 have shown a higher propensity for amyloid aggregation. Therefore, their solubilization could be even more difficult, rendering their detection unachievable. In our experiments, the setting up of a refolding procedure was a crucial step in the whole process and needed to be validated by evaluating the functionality of both moieties. The adhesiveness of the chimeras was easily

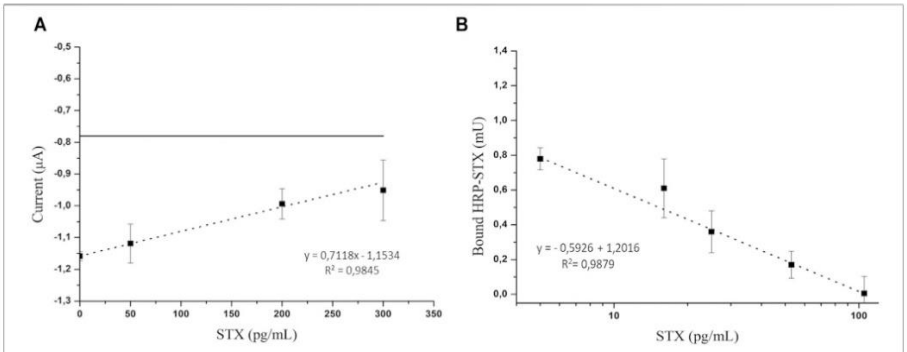

FIGURE 5 | (A) Electrochemical detection of the competitive assay using a STX concentration in the range from 0 to 300 pg/ml. The horizontal line indicates the electrochemical background signal; **(B)** optical detection of the competitive assay using an STX concentration in the range from 0 to 100 pg/ml.

ascertained although assessing the binding capacity of the ScFvs was trickier.

Vmh2-ScFv$_{STX}$ and Vmh2-ScFv$_{DA}$ were immobilized on pristine MBs since MBs are often used to develop optical or electrochemical immunosensors, thanks to their own characteristics. They show a large surface to the volume ratio, a wide surface area, and, most importantly, they can be recovered using a magnetic field (Bilal et al., 2018), allowing their usage as a carrier to pre-concentrate the analytes and to enhance the sensitivity of the systems (Toldrà et al., 2021). Both chimeras were almost completely immobilized on this surface without the need of any chemical derivatization. Concerning the functionality of the ScFvs moiety, a different behavior between the two fusion proteins was observed. Vmh2-ScFv$_{DA}$ bound a lower amount of the labeled toxin and was less stable, with respect to Vmh2-ScFv$_{STX}$, as tested by the optical assay. This difference could be due to an unsatisfactory refolding process of Vmh2-ScFv$_{DA}$, making the optical competitive assay unachievable. On the other hand, the competitive assay was accomplished using the electrochemical technique. Indeed, the calculated LOD (0.35 ng/ml) was higher than that (0.1 ng/ml) described by Kania et al. (2003), while it was lower than that recently developed by Nelis et al. (2021), whose LOD is 1.7 ng/ml.

A more complete characterization of the antigen-binding capability was achieved in the case of Vmh2-ScFv$_{STX}$. This chimera was able to compete in solution with a commercial antibody against STX, thus confirming its functionality in STX binding. Both optical and electrochemical detection were used to measure STX in a competitive assay obtaining very low LODs, 1.7 pg/ml and 52 pg/ml, respectively. The sensitivity of the optical platform is comparable to that (1.2 pg/ml) recently obtained by Jin et al. (2019), who developed an ultrasensitive immunosensor to detect traces of STX based on a magnetic gold electrode, antibody-functionalized MBs, and palladium-doped graphitic carbon nitride nano-sheets, which possess a peroxidase-like activity. Even the analyte concentration range of our electrochemical detection (0–300 pg/ml) is comparable to that obtained by Jin et al. (2019) (0–400 pg/ml). On the other hand, our immobilization procedure is innovative, very easy to implement, and smart, allowing the direct functionalization of MBs with ScFvs.

DATA AVAILABILITY STATEMENT

The original contributions presented in the study are included in the article further inquiries can be directed to the corresponding author.

AUTHOR CONTRIBUTIONS

IS performed most of the experiments and wrote the manuscript draft; DIB performed the electrochemistry experiments and contributed to writing the manuscript draft; MGBB analyzed the electrochemistry data and was involved in the development of the project; PG and AP were involved in the project supervision and administration, writing, reviewing, and editing the manuscript.

FUNDING

This project was funded by the Italian Ministry of Education, Universities, and Research and the Spanish Centre for the Development of Industrial Technology (CDTI) and co-funded by the European Union's Horizon 2020 research and innovation program under the framework of ERA-NET Cofund MarTERA (Maritime and Marine Technologies for a new Era), FLAshMoB, Functional Amyloid chimera for Marine Biosensing (ID: 172).

REFERENCES

Bayry, J., Aimanianda, V., Guijarro, J. I., Sunde, M., and Latgé, J.-P. (2012). Hydrophobins-unique Fungal Proteins. *Plos Pathog.* 8, e1002700–9. doi:10.1371/journal.ppat.1002700

Berman, F. W., LePage, K. T., and Murray, T. F. (2002). Domoic Acid Neurotoxicity in Cultured Cerebellar Granule Neurons Is Controlled Preferentially by the NMDA Receptor Ca2+ Influx Pathway. *Brain Res.* 924, 20–29. doi:10.1016/S0006-8993(01)03221-8

Bilal, M., Zhao, Y., Rasheed, T., and Iqbal, H. M. N. (2018). Magnetic Nanoparticles as Versatile Carriers for Enzymes Immobilization: A Review. *Int. J. Biol. Macromolecules* 120, 2530–2544. doi:10.1016/j.ijbiomac.2018.09.025

Cusick, K., and Sayler, G. (2013). An Overview on the Marine Neurotoxin, Saxitoxin: Genetics, Molecular Targets, Methods of Detection and Ecological Functions. *Mar. Drugs* 11, 991–1018. doi:10.3390/md11040991

Gravagnuolo, A. M., Morales-Narváez, E., Matos, C. R. S., Longobardi, S., Giardina, P., and Merkoçi, A. (2015). On-the-Spot Immobilization of Quantum Dots, Graphene Oxide, and Proteins via Hydrophobins. *Adv. Funct. Mater.* 25, 6084–6092. doi:10.1002/adfm.201502837

Greer, B., McNamee, S. E., Boots, B., Cimarelli, L., Guillebault, D., Helmi, K., et al. (2016). A Validated UPLC-MS/MS Method for the Surveillance of Ten Aquatic Biotoxins in European Brackish and Freshwater Systems. *Harmful Algae* 55, 31–40. doi:10.1016/j.hal.2016.01.006

Jin, X., Chen, J., Zeng, X., Xu, L., Wu, Y., and Fu, F. (2019). A Signal-On Magnetic Electrochemical Immunosensor for Ultra-sensitive Detection of Saxitoxin Using Palladium-Doped Graphitic Carbon Nitride-Based Non-competitive Strategy. *Biosens. Bioelectron.* 128, 45–51. doi:10.1016/j.bios.2018.12.036

Jung, Y., Jeong, J. Y., and Chung, B. H. (2008). Recent Advances in Immobilization Methods of Antibodies on Solid Supports. *Analyst* 133, 697–701. doi:10.1039/b800014j

Kania, M., Kreuzer, M., Moore, E., Pravda, M., Hock, B., and Guilbault, G. (2003). Development of Polyclonal Antibodies against Domoic Acid for Their Use in Electrochemical Biosensors. *Anal. Lett.* 36, 1851–1863. doi:10.1081/AL-120023618

Kirkland, B. H., and Keyhani, N. O. (2011). Expression and Purification of a Functionally Active Class I Fungal Hydrophobin from the Entomopathogenic Fungus Beauveria Bassiana in *E. coli*. *J. Ind. Microbiol. Biotechnol.* 38, 327–335. doi:10.1007/s10295-010-0777-7

Kwan, A. H. Y., Winefield, R. D., Sunde, M., Matthews, J. M., Haverkamp, R. G., Templeton, M. D., et al. (2006). Structural Basis for Rodlet Assembly in Fungal Hydrophobins. *Proc. Natl. Acad. Sci.* 103, 3621–3626. doi:10.1073/pnas.0505704103

Laaksonen, P., Kainlauri, M., Laaksonen, T., Shchepetov, A., Jiang, H., Ahopelto, J., et al. (2010). Interfacial Engineering by Proteins: Exfoliation and Functionalization of Graphene by Hydrophobins. *Angew. Chem. Int. Edition* 49, 4946–4949. doi:10.1002/anie.201001806

Lange, C., and Rudolph, R. (2009). Suppression of Protein Aggregation by L-Arginine. *Curr. Pharm. Biotecnol.* 10, 408–414. doi:10.2174/138920109788488851

Longobardi, S., Gravagnuolo, A. M., Funari, R., Della Ventura, B., Pane, F., Galano, E., et al. (2015). A Simple MALDI Plate Functionalization by Vmh2 Hydrophobin for Serial Multi-Enzymatic Protein Digestions. *Anal. Bioanal. Chem.* 407, 487–496. doi:10.1007/s00216-014-8309-3

Nelis, J. L. D., Migliorelli, D., Mühlebach, L., Generelli, S., Stewart, L., Elliott, C. T., et al. (2021). Highly Sensitive Electrochemical Detection of the marine Toxins Okadaic Acid and Domoic Acid with Carbon Black Modified Screen Printed Electrodes. *Talanta* 228, 122215. doi:10.1016/j.talanta.2021.122215

Piscitelli, A., Cicatiello, P., Gravagnuolo, A. M., Sorrentino, I., Pezzella, C., and Giardina, P. (2017a). Applications of Functional Amyloids from Fungi: Surface Modification by Class I Hydrophobins. *Biomolecules* 7, 45. doi:10.3390/biom7030045

Piscitelli, A., Pennacchio, A., Cicatiello, P., Politi, J., De Stefano, L., and Giardina, P. (2017b). Rapid and Ultrasensitive Detection of Active Thrombin Based on the Vmh2 Hydrophobin Fused to a Green Fluorescent Protein. *Biosens. Bioelectron.* 87, 816–822. doi:10.1016/j.bios.2016.09.052

Piscitelli, A., Pennacchio, A., Longobardi, S., Velotta, R., and Giardina, P. (2017c). Vmh2 Hydrophobin as a Tool for the Development of "Self-Immobilizing" Enzymes for Biosensing. *Biotechnol. Bioeng.* 114, 46–52. doi:10.1002/bit.26049

Pulido-Tofiño, P., Barrero-Moreno, J. M., and Pérez-Conde, M. C. (2000). Flow-through Fluoroimmunosensor for Isoproturon Determination in Agricultural Foodstuff. *Analytica Chim. Acta* 417, 85–94. doi:10.1016/S0003-2670(00)00920-X

Puopolo, R., Sorrentino, I., Gallo, G., Piscitelli, A., Giardina, P., Le Goff, A., et al. (2021). Self-assembling Thermostable Chimeras as New Platform for Arsenic Biosensing. *Sci. Rep.* 11, 2991. doi:10.1038/s41598-021-82648-9

Sorrentino, I., Gargano, M., Ricciardelli, A., Parrilli, E., Buonocore, C., de Pascale, D., et al. (2020). Development of Anti-bacterial Surfaces Using a Hydrophobin Chimeric Protein. *Int. J. Biol. Macromolecules* 164, 2293–2300. doi:10.1016/j.ijbiomac.2020.07.301

Sorrentino, I., Giardina, P., and Piscitelli, A. (2019). Development of a Biosensing Platform Based on a Laccase-Hydrophobin Chimera. *Appl. Microbiol. Biotechnol.* 103, 3061–3071. doi:10.1007/s00253-019-09678-2

Toldrà, A., Andree, K. B., Roque, A., Lowenthal, A., Rozenberg, Y., Furones, M. D., et al. (2021). Use of Anionic Polymer-Coated Magnetic Beads to Pre-concentrate Ostreid Herpesvirus 1 from Seawater: Application to a UV Disinfection Treatment. *Aquaculture* 536, 736452. doi:10.1016/j.aquaculture.2021.736452

Vilariño, N., Fonfría, E., Louzao, M. C., and Botana, L. (2009). Use of Biosensors as Alternatives to Current Regulatory Methods for marine Biotoxins. *Sensors* 9, 9414–9443. doi:10.3390/s91109414

Wösten, H. A. B., and de Vocht, M. L. (2000). Hydrophobins, the Fungal Coat Unravelled. *Biochim. Biophys. Acta (Bba) - Rev. Biomembranes* 1469, 79–86. doi:10.1016/S0304-4157(00)00002-2

Wösten, H. A., Schuren, F. H., and Wessels, J. G. (1994). Interfacial Self-Assembly of a Hydrophobin into an Amphipathic Protein Membrane Mediates Fungal Attachment to Hydrophobic Surfaces. *EMBO J.* 13, 5848–5854. doi:10.1002/j.1460-2075.1994.tb06929.x

Yusakul, G., Nuntawong, P., Sakamoto, S., Ratnatilaka Na Bhuket, P., Kohno, T., Kikkawa, N., et al. (2017). Bacterial Expression of a Single-Chain Variable Fragment (scFv) Antibody against Ganoderic Acid a: A Cost-Effective Approach for Quantitative Analysis Using the Scfv-Based Enzyme-Linked Immunosorbent Assay. *Biol. Pharm. Bull.* 40, 1767–1774. doi:10.1248/bpb.b17-00531

Conflict of Interest: Authors DIB and MBGG are employed by the company Metrohm DropSens.

The remaining authors declare that the research was conducted in the absence of any commercial or financial relationships that could be construed as a potential conflict of interest.

Publisher's Note: All claims expressed in this article are solely those of the authors and do not necessarily represent those of their affiliated organizations, or those of the publisher, the editors, and the reviewers. Any product that may be evaluated in this article, or claim that may be made by its manufacturer, is not guaranteed or endorsed by the publisher.

Chapter 5

5. Development of biosensing platforms based on natural and engineered laccase

The own characteristics of the laccase enzyme and its ability to oxidize aromatic and phenolic compounds, that represent the most common pollutants, make these biomolecules extremely useful in a wide range of application fields. To better describe the laccase enzyme and its functions, in the section 5.1 is reported the review of which I am the first author. In the manuscript it is explained the biocatalytic nature of the laccase, the molecular engineering methods to build highly efficient biocatalysts and its exploitation in several applications from bioremediation to pharmaceutical field, from food industry to biosensing field. For this last application, for example, the laccase enzymes present many advantages such as their capability to catalyze electron-transfer reactions without additional cofactors and a good stability. Indeed, many laccases produced by a plethora of microorganisms have been employed for the development of electrochemical and optical biosensors to detect phenolic compounds in different matrices [85].
In this context, we developed electrochemical biosensors by the usage of the laccase PoxA1b from *P. ostreatus* and recombinantly expressed in *Pichia pastoris* yeast, to detect different aromatic compounds. Moreover, to increase and facilitate the enzyme immobilization on several surfaces, PoxA1b has been genetically fused to the class I hydrophobin Vmh2. Thus, the obtained chimeric protein is endowed with the enzymatic activity of the laccase and the adhesive capability of the hydrophobin. Since PoxA1b can adhere on a hydrophobic polystyrene surface with a low immobilization yield, probably due to its glycosylation grade, for each developed biosensors the performances of the chimeric protein PoxA1b-Vmh2 have been compared to those of the free PoxA1b.
In the paper of the section 5.2, the PoxA1b-Vmh2 protein has been immobilized on few-layer graphene, through an exfoliation process starting from graphite, and then used to electrochemically detect phenolic compounds. In this paper, my relevant contribution, as first author, is related to the proteins production and the optimization of the immobilization process on the carbon nanomaterial. Then the French partners performed the nanomaterial deposition on a Glass Carbon Electrode to electrochemically detect catechol and dopamine.
In the section 5.3 the development of the electrochemical biosensor for the detection of catechol and dopamine through the immobilization of the laccase on the multi walled carbon nanotubes (MWCNT) is described. Instead, exploiting the efficient adsorption of anthraquinones at CNT electrodes, an electrochemical biosensor to detect anthracene has been developed using either laccase in solution, CNT-supported laccase or laccase immobilized on magnetic beads (section 5.4). Due to my skills in recombinant protein

production and laccase manipulation, in both papers I was mainly involved in the production of PoxA1b and PoxA1b-Vmh2 proteins.
Finally, in the section 5.5 the paper under preparation related to my work at the University of Oviedo, Spain, is reported. Taking advantages from the immobilization of the laccase chimera on the commercial micropipette polypropylene tips, a rapid, easy to use, and innovative electrochemical system has been developed for the detection of the caffeic acid in real samples.

5.1 Beyond natural laccases: extension of their potential applications by protein engineering

Applied Microbiology and Biotechnology
https://doi.org/10.1007/s00253-019-10147-z

MINI-REVIEW

Beyond natural laccases: extension of their potential applications by protein engineering

Ilaria Stanzione[1] · Cinzia Pezzella[2] · Paola Giardina[1] · Giovanni Sannia[1] · Alessandra Piscitelli[1]

Received: 15 July 2019 / Revised: 6 September 2019 / Accepted: 17 September 2019

Abstract
Laccases bring exciting promises into the green industries, and the development of enzymes with improved properties is further raising their exploitation potential. Molecular engineering methods to build highly efficient catalysts both through rational and random mutagenesis were extensively applied. Moreover, computational approaches are becoming always more reliable in aiding proper design of efficient and tailored catalyst for specific applications. In this review, the results of the last 10 years about industrial application of engineered laccases in different fields are analyzed. Tailoring laccase towards a target substrate and defining a proper screening strategy for the selection of the "jackpot mutant" represent the keys of a winning mutagenesis pathway. Likewise, laccase chimerae, built by the fusion of laccases with relevant proteins, emerged as an added value in the designing of flexible and well-rounded biocatalysts. Despite being promising in most of the reported examples, evolved laccases are currently tested at a laboratory scale and a feedback from the industry world is continuously required to strengthen the biotechnological exploitation of these improved enzymes.

Keywords Chimeric laccase · Rational design · Random evolution · Computational approaches

Introduction

One of the major challenges of the next future is the development of technologies that can provide the increasing numbers of daily life products while consuming fewer resources and having a lesser environmental footprint. Biocatalysts can make an impact since enzymatic processes generally lead to reduced contributions to global warming. Although the first discovery of laccases dates back to the mid-nineteenth century, these enzymes, with their large substrate specificity and wide range of applications, are still very relevant in the replacement of conventional chemical processes in many industrial fields. Laccases (*p*-diphenol-dioxygen oxidoreductases; EC 1.10.3.2) are well-known copper oxidoreductases (Cañas and Camarero 2010; Giardina et al. 2010; Hakulinen and Rouvinen 2015; Jones and Solomon 2015; Martins et al. 2015) produced in fungi, plants, and bacteria, able to catalyze the oxidation of a wide range of phenolic and non-phenolic compounds using oxygen as electron acceptor and producing water as the only by-product (Giardina et al. 2010). Regardless of their very similar structures, laccases exhibit a wide range of redox potential, from + 430 to + 800 mV (*vs.* normal hydrogen electrode) (Cambria et al. 2012), and those from basidiomycetous fungi display the highest redox potential. From a biotechnological perspective, high redox potential laccases are much more interesting, since the higher the redox potential, the wider the range of oxidized substrates. Since the first launch of a commercial product based on a laccase enzyme by Novozyme (Novo Nordisk, Denmark) in 1996, laccases are being employed successfully in the industry. Exploitation of laccases spans from bioremediation to the pharmaceutical field, and many reviews addressing laccase applications have been published in the last years (Pezzella et al. 2015; Sharma et al. 2018), also dealing with more specific applications such as in the food industry (Osma et al. 2010), in the synthesis of high added value compounds (Polak and Jarosz-Wilkolazka 2012; Piscitelli et al. 2012), in grafting reactions (Kudanga et al. 2011), in bioremediation (Chandra and Chowdhary 2015; Zucca et al. 2016; Yang et al. 2017), in biorefinery (Kudanga and Le Roes-Hill 2014;

Ilaria Stanzione and Cinzia Pezzella contributed equally to this work.

✉ Alessandra Piscitelli
apiscite@unina.it

[1] Department of Chemical Sciences, University Federico II, Naples, Italy

[2] Department of Agricultural Sciences, University Federico II, via Cintia 4, 80126 Naples, Italy

Published online: 13 December 2019

Roth and Spiess 2015; Fillat et al. 2017), in biosensing (Rodríguez-Delgado et al. 2015), in the development of bioelectronic devices (Le Goff et al. 2015), and in the pulp and paper industry (Singh and Arya 2019).

However, laccases' full potential is still untapped, and some bottlenecks are the lack of biocatalysts with the required selectivity, their compatibility with the rigorous process conditions, their low production level, and their scarce commercial availability (Martínez et al. 2017). Many concerted approaches are being pursued and/or envisaged to address the existing challenges and boost the exploitation of laccases (Fig. 1): (i) exploration of the biodiversity of microorganisms living in extreme habitats to discover enzymes endowed with desirable characteristics (Cruz Ramírez et al. 2012; Ghatge et al. 2018; Siroosi et al. 2018; Zerva et al. 2019), (ii) enzyme immobilization to allow reuse of the biocatalyst with benefits in terms of costs and enzyme performances (Fernández-Fernández et al. 2013), (iii) recombinant production in homologous or heterologous hosts with the aim to increase the cost-effectiveness of the production of these enzymes (Piscitelli et al. 2010), (iv) protein engineering with the aim of both improving enzymatic features and generating enzymes with tailor-made properties for different fields of application (Mate and Alcalde 2015; Pardo and Camarero 2015), and (v) metagenomic analysis to identify enzymes with novel properties from the unculturable component of microbiomes (Fang et al. 2011; Ausec et al. 2017; Dandare et al. 2019).

Among the abovementioned approaches, the present review is aimed at highlighting the progress towards applications of laccases engineered through both rational and random approaches. Moreover, the potentialities of chimeric proteins in which laccases are fused with other functional proteins/domains, to extend their scope, are also pointed out.

Engineered laccases by rational and random approaches

Most of the papers about laccase engineering published in the last 10 years were generally aimed at improving laccase properties and not directly linked to their industrial exploitation. Researchers extensively used molecular engineering methods to design highly efficient laccases through both rational and random mutagenesis, e.g., Maté et al. 2010; Miele et al. 2010; Pardo et al. 2012; Furukawa et al. 2013; Mate et al. 2013a, b; Nasoohi et al. 2013; Khodakarami et al. 2018. In other papers, some specific targets were addressed, even if no application was tested. Among these, some studies were devoted to increase laccase tolerance in stressful conditions (Mollania et al. 2011; Liu et al. 2013; Mateljak et al. 2019a). For example, Liu et al. (2013) developed a directed evolution protocol to improve the resistance of a *Trametes versicolor* laccase in ionic liquids (ILs), with the aim to boost laccase exploitation in lignin degradation. ILs are a new class of solvents which display very interesting solubility properties in industrial applications, particularly lignin processing. After two rounds of directed evolution, the author developed a laccase variant endowed with about 4.5-fold higher activity than wild type in the presence of 15% (v/v) [EMIM] [$EtSO_4$], a prime IL for application in biomass treatment. Very recently, computationally designed protein building blocks (predicted by SCHEMA-RASPP algorithm) from three high redox potential

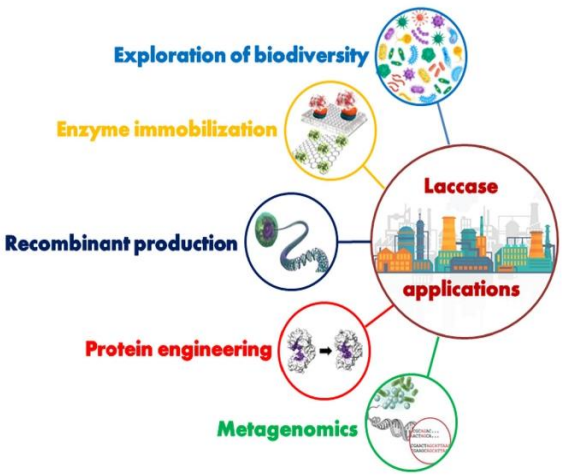

Fig. 1 Strategies adopted to boost the exploitation of laccases

fungal laccase orthologs (~ 70% protein sequence identity) were shuffled and assembled in vivo into *Saccharomyces cerevisiae* (Mateljak et al. 2019a). An enriched library of shuffled thermostable laccases with considerable sequence diversity was rapidly generated. Several variants displayed modified activity preferences for particular substrates and improved stability at acidic pH. Sequence analysis of selected enzymes helped to shed light on the recognition of specific residues involved in substrate oxidation (Mateljak et al. 2019a).

Nowadays, computational analyses proved to be robust approaches to reliably forecast specific enzyme regions to be mutated with reduction of the screening efforts. Indeed, the combination of computational approach with experimental validation has been fruitfully and always more frequently tested for designing efficient and tailored catalysts for specific applications (Monza et al. 2015; Santiago et al. 2016; Giacobelli et al. 2017; Díaz et al. 2018; Mateljak et al. 2019b). By combination of computational design with directed evolution, Mateljak and coworkers created a laccase library with the aim to increase enzyme activity towards high-redox-potential mediators (Mateljak et al. 2019b). As a result of this strategy, an enhancement of the T1 redox potential was obtained, with a concomitant improvement in thermal and acidic pH stability of the enzyme. The substitution of hydrophobic residues surrounding the T1 Cu site was considered responsible for these effects.

Several application tests of the engineered laccases were performed at a laboratory scale, and mainly in the bioremediation field, while scattered examples are present in other sectors.

Engineered laccases in bioremediation

The exploitation of laccases in bioremediation processes was the object of blooming research in the last decades, occupying the widest slice (~ 30%) of published examples on laccase biotechnological uses (Pezzella et al. 2015; Mate and Alcalde 2017). In this scenario, laccase engineering offered the potential to enrich the portfolio of exploitable biocatalysts, providing new enzymes, with improved efficiency in selected processes (Table 1).

Laccases were reported to oxidize a wide range of environmental pollutants, including polycyclic aromatic hydrocarbons (PAHs), recalcitrant dyes, organophosphorous compounds, and endocrine disruptor chemicals (EDCs) (Sharma et al. 2018). Two mechanisms were postulated in the laccase-mediated bioremediation (Jeon and Chang 2013): (i) the oxidative bond cleavage, resulting into the formation of less toxic products and (ii) the oxidative coupling, leading to polymerization of polluting molecules, which can then be subsequently removed by filtration/sedimentation. The occurrence of the alternative mechanisms depends on several factors (i.e., the nature of the oxidizable substrate, the half-life of the corresponding radical, the laccase redox potential) and strives towards the oxidative bond cleavage in the presence of redox mediators (Sharma et al. 2018).

A plethora of both fungal and bacterial laccases from different sources was tested for bioremediation processes, exploring their diversity in substrate specificity, as well as their ability to withstand with the harsh conditions which usually characterize polluted wastewaters, i.e., extreme pHs, high salt concentration, and presence of organic solvents (Majeau et al. 2010). Nakagawa et al swapped N- and C-terminal domains between Lcc4 and Lcc1 from *Lentinula edodes* and expressed the mutated laccase in tobacco cell culture, with the idea to combine the efficient secretion of Lcc1 with the broad substrate reactivity of Lcc4 (Nakagawa et al. 2010). The resulting Lcc4/1 enzyme, besides exhibiting properties that are intermediate between those of the parental enzymes, proved to be more efficient, compared to Lcc1, in decolorizing RBBR and poly-R478, even if the latter is only in the presence of a redox mediator (Nakagawa et al. 2011).

POXA1b laccase from *Pleurotus ostreauts* was the target of several rounds of random and semi-rational mutagenesis (Festa et al. 2008; Miele et al. 2010; Piscitelli et al. 2011). Its high redox potential and remarkable stability at alkaline pH make this enzyme an ideal candidate for environmental applications (Pezzella et al. 2017). Two evolved variants, selected for their improved catalytic activity towards the phenolic substrate, 2,6-DMP, were tested for their ability to decolorize industrial dyes with complex trisazo-, polyazo-, and stilbene-type structures (Miele et al. 2010). Both mutants displayed a wider dye degradation specificity compared to the wild type, resulting in the ability to decolorize the recalcitrant stilbene-type dye. Interestingly, one of these mutants also displayed an increased stability at acidic pH, besides storing its stability at alkaline pH. Inspection of protein models of the evolved mutants allowed localization of mutations in the loops next to the substrate-binding pocket, ascribing a potential role in the interaction of the enzyme with the reducing substrate (Miele et al. 2010). A panel of twelve POXA1b improved variants, selected after three random mutagenesis rounds according to different criteria (activity *vs* phenolic and non-phenolic substrates at different pHs, pH stability), was applied to the decolorization of different textile wastewater models characterized by different composition, pH, and salt concentration (Piscitelli et al. 2011). These mutants displayed further unpredictable enhanced stability features, which made them best suited candidates for wastewater treatment. As a fact, seven out of twelve variants provided an increased decolorization of the acid wastewater model with respect to the wild type (Piscitelli et al. 2011). Among the panel of POXA1b mutants reported by Piscitelli and coworkers (Piscitelli et al. 2011), 1H6C deserved attention for its higher redox potential with respect to the wild type (Macellaro et al. 2014a). This variant was investigated in the treatment of EDCs with different chemical structures, drawing a complex picture of results. 1H6C displayed a higher BPA

Table 1 Application of engineered laccases to target processes

Laccase engineering	Target process	Reference
Laccase Lcc4/1, composed of the N-terminus of the Lcc4 and the C-terminus of the Lcc1 laccases from *Lentinula edodes*	RBBR and Poly-R478 decolorization	Nakagawa et al. 2010
Pleurotus ostreatus POXA1b mutants (2L4A, 3L7H) obtained through random mutagenesis	Decolorization of industrial dyes with different chemical structures	Miele et al. 2010
Site-directed mutagenesis of *Trametes versicolor* laccase (TvL) addressing four Phe residues in key positions of the binding pocket	Bisphenol A (BPA) degradation	Galli et al. 2011
Twelve *P. ostreatus* POXA1b mutants obtained through three generations of random mutagenesis	Decolorization of industrial wastewaters	Piscitelli et al. 2011
Lac15 form marine metagenomic library, devoid of C-terminal residues	Hair coloring at alkaline pH	Fang et al. 2014
P. ostreatus POXA1b mutant, 1H6C, deriving from a combination of random and rational mutagenesis approaches	Degradation of Endocrine disrupting compounds (EDCs)	Macellaro et al. 2014a
PM1 laccase mutant (Chu-B) obtained after several rounds of evolution and hybrid approaches	H_2O electrolysis	Pita et al. 2014
Myceliophtora albomyces laccase mutant, rationally designed	Aniline oxidation	Santiago et al. 2016
Alkaline laccase mutant from *M. thermophila* obtained through random mutagenesis	Synthesis of C–N heteropolymeric dyes	Vicente et al. 2016
Bacillus pumilus CotA mutant (GWLF), obtained by combination of rational and computer-aided approaches	Decolorization of industrial dyes Evans blue decolorization and detoxification	Chen et al. 2017 Xia et al. 2019
Rheinheimera sp. laccase mutant (ΔRhLacc) obtained through random mutagenesis	Deinking of old newspaper Indigo carmine decolorization	Gupta et al. 2019
Bacillus licheniformis CotA laccase mutant obtained through combination of random and rational mutagenesis	Bioelectrocatalytic reduction of O_2	Lopes et al. 2019
CotA variant obtained by DNA shuffling	Indigo carmine and Congo red decolorization	Ouyang and Zhao 2019
CueO mutant obtained after directed evolution	Enzymatic biofuel cells	Zhang et al. 2019

degradation with respect to POXA1b in the absence of any mediator, while this difference was annulled by the addition of redox mediators (Macellaro et al. 2014b). Interestingly, the two enzymes displayed an opposite behavior in nonylphenol degradation, in response to different mediators: in the presence of ABTS, 1H6C was more effective than POXA1b, whereas in the presence of acetosyringone (AS), POXA1b proved to be more efficient than its variant. Furthermore, 1H6C was much less efficient than the wild type in methyl-, butyl-parabens degradation. Taken together, these data highlighted how laccase reactivity is an intricate multidimensional issue, in which the electron transfer driving force is a key factor influenced not only by T1 E^0, but also by the right position of the substrate in the binding pocket (Giacobelli et al. 2017).

Consistent with this idea, BPA degradation was achieved by testing different *T. versicolor* TvL single-point mutants, designed to allow the oxidation of bulky phenolic substrates (Galli et al. 2011). Four phenylalanine residues in key positions at the entrance of the binding pocket were replaced by smaller-sized, but still apolar, alanines. A double mutant, combining the mutations causing the highest oxidation extents of bulky substrates, was the most effective in BPA degradation (Galli et al. 2011).

A rational mutagenesis approach, supported by a computer-aided design program, was applied to increase the specificity of *Bacillus pumilus* CotA laccase towards ABTS, as well as its thermostability (Chen et al. 2017). Analogously to what was observed for POXA1b mutagenesis, the introduced mutations also induced an unexpected enhancement in pH stability, probably as a result of the strengthened hydrogen bonding and electrostatic interactions. This feature encouraged the use of this engineered laccase in the decolorization of some industrial dyes under alkaline conditions. When compared to the wild type, CotA mutant was more efficient in the degradation of methyl red, RBBR, and AB129 dyes (Chen et al. 2017). The same CotA mutant was further engineered to improve its functional expression in *Pichia pastoris* (Xia et al. 2019). The resulting variant was found able to efficiently decolorize and detoxify the carcinogenic dye Evans blue, catalyzing the transformation of the azo bond into N_2, instead of toxic aniline compounds (Xia et al. 2019). Finally, very recently, Gupta et al. (2019) reported an interesting example of application of mutated laccase, which witnessed the importance of the other copper sites, besides T1 center, in laccase functionality. By means of a random mutagenesis approach, the authors isolated a truncated variant of a novel laccase from *Rheinheimera* sp., devoid of domain 3 containing T1 copper center. Surprisingly, the truncated mutant preserved the performances of wild type in deinking of old newspaper and degradation of indigo dye, if external copper was added (Gupta et al. 2019). The mutant was also less affected by pH and temperature inactivation than the wild type. In silico analysis revealed substantial structural differences in the truncated

mutant, such as the complete absence of beta turns, assumed to be responsible for the greater stability of the variant with respect to wild type (Gupta et al. 2019).

The reviewed data indicate that besides the mutations aimed at enlarging the substrate binding pocket (Galli et al. 2011), the positive effect observed in pollutant removal is almost unpredictable a priori. The success of a laccase-based bioremediation process relies on the combination of two main factors: the specificity towards the target xenobiotic and the tolerance to the conditions in which the biocatalyst is used. In order to achieve this hit, future laccase engineering will have to focus on both these targets, stressing the usefulness of in silico simulations in unveiling the molecular determinants for the efficient oxidation of a target molecule (Pardo et al. 2016), as well as designing high-throughput screening protocols for the selection of evolved variants more suitable to the final operative conditions.

Engineered laccases in other sectors

The design of laccases tailored for several case-specific applications was also fruitfully applied. A reliable in silico protocol, combining classical and quantum mechanics, aimed towards improving both substrate binding and electron transfer, allowed to predict and validate a laccase mutant with enhanced performances in aniline oxidation (Santiago et al. 2016). Laccase variants designed to cope to harsh process conditions required for specific applications, were selected after several rounds of evolution and hybrid approaches (Pita et al. 2014; Lopes et al. 2019). A CotA mutant from *Bacillus licheniformis*, operating in basic media and seawater, was effective in catalyzing the bioelectrocatalytic O_2 reduction, suggesting a prospective enzyme application for sustainable production of energy from seawater and oxygen (Lopes et al. 2019). Similarly, a PM1 laccase variant, specifically selected for high resistance to anionic inhibitors, i.e., halide and hydroxyls, was applied to H_2O electrolysis with high O_2 production, assuring high durability of the enzymatic electrode (Pita et al. 2014).

Two interesting examples demonstrate the effectiveness of a screening system focused on the final application (Vicente et al. 2016; Zhang et al. 2019). An alkaline laccase mutant form *Myceliophthora thermophila* was chosen and further evolved for the synthesis of the C–N polydye at basic pHs. Over 11,500 clones derived form 3 rounds of directed and focused evolution were screened through a high-throughput colorimetric assay, and a variant with 3.5-fold improved activity relative to that of the wild type was selected (Vicente et al. 2016). Zhang et al. (2019) developed a robust electrochemical screening system for the directed evolution of CueO laccase with an efficient immobilization on electrodes from crude cell extracts. A CueO variant, with two mutations mapped adjacently to the coordinated ligands of the T1 Cu site, was obtained with a significantly increased onset potential, and an enhancement of power output when applied to the cathode of the enzymatic biofuel cell (Zhang et al. 2019).

Chimeric laccases

During the last 10 years, different hosts have been used to develop chimeric laccases combining their abilities to those of various relevant proteins with the aim to adapt their scope to ad hoc applications.

One of the first chimeric laccase was obtained fusing a *Pycnoporus cinnabarinus* laccase to the C-terminal linker and carbohydrate-binding module (CBM) of *Aspergillus niger* cellobiohydrolase B (CBHB) (Ravalason et al. 2009) and produced in *A. niger*. The authors demonstrated that the laccase-CBM, endowed with a carbohydrate-binding capability, displayed an enhanced biobleaching ability. Furthermore, subsequent studies showed that laccase-CBM/HBT (1-hydroxybenzotriazole) treatment led to a better preservation of the pulp properties. This effect was probably due to fiber surface modifications involving the action of the CBM. Transmission electron microscopy examination of pulp fibers indicated retention of laccase-CBM inside the pulp fibers due to CBM binding and an increased external micro-fibrillation of the fibers due to enzymatic treatments (Ravalason et al. 2012). Shortly after, other two chimerae were developed and expressed in *Escherichia coli* by Ribeiro et al. (2011) combining the *Bacillus subtilis* CotA laccase with xynA xylanase or with its thermostable variant xynAG3. The effect of the chimeric enzyme on the bleaching of cellulose pulp was tested. The release of phenolic compounds from pulp by the CotA-XynAG3 chimera was 2.3-fold higher than that of the parental enzyme mixture, showing that the physical proximity of the two catalytic domains synergistically enhanced activities of each enzyme.

In research on new sustainable pretreatments for lignocellulosic raw material valorisation, laccases offer the possibility to increase the yield of sugar recovery due to alteration of lignin hydrophobicity and porosity (Giacobbe et al. 2018). A chimeric laccase was created by insertion of the β-1,3–1,4-glucanase (*bglS*) gene into the *cotA* coding sequence, and its hydrolytic activity was assayed against natural milled sugarcane bagasse (Furtado et al. 2013). The hydrolytic activity of the chimeric enzyme was 20% higher than that of the equimolar mixtures of the separate parental enzymes in the presence of ABTS as mediator.

During recent years, the production of designed cellulosomes has gained increasing attention (Bayer 2017). A designed cellulosome is a chimeric system able to boost degradative potential of a single enzyme through a highly ordered structural organization that enables enzyme synergy among the multiple enzymatic activities. These complexes are based on a combination of scaffoldins, cohesins, and dockerins. Scaffoldins are non-

catalytic subunits serving as a docking backbone containing both a cellulose-specific carbohydrate-binding module (CBM) and multiple cohesin modules. In turn, cohesins specifically interact with dockerins, which carry different enzymatic subunits. Hyeon and coworkers recombinantly expressed in *E. coli* the scaffoldin miniCbpA and the chimeric laccase, composed by CueO and the dockerin of a cellulosome system (Hyeon et al. 2014). When applied to the pretreatment of barley straw, the CueO-miniCbpA almost doubled the amount of reduced sugar and, consequently, the bioethanol yield. Davidi and colleagues worked on the integration of the laccase from *Thermobifida fusca* into a bacterial cellulosome alongside two cellulases and a xylanase (Davidi et al. 2016). A new chimeric enzyme (Xyn-c-Lac) formed by a dockerin, a xylanase, and a laccase was expressed in *E. coli* and its activity was tested on a wheat straw substrate to evaluate the benefits of the simultaneous degradation of the three main components of lignocellulose. The presence of Xyn-c-Lac into the designed cellulosome machinery allowed a twofold increase in the amount of reducing sugar production compared with cellulosome lacking the laccase. This result proved the effectiveness of the proximity among the enzymatic components of the designed cellulosome.

Furukawa et al. (2013) and Iiyoshi et al. (2017) had the idea to directly express a chimeric laccase in plant cells to develop low-lignin plants facilitating their conversion into biofuels. Thus, a chimeric laccase composed by the *T. versicolor* fungal laccase (Lac) and a bacterial cellulose-binding module domain (CBD) was produced both in the rice plant *Oryza sativa* (Furukawa et al. 2013) and in the dicot model plant *Arabidopsis thaliana* (Iiyoshi et al. 2017). Albeit both transgenic plants showed normal morphology and growth, an increased sugar yield was obtained after their treatment, confirming the hypothesis that the Lac-CBD expression triggered structural changes in the cell wall composition.

Inspired by the cellulosome action, a fascinating approach to enhance laccase catalyzed-melanin degradation by bringing the enzyme in proximity to its substrate, was proposed by Shin et al (Shin et al. 2019). The authors fused the *E. coli* laccase CueO to the dockerin domain of endoglucanase B from *Clostrium cellulovorans*. The chimera was designed to be brought directly on the melanin substrate by the interaction with a scaffoldin fused to the melanin-binding peptide (MBP). By combining laccase activity on melanin with the synergistic action of a dockerin-fused peroxidase, an enzymatic complex for efficient melanin degradation via hydrogen peroxide circulation was realized (Shin et al. 2019).

The fusion of laccases to self-assemble and adhesive hydrophobins allowed to functionalize different material surfaces (Fokina et al. 2016; Sorrentino et al. 2019). Fokina et al. succeeded in designing a functional chimeric protein composed of LccC from *Aspergillus nidulans* and the hydrophobin DewA. Since the chimera was efficiently secreted in the extracellular medium, the culture broth was directly used for coating of glass and polystyrene, without additional purification steps (Fokina et al. 2016). Taking advantage of the same procedure, but implementing its great potentialities, Sorrentino et al. (2019) immobilized the *Pleurotus ostreatus* POXA1b-Vmh2 chimera on polystyrene multi-well plates and developed a rapid and easy-to-use biosensing platform for the detection of phenolic compounds (L-DOPA and caffeic acid) in different matrices. The method was based on the use of the analytes as competing inhibitors of the laccase-catalyzed ABTS oxidation (Sorrentino et al. 2019).

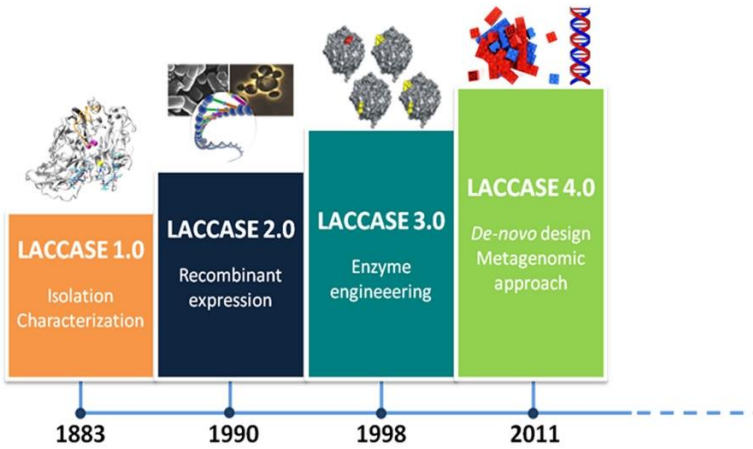

Fig. 2 Temporary evolution of the laccase green era

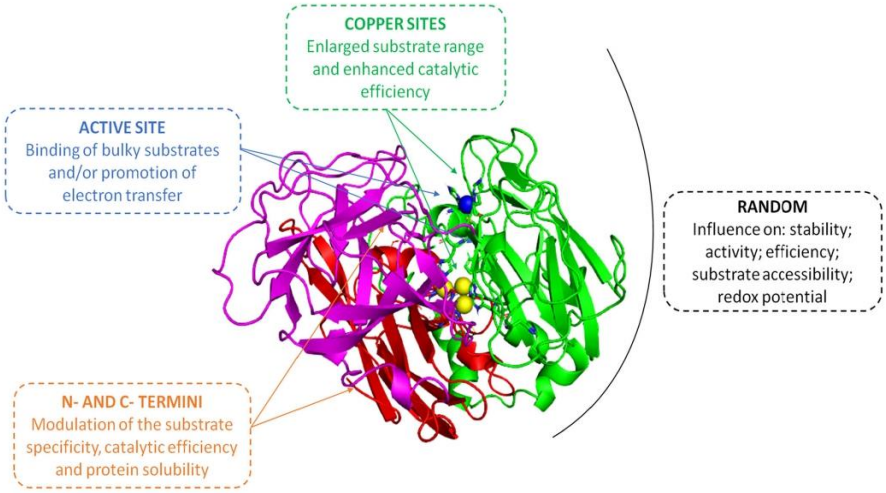

Fig. 3 Target regions for laccase mutations

Concluding remarks

When Yoshida discovered firstly a laccase from the Japanese lacquer tree, he could have ever expected neither its enormous potential nor the opening of a green era revolution (Fig. 2). Nowadays, it is well clear to the whole laccase researcher community that natural and/or engineered laccases are at the peak of that revolution. The challenge at this point is to produce at high titers these enzymes and to develop laccases with exciting and tailored biotechnological properties through the combination of laboratory evolution with both rational and semi-rational strategies. Results of the last 10 years surveyed in this review single out how the promising future foreseen for laccases is becoming truer and truer, but it cannot disregard a continuous feedback with the industry world. In fact, although an improvement in enzyme performances was reported for engineered laccases compared to the corresponding wild type (Fig. 3), in most of the cases, the "gained" ability is not directly related to the property for which the engineered enzyme was specifically designed/selected. Therefore, when performing a rational approach, the winning strategy relies on *à la carte* designing a laccase towards a specific substrate. On the other

Fig. 4 Engineered laccase chimera

hand, a proper screening strategy for the selection of the "jackpot mutant" for a specific application is mandatory in the case of random mutagenesis. In this scenario, the assistance of computational approaches represents a substantial added value in aiding proper design of an efficient and tailored catalyst for specific applications. Furthermore, the combination of laccase activity—natural or even improved—with the ability of relevant proteins proved to be an added value in the establishment of a flexible and well-rounded biocatalyst (Fig. 4). Fueled by these hints, the exciting perspectives of the metagenomic approach (Ye et al. 2010; Fang et al. 2011; Ausec et al. 2017; Yue et al. 2017; Qu et al. 2018; Yang et al. 2018; Dandare et al. 2019), and of the *de-novo* design (Glykys et al. 2011) foster the beginning of a laccase 4.0 era (Fig. 2) that will accelerate the strengthening of the industrial application of laccases. Now, it is up to the industry and the scientists to stay tuned.

Compliance with ethical standards

Conflict of interest The authors declare that they have no conflict of interest.

Ethical approval This article does not contain any studies with human participants or animals performed by any of the authors.

References

Ausec L, Berini F, Casciello C, Cretoiu MS, van Elsas JD, Marinelli F, Mandic-Mulec I (2017) The first acidobacterial laccase-like multicopper oxidase revealed by metagenomics shows high salt and thermo-tolerance. Appl Microbiol Biotechnol 101:6261–6276. https://doi.org/10.1007/s00253-017-8345-y

Bayer EA (2017) Cellulosomes and designer cellulosomes: why toy with Nature? Env Microbiol Rep 9:14–15. https://doi.org/10.1111/1758-2229.12489

Cambria MT, Gullotto D, Garavaglia S, Cambria A (2012) In silico study of structural determinants modulating the redox potential of Rigidoporus lignosus and other fungal laccases. J Biomol Struct Dyn 30:89–101. https://doi.org/10.1080/07391102.2012.674275

Cañas AI, Camarero S (2010) Laccases and their natural mediators: biotechnological tools for sustainable eco-friendly processes. Biotechnol Adv 28:694–705. https://doi.org/10.1016/j.biotechadv.2010.05.002

Chandra R, Chowdhary P (2015) Properties of bacterial laccases and their application in bioremediation of industrial wastes. Environ Sci Process Impacts 17:326–342. https://doi.org/10.1039/c4em00627e

Chen Y, Luo Q, Zhou W, Xie Z, Cai YJ, Liao XR, Guan ZB (2017) Improving the catalytic efficiency of *Bacillus pumilus* CotA-laccase by site-directed mutagenesis. Appl Microbiol Biotechnol 101:1935–1944. https://doi.org/10.1007/s00253-016-7962-1

Cruz Ramírez MG, Rivera-Rios JM, Téllez-Jurado A, Maqueda Gálvez AP, Mercado-Flores Y, Arana-Cuenca A (2012) Screening for thermotolerant ligninolytic fungi with laccase, lipase, and protease activity isolated in Mexico. J Environ Manag 95:256–259. https://doi.org/10.1016/j.jenvman.2010.10.045

Dandare SU, Young JM, Kelleher BP, Allen CCR (2019) The distribution of novel bacterial laccases in alpine paleosols is directly related to soil stratigraphy. Sci Total Environ 671:19–27. https://doi.org/10.1016/j.scitotenv.2019.03.250

Davidi L, Moraïs S, Artzi L, Knop D, Hadar Y, Arfi Y, Bayer EA (2016) Toward combined delignification and saccharification of wheat straw by a laccase-containing designer cellulosome. Proc Natl Acad Sci U S A 113:1–6. https://doi.org/10.1073/pnas.1608012113

Díaz R, Yuridia MF, Díaz-Godínez G, Herrera-Zúñiga LD, Álvarez-Cervantes J, Anducho-Reyes MA (2018) In silico generation of laccase mutants from lacc 6 of *Pleurotus ostreatus* and bacterial enzymes. BioResources 13:8113–8131. https://doi.org/10.15376/biores.13.4.8113-8131

Fang Z, Li T, Wang Q, Zhang X, Peng H, Fang W, Hong Y, Ge H, Xiao Y (2011) A bacterial laccase from marine microbial metagenome exhibiting chloride tolerance and dye decolorization ability. Appl Microbiol Biotechnol 89:1103–1110. https://doi.org/10.1007/s00253-010-2934-3

Fang Z, Zhou P, Chang F, Yin Q, Fang W, Yuan J, Zhang X, Xiao Y (2014) Structure-based rational design to enhance the solubility and thermostability of a bacterial laccase Lac15. PLoS One 9:1–6. https://doi.org/10.1371/journal.pone.0102423

Fernández-Fernández M, Sanromán MÁ, Moldes D (2013) Recent developments and applications of immobilized laccase. Biotechnol Adv 31:1808–1825. https://doi.org/10.1016/j.biotechadv.2012.02.013

Festa G, Autore F, Fraternali F, Giardina P, Sannia G (2008) Development of new laccases by directed evolution: functional and computational analyses. Proteins 72:25–34. https://doi.org/10.1002/prot.21889

Fillat Ú, Ibarra D, Eugenio M, Moreno A, Tomás-Pejó E, Martín-Sampedro R (2017) Laccases as a potential tool for the efficient conversion of lignocellulosic biomass: a review. Fermentation 3:17. https://doi.org/10.3390/fermentation3020017

Fokina O, Fenchel A, Winandy L, Fischer R (2016) Immobilization of LccC laccase from *Aspergillus nidulans* on hard surfaces via fungal hydrophobins. Appl Environ Microbiol 82:6395–6402. https://doi.org/10.1128/aem.01413-16

Furtado GP, Ribeiro LF, Lourenzoni MR (2013) Enzyme shows synergistic sugar release from milled sugarcane bagasse. Protein Eng Des Sel 26:15–23. https://doi.org/10.1093/protein/gzs057

Furukawa T, Sawaguchi C, Watanabe A, Takahashi M, Nigorikawa M, Furukawa K, Iimura Y, Kajita S, Oguchi T, Ito Y, Sonoki T (2013) Application of fungal laccase fused with cellulose-binding domain to develop low- lignin rice plants. J Biosci Bioeng 116:616–619. https://doi.org/10.1016/j.jbiosc.2013.05.007

Galli C, Gentili P, Jolivalt C, Madzak C, Vadalà R (2011) How is the reactivity of laccase affected by single-point mutations? Engineering laccase for improved activity towards sterically demanding substrates. Appl Microbiol Biotechnol 91:123–131. https://doi.org/10.1007/s00253-011-3240-4

Ghatge S, Yang Y, Song WY, Kim TY, Hur HG (2018) A novel laccase from thermoalkaliphilic bacterium *Caldalkalibacillus thermarum* strain TA2.A1 able to catalyze dimerization of a lignin model compound. Appl Microbiol Biotechnol 102:4075–4086. https://doi.org/10.1007/s00253-018-8898-4

Giacobbe S, Pezzella C, Lettera V, Sannia G (2018) Bioresource technology laccase pretreatment for agrofood wastes valorization. Bioresour Technol 265:59–65. https://doi.org/10.1016/j.biortech.2018.05.108

Giacobelli VG, Monza E, Fatima Lucas M, Pezzella C, Piscitelli A, Guallar V, Sannia G (2017) Repurposing designed mutants: a valuable strategy for computer-aided laccase engineering-the case of POXA1b. Catal Sci Technol 7:515–523. https://doi.org/10.1039/c6cy02410f

Giardina P, Faraco V, Pezzella C, Piscitelli A, Vanhulle S, Sannia G (2010) Laccases: a never-ending story. Cell Mol Life Sci 67:369–385. https://doi.org/10.1007/s00018-009-0169-1

Glykys DJ, Szilvay GR, Tortosa P, Suárez Diez M, Jaramillo A, Banta S (2011) Pushing the limits of automatic computational protein design: design, expression, and characterization of a large synthetic

protein based on a fungal laccase scaffold. Syst Synth Biol 5:45–58. https://doi.org/10.1007/s11693-011-9080-9

Gupta V, Balda S, Gupta N, Capalash N, Sharma P (2019) Functional substitution of domain 3 (T1 copper center) of a novel laccase with Cu ions. Int J Biol Macromol 123:1052–1061. https://doi.org/10.1016/j.ijbiomac.2018.11.174

Hakulinen N, Rouvinen J (2015) Three-dimensional structures of laccases. Cell Mol Life Sci 72:857–868. https://doi.org/10.1007/s00018-014-1827-5

Hyeon J, Kyou S, Hee D, Ryu S, Kim M, Lee S, Ok S (2014) Enzymatic degradation of lignocellulosic biomass by continuous process using laccase and cellulases with the aid of scaffoldin for ethanol production. Process Biochem 49:1266–1273. https://doi.org/10.1016/j.procbio.2014.05.004

Iiyoshi R, Oguchi T, Furukawa T, Iimura Y (2017) Expression of a fungal laccase fused with a bacterial cellulose-binding module improves the enzymatic saccharification efficiency of lignocellulose biomass in transgenic *Arabidopsis thaliana*. Transgenic Res 26:753–761. https://doi.org/10.1007/s11248-017-0043-0

Jeon JR, Chang YS (2013) Laccase-mediated oxidation of small organics: bifunctional roles for versatile applications. Trends Biotechnol 31:335–341. https://doi.org/10.1016/j.tibtech.2013.04.002

Jones SM, Solomon EI (2015) Electron transfer and reaction mechanism of laccases. Cell Mol Life Sci 72:869–883. https://doi.org/10.1007/s00018-014-1826-6

Khodakarami A, Goodarzi N, Hoseinzadehdehkordi M, Amani F, Khodaverdian S, Khajeh K, Ghazi F, Ranjbar B, Amanlou M, Dabirmanesh B (2018) Rational design toward developing a more efficient laccase: catalytic efficiency and selectivity. Int J Biol Macromol 112:775–779. https://doi.org/10.1016/j.ijbiomac.2018.02.019

Kudanga T, Le Roes-Hill M (2014) Laccase applications in biofuels production: current status and future prospects. Appl Microbiol Biotechnol 98:6525–6542. https://doi.org/10.1007/s00253-014-5810-8

Kudanga T, Nyanhongo GS, Guebitz GM, Burton S (2011) Potential applications of laccase-mediated coupling and grafting reactions: a review. Enzym Microb Technol 48:195–208. https://doi.org/10.1016/j.enzmictec.2010.11.007

Le Goff A, Holzinger M, Cosnier S (2015) Recent progress in oxygen-reducing laccase biocathodes for enzymatic biofuel cells. Cell Mol Life Sci 72:941–952. https://doi.org/10.1007/s00018-014-1828-4

Liu H, Zhu L, Bocola M, Chen N, Spiess AC, Schwaneberg U (2013) Directed laccase evolution for improved ionic liquid resistance. Green Chem 15:1348–1355. https://doi.org/10.1039/c3gc36899h

Lopes P, Koschorreck K, Nedergaard Pedersen J, Ferapontov A, Lörcher S, Skov Pedersen J, Urlacher VB, Ferapontova EE (2019) *Bacillus Licheniformis* CotA laccase mutant: electrocatalyticreduction of O 2 from 0.6 V (SHE) at pH 8 and in seawater. Chem Electro Chem 6:2043–2049. https://doi.org/10.1002/celc.201900363

Macellaro G, Baratto MC, Piscitelli A, Pezzella C, De Biani FF, Palmese A, Piumi F, Record E (2014a) Effective mutations in a high redox potential laccase from *Pleurotus ostreatus*. https://doi.org/10.1007/s00253-013-5491-8

Macellaro G, Pezzella C, Cicatiello P, Sannia G, Piscitelli A (2014b) Fungal laccases degradation of endocrine disrupting compounds. Biomed Res Int 2014:1–8. https://doi.org/10.1155/2014/614038

Majeau JA, Brar SK, Tyagi RD (2010) Laccases for removal of recalcitrant and emerging pollutants. Bioresour Technol 101:2331–2350. https://doi.org/10.1016/j.biortech.2009.10.087

Martínez AT, Ruiz-Dueñas FJ, Camarero S, Serrano A, Linde D, Lund H, Vind J, Tovborg M, Herold-Majumdar OM, Hofrichter M, Liers C, Ullrich R, Scheibner K, Sannia G, Piscitelli A, Pezzella C, Sener ME, Kılıç S, van Berkel WJH, Guallar V, Lucas MF, Zuhse R, Ludwig R, Hollmann F, Fernández-Fueyo E, Record E, Faulds CB, Tortajada M, Winckelmann I, Rasmussen JA, Gelo-Pujic M, Gutiérrez A, del Río JC, Rencoret J, Alcalde M (2017) Oxidoreductases on their way to industrial biotransformations. Biotechnol Adv 35:815–831. https://doi.org/10.1016/j.biotechadv.2017.06.003

Martins LO, Durão P, Brissos V, Lindley PF (2015) Laccases of prokaryotic origin: enzymes at the interface of protein science and protein technology. Cell Mol Life Sci 72:911–922. https://doi.org/10.1007/s00018-014-1822-x

Mate DM, Alcalde M (2015) Laccase engineering: from rational design to directed evolution. Biotechnol Adv 33:25–40. https://doi.org/10.1016/j.biotechadv.2014.12.007

Mate DM, Alcalde M (2017) Laccase: a multi-purpose biocatalyst at the forefront of biotechnology. Microb Biotechnol 10:1457–1467. https://doi.org/10.1111/1751-7915.12422

Maté D, García-Burgos C, García-Ruiz E, Ballesteros AO, Camarero S, Alcalde M (2010) Laboratory evolution of high-redox potential laccases. Chem Biol 17:1030–1041. https://doi.org/10.1016/j.chembiol.2010.07.010

Mate DM, Garcia-Ruiz E, Camarero S, Shubin VV, Falk M, Shleev S, Ballesteros AO, Alcalde M (2013a) Switching from blue to yellow: altering the spectral properties of a high redox potential laccase by directed evolution. Biocatal Biotransf 31:8–21. https://doi.org/10.3109/10242422.2012.749463

Mate DM, Gonzalez-Perez D, Falk M, Kittl R, Pita M, De Lacey AL, Ludwig R, Shleev S, Alcalde M (2013b) Blood tolerant laccase by directed evolution. Chem Biol 20:223–231. https://doi.org/10.1016/j.chembiol.2013.01.001

Mateljak I, Monza E, Lucas MF, Guallar V, Aleksejeva O, Ludwig R, Leech D, Shleev S, Alcalde M (2019a) Increasing redox potential, redox mediator activity, and stability in a fungal laccase by computer-guided mutagenesis and directed evolution. ACS Catal 9:4561–4572. https://doi.org/10.1021/acscatal.9b00531

Mateljak I, Rice A, Yang K, Tron T, Alcalde M (2019b) The generation of thermostable fungal laccase chimeras by SCHEMA-RASPP structure-guided recombination in vivo. ACS Synth Biol 8:833–843. https://doi.org/10.1021/acssynbio.8b00509

Miele A, Giardina P, Sannia G, Faraco V (2010) Random mutants of a *Pleurotus ostreatus* laccase as new biocatalysts for industrial effluents bioremediation. J Appl Microbiol 108:998–1006. https://doi.org/10.1111/j.1365-2672.2009.04505.x

Mollania N, Khajeh K, Ranjbar B, Hosseinkhani S (2011) Enhancement of a bacterial laccase thermostability through directed mutagenesis of a surface loop. Enzym Microb Technol 49:446–452. https://doi.org/10.1016/j.enzmictec.2011.08.001

Monza E, Lucas MF, Camarero S, Alejaldre LC, Martínez AT, Guallar V (2015) Insights into laccase engineering from molecular simulations: toward a binding-focused strategy. J Phys Chem Lett 6:1447–1453. https://doi.org/10.1021/acs.jpclett.5b00225

Nakagawa Y, Sakamoto Y, Kikuchi S, Sato T, Yano A (2010) A chimeric laccase with hybrid properties of the parental *Lentinula edodes* laccases. Microbiol Res 165:392–401. https://doi.org/10.1016/j.micres.2009.08.006

Nakagawa Y, Toda Y, Yamamura H, Hayakawa M, Iimura Y (2011) FLO11 is essential for pellicle formation by wild pellicle-forming yeasts isolated from contaminated wines. J Biosci Bioeng 111:7–9

Nasoohi N, Khajeh K, Mohammadian M, Ranjbar B (2013) International Journal of Biological Macromolecules Enhancement of catalysis and functional expression of a bacterial laccase by single amino acid replacement. Int J Biol Macromol 60:56–61. https://doi.org/10.1016/j.ijbiomac.2013.05.011

Osma JF, Toca-Herrera JL, Rodríguez-Couto S (2010) Uses of laccases in the food industry. Enzyme Res 2010:1–8. https://doi.org/10.4061/2010/918761

Ouyang F, Zhao M (2019) Enhanced catalytic efficiency of CotA-laccase by DNA shuffling. Bioengineered 10:182–189. https://doi.org/10.1080/21655979.2019.1621134

Pardo I, Camarero S (2015) Exploring the oxidation of lignin-derived phenols by a library of laccase mutants. 15929–15943. https://doi.org/10.3390/molecules200915929

Pardo I, Vicente AI, Mate DM, Alcalde M, Camarero S (2012) Development of chimeric laccases by directed evolution. Biotechnol Bioeng 109:2978–2986. https://doi.org/10.1002/bit.24588

Pardo I, Santiago G, Gentili P, Lucas F, Monza E, Medrano FJ, Galli C, Martínez AT, Guallar V, Camarero S (2016) Re-designing the substrate binding pocket of laccase for enhanced oxidation of sinapic acid. Catal Sci Technol 6:3900–3910. https://doi.org/10.1039/c5cy01725d

Pezzella C, Guarino L, Piscitelli A (2015) How to enjoy laccases. Cell Mol Life Sci 72:923–940. https://doi.org/10.1007/s00018-014-1823-9

Pezzella C, Guido V, Lettera V, Olivieri G, Cicatiello P, Sannia G, Piscitelli A (2017) A step forward in laccase exploitation: recombinant production and evaluation of techno-economic feasibility of the process. J Biotechnol 259:175–181. https://doi.org/10.1016/j.jbiotec.2017.07.022

Piscitelli A, Cinzia P, Paola G, Vincenza F, Sannia G (2010) Heterologous laccase production and its role in industrial applications. Bioeng Bugs 1:252–262. https://doi.org/10.4161/bbug.1.4.11438

Piscitelli A, Del Vecchio C, Faraco V, Giardina P, MacEllaro G, Miele A, Pezzella C, Sannia G (2011) Fungal laccases: versatile tools for lignocellulose transformation. C R Biol 334:789–794. https://doi.org/10.1016/j.crvi.2011.06.007

Piscitelli A, Amore A, Faraco V (2012) Last advances in synthesis of added value compounds and materials by laccasemediated biocatalysis

Pita M, Mate DM, Gonzalez-Perez D, Shleev S, Fernandez VM, Alcalde M, De Lacey AL (2014) Bioelectrochemical oxidation of water. J Am Chem Soc 136:5892–5895. https://doi.org/10.1021/ja502044j

Polak J, Jarosz-Wilkolazka A (2012) Fungal laccases as green catalysts for dye synthesis. Process Biochem 47:1295–1307. https://doi.org/10.1016/j.procbio.2012.05.006

Qu W, Liu T, Wang D, Hong G, Zhao J (2018) Metagenomics-based discovery of Malachite green-degradation gene families and enzymes from mangrove sediment. Front Microbiol 9:1–11. https://doi.org/10.3389/fmicb.2018.02187

Ravalason H, Herpoël-gimbert I, Record E, Bertaud F, Petit-conil M, Sigoillot J (2009) Fusion of a family 1 carbohydrate binding module of *Aspergillus niger* to the *Pycnoporus cinnabarinus* laccase for efficient softwood kraft pulp biobleaching. 142:220–226. https://doi.org/10.1016/j.jbiotec.2009.04.013

Ravalason H, Bertaud F, Herpoël-gimbert I, Meyer V, Ruel K, Joseleau J, Grisel S, Olivé C, Sigoillot J, Petit-conil M (2012) Laccase / HBT and laccase-CBM / HBT treatment of softwood kraft pulp: impact on pulp bleachability and physical properties. Bioresour Technol 121:68–75. https://doi.org/10.1016/j.biortech.2012.06.077

Ribeiro LF, Furtado GP, Lourenzoni MR, Costa-filho AJ, Santos CR, Nogueira SCP, Betini JA, Polizeli MDL, Murakami MT, Ward RJ (2011) Engineering bifunctional laccase-xylanase chimeras for improved catalytic performance. 286:43026–43038. https://doi.org/10.1074/jbc.M111.253419

Rodríguez-Delgado MM, Alemán-Nava GS, Rodríguez-Delgado JM, Dieck-Assad G, Martínez-Chapa SO, Barceló D, Parra R (2015) Laccase-based biosensors for detection of phenolic compounds. TrAC - Trends Anal Chem 74:21–45. https://doi.org/10.1016/j.trac.2015.05.008

Roth S, Spiess AC (2015) Laccases for biorefinery applications: a critical review on challenges and perspectives. Bioprocess Biosyst Eng 38:2285–2313. https://doi.org/10.1007/s00449-015-1475-7

Santiago G, De Salas F, Lucas MF, Monza E, Acebes S, Martinez ÁT, Camarero S, Guallar V (2016) Computer-aided laccase engineering: toward biological oxidation of arylamines. ACS Catal 6:5415–5423. https://doi.org/10.1021/acscatal.6b01460

Sharma A, Jain KK, Jain A, Kidwai M, Kuhad RC (2018) Bifunctional in vivo role of laccase exploited in multiple biotechnological applications. Appl Microbiol Biotechnol 102:10327–10343. https://doi.org/10.1007/s00253-018-9404-8

Shin SK, Hyeon JE, Joo YC, Jeong DW, You SK, Han SO (2019) Effective melanin degradation by a synergistic laccase-peroxidase enzyme complex for skin whitening and other practical applications. Int J Biol Macromol 129:181–186. https://doi.org/10.1016/j.ijbiomac.2019.02.027

Singh G, Arya SK (2019) Utility of laccase in pulp and paper industry: a progressive step towards the green technology. Int J Biol Macromol 134:1070–1084. https://doi.org/10.1016/j.ijbiomac.2019.05.168

Siroosi M, Amoozegar MA, Khajeh K, Dabirmanesh B (2018) Decolorization of dyes by a novel sodium azide-resistant spore laccase from a halotolerant bacterium, *Bacillus safensis* sp. strain S31. Water Sci Technol 77:2867–2875. https://doi.org/10.2166/wst.2018.281

Sorrentino I, Giardina P, Piscitelli A (2019) Development of a biosensing platform based on a laccase-hydrophobin chimera. Appl Microbiol Biotechnol 103:3061–3071. https://doi.org/10.1007/s00253-019-09678-2

Vicente AI, Viña-Gonzalez J, Santos-Moriano P, Marquez-Alvarez C, Ballesteros AO, Alcalde M (2016) Evolved alkaline fungal laccase secreted by *Saccharomyces cerevisiae* as useful tool for the synthesis of C–N heteropolymeric dye. J Mol Catal B Enzym 134:323–330. https://doi.org/10.1016/j.molcatb.2016.10.004

Xia J, Wang Q, Luo Q, Chen Y, Liao XR, Guan ZB (2019) Secretory expression and optimization of *Bacillus pumilus* CotA-laccase mutant GWLF in *Pichia pastoris* and its mechanism on Evans blue degradation. Process Biochem 78:33–41. https://doi.org/10.1016/j.procbio.2018.12.034

Yang J, Li W, Bun Ng T, Deng X, Lin J, Ye X (2017) Laccases: production, expression regulation, and applications in pharmaceutical biodegradation. Front Microbiol 8. https://doi.org/10.3389/fmicb.2017.00832

Yang Q, Zhang M, Zhang M, Wang C, Liu Y, Fan X, Li H (2018) Characterization of a novel, cold-adapted, and thermostable laccase-like enzyme with high tolerance for organic solvents and salt and potent dye decolorization ability, derived from a marine metagenomic library. Front Microbiol 9:1–9. https://doi.org/10.3389/fmicb.2018.02998

Ye M, Li G, Liang WQ, Liu YH (2010) Molecular cloning and characterization of a novel metagenome-derived multicopper oxidase with alkaline laccase activity and highly soluble expression. Appl Microbiol Biotechnol 87:1023–1031. https://doi.org/10.1007/s00253-010-2507-5

Yue Q, Yang Y, Zhao J, Zhang L, Xu L, Chu X, Liu X, Tian J, Wu N (2017) Identification of bacterial laccase cueO mutation from the metagenome of chemical plant sludge. Bioresour Bioprocess 4. https://doi.org/10.1186/s40643-017-0178-0

Zerva A, Koutroufini E, Kostopoulou I, Detsi A, Topakas E (2019) A novel thermophilic laccase-like multicopper oxidase from *Thermothelomyces thermophila* and its application in the oxidative cyclization of 2′,3,4-trihydroxychalcone. New Biotechnol 49:10–18. https://doi.org/10.1016/j.nbt.2018.12.001

Zhang L, Cui H, Zou Z, Garakani TM, Novoa-Henriquez C, Jooyeh B, Schwaneberg U (2019) Directed evolution of a bacterial laccase (CueO) for enzymatic biofuel cells. Angew Chem Int Ed 58:4562–4565. https://doi.org/10.1002/anie.201814069

Zucca P, Cocco G, Sollai F, Sanjust E (2016) Fungal laccases as tools for biodegradation of industrial dyes. Biocatalysis 1:82–108. https://doi.org/10.1515/boca-2015-0007

5.2 From Graphite to Laccase Biofunctionalized Few-Layer Graphene: A “One Pot” Approach Using a Chimeric Enzyme

International Journal of
Molecular Sciences

MDPI

Article

From Graphite to Laccase Biofunctionalized Few-Layer Graphene: A "One Pot" Approach Using a Chimeric Enzyme

Ilaria Sorrentino [1,2†], Ilaria Stanzione [2,†], Yannig Nedellec [1], Alessandra Piscitelli [2,*], Paola Giardina [2] and Alan Le Goff [1,*]

[1] Department of Molecular Chemistry, University Grenoble Alpes, CNRS, 38000 Grenoble, France; ilaria.sorrentino@univ-grenoble-alpes.fr (I.S.); yannig.nedellec@univ-grenoble-alpes.fr (Y.N.)
[2] Department of Chemical Sciences, University Federico II, 80126 Naples, Italy; ilaria.stanzione@unina.it (I.S.); giardina@unina.it (P.G.)
* Correspondence: apiscite@unina.it (A.P.); alan.le-goff@univ-grenoble-alpes.fr (A.L.G.)
† These authors contributed equally to the work

Received: 28 April 2020; Accepted: 22 May 2020; Published: 26 May 2020

Abstract: A chimeric enzyme based on the genetic fusion of a laccase with a hydrophobin domain was employed to functionalize few-layer graphene, previously exfoliated from graphite in the presence of the hydrophobin. The as-produced, biofunctionalized few-layer graphene was characterized by electrochemistry and Raman spectroscopy, and finally employed in the biosensing of phenols such as catechol and dopamine. This strategy paves the way for the functionalization of nanomaterials by hydrophobin domains of chimeric enzymes and their use in a variety of electrochemical applications.

Keywords: laccase; hydrophobin; graphene

1. Introduction

Graphene is a two-dimensional sheet of sp^2-hybridized carbon that exhibits unparalleled properties such as high planar surface, superlative mechanical strength, and remarkable thermal and electrical conductivity. Due to its extraordinary structure and fascinating properties, graphene is the most studied nanomaterial and can be integrated as the core of cutting-edge devices in many types of applications, ranging from microelectronics to electrochemical energy harvesting systems [1–8]. In biosensing in particular, graphene acts as a conductive platform for biomolecule immobilization and electrochemical detection of bioanalytes [9–14]. Graphene-based electrochemical biosensing has relied on the recent developments in the study of graphene electrochemical properties, its production, and biofunctionalization. Different techniques have been investigated for the production of graphene such as scotch-tape transfer, chemical vapor deposition (CVD) growth, and chemically or electrochemically reduced graphene oxide. These strategies lead to different nanomaterials in terms of size, edge and basal defects, number of layers, and oxygenated defect content. Although CVD produces a large surface of monolayer graphene, soft exfoliation of graphite has also been able to provide low-cost access to few-layer graphene (FLG) dispersions. The dispersion stability is one of the main challenges to address during the exfoliation procedure, as in general, the re/aggregation of exfoliated material is minimized by using organic solvents or surfactant–water solutions [15–17]. Like other nanomaterials, graphene is a very suitable platform for enzyme immobilization thanks to its high surface area, dispersion in solution, and tunable surface chemistry. Intense efforts have been devoted to this research field in the last five years, resulting in the immobilization of different enzymes for various applications [18]. However, the hydrophobic interactions driving the direct immobilization of active proteins on graphene surface are often difficult to achieve, and modifications

of the protein 3D structures can occur with detrimental effects on their functionality [19]. Two main approaches have been implemented, and often combined, to overcome this issue, such as the use of graphene oxide (GO) whose surface is more hydrophilic, or the exploitation of graphene-based composites, such as microcellulose, chitosan, and various metal oxides [18].

Recently, proteins prone to forming amyloid structures have been proven to be able to biofunctionalize graphene. In this respect, the fungal self-assembling class I hydrophobin Vmh2 from *Pleurotus ostreatus* has been successfully exploited to disperse and stabilize FLG in ethanol–water mixtures by ultrasonic wave exfoliation. [20] Hydrophobins (HFB) are a family of small self-assembling proteins produced by filamentous fungi, and can be divided into two classes that differ for the nature of the amphipathic layers that they form. Fibrillar structures formed by class I HFB are extremely robust, are disassembled only in strong acids, and share structural properties with amyloid fibrils [21]. HFB efficiently adheres to several hydrophobic surfaces, including 2D materials, such as graphene [20]. This ability has been further exploited by genetic fusion of the hydrophobin to biotechnologically relevant proteins that can be immobilized on various surfaces, obtaining the so-called "self-immobilizing" proteins/enzymes [22]. Recently a new chimeric protein was designed to combine the HFB Vmh2 with a laccase enzyme (Lac), Lac-Vmh2 [23]. Laccases (*p*-diphenol-dioxygenoxidoreductases; EC 1.10.3.2) are multicopper oxidases able to catalyze the oxidation of a wide range of aromatic substrates using oxygen as co-substrate and producing water as the only by-product. These enzymes are promising biocatalysts with possible applications in bioremediation, chemical synthesis, biobleaching of paper pulp, and biosensing [24]. Laccases have been immobilized on various carriers, using different methods with both advantages and drawbacks. Among the various enzymes, the laccase POXA1b from *P. ostreatus* was chosen for its peculiar characteristics such as its stability and activity in a wide range of pHs and temperatures, as well as its high redox potential [25]. The produced Lac-Vmh2 allowed achievement of simple and stable immobilization of the enzyme on polystyrene [23].

The main purpose of this work was to advance the biofunctionalization of graphene with Vmh2, immobilizing laccase on FLG by using the fusion protein Lac-Vmh2 through a "one-pot" approach. The presented method is easy, eco-friendly, and versatile, because, in principle, a wide variety of different HFB chimera proteins can be used in this one-pot exfoliation/functionalization procedure. As a proof of concept, the as-prepared Lac-Vmh2/FLG was used for the modification of Glassy Carbon (GC) electrodes to build an electrochemical sensor for phenolic compounds, such as catechol, a well-known environmental pollutant, and dopamine, a renowned neurotransmitter.

2. Results and Discussion

2.1. Laccase Immobilization on FLG

Graphite exfoliation was carried out, as previously described, by exposing mixtures of Vmh2 protein and graphite to ultrasonic waves [20]. Vmh2-exfoliated graphene is generally stable in 60% ethanol (EtOH) thanks to the presence of the HFB. On the other hand, enzymes are usually used and stable in aqueous buffers. Thus, conditions have to be assessed to preserve both the stability of graphene dispersion and the enzyme activity. The wild-type PoxA1b laccase and Lac-Vmh2 were dialyzed toward different ethanol concentration (20%, 40%, 50% and 60% EtOH,) and 10 mM Tris-HCl pH 8, in order to test the stability of the enzyme in these conditions. Concomitantly, the Vmh2 graphene samples in 60% EtOH were centrifuged and pellets were solubilized with or without the addition of 0.05 mg mL^{-1} of Vmh2 in the same conditions tested for enzymatic stability. The optimal condition for the graphene stability was 50% EtOH + Vmh2 and 40% EtOH + Vmh2 (Figure S1). On the other hand, the enzyme stability was reasonable up to 40% EtOH (Table S1). Thus, looking both at the enzyme and the graphene stability, the 40% EtOH was selected as the optimal solvent for graphite exfoliation in the presence of laccase.

To study and optimize the condition of laccase immobilization on the FLG, several tests were performed (Figure 1). Addition of the enzymes (wild-type or chimera) was performed after exfoliation of graphite in the presence of Vmh2 (route A). Addition of the enzyme solutions to

graphite powder was performed at the beginning of the exfoliation (route B). Or, in situ exfoliation of graphite with Vmh2 was followed by the addition of the enzymes in the last 10 min of sonication (route C). Each route was compared by measuring the enzymatic activity [25] of the biofunctionalized FLG (previously separated after centrifugation at 13,000 rpm for 15 min) obtained after centrifugation. Results are displayed in Table S2. Route A led to final no enzymatic activity, indicating that negligible amounts of enzymes can be immobilized on FLG after exfoliation of graphite with Vmh2. When the chimera was used to exfoliate graphene from graphite (route B), the extensive ultrasonication time led to a complete loss of the enzymatic activity of laccase. To avoid a long exposure of the enzymes to ultrasonic waves, route C was used in the course of this work. In the latter route, wild-type or chimera were added during the last 10 min of the exfoliation process in order to prevent enzyme inactivation. An immobilization yield of 5% and 11%, for PoxA1b or Lac-Vmh2, respectively, was estimated, considering the enzymatic activity before and after immobilization. According to the activity of the immobilized Lac-Vmh2, this corresponded to an enzyme loading of about 0.4 U per mg of FLG (Table 1). Lac-Vmh2 showed a slight increased amount of attached enzyme as compared to the wild-type enzyme. Indeed, POXA1b was able to stick to graphene, as already observed using polystyrene [23]. Nevertheless, the stability of the biofunctionalized graphene obtained with Lac-Vmh2 was higher than that of the wild-type enzyme, in terms of both activity and adhesion (Table 1).

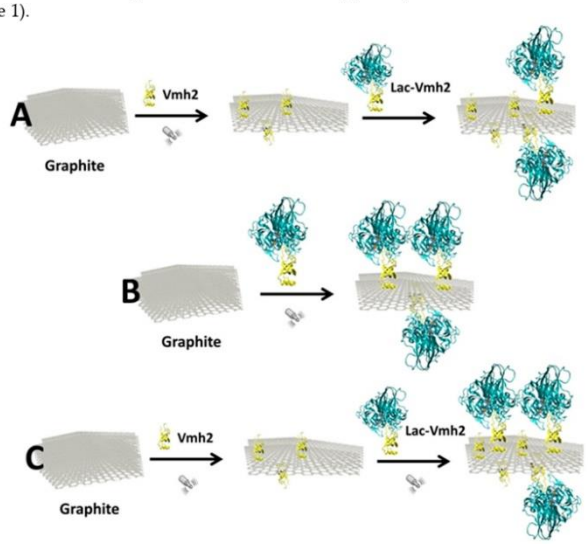

Figure 1. Tests performed to exfoliate and biofunctionalize graphite with laccase chimera, Lac-Vmh2. (**A**): graphite exfoliation in the presence of Vmh2 (~ 5h) and subsequent addition of Lac-Vmh2; (**B**): graphite exfoliation in the presence of both Vmh2 and Lac-Vmh2 (~ 5h); (**C**): graphite exfoliation in the presence of Vmh2 (~ 5h) and addition of Lac-Vmh2 in the last 10 min of exfoliation.

Table 1. Summary of the sample enzymatic activity and their characteristics.

Samples	Units in Milligrams of Graphene (U $^{mg-1}$)	$t_{1/2}$ (Days)	Activity after Washing
Graphene/PoxA1b	0.3 ± 0.1	17	Stable up to the second wash
Graphene/Lac-Vmh2	0.4 ± 0.1	26	Stable up to the fourth wash

The biofunctionalized graphene was stable at least for 30 days (Figure 2A).

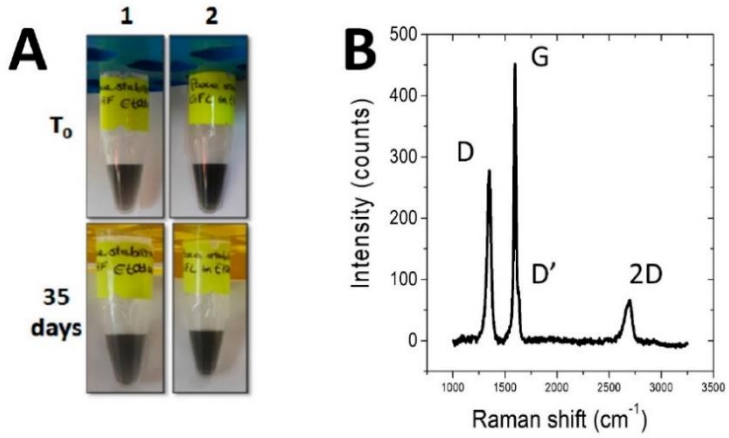

Figure 2. (**A**) Stability of graphene dispersion at time zero and after 35 days: lane1: Graphene/PoxA1b; lane 2: Graphene/Lac-Vmh2. (**B**) Representative Raman spectrum of a Lac-Vmh2-biofunctionlized few-layer graphene (FLG) film.

Raman spectroscopy was also performed in order to characterize the number of graphene layers for these biofunctionalized FLG (Figure 2B). According to Ferrari's work [26], the high-energy band observed at 2700 cm^{-1} stems for the presence of only few graphene layers (<5 layers), as already observed in the case of the native Vmh2 hydrophobin [20]. It is noteworthy that the Raman spectrum was also performed after several months on the same stock solution of Lac-Vmh2-functionalized FLG without showing any restacking nor aggregation phenomena.

2.2. Exploitation of Biofunctionalized FLG in Electrochemical Biosensing

GC electrodes were then modified by drop-casting a solution of biofunctionalized FLG. The incubation was performed at room temperature until the electrode was completely dry, and then several washes with citrate-phosphate buffer pH 5.0 were executed to eliminate the unbound sample.

Figure 3 displays a typical SEM image of biofunctionalized FLG deposited onto planar gold electrode. This underlines the homogenous dispersion of FLG both in solution and at the surface of the electrode. According to size distribution study, the sizes of biofunctionalized FLG are mostly below 2 μm^2. These nanostructured bioelectrodes were employed for biosensing experiments. The principle of laccase biosensors is based on the enzymatic oxidation of phenols or o-diphenols into quinones, the latter being subsequently reduced at the nanostructured electrode polarized at a redox potential required for the electroreduction of quinone into phenols, that is, E = −0.2 V vs. saturated calomel electrode (SCE). The regeneration of the catechol derivative triggers an amplification cycle of "enzymatic oxidation/electrochemical reduction", which increases biosensing sensitivity.

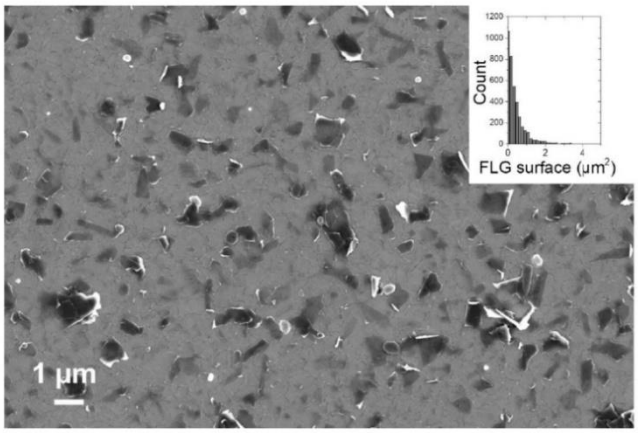

Figure 3. SEM image of biofunctionalized FLG at the surface of a gold electrode; (inset) size distribution of biofunctionalized FLG obtained by ImageJ.

Addition of both catechol and dopamine was monitored at Lac-Vmh2-biofunctionalized FLG electrodes. Figure 4A displays a representative chronoamperometry experiment performed upon the addition of catechol.

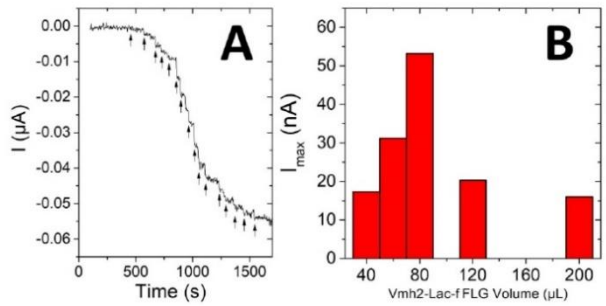

Figure 4. (**A**) Chronoamperometry performed at Lac-Vmh2-biofunctionlized FLG electrode after successive additions of catechol (indicated by the arrows, applied potential = −0.2 V vs. saturated calomel electrode (SCE), 0.1 M Phosphate-buffered saline (PBS), pH 6, 25 °C). (**B**) Plot of the maximum current towards volume of drop-coated Lac-Vmh2-biofunctionlized FLG solutions.

Chronoamperometry at different volumes of FLG (Figure 4B) were performed, showing that an optimum value of biofunctionalized FLG was reached after the drop-coating of 80 µL (16 mU) solution on GC electrodes. These experiments underlined the fact that an optimal volume of FLG was needed in order to maximize the amount of immobilized enzymes while also providing efficient diffusion of catechol into the nanostructured FLG conductive film. In order to indirectly confirm the interaction between the Vmh2 domain of the chimera and graphene layer, the wild-type POXA1b was also used in the exfoliation process of FLG. However, on the contrary to the Lac-Vmh2-biofunctionlized FLG electrode (Figure 4A), negligible current was observed for catechol oxidation, underlining the fact that less adsorption of POXA1b was observed on FLG. This also demonstrated the important role of the Vmh2 domain in order to immobilize laccase at the surface of FLG.

Figure 5 displays the calibration curves for catechol and dopamine recorded at these electrodes. The shape of the curves was governed by the enzymatic reaction that was reliability modelized according to typical Michaelis–Menten kinetics. Table 2 summarizes the electrochemical characteristics of the modelized curves.

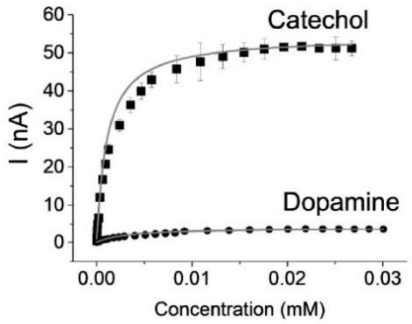

Figure 5. Plot of the catalytic current towards increasing concentrations of (■) catechol and (●) dopamine for electrodes (measurements performed by chronoamperometry at E = −0.2 V vs. SCE, 0.1 M PBS, pH 6, 25 °C).

Table 2. Electrochemical characteristics obtained after modelization of the curve according Michaelis–Menten kinetics; equation: $I = (I_{MAX} \times [substrate])/(K_M + [substrate])$.

Substrate	K_M (mM)	I_{MAX} (nA cm^{-2})	R^2
Catechol	1.1	775.7	0.99
Dopamine	3.0	55.5	0.95

The apparent Michaelis–Menten constant (K_{Mapp}) reflected the enzyme-substrate affinity, which was higher in the case of dopamine when compared to catechol for laccase. A lower Km value is advantageous in the case of laccase-based sensors in order to observe linear range with a minimal limit of detection and a maximal sensitivity. Laccase has a better affinity for catechol compared to dopamine. This is the reason why biosensors based on laccases always exhibit better performance towards catechol as compared to dopamine.

The linear part of the curve is shown in Figure 6.

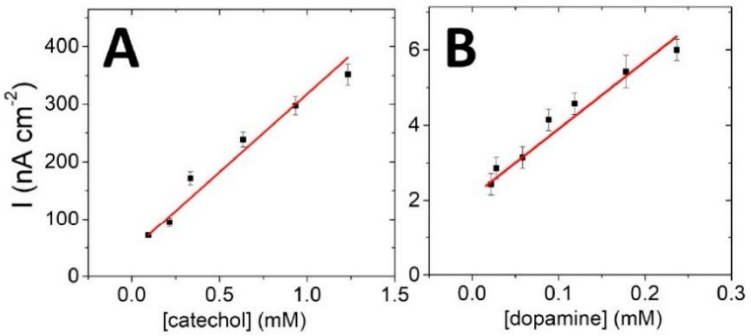

Figure 6. Plot of the linear part of the catalytic current density towards concentration of (**A**) catechol and (**B**) dopamine ($E_{applied}$ = −0.2 V vs. SCE, 0.1 M PBS, pH 6, 25 °C).

Limit of detection (LOD) of 20 μM was separately measured for both catechol and dopamine, with sensitivity of 0.27 mA M^{-1} cm^{-2} (R^2 = 0.97) towards catechol and 16.4 μA M^{-1} cm^{-2} (R^2 = 0.96) towards dopamine being measured with respective linear ranges of 20 to 1000 μM and 20 to 250 μM. Although the most efficient phenolic biosensors are based on a combination of tyrosinases and laccases, [27,28] or based on the use of redox hydrogels [29,30], this type of nanostructured biosensor approaches the performances of other types of biosensors that associate graphene and laccases [29,31,32]

3. Materials and Methods

All products were purchased from Sigma-Aldrich and were used without further purification. All solvents were of analytical grade. Distilled water was passed through a Milli-Q water purification system to obtain ultrapure water at 18.2 MΩ cm^{-1}. Phosphate-buffered saline (PBS) solution was prepared from Milli-Q water.

3.1. Electrochemical Measurements

The electrochemical experiments were carried out in a three-electrode electrochemical cell using Ametek Multipotentiostat Princeton Applied Research (Wokingham, UK). A Pt wire was used as the counter electrode and the saturated calomel electrode (SCE) served as the reference electrode. All experiments were conducted at room temperature. All simulated curves were obtained via Origin Pro 9.0. Error bars were estimated from three measurements recorded per sample.

3.2. Laccase Enzymes

Both fusion proteins Lac-Vmh2 and wild-type enzyme POXA1b were produced and secreted by the yeast *Pichia pastoris* in the culture media. The supernatant, after centrifugation for 15 min at 6000 rpm at 4 °C, was concentrated and dialyzed towards 50 mM Tris-HCl buffer, pH 8.0, using Centricon Centrifugal Filter Units 10kDa (Merck, Darmstadt, Germany). The laccase enzymes are used without additional purification steps. The total protein concentration was determined using the Pierce 660 method (Thermo Fischer Scientific, Waltham, Massachusetts, MA, USA) and using (Bovine Serum Albumin) BSA as the standard. The laccase activity was assayed at room temperature, monitoring the oxidation of ABTS (2,2′-azino-bis(3-ethylbenzothiazoline-6-sulphonic acid)) at 420 nm ($\varepsilon_{420\,nm}$ = 3.6 × 10^4 M^{-1} cm^{-1})—the assay mixture contained 2 mM ABTS and 0.1 M sodium citrate buffer, pH 3.0.

3.3. In Situ Exfoliation of Graphite

Graphite powder, 1 mg/mL (Aldrich, 332461, mesh number of grains +100, >75%), was exfoliated in batches of 7.5 mL of 60% *v/v* ethanol (EtOH) in MilliQ water (in 20 mL flasks) and 7.5 mL of 50 µg/mL Vmh2, using a medium power tip sonicator (Ultrasound SONOPLUS HD3200, maximum power 200 W, working frequency 20 kHz, KE-76 probe, running at 15% amplitude. BANDELIN, Berlin Germany) and cooling the system in an ice bath. The exfoliation was stopped when the energy value was 450 KJ (about 5 h of sonication time). To remove the unexfoliated material, consecutive 40 min centrifugations at increased centrifugal force were performed (40×, 160× and 620× *g*). We characterized and used the dispersions obtained after the last centrifugation.

Three types of experiments were tested with the laccase enzymes:

- A 7 mL solution of PoxA1b or Lac-Vmh2 in 40% EtOH was added to Vmh2-exfoliated graphene and incubated at 4°C whilst stirring continuously.
- The immobilization was performed by adding the wild-type or chimeric enzyme solution to graphite powder at the beginning of the exfoliation.
- The wild-type or chimeric enzyme solution was added during the last 10 min of exfoliation. Indeed, the inactivation of the enzyme when higher sonication time was used has been previously verified. The process was performed normalizing the activity units (4 U_{tot} for both) between wild-type POXA1b and Lac-Vmh2 (0.16 mg and 0.44 mg, respectively).

4. Conclusions

This work shows that Lac-Vmh2 chimera enzyme can be used both as a surfactant of FLG while also providing enzymatic activity to biofunctionalized nanomaterials. This original biofunctionalization technique represents a soft and biocompatible technique compared to the use of more classic long-alkyl-chain surfactants, leading to stable exfoliation of FLGs. The possibility to merge Vmh2 with active enzymes into chimera enzymes brings novel physico-chemical properties to this exfoliation technique. Here, deposition of these biofunctionalized FLGs on electrodes affords the fabrication of catechol and dopamine biosensors. This novel strategy of functionalizing carbon nanomaterials with specific chimeric enzymes paves the way for the development of many types of novel chimeric enzymes that can be developed for a variety of applications involving multienzymatic systems and biofunctionalization of nanomaterials.

Supplementary Materials: Supplementary materials can be found at www.mdpi.com/1422-0067/21/11/3741/s1. Figure S1: Stability of graphene dispersion in different solvents; Table S1: $t_{1/2}$ of laccases in different buffers; Table S2: Summary of the immobilization experiments.

Author Contributions: Experiments, I.St. and I.So.; Raman spectroscopy, Y.N.; writing—review and editing, A.L.G., A.P., and P.G.; supervision, A.L.G., A.P., and P.G.; project administration, A.L.G., A.P., and P.G.; funding acquisition, A.L.G., A.P., and P.G.; I.St. and I.So. contributed equally to this work. All authors have read and agreed to the published version of the manuscript.

Funding: This project is funded by the Italian Education, University and Research Ministry (MIUR) and the French National Research Agency (ANR), and co-funded by European Union's Horizon 2020 research and innovation program under the framework of ERA-NET Cofund MarTERA (Maritime and Marine Technologies for a new Era), FLAshMoB, Functional Amyloid chimera for Marine Biosensing (ID: 172). This work was also supported by the Agence Nationale de la Recherche through the LabEx ARCANE programme (ANR-11-LABX-0003-01) and the Graduate School on Chemistry, Biology and Health of Univ Grenoble Alpes CBH-EUR-GS (ANR-17-EURE-0003). The authors acknowledge support from the plateforme de Chimie NanoBio ICMG FR 2607 (PCN-ICMG).

Conflicts of Interest: The authors declare no conflict of interest.

References

1. Pumera, M. Voltammetry of carbon nanotubes and graphenes: excitement, disappointment, and reality. *Chem. Rec.* **2012**, *12*, 201–213, doi:10.1002/tcr.201100027.

2. Brownson, D.A.C.; Lacombe, A.C.; Gómez-Mingot, M.; Banks, C.E. Graphene oxide gives rise to unique and intriguing voltammetry. *Rsc. Adv.* **2011**, *2*, 665–668, doi:10.1039/C1RA00743B.
3. Brownson, D.A.C.; Munro, L.J.; Kampouris, D.K.; Banks, C.E. Electrochemistry of graphene: not such a beneficial electrode material? *Rsc. Adv.* **2011**, *1*, 978–988, doi:10.1039/C1RA00393C.
4. Kampouris, D.K.; Banks, C.E. Exploring the physicoelectrochemical properties of graphene. *Chem. Commun.* **2010**, *46*, 8986–8988, doi:10.1039/C0CC02860F.
5. Novoselov, K.S.; Fal'ko, V.I.; Colombo, L.; Gellert, P.R.; Schwab, M.G.; Kim, K. A roadmap for graphene. *Nature* **2012**, *490*, 192–200, doi:10.1038/nature11458.
6. Ferrari, A.C.; Bonaccorso, F.; Fal'ko, V.; Novoselov, K.S.; Roche, S.; Bøggild, P.; Borini, S.; Koppens, F.H.L.; Palermo, V.; Pugno, N.; et al. Science and technology roadmap for graphene, related two-dimensional crystals, and hybrid systems. *Nanoscale* **2015**, *7*, 4598–4810, doi:10.1039/C4NR01600A.
7. Zhang, F.; Li, Y.-H.; Li, J.-Y.; Tang, Z.-R.; Xu, Y.-J. 3D graphene-based gel photocatalysts for environmental pollutants degradation. *Environ. Pollut.* **2019**, *253*, 365–376, doi:10.1016/j.envpol.2019.06.089.
8. Zhang, N.; Yang, M.-Q.; Liu, S.; Sun, Y.; Xu, Y.-J. Waltzing with the Versatile Platform of Graphene to Synthesize Composite Photocatalysts. *Chem. Rev.* **2015**, *115*, 10307–10377, doi:10.1021/acs.chemrev.5b00267.
9. Fritea, L.; Tertis, M.; Sandulescu, R.; Cristea, Chapter Eleven - C. Enzyme–Graphene Platforms for Electrochemical Biosensor Design With Biomedical Applications. In *Methods in Enzymology*; Kumar, C.V., Eds.; Academic Press (Cambridge, Massachusetts, MA, USA): 2018; Vol. 609, pp. 293–333.
10. Pumera, M. Graphene in biosensing. *Mater. Today* **2011**, *14*, 308–315, doi:10.1016/S1369-7021(11)70160-2.
11. Zhang, W.; Jia, B.; Furumai, H. Fabrication of graphene film composite electrochemical biosensor as a pre-screening algal toxin detection tool in the event of water contamination. *Sci. Rep.* **2018**, *8*, 1–10, doi:10.1038/s41598-018-28959-w.
12. Lalaoui, N.; Le Goff, A.; Holzinger, M.; Mermoux, M.; Cosnier, S. Wiring Laccase on Covalently Modified Graphene: Carbon Nanotube Assemblies for the Direct Bio-electrocatalytic Reduction of Oxygen. *Chem. Eur. J.* **2015**, *21*, 3198–3201, doi:10.1002/chem.201405557.
13. Le Goff, A.; Reuillard, B.; Cosnier, S. A Pyrene-Substituted Tris(bipyridine)osmium(II) Complex as a Versatile Redox Probe for Characterizing and Functionalizing Carbon Nanotube- and Graphene-Based Electrodes. *Langmuir* **2013**, *29*, 8736–8742, doi:10.1021/la401712u.
14. Fritea, L.; Le Goff, A.; Putaux, J.-L.; Tertis, M.; Cristea, C.; Sandulescu, R.; Cosnier, S. Design of a reduced-graphene-oxide composite electrode from an electropolymerizable graphene aqueous dispersion using a cyclodextrin-pyrrole monomer. Application to dopamine biosensing. *Electrochim. Acta* **2015**, *178*, 108–112, doi:10.1016/j.electacta.2015.07.124.
15. Keeley, G.P.; O'Neill, A.; Holzinger, M.; Cosnier, S.; Coleman, J.N.; Duesberg, G.S. DMF-exfoliated graphene for electrochemical NADH detection. *Phys. Chem. Chem. Phys.* **2011**, *13*, 7747–7750, doi:10.1039/C1CP20060G.
16. Lotya, M.; Hernandez, Y.; King, P.J.; Smith, R.J.; Nicolosi, V.; Karlsson, L.S.; Blighe, F.M.; De, S.; Wang, Z.; McGovern, I.T.; et al. Liquid Phase Production of Graphene by Exfoliation of Graphite in Surfactant/Water Solutions. *J. Am. Chem. Soc.* **2009**, *131*, 3611–3620, doi:10.1021/ja807449u.
17. Smith, R.J.; Lotya, M.; Coleman, J.N. The importance of repulsive potential barriers for the dispersion of graphene using surfactants. *New J. Phys.* **2010**, *12*, 125008, doi:10.1088/1367-2630/12/12/125008.
18. Ramakrishna, T.R.B.; Nalder, T.D.; Yang, W.; Marshall, S.N.; Barrow, C.K. Controlling enzyme function through immobilisation on graphene, graphene derivatives and other two dimensional nanomaterials. *J. Mater. Chem. B* **2018**, *6*, 3200–3218, doi:10.1039/C8TB00313K.
19. Rodrigues, R.C.; Ortiz, C.; Berenguer-Murcia, Á.; Torres, R.; Fernández-Lafuente, R. Modifying enzyme activity and selectivity by immobilization. *Chem. Soc. Rev.* **2013**, *42*, 6290–6307, doi:10.1039/C2CS35231A.
20. Gravagnuolo, A.M.; Morales-Narváez, E.; Longobardi, S.; da Silva, E.T.; Giardina, P.; Merkoçi, A. In Situ Production of Biofunctionalized Few-Layer Defect-Free Microsheets of Graphene. *Adv. Funct. Mater.* **2015**, *25*, 2771–2779, doi:10.1002/adfm.201500016.
21. Zampieri, F.; Wösten, H.A.B.; Scholtmeijer, K. Creating Surface Properties Using a Palette of Hydrophobins. *Materials* **2010**, *3*, 4607–4625, doi:10.3390/ma3094607.
22. Piscitelli, A.; Pennacchio, A.; Longobardi, S.; Velotta, R.; Giardina, P. Vmh2 hydrophobin as a tool for the development of "self-immobilizing" enzymes for biosensing. *Biotechnol. Bioeng.* **2017**, *114*, 46–52, doi:10.1002/bit.26049.

23. Sorrentino, I.; Giardina, P.; Piscitelli, A. Development of a biosensing platform based on a laccase-hydrophobin chimera. *Appl. Microbiol. Biotechnol.* **2019**, *103*, 3061–3071, doi:10.1007/s00253-019-09678-2.
24. Pezzella, C.; Guarino, L.; Piscitelli, A. How to enjoy laccases. *Cell. Mol. Life Sci.* **2015**, *72*, 923–940, doi:10.1007/s00018-014-1823-9.
25. Pezzella, C.; Giacobelli, V.G.; Lettera, V.; Olivieri, G.; Cicatiello, P.; Sannia, G.; Piscitelli, A. A step forward in laccase exploitation: Recombinant production and evaluation of techno-economic feasibility of the process. *J. Biotechnol.* **2017**, *259*, 175–181, doi:10.1016/j.jbiotec.2017.07.022.
26. Ferrari, A.C.; Meyer, J.C.; Scardaci, V.; Casiraghi, C.; Lazzeri, M.; Mauri, F.; Piscanec, S.; Jiang, D.; Novoselov, K.S.; Roth, S.; et al. Raman Spectrum of Graphene and Graphene Layers. *Phys. Rev. Lett.* **2006**, *97*, 187401, doi:10.1103/PhysRevLett.97.187401.
27. Yaropolov, A.I.; Kharybin, A.N.; Emnéus, J.; Marko-Varga, G.; Gorton, L. Flow-injection analysis of phenols at a graphite electrode modified with co-immobilised laccase and tyrosinase. *Anal. Chim. Acta* **1995**, *308*, 137–144, doi:10.1016/0003-2670(94)00404-A.
28. Freire, R.S.; Thongngamdee, S.; Durán, N.; Wang, J.; Kubota, L.T. Mixed enzyme (laccase/tyrosinase)-based remote electrochemical biosensor for monitoring phenolic compounds. *Analyst* **2002**, *127*, 258–261, doi:10.1039/B110011D.
29. Rodríguez-Delgado, M.M.; Alemán-Nava, G.S.; Rodríguez-Delgado, J.M.; Dieck-Assad, G.; Martínez-Chapa, S.O.; Barceló, D.; Parra, R. Laccase-based biosensors for detection of phenolic compounds. *Trac. Trends Anal. Chem.* **2015**, *74*, 21–45, doi:10.1016/j.trac.2015.05.008.
30. Ferry, Y.; Leech, D. Amperometric Detection of Catecholamine Neurotransmitters Using Electrocatalytic Substrate Recycling at a Laccase Electrode. *Electroanalysis* **2005**, *17*, 113–119, doi:10.1002/elan.200403069.
31. Palanisamy, S.; Ramaraj, S.K.; Chen, S.-M.; Yang, T.C.K.; Yi-Fan, P.; Chen, T.-W.; Velusamy, V.; Selvam, S. A novel Laccase Biosensor based on Laccase immobilized Graphene-Cellulose Microfiber Composite modified Screen-Printed Carbon Electrode for Sensitive Determination of Catechol. *Sci. Rep.* **2017**, *7*, 1–12, doi:10.1038/srep41214.
32. Boujakhrout, A.; Jimenez-Falcao, S.; Martínez-Ruiz, P.; Sánchez, A.; Díez, P.; Pingarrón, J.M.; Villalonga, R. Novel reduced graphene oxide–glycol chitosan nanohybrid for the assembly of an amperometric enzyme biosensor for phenols. *Analyst* **2016**, *141*, 4162–4169, doi:10.1039/C5AN02640G.

5.3 Carbon-nanotube-supported POXA1b laccase and its hydrophobin chimera for oxygen reduction and picomolar phenol biosensing

8 (2021) 100074

Contents lists available at ScienceDirect

Biosensors and Bioelectronics: X

journal homepage: www.journals.elsevier.com/biosensors-and-bioelectronics-x

Carbon-nanotube-supported POXA1b laccase and its hydrophobin chimera for oxygen reduction and picomolar phenol biosensing

Ilaria Sorrentino [a], Ilaria Stanzione [b], Alessandra Piscitelli [b], Paola Giardina [b,*], Alan Le Goff [a,*]

[a] Department of Molecular Chemistry, University Grenoble Alpes, CNRS, 38000, Grenoble, France
[b] Department of Chemical Sciences, University Federico II, 80126, Naples, Italy

ARTICLE INFO

Keywords:
Laccase
Hydrophobin
Carbon nanotubes
Catechol
Dopamine
Biosensing

ABSTRACT

The immobilization of POXA1b laccase and its hydrophobin-fused chimera was performed at pristine Multi-walled Carbon Nanotube (MWCNT) and MWCNT-modified electrodes by electrografting of a 2-diazoniumanthraquinone salt. The influence of the hydrophobin domain and the MWCNT functionalization with anthraquinone groups towards immobilization of laccase was compared by direct electrochemistry under O_2 and electrochemical biosensing of phenols. The hydrophobin domain affords the stable dispersion of MWCNT in water/ethanol, while being detrimental to the direct electron transfer between POXA1b and the electrode. On the contrary, the stronger hydrophobic interactions between anthraquinone and laccase affords direct electrochemistry of POXA1b and enabled the design of a highly sensitive phenol biosensor, reaching a limit-of-detection (LOD) of 2 pM and sensitivity of 23,600 mA L $mmol^{-1}$ cm^{-2} for catechol, and a LOD of 15 nM and sensitivity of 0.053 mA L $mmol^{-1}$ cm^{-2} for dopamine.

1. Introduction

The use of nanostructured carbons such as carbon nanotubes (CNTs) or graphene have tremendously improved the performance of biosensors (Holzinger et al., 2017; Sotiropoulou et al., 2003; Valentini et al., 2013). In particular, the nanowire morphology of CNTs, coupled with excellent conductivity and biocompatibility, have made CNTs a material of choice for biosensor electrodes (Holzinger et al., 2017). CNT electrode films exhibit high electroactive area and can be easily modified by many types of reactions to attach biomolecules (Le Goff and Holzinger, 2018). Their thin nanowire morphology can also make them excellent candidates for closely approaching the catalytic pocket and activating direct electron transfer (DET) with many enzymes, even those possessing deeply embedded active sites.

Laccases (*p*-diphenol-dioxygenoxidoreductases; EC 1.10.3.2) are multicopper oxidases involved in the catalysis of the oxidation of a wide range of aromatic substrates using oxygen as a co-substrate and water as the only by-product. These metalloenzymes are envisioned as renewable biocatalysts in many applications such as bioremediation, organic synthesis, biobleaching, biofuel cells and biosensing (Le Goff et al., 2015; Mano and de Poulpiquet, 2017; Pezzella et al., 2015). Among the laccase family, POXA1b from *Pleurotus ostreatus* has peculiar characteristics such as its stability and activity over a wide range of pHs and temperatures, as well as its high redox potential (Pezzella et al., 2017). Recently, we demonstrated that the class I hydrophobin Vmh2 from the same fungus *P. ostreatus*, was able to disperse graphene by ultrasonic wave exfoliation from graphite (Gravagnuolo et al., 2015). Hydrophobins strongly interact with several hydrophobic surfaces such as Teflon (Askolin et al., 2006; Portaccio et al., 2015; White, 2004), polystyrene (Wang et al., 2010), silicon (De Stefano et al, 2007, 2009), steel (Longobardi et al., 2015), and graphene (Gravagnuolo et al., 2015). This appealing ability has been further extended to laccases by genetic fusion of the hydrophobin to POXA1b(Sorrentino et al., 2019a,b), allowing achievement of simple and stable immobilization of the enzyme on different surfaces such as polystyrene or graphene sheets (Sorrentino et al, 2019, 2020). These biofunctionalized surfaces were then employed in the design of laccase-based phenol biosensors(Sorrentino et al., 2020).

The main objective of this work was to study the interaction of both POXA1b and its hydrophobin-fused chimera, POXA1b-Vmh2, with Multi-Walled CNT (MWCNT) sidewalls. MWCNTs were modified using diazonium electrografting in order to introduce anthraquinone groups which are known to increase the hydrophobicity of the electrode surface and interact with the substrate pocket of laccases (Bourourou et al., 2013; Sorrentino et al., 2019a,b; Sosna et al., 2012). Herein, we

* Corresponding authors.
E-mail addresses: giardina@unina.it (P. Giardina), alan.le-goff@univ-grenoble-alpes.fr (A.L. Goff).

https://doi.org/10.1016/j.biosx.2021.100074
Received 28 January 2021; Received in revised form 11 May 2021; Accepted 2 June 2021
Available online 20 June 2021

investigated for the first time the influence of anthraquinone-modified MWCNTs on the immobilization of POXA1b and POXA1b-Vmh2. In addition, direct electrochemistry in the presence of O_2 was explored as well as electroenzymatic oxidation of catechol and dopamine by these bioelectrodes.

2. Materials and methods

2.1. General procedure

Multi-Walled Carbon Nanotube (MWCNTs, > 99% purity) and all other reagents were purchased from Sigma-Aldrich (Saint Louis, Missouri, USA) and were used without further purification. All chemicals employed in this work were of analytical grade. All solutions were prepared with Milli-Q deionised water (18.2 MΩ cm−1). Freshly prepared solutions were used in all experiments by diluting the corresponding standard stock solution.

The electrochemical experiments were performed with a conventional three-electrode electrochemical cell using either a Biologic VMP3 Multi Potentiostat or Ametek Multipotentiostat Princeton Applied Research (Wokingham, UK). MWCNT bioelectrodes were used as working electrodes, with a saturated calomel (SCE) and a platinum (Pt) wire acting as the reference and counter electrode, respectively. All experiments were conducted at room temperature. All simulated curves were obtained via Origin Pro 9.0. Error bars were estimated from three measurements recorded per sample.

2.2. Preparation of the glassy carbon-modified MWCNT electrode

The working electrodes were modified glassy carbon electrodes (3 mm diameter). 5 mg mL^{-1} N-Methylpyrrolidone (NMP) dispersions of MWCNTs (purity > 99% Sigma-Aldrich) were prepared by 30 min in an ultrasonic bath (Fisher scientific FB 15050) until a homogeneous black suspension was obtained. Then 20 μL of the MWCNTs solution was drop-casted on a glassy carbon electrode (GCE) and NMP was removed under vacuum to obtain a 5-μm-thick film. Then, these MWCNT-coated glassy carbons electrodes were modified by electrografting in a 2 mM 2-diazoniumanthraquinone tetrafluoroborate solution in 0.1 tetrabutylammonium perchlorate (TBAP)/MeCN according to previously-described procedures(Sorrentino et al., 2019a,b). After incubation, the electrodes were washed with MeCN and water.

2.3. Laccase enzyme

Both wild-type enzyme POXA1b and fusion protein POXA1b-Vmh2 were produced as recombinant proteins by the yeast *Pichia pastoris* and secreted in the culture media. The supernatant, following centrifugation for 15 min at 6000 rpm at 4 °C, was concentrated and dialyzed against 50 mM Tris-HCl buffer, pH 8.0, using Centricon Centrifugal Filter Units 10 kDa (Sartorius Vivaspin®). The enzymes were used without additional purification steps.

The laccase activity was assayed by monitoring at 420 nm ($\varepsilon_{420\ nm} = 3.6 \times 10^4\ M^{-1}\ cm^{-1}$) the oxidation of ABTS (2,2′-azino-bis (3-ethylbenzothiazoline-6-sulphonic acid)) at room temperature: the assay solution contained 2 mM ABTS and 50 mM phosphate/citrate buffer, pH 3.0.

2.4. Immobilization of laccase enzymes

The modified MWCNT electrodes were incubated with 20 μL of both enzymes POXA1b and POXA1b-Vmh2 (1 U mL^{-1}), in concentrate condition with POXA1b 100 U mL^{-1}, for 2 h at room temperature. Electrodes were then rinsed with 50 mM Tris-HCl buffer solution at pH = 8 and stored at 4 °C.

3. Results and discussion

3.1. Properties of POXA1b and POXA1b-Vmh2 as a MWCNT dispersant

In line with our results on the exfoliation of graphite in the presence of POXA1b-Vmh2 (Sorrentino et al., 2020), the properties of this chimera as a MWCNT surfactant was investigated. Aqueous surfactants such as sodium dodecyl sulfate (SDS) are used to facilitate the preparation of CNT dispersions and their ease of manipulation. However, most surfactants are detrimental to enzyme activity since these molecules are also well-known enzyme denaturants. As shown in Fig. 1, the addition of POXA1b-Vmh2 to a suspension of MWCNTs improved the dispersion stability after sonication for 10 min and centrifugation.

This underlines the surfactant ability of POXA1b-Vmh2 owing to the adhesion properties of the hydrophobin domain towards hydrophobic surface such as MWCNT sidewalls. These results prompted us to study both POXA1b and POXA1b-Vmh2 immobilized at the surface of MWCNT electrodes for bioelectrochemical applications.

3.2. Direct electrochemistry of POXA1b and POXA1b-Vmh2 on pristine MWCNT and anthraquinone-modified MWCNTs

First, the direct electrochemistry of immobilized POXA1b and POXA1b-Vmh2 was studied under Ar and O_2 at pH 5. Fig. 2 shows the direct electrochemistry of POXA1b and POXA1b-Vmh2 on nonmodified and anthraquinone-modified MWCNTs (AQ-MWCNT). AQ-MWCNT were prepared as previously-described (Gentil et al., 2018), by the electrografting of 2-diazoniumanthraquinone tetrafluroroborate in MeCN.

No direct bioelectrocatalytic reduction of O_2 was observed for both POXA1b and POXA1b-Vmh2 on nonmodified MWCNT (curve a, Fig. 2). On AQ-MWCNT, no DET is observed for POXA1b-Vmh2 (data not shown). On the contrary, an irreversible electrocatalytic reduction signal is observed for POXA1b immobilized on AQ-MWCNT (curve b, Fig. 2). Maximum current densities of 150 μA cm^{-2} were observed at 0.1 V *vs.* SCE. Under Ar (black curve b, Fig. 2), a tiny reversible redox system is observed at $E_{1/2} = +0.41$ V vs. SCE or 0.65 V vs. NHE ($\Delta E = 58$ mV), corresponding to an enzyme surface coverage of 5 pmol cm^{-2}. This is the first report of the measurement of the redox potential of POXA1b laccase by direct electrochemistry. It is in good agreement with the redox potential of the T1 copper centre of POXA1b measured at +0.650 V vs. NHE (Garzillo et al., 2001; Pezzella et al., 2017). These results are indicative of a direct wiring of POXA1b on AQ-MWCNT owing to the favourable orientation of the enzyme. This type of behaviour has already been evidenced for *Trametes* laccases (Bourourou et al., 2013; Lalaoui et al, 2015, 2016). However, the fact that no DET is observed for POXA1b-Vmh2 either on nonmodified or AQ-MWCNT electrodes likely indicates that the Vmh2 domain might hinder the electron transfer to the T1 site by adding an insulating domain as well as increased distance between the copper centre and the surface of the electrode. These results prompted us to explore the properties of these two types of modified electrodes towards catechol and dopamine sensing. These biosensors do not rely on direct electron transfer but rather on the efficient immobilization of POXA1b on electrodes either by the chimeric POXA1b-Vmh2 or by the immobilization of POXA1b on AQ-MWCNTs.

3.3. Catechol and dopamine detection by POXA1b and POXA1b-Vmh2 on pristine MWCNT and anthraquinone-modified MWCNTs

Native POXA1b and POXA1b-Vmh2 were compared towards catechol oxidation after their immobilization on MWCNT and AQ-MWCNT electrodes. Catechol biosensing is based on the ability of immobilized laccase to oxidize o-diphenols into quinones in the presence of oxygen. Quinone is subsequently reduced at the electrode poised at a redox potential of E = −0.2 V vs. SCE. The electrogeneration of the phenol derivative induces an amplification cycle of "enzymatic oxidation/

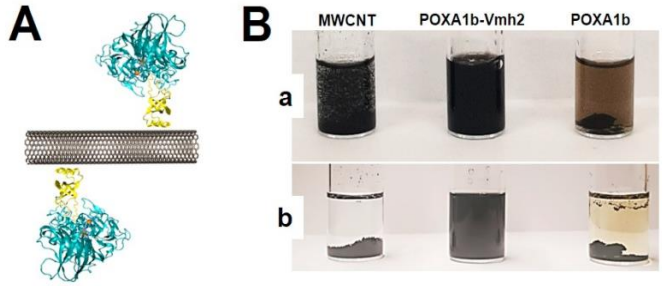

Fig. 1. Panel A: cartoon of POXA1b-Vmh2 bound to a CNT. Panel B: Photograph of the MWCNTs dispersions after ultrasonication and centrifugation in 50% water/ethanol solution (1 mg mL $^{-1}$) before (a) and (b) after 50 days.

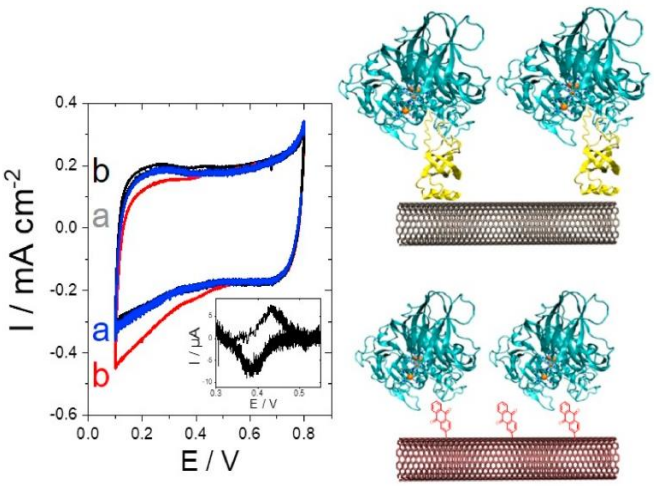

Fig. 2. A schematic representation of POXA1b-Vmh2 and POXA1b immobilized at MWCNT and AQ-MWCNT electrodes, respectively, and corresponding CVs for POXA1b-Vmh2 immobilized at an MWCNT electrode under (a, gray) Ar and (a, blue) O_2 and POXA1b immobilized at an AQ-MWCNT electrode under (b, black) Ar and (b, red) O_2 at pH = 5 (0.1 M phosphate/citrate buffer, v = 10 mV s^{-1}); (inset) Background-subtracted CV of the POXA1b-modified AQ-MWCNT electrode under Ar. (For interpretation of the references to color in this figure legend, the reader is referred to the Web version of this article.)

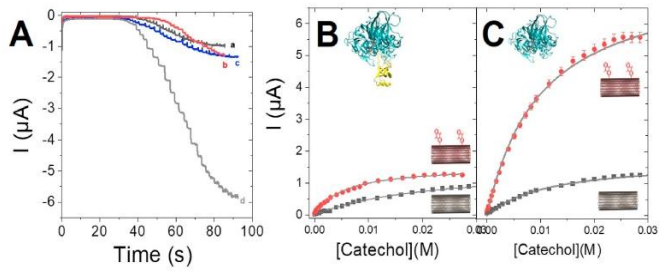

Fig. 3. (A) Chronoamperometry measurements after successive additions of catechol between 0 and 0.03 M for POXA1b-Vmh2 immobilized on (a, black) MWCNT and (b, red) AQ-MWCNT electrodes and POXA1b immobilized on (c, blue) MWCNT and (d, gray) AQ-MWCNT electrodes; Corresponding plot of the catalytic current towards increasing concentrations of catechol for (B) POXA1b-Vmh2 and (C) POXA1b immobilized on MWCNT and AQ-MWCNT electrodes and corresponding fitting curves (gray line) Measurements performed by chronoamperometry at E = −0.2 V vs. SCE, 0.1 M phosphate/citrate buffer, pH 5, 25 °C). Fitting curves were obtained using Origin PRO 9.0 software. (For interpretation of the references to color in this figure legend, the reader is referred to the Web version of this article.)

electrochemical reduction". Amperometric biosensing of catechol is performed by chronoamperometry at different catechol concentrations. Fig. 3 displays chronoamperometry experiments for POXA1b-Vmh2 and POXA1b immobilized (0.02 U for both enzymes) on modified and non-modified MWCNT electrodes.

A typical Michaelis-Menten-type curve was obtained for all electrodes and modelized with the Michaelis-Menten equation. Electrochemical characteristics for all electrodes are displayed in Table 1.

Interestingly, similar curves were obtained for POXA1b and POXA1b-Vmh2 on MWCNT electrodes (black curves from Fig. 3B–C). An increased K_M^{APP} value for POXA1b-Vmh2 might indicate a possible conformation change in the immobilized chimeric enzyme on MWCNTs. This arises from a strong interaction between CNT sidewalls and Vmh2, as confirmed by the high dispersibility of MWCNT in POXA1b-Vmh2 solutions. POXA1b-Vmh2 immobilized on MWCNT electrodes does not show any significant improvement, indicating that the presence of anthraquinone groups at the surface of MWCNT sidewalls does not influence the immobilization or orientation of laccase. On the contrary, POXA1b immobilized on AQ-MWCNT exhibits an almost four-fold increase in maximum current densities (red curve, Fig. 3C). This is in agreement with results observed by direct electrochemistry and the ability of anthraquinone to strongly interact with the substrate pocket of laccase, as already studied by electrochemistry and DFT calculations on *Trametes* laccase (Lalaoui et al., 2016).

3.4. Dopamine and catechol biosensors

Owing to the excellent Michaelis-Menten characteristics of POXA1b laccase immobilized on AQ-MWCNT electrodes, both catechol and dopamine sensors were optimized for this particular configuration. Highly-concentrated POAX1b (2 U, about 100 times more concentrated) was immobilized on anthraquinone-modified MWCNTs to maximize the enzymatic response towards catechol and dopamine. Fig. S1A displays the expected Michaelis-Menten-type dependence for both catechol and dopamine. As expected, high maximum current densities of 25.7 μA were obtained at high catechol concentration. Lower apparent K_M^{APP} values for dopamine (15 mM) were obtained compared to catechol (0.6 mM), owing to the higher affinity of laccase towards catechol.

Fig. 4 shows the presence of two consecutives linear regions for both catechol and dopamine, as has been observed in many enzyme-based phenol sensors(Rodríguez-Delgado et al., 2015).

Two linear regions were identified between 2 and 30 pM and 0.1–800 μM with corresponding sensitivities of 23,600 ($R^2 = 0.972$) and 0.28 ($R^2 = 0.992$) mA L $mmol^{-1}$ cm^{-2} for catechol (Fig. 4A and B), respectively. For dopamine, two linear regions were identified between 0.015-90 μM and 30-30 μM with corresponding sensitivities of 0.053 ($R^2 = 0.975$) and 0.033 ($R^2 = 0.999$) mA L $mmol^{-1}$ cm^{-2} (Fig. 4C and D), respectively. Excellent biosensing characteristics make this biosensor one of the most sensitive biosensors based on laccase for both catechol and dopamine. Furthermore, no chronoamperometric response was observed during biosensing experiments after the addition of two interferents, 50 μM ascorbic acid and 50 μM uric acid. It is noteworthy that these biosensing performances are several orders of magnitude higher as compared to our previously-developed hydrophobin-fused chimera Vmh2-POXA1b immobilized on few-layer graphene.(Sorrentino et al., 2020). This likely accounts for the nonoptimized functionalization

Table 1
Simulated Electrochemical characteristics obtained from the plot of the catalytic current towards increasing concentrations of catechol in Fig. 3B–C.

		K_M^{APP} (mol L^{-1})	I_{max} (μA)	R^2
POXA1b	MWCNT	0.010 (±0.001)	1.74 (±0.10)	0.998
	AQ-MWCNT	0.011 (±0.001)	7.62 (±0.05)	0.992
POXA1b-Vmh2	MWCNT	0.022 (±0.002)	1.54 (+/0.04)	0.997
	AQ-MWCNT	0.007 (±0.001)	1.55 (±0.05)	0.991

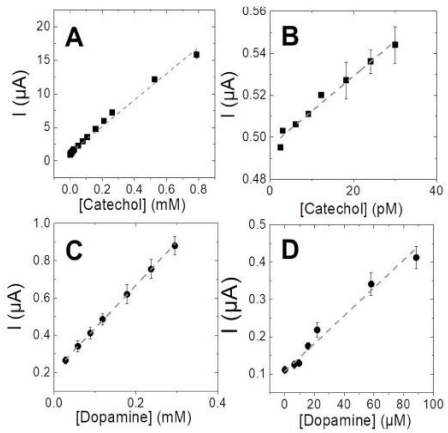

Fig. 4. Linear sections of the plots for catalytic current towards catechol (A, B) and dopamine (C, D) concentration.

of graphene nanosheets with chimera laccase and the superior conductivity of MWCNT films as compared to biofunctionalized graphene. Table 2 and summarizes previously-developed biosensors based on tyrosinases and laccases for catechol and dopamine. The POXA1b-modifed AQ-MWCNT electrode outperforms most laccase-based biosensors for catechol and provides higher limit-of-detection compared to nanostructured biosensors based on both laccase or tyrosinase. For dopamine sensing, AQ-MWCNT-supported POXA1b approaches the best performances of other types of laccase and tyrosinase biosensors.

Furthermore, the stability of this sensor was tested at high salinity from 0 to 0.5 M NaCl to estimate its ability to operate in seawater samples. It is well known that the extensively studied *Trametes* laccases are highly sensitive towards chloride inhibition(Le Goff et al., 2015; Mano and de Poulpiquet, 2017; Vaz-Dominguez et al., 2008). Here, owing to the exceptional stability of POXA1b at high chloride concentration, the nanostructured biosensor retains 30% of its initial activity at 0.5 M NaCl (Fig. S1B).

4. Conclusion

In this work, we investigated the electrochemical characteristics of POXA1b and its hydrophobin-based fused chimera on functionalized MWCNTs, either for direct electroenzymatic reduction of O_2 or indirect electrochemical biosensing of catechol and dopamine. While POXA1b-Vmh2 gives access to stable CNT dispersions in water/ethanol mixtures, its Vmh2 increases the distance between the electrode surface and the enzyme active site. This prevents its use in direct electrochemistry. On the contrary, anthraquinone-modified MWCNTs are able to efficiently immobilize POXA1b laccase, showing, for the first time for this particular laccase, direct electrocatalytic reduction of O_2. The fact that anthraquinone greatly improves POXA1b immobilization, and not for POXA1b-Vmh2, is indicative of the fact that the Vmh2 domain competes with the hydrophobic patch at the surface of the native POXA1b for the efficient immobilization of the enzyme. The combination of AQ-MWCNT with POXA1b gives access to a highly sensitive biosensor for catechol and dopamine, leading to unprecedented picomolar detection for catechol and micromolar detection of dopamine, accompanied with respective sensitivities of 23,600 mA L $mmol^{-1}$ cm^{-2} and 0.053 mA L $mmol^{-1}$. This work provides new insights into the nature of the interactions of POXA1b and its chimera at the surface of MWCNTs. While

Table 2
Electrochemical characteristics of biosensors based on tyrosinases and laccases for catechol and dopamine electrochemical biosensing.

Catechol biosensor	Enzyme	Linear range	Sensitivity (mA L mmol-1 cm^{-2})	References
POxA1b/AQ-MWCNT	POXA1b	2–30 pM 0.1–800 μM	23,600 0.28	This work
POxA1b-vmh2/graphene	POXA1b	20–1000 μM	0.00027	Sorrentino et al. (2020)
Graphene/cellulose microfiber	*Trametes versicolor*	0.085–210 μM	0.0009	Palanisamy et al. (2017)
reduced graphene oxide/chitosan	*Rhus vernicifera* laccase	7–700 μM	0.00011	Zhou et al. (2013)
tungsten disulfide nanotubes	Tyrosinase	0.6–70 μM	0.151	Palomar et al. (2020)
CNT + CaCO3 nanoparticles	Tyrosinase	1–8 μM	35.7	Bujduveanu et al. (2013)
Gold nanoparticle + screen printed carbon electrode	tyrosinase	1.1–80 μM	49	Karim et al. (2014)
screen-printed carbon electrode	horseradish peroxidase/ tyrosinase	0.120–43 μM	0.00185	Chang et al. (2002)
circular glassy carbon electrode	Tyrosinase	0–0.631 μM	0.213	Adamski et al. (2010)
CPE-Tyr-Inc (incorporated lyophilized Tyr) **CPE-Tyr (graphite)** **CBPE-Tyr (carbon black**	Tyrosinase	2.5–17.5 μM 5–85 μM 0.013–150 μM	1400 1640 1720	Nadifiyine et al. (2013)
single-wall carbon nanotubes (SWCNTs) and polyaniline (PANI)	Tyrosinase	0.25–92 μM	0.144	Wang et al. (2013)
Tyr-AuNPs-DHP/GCE	Tyrosinase	2.5–95 μM	0.115	Campanhã Vicentini et al. (2016)
GCE/hybrid/enzyme/membrane	Tyrosinase or laccase	0–300 μM	310	Vlamidis et al. (2017)
Dopamine biosensor				
POxA1b/AQ-MWCNT	POXA1b	0.01–90 μM 30–300 μM	0.053 0.033	This work
POxA1b-vmh2/graphene	POXA1b	20–250 μM	0.000016	Sorrentino et al. (2020)
Si/MWCNT/Screen-printed electrode	*Trametes versicolor laccase*	1.3–85.5 μM	2.787	Li et al. (2012)
3-mercaptopropionic acid-modified gold electrode	*Agaricus bisporus* laccase	0.5–13 μM 47–430 μM	1.95 0.92	Shervedani and Amini (2012)
tungsten disulfide nanotubes	Commercial Tyrosinase	0.5–10 μM 10–40 μM	0.0087 0.0048	Palomar et al. (2020)
CNT + CaCO3 nanoparticles	Commercial Tyrosinase	0.015–30 μM	3.57	Bujduveanu et al. (2013)
CNT/glutaraldehyde/PEDOT on gold microelectrode array	Commercial Tyrosinase	100–500 μM	1120	Lete et al. (2015)
SWNT/Ppy	Commercial tyrosinase	5–50 μM	0.467	Min and Yoo (2009)

the Vmh2 domain provides a soft functionalization route for immobilization of redox enzymes, the fusion protein still needs more developments that take into account the nature of the interactions with the corresponding surface as well as the accessibility of both the substrate and electrons, especially for bioelectrocatalytic applications. Owing to the wide spectrum of phenolic substrates of laccase and the stability of POXA1b in harsh conditions, this work paves the way for the use of this particular enzyme for many types of laccase-based electrochemical biosensors, while also providing future directions for the engineering of new chimera redox proteins.

CRediT authorship contribution statement

Ilaria Sorrentino: Experiments. **Ilaria Stanzione:** Experiments. **Alessandra Piscitelli:** Writing – review & editing, Supervision, Project administration, Funding acquisition. **Paola Giardina:** Writing – review & editing, Supervision, Project administration, Funding acquisition. **Alan Le Goff:** Writing – review & editing, Supervision, Project administration, Funding acquisition.

Declaration of competing interest

The authors declare that they have no known competing financial interests or personal relationships that could have appeared to influence the work reported in this paper.

Acknowledgements

This project is funded by the Italian Education, University and Research Ministry (MIUR) and the French National Research Agency (ANR), and co-funded by European Union's Horizon 2020 research and innovation program under the framework of ERA-NET Cofund MarTERA (Maritime and Marine Technologies for a new Era), FLAshMoB, Functional Amyloid chimera for Marine Biosensing (ID: 172). This work was also supported by the Agence Nationale de la Recherche through the LabEx ARCANE programme (ANR-11-LABX-0003-01) and the Graduate School on Chemistry, Biology and Health of Univ Grenoble Alpes CBH-EUR-GS (ANR-17-EURE-0003). The authors acknowledge support from the plateforme de Chimie NanoBio ICMG FR 2607 (PCN-ICMG).

Appendix A. Supplementary data

Supplementary data to this article can be found online at https://doi.org/10.1016/j.biosx.2021.100074.

References

Adamski, J., Nowak, P., Kochana, J., 2010. Electrochim. Acta 55, 2363–2367. https://doi.org/10.1016/j.electacta.2009.11.099.
Askolin, S., Linder, M., Scholtmeijer, K., Tenkanen, M., Penttilä, M., de Vocht, M.L., Wösten, H.A.B., 2006. Biomacromolecules 7, 1295–1301. https://doi.org/10.1021/bm050676s.
Bourourou, M., Elouarzaki, K., Lalaoui, N., Agnès, C., Le Goff, A., Holzinger, M., Maaref, A., Cosnier, S., 2013. Chem. Eur J. 19, 9371–9375. https://doi.org/10.1002/chem.201301043.
Bujduveanu, M.-R., Yao, W., LeGoff, A., Gorgy, K., Shan, D., Diao, G.-W., Ungureanu, E.-M., Cosnier, S., 2013. Electroanalysis 25, 613–619. https://doi.org/10.1002/elan.201200245.
Campanhã Vicentini, F., Garcia, L.L.C., Figueiredo-Filho, L.C.S., Janegitz, B.C., Fatibello-Filho, O., 2016. Enzym. Microb. Technol. 84, 17–23. https://doi.org/10.1016/j.enzmictec.2015.12.004.
Chang, S.C., Rawson, K., McNeil, C.J., 2002. Biosens. Bioelectron. 17, 1015–1023. https://doi.org/10.1016/S0956-5663(02)00094-5.

De Stefano, L., Rea, I., Armenante, A., Giardina, P., Giocondo, M., Rendina, I., 2007. Langmuir 23, 7920–7922. https://doi.org/10.1021/la701189b.
De Stefano, L., Rea, I., De Tommasi, E., Rendina, I., Rotiroti, L., Giocondo, M., Longobardi, S., Armenante, A., Giardina, P., 2009. Eur. Phys. J. E 30, 181. https://doi.org/10.1140/epje/i2009-10481-y.
Garzillo, A.M., Colao, M.C., Buonocore, V., Oliva, R., Falcigno, L., Saviano, M., Santoro, A.M., Zappala, R., Bonomo, R.P., Bianco, C., Giardina, P., Palmieri, G., Sannia, G., 2001. J. Protein Chem. 20, 191–201. https://doi.org/10.1023/A:1010954812955.
Gentil, S., Che Mansor, S.M., Jamet, H., Cosnier, S., Cavazza, C., Le Goff, A., 2018. ACS catal. https://doi.org/10.1021/acscatal.8b00708, 3957-3964.
Gravagnuolo, A.M., Morales-Narváez, E., Longobardi, S., da Silva, E.T., Giardina, P., Merkoçi, A., 2015. Adv. Funct. Mater. 25, 2771–2779. https://doi.org/10.1002/adfm.201500016.
Holzinger, M., Le Goff, A., Cosnier, S., 2017. Sensors 17, 1010. https://doi.org/10.3390/s17051010.
Karim, MdN., Lee, J.E., Lee, H.J., 2014. Biosens. Bioelectron. 61, 147–151. https://doi.org/10.1016/j.bios.2014.05.011.
Lalaoui, N., David, R., Jamet, H., Holzinger, M., Le Goff, A., Cosnier, S., 2016. ACS Catal. 6, 4259–4264. https://doi.org/10.1021/acscatal.6b00797.
Lalaoui, N., LeGoff, A., Holzinger, M., Mermoux, M., Cosnier, S., 2015. Chem. Eur J. 21, 3198–3201. https://doi.org/10.1002/chem.201405557.
Le Goff, A., Holzinger, M., 2018. Sustainable Energy Fuels 2, 2555–2566. https://doi.org/10.1039/C8SE00374B.
Le Goff, A., Holzinger, M., Cosnier, S., 2015. Cell. Mol. Life Sci. 72, 941–952. https://doi.org/10.1007/s00018-014-1828-4.
Lete, C., Lupu, S., Lakard, B., Hihn, J.-Y., del Campo, F.J., 2015. J. Electroanal. Chem. 744, 53–61. https://doi.org/10.1016/j.jelechem.2015.03.005.
Li, Y., Zhang, L., Li, M., Pan, Z., Li, D., 2012. Chem. Cent. J. 6, 103. https://doi.org/10.1186/1752-153X-6-103.
Longobardi, S., Gravagnuolo, A.M., Funari, R., Della Ventura, B., Pane, F., Galano, E., Amoresano, A., Marino, G., Giardina, P., 2015. Anal. Bioanal. Chem. 407, 487–496. https://doi.org/10.1007/s00216-014-8309-3.
Mano, N., de Poulpiquet, A., 2017. O2 Chem. Rev. 118, 2392–2468. https://doi.org/10.1021/acs.chemrev.7b00220.
Min, K., Yoo, Y.J., 2009. Talanta 80, 1007–1011. https://doi.org/10.1016/j.talanta.2009.08.032.
Nadifiyine, S., Haddam, M., Mandli, J., Chadel, S., Blanchard, C.C., Marty, J.L., Amine, A., 2013. Anal. Lett. 46, 2705–2726. https://doi.org/10.1080/00032719.2013.811679.
Palanisamy, S., Ramaraj, S.K., Chen, S.-M., Yang, T.C.K., Yi-Fan, P., Chen, T.-W., Velusamy, V., Selvam, S., 2017. Sci. Rep. 7, 1–12. https://doi.org/10.1038/srep41214.
Palomar, Q., Gondran, C., Lellouche, J.-P., Cosnier, S., Holzinger, M., 2020. J. Mater. Chem. B 8, 3566–3573. https://doi.org/10.1039/C9TB01926J.
Pezzella, C., Giacobelli, V.G., Lettera, V., Olivieri, G., Cicatiello, P., Sannia, G., Piscitelli, A., 2017. J. Biotechnol. 259, 175–181. https://doi.org/10.1016/j.jbiotec.2017.07.022.
Pezzella, C., Guarino, L., Piscitelli, A., 2015. Cell. Mol. Life Sci. 72, 923–940. https://doi.org/10.1007/s00018-014-1823-9.
Portaccio, M., Gravagnuolo, A.M., Longobardi, S., Giardina, P., Rea, I., De Stefano, L., Cammarota, M., Lepore, M., 2015. Appl. Surf. Sci. 351, 673–680. https://doi.org/10.1016/j.apsusc.2015.05.182.
Rodríguez-Delgado, M.M., Alemán-Nava, G.S., Rodríguez-Delgado, J.M., Dieck-Assad, G., Martínez-Chapa, S.O., Barceló, D., Parra, R., 2015. Trac. Trends Anal. Chem. 74, 21–45. https://doi.org/10.1016/j.trac.2015.05.008.
Shervedani, R.K., Amini, A., 2012. Bioelectrochemistry 84, 25–31. https://doi.org/10.1016/j.bioelechem.2011.10.004.
Sorrentino, I., Gentil, S., Nedellec, Y., Cosnier, S., Piscitelli, A., Giardina, P., LeGoff, A., 2019a. ChemElectroChem 5, 1–6. https://doi.org/10.1002/celc.201801264.
Sorrentino, I., Giardina, P., Piscitelli, A., 2019b. Appl. Microbiol. Biotechnol. 103, 3061–3071. https://doi.org/10.1007/s00253-019-09678-2.
Sorrentino, I., Stanzione, I., Nedellec, Y., Piscitelli, A., Giardina, P., Le Goff, A., 2020. Int. J. Mol. Sci. 21, 3741. https://doi.org/10.3390/ijms21113741.
Sosna, M., Stoica, L., Wright, E., Kilburn, J.D., Schuhmann, W., Bartlett, P.N., 2012. Phys. Chem. Chem. Phys. 14, 11882.
Sotiropoulou, S., Gavalas, V., Vamvakaki, V., Chaniotakis, N.A., 2003. Biosens. Bioelectron. 18, 211–215. https://doi.org/10.1016/S0956-5663(02)00183-5.
Valentini, F., Carbone, M., Palleschi, G., 2013. Anal. Bioanal. Chem. 405, 451–465. https://doi.org/10.1007/s00216-012-6351-6.
Vaz-Dominguez, C., Campuzano, S., Rüdiger, O., Pita, M., Gorbacheva, M., Shleev, S., Fernandez, V.M., De Lacey, A.L., 2008. Laccase electrode for direct electrocatalytic reduction of O_2 to H_2O with high-operational stability and resistance to chloride inhibition. Biosens. Bioelectron. 24, 531–537. https://doi.org/10.1016/j.bios.2008.05.002.
Vlamidis, Y., Gualandi, I., Tonelli, D., 2017. J. Electroanal. Chem. 799, 285–292. https://doi.org/10.1016/j.jelechem.2017.06.012.
Wang, B., Zheng, J., He, Y., Sheng, Q., 2013. Sensor. Actuator. B Chem. 186, 417–422. https://doi.org/10.1016/j.snb.2013.06.016.
Wang, Z., Lienemann, M., Qiau, M., Linder, M.B., 2010. Langmuir 26, 8491–8496. https://doi.org/10.1021/la101240e.
White, S.H., 2004. Protein Sci. 13, 1948–1949. https://doi.org/10.1110/ps.04712004.
Zhou, X.-H., Liu, L.-H., Bai, X., Shi, H.-C., 2013. Sensor. Actuator. B Chem. 181, 661–667. https://doi.org/10.1016/j.snb.2013.02.021.

5.4 The Laccase mediator system at carbon nanotubes for anthracene oxidation and femtomolar electrochemical biosensing

Analyst

ROYAL SOCIETY OF CHEMISTRY

PAPER

View Article Online
View Journal | View Issue

Cite this: *Analyst*, 2022, **147**, 897

The laccase mediator system at carbon nanotubes for anthracene oxidation and femtomolar electrochemical biosensing†

Ilaria Sorrentino, [a] Marie Carrière,[a] Hélène Jamet,[a] Ilaria Stanzione, [b] Alessandra Piscitelli, [b] Paola Giardina *[b] and Alan Le Goff *[a]

We investigated the use of POXA1b laccase from *Pleurotus ostreatus* for the oxidation of anthracene into anthraquinone. We show that different pathways can occur depending on the nature of the redox mediator combined to laccase, leading to different structural isomers. The laccase combined with 2,2'-azine-bis(3-ethylbenzothiazoline-6-sulfonic acid (ABTS) leads to the formation of 1,4-anthraquinone and/or 1,2-anthraquinone. The unprecedented role of carbon nanotubes (CNTs) as redox mediators for oxidation of anthracene into 9,10-anthraquinone is shown and corroborated by density-functional theory (DFT) calculations. Owing to the efficient adsorption of anthraquinones at CNT electrodes, anthracene can be detected with low limit-of-detection using either laccase in solution, CNT-supported laccase or laccase immobilized at magnetic beads exploiting the adhesive property of a chimeric hydrophobin-laccase.

Received 18th November 2021,
Accepted 2nd February 2022
DOI: 10.1039/d1an02091a

rsc.li/analyst

Introduction

Polycyclic aromatic hydrocarbons (PAHs), aromatic molecules consisting of at least two fused benzenic rings, are well-known environmental and food pollutants. Accumulating PAHs have detrimental effects on flora and fauna and are an increasing health problem as human carcinogens. PAHs can be either produced by food processing (baking, smoking, roasting) or introduced by contamination. PAHs can also be a marker of important environmental pollution of water by oil. Current methods for PAH sensing are based on gas or liquid chromatography coupled to mass spectrometry, fluorimetry or UV-visible spectroscopy.[1] In order to avoid these heavy laboratory instrumentation and/or expensive light sources, electrochemical sensors have represented an easy-to-use and inexpensive alternative. However, PAHs are difficult to detect by electrochemical methods. Most PAHs have high and irreversible oxidation potential. This is the reason why most electrochemical sensors rely on high-potential detection or rely on the detection of oxidized hydroxylated PAHs.[1]

Enzyme-based electrochemical biosensors have relied on both the specificity of enzyme towards specific substrates and the catalytic activity of enzyme to provide high sensitive responses.[2,3] Furthermore, enzyme-based biosensors also rely on the ability of enzymes to perform specific reactions in water at room temperature and atmospheric pressure. During the last decade, the combination of enzymes with nanomaterials have led to tremendous progress in biosensor design and sensitivity.[3–5] In particular, carbon nanotubes (CNTs) have represented a multifunctional material, combining high affinity and biocompatibility towards enzymes, improved electron transfer rates and conductivity and high electroactive surfaces.[2–4,6] Magnetic beads have also represented a versatile material with many advantages in biosensing.[7,8] Apart from their ability to be modified with many types of biomolecules, the use of magnetic beads allows the catalyst or the analyte to be separated or concentrated from the medium.[7,8] Furthermore, magnetic particles can also carry analytes or transducers in microfluidic chips for multiplex analysis.[9,10]

Laccases (*p*-diphenol-dioxygenoxidoreductases; EC 1.10.3.2) are copper-containing oxidases, catalyzing the oxidation of a wide range of aromatic substrates while concomitantly reducing O_2 into water. These metalloenzymes are used or envisioned in industrial applications such as remediation, bleaching, biosensing and fuel cells.[11–13] The active site of laccase is composed of a type 2/type 3 trinuclear copper cluster where O_2 is reduced into water. Electrons are transferred from a mononuclear type 1 copper centre, near the surface of the protein, where the substrate is oxidized. POXA1b, a laccase from *Pleurotus ostreatus*, possess interesting properties for many applications: high stability, high enzymatic activity over a wide

[a]*Univ. Grenoble Alpes, CNRS, DCM, 38000 Grenoble, France. E-mail: alan.le-goff@univ-grenoble-alpes.fr*
[b]*Department of Chemical Sciences, University of Naples Federico II, 80126 Naples, Italy. E-mail: giardina@unina.it*
†Electronic supplementary information (ESI) available: Experimental details, Fig. S1. See DOI: 10.1039/d1an02091a

range of pHs and temperatures and a high redox potential.[14,15] We recently investigated this particular laccase at modified graphene and CNT-based electrodes.[12] For biosensing applications, laccases have been mostly studied for the detection of *ortho*-diphenol substrates such as catechol or dopamine.[16–19] We recently produced in *Pichia pastoris* a chimera by fusion of POXA1b with a hydrophobin, a self-assembling adhesive protein produced by the same fungus *P. ostreatus*, making laccase prone to be immobilized at different types of materials such polystyrene beads, graphene nanosheets or CNTs.[16,18,20]

Laccase redox mediators, the most common being the diammonium salt of 2,2′-azine-bis(3-ethylbenzothiazoline-6-sulfonic acid (ABTS), have been used for many years, acting as electron relays when laccase are immobilized at electrode surface[12,13] or acting as an enhancer/promoter of the ability of laccase to catalyze the oxidation of high potential nonphenolic substrate.[21] Several studies have shown that this so-called laccase-mediator system is able to oxidize several PAHs such as anthracene or benzo(a)pyrene into quinoid products.[22–24] In this work, we intend to design the first example of a PAH electrochemical enzyme sensor by exploring the oxidation of PAHs by laccase and the detection of the quinoid products at multi-walled CNT (MWCNT) electrodes. Porous carbon materials are notorious adsorbents of PAHs, owing to the strong pi–pi-stacking of pi-extended aromatic with CNT sidewalls of CNTs or graphene-based materials.[25–32] We therefore investigate the oxidation of PAH by laccase and the subsequent adsorption and detection of their corresponding enzymatically-oxidized products at MWCNT electrodes. We also investigated the role of CNTs as redox mediator of anthracene oxidation. The versatility of this biosensing strategy was finally studied by using laccase either in solution or immobilized at both CNT and magnetic beads.

Results and discussion

Electrochemical study of the adsorption of anthraquinone on MWCNT electrodes

In order to develop a biosensor based on the detection of oxidation products of anthracene, the detection of adsorbed anthraquinone at MWCNTs was investigated. Among the products of anthracene oxidation, either by chemical or biochemical processes, the main redox-active products of anthracene oxidation are either 1,4-anthraquinone, 1,2-anthraquinone and 9,10-anthraquinone,[33,34] while co-products or products of further oxidation are non-electroactive. In particular, major products of anthracene oxidation by the white rot fungus *P. ostreatus* have been identified as 9,10-anthraquinone and anthracene *trans*-1,2-dihydrodiol.[34] First, the ability of MWCNT electrodes to detect anthraquinone derivatives were tested on two anthraquinone isomers, 1,4-anthraquinone and 9,10-anthraquinone. MWCNTs are well-known to strongly interact with polycyclic aromatics *via* pi–pi interactions with CNT sidewalls. Fig. 1 shows the electrochemical response of MWCNT electrodes previously incubated in a 1 mM solution of

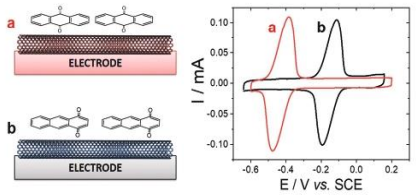

Fig. 1 Schematic representation of adsorbed (a) 9,10-anthraquinone and 1,4-anthraquinone at MWCNT electrode and CV of the modified MWCNT electrodes performed in 0.1 M McIlvaine buffer pH 5 (v = 10 mV s^{-1}, pH 7) after incubation (10 min, 25 °C) of the MWCNT electrode in a 1 mM MeCN solution of (a) 9,10-anthaquinone and (b) 1,4-anthraquinone.

1,4-anthraquinone or 9,10-anthraquinone in MeCN. In order to avoid any interferences from redox-active impurities, high-purity (99%) MWCNTs were chosen. No background electroactivity of the MWCNT electrode was observed in the experimental potential window.

The electrodes were further washed and the adsorption of respective anthraquinones was studied in 0.1 M phosphate buffer. The expected redox reversible systems observed at $E_{p,1/2}$ = −0.43 V (ΔE = 90 mV) and $E_{p,1/2}$ = −0.12 V *vs.* SCE correspond to the redox potential of 9,10-anthraquinone and 1,4-anthraquinone respectively. Both systems correspond to the two-electron/two-proton oxidation of anthraquinone into their corresponding bis-paraphenol product.[35–37] According to integration of the charge, similar maximum surface concentrations of 0.82 and 0.71 nmol cm^{-2} were measured for 1,4-anthraquinone and 9,10-anthraquinone respectively.

With the aim of further describing the adsorption of anthraquinone at MWCNTs, an equilibrium isotherm model was investigated using different concentrations of anthraquinone (Fig. 2).

The adsorption isotherm was studied by investigating the anthraquinone redox system by square-wave voltammetry

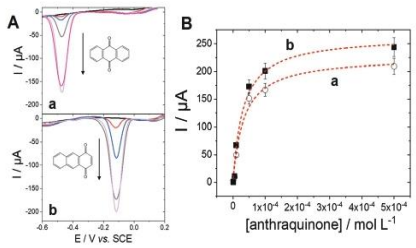

Fig. 2 (A) SWV and (B) corresponding plot of the peak current against anthraquinone concentration (0.1 M McIlvaine buffer pH 5, 25 °C, pulse height = 25 mV, pulse width = 0.5 s, step height = −5 mV) performed after incubation (10 min, 25 °C) of the MWCNT electrode in a MeCN solution of (a, ○) 9,10-anthaquinone and (b, ■) 1,4-anthraquinone at different concentrations.

(SWV) obtained after incubation at different anthraquinone concentrations. SWV is employed as it provides high sensitivity towards the detection of such reversible redox signals, reducing signal-to-noise ratio and background capacitive currents. As expected, the intensity of the peak for each anthraquinone increases when increasing the incubating concentration until reaching a plateau. This behaviour was well modelized by using a simple Langmuir isotherm model according to eqn (1):[38–40]

$$I_{p,eq} = \frac{I_{p,max} \times K_{AQ} \times [AQ]}{1 + K_{AQ} \times [AQ]} \quad (1)$$

where $I_{p,eq}$ is the equilibrium peak current, $I_{p,max}$ is the peak current at saturating concentrations of 1.4-anthraquinone or 9,10-anthraquinone and K_{AQ} is the association constant between AQ and MWCNT surface in MeCN at 25 °C. For 1,4-anthraquinone, the best fit (R^2 = 0.98) was achieved with a $I_{p,max}$ = 260(±16) μA and $K_{1,4\text{-}AQ}$ = 3.2(±0.7) × 10^5 L mol^{-1}. For 9,10-anthraquinone, the best fit (R^2 = 0.98) was achieved with a $I_{p,max}$ = 230(±15) μA and $K_{9,10\text{-}AQ}$ = 3.0(±0.7) × 10^5 L mol^{-1}. For comparison, an association constant 1 to 2 × 10^3 L mol^{-1} have been measured for pyrene and different types of pyrene-based derivatives.[27,40,41] As expected, both anthraquinone derivatives exhibit the same interaction mechanism with MWCNT sidewalls. These results underline that MWCNT electrodes are able to reproducibly adsorb and detect anthraquinone isomers *via* a Langmuir-type reversible model.

Electrochemical detection of the products of anthracene oxidation by free and adsorbed laccase with and without ABTS

Using the ability of MWCNT electrodes to detect anthraquinone derivatives, we investigate the detection of the products of the enzymatic oxidation of anthracene by laccase, either in solution or adsorbed at the surface of the MWCNT electrodes. In most cases, the use of a redox mediator such as ABTS is required for laccases to be able to oxidize nonphenolic compounds such as PAHs.[21] POXA1b laccase was chosen for its high redox potential, high activity and stability and its thermophilic character[42] suitable for the oxidation of nonphenolic compounds. We have recently shown its facile adsorption on MWCNT electrodes for sensitive catechol and dopamine sensing.[20] Fig. 3 shows the detection of anthraquinone products at different concentrations of anthracene in the presence of POXA1b laccase in solution or adsorbed at MWCNT electrodes, with and without ABTS. When laccase is used in solution, no anthraquinone derivatives were detected at room temperature after incubation of laccase (1 U mL^{-1}) and 100 μM of anthracene. When temperature is increased to 40 °C, traces of 9,10-anthraquinone are detected at MWCNT electrodes with maximum SWV peak current of 5.5 μA (E_p = −0.42 V) at 100 μM of anthracene (Fig. 3A). When the incubation is performed in the presence of ABTS (20 mM), a SWV peak is observed at E_p = −0.06 V, likely corresponding to the production of 1,2- or/and 1,4-anthraquinone (Fig. 3B). This product is detected at extremely low limit-of-detection of 0.1 fM and the signal levels off at current values of 122 μA at 100 μM of anthracene. At this concentration, a small peak is also observed at E_p = −0.42 V, corresponding to the concomitant formation of 9,10-anthraquinone, only observed at high anthracene concentrations.

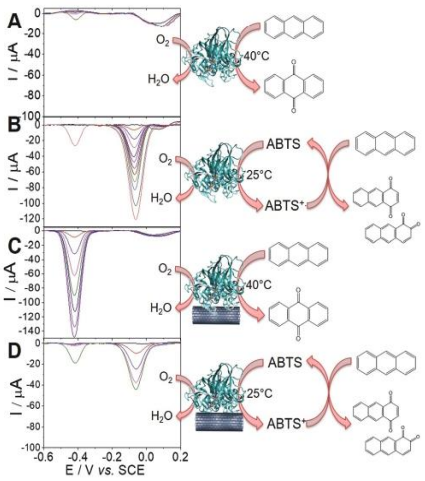

Fig. 3 (A) SWV (0.1 M McIlvaine buffer pH 5, 25 °C, pulse height = 25 mV, pulse width = 0.5 s, step height = −5 mV) for the detection of different concentrations of anthracene (0, 0.1 nM, 100 nM, 1 μM and 100 μM) after incubation (10 min) of the MWCNT electrode in a solution of 1 U mL^{-1} of laccase and anthracene left to react for 2 h at 40 °C min; (B) SWV for the detection of different concentrations of anthracene (0, 0.1 fM, 0.5 fM, 1 fM, 10 fM, 50 fM, 0.1 pM, 1 pM, 10 pM, 0.05 nM, 1 μM and 100 μM) after incubation (10 min) of the MWCNT electrode in a solution of 1 U mL^{-1} of laccase and ABTS left to react for 1 h at 25 °C min; (C) SWV for the detection of different concentrations of anthracene (0, 0.1 nM, 10 nM, 0.1 μM, 1 μM, 10 μM and 100 μM) after incubation (10 min) of a POXA1b modified electrode in a solution of anthracene left to react for 2 h at 40 °C; (D) SWV for the detection of different concentrations of anthracene after incubation (10 min) of a POXA1b-modified electrode in a solution of anthracene (0, 0.1 nM, 100 nM, 1 μM and 100 μM) and ABTS left to react for 1 h at 25 °C.

For MWCNT-supported laccases, without addition of ABTS, 9,10-anthraquinone is detected at concentrations of 0.1 nM, levelling at 100 μM with maximum current of −148 μA (Fig. 3C). When ABTS is used in solution with MWCNT-supported laccase, 1,2- or/and 1,4-anthraquinone is mostly detected with maximum current of 45 μA at E_p = −0.06 V at 100 μM of anthracene, with the concomitant formation of 9,10-anthraquinone at E_p = −0.41 V (Fig. 3D).

These results show that the formation of these anthraquinone isomers can be obtained from the enzymatic oxidation of anthracene by laccases, depending on the conditions and the presence and nature of the redox mediator. When ABTS is used either with laccase in solution or adsorbed on MWCNTs, 1,2- and or 1,4-anthraquinone are the major products of the

oxidation of anthracene. The fact that negligible amounts of anthraquinone is observed when laccase is used in solution without ABTS is expected from the fact that laccases are known to have poor oxidation ability of nonphenolic substrates without the addition of a redox mediator. However, owing to the stability of POXA1b at temperature up to 40 °C, traces of 9,10-anthraquinone can still be observed. More interestingly, despite the fact that adsorbed laccase is present in low amounts as compared to laccase in solution (2 U), the formation of 9,10-anthraquinone is detected when laccases is adsorbed at MWCNT electrodes, without the need of a redox mediator in solution.

To further investigate the role of MWCNTs in the oxidation of anthracene by laccases in the absence of ABTS, DFT calculations were done. The idea was to compare the electronic structure of the anthracene adsorbed at MWCNT electrodes or in solution. To modelize the anthracene adsorbed at MWCNT electrodes, we used a graphene ribbon of 18 × 12 Å^2. Fig. 4 reports the highest occupied orbitals HOMO, HOMO−1 of the two systems. The orbitals involved in the oxidation of the anthracene are the HOMO for the molecule isolated and the HOMO−1 for the anthracene adsorbed on the graphene. These two orbitals are localized similarly on carbon atoms of anthracene but the energy of the orbital involved for the model of the anthracene adsorbed is higher in energy (−6.93 eV against −7.29 eV). Therefore, DFT calculations underline the fact that anthracene is easier to oxidize when adsorbed at the surface of MWCNTs. This explains the difference of reactivity observed experimentally and that laccases do not need redox mediators such as ABTS when anthracene is adsorbed on MWCNTs, the latter acting as oxidation promoters.

SWV experiments performed in the best conditions, *i.e.* adsorbed laccases without ABTS and laccase in solution with ABTS, were modelized using adsorption isotherms considering the fact that a pseudo-equilibrium is reached during the oxidation of anthracene (Fig. 5A). No accurate model was obtained using a simple Langmuir isotherm, likely arising from the presence of a mixture of enzymes, anthracene and anthraquinone at MWCNT electrodes. In this particular case

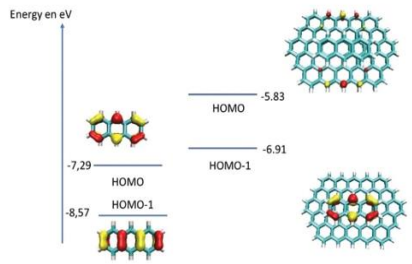

Fig. 4 Schematic representation of the highest occupied orbitals for the anthracene and for the model of the anthracene adsorbed at MWCNT electrodes.

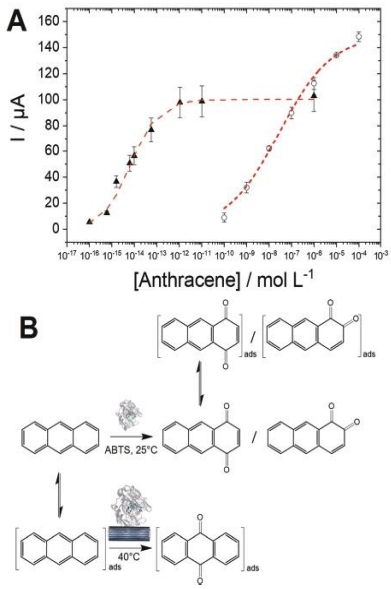

Fig. 5 (A) Logarithmic plot of the SWV peak current towards anthracene concentration for the detection of anthracene at MWWCNT electrode from (▲) a solution of 1 U mL^{-1} of laccase and ABTS left to react for 1 h at 25 °C min and (○) from a POXA1b-modified MWCNT electrode in a solution of anthracene left to react for 2 h at 40 °C; (B) hypothesized mechanism for the formation of 1,4-anthraquinone and 9,10-anthraquinone and their adsorption on MWCNT.

where heterogeneity of adsorptions might be caused by a complicated mixture at such porous surface, the Freundlich model was successfully used to fit the experimental data, according to eqn (2):[38,43]

$$I_{p,eq} = \frac{I_{p,max} \times (K_{AQ}^{app} \times [\text{anthracene}])^n}{1 + (K_{AQ}^{app} \times [\text{anthracene}])^n} \quad (2)$$

where $I_{p,eq}$ is the equilibrium peak current, $I_{p,max}$ is the peak current at saturating concentrations of anthracene and K_{AQ} is the association constant between the as-produced anthraquinone (AQ) derivative and the MWCNT surface in water and n is Langmuir–Freundlich coefficient number. Table 1 shows the

Table 1 Fitting parameters for the Langmuir–Freundlich isotherm model from Fig. 5A

	$I_{p,max}$	K_{AQ}^{app} (L mol^{-1})	n	R^2
Laccase/ABTS	100(±9)	1.5×10^{14}	0.7(±0.1)	0.975
Laccase/MWCNT	150(±7)	3.5×10^{7}	0.4(±0.1)	0.997

Langmuir–Freundlich model parameters obtained from fitting curves of Fig. 5A.

The high apparent value of K_{AQ} of 1.5×10^{14} L mol^{-1} for the laccase/ABTS mediator system is likely due to the high efficiency of the enzymatic oxidation, which maximizes the formation of 1,4-anthraquinone and its subsequent adsorption on MWCNT surfaces. The K_{AQ}^{app} value is also several order of magnitude higher compared to the K_{AQ} value measured for anthraquinone adsorption in MeCN. This is expected from the stronger pi–pi interaction between anthraquinone and CNT sidewalls in water as compared to MeCN. K_{AQ}^{app} value of 3.5×10^{7} L mol^{-1} for MWCNT-supported laccase, is indicative of a less-efficient oxidation process as compared to the laccase/ABTS mediator system, generating lower amounts of 9,10-anthraquinone. The fact that higher I_p^{max} of 150 μA is obtained for the MWCNT-supported laccase system likely arises from two reasons.

The oxidation process, in this case, is driven by the adsorption of anthracene which might have higher amounts of binding site on MWCNT sidewalls as compared to anthraquinone. ABTS can also possibly compete with anthraquinone towards binding sites in the case of the laccase/ABTS system. These results indicate that two major pathways are involved in the anthracene oxidation by laccases (Fig. 5B). First, the most sensitive and efficient way is the use of the laccase/ABTS system in solution. This allows the fast generation of 1,4-anthraquinone, which is subsequently adsorbed on MWCNTs and detected by SWV at detection limits as low as 0.1 fM. A second pathway is observed in the case of MWCNT-supported laccase, producing specifically 9,10-anthraquinone. The fact that this reaction is only observed when laccase is immobilized on MWCNT implies that MWCNT plays the role of the redox mediator by oxidizing adsorbed anthracene. Electrons are likely transferred from MWCNTs to the laccase active site, affording the oxidation of anthracene into 9,10-anthraquinone. We recently demonstrated that POXA1b could favourably transfer electrons between the T1 active site and the electrode for direct oxygen reduction.[20] This pathway leads to the preferred formation of 9,10-anthraquinone over 1,4- and 1,2-anthraquinone. The selectivity of the oxidation of anthracene *via* these two pathways is still not clearly understood. However, we can hypothesize that a radical intermediate formed by anthracene oxidation is likely stabilized by pi–pi interactions with MWCNTs. It is noteworthy that the high-potential electro-oxidation of anthracene at CNT-based electrodes leads to the formation of 9,10-anthaquinone.[44]

Anthracene and PAH biosensing performances

Owing to the logarithmic scale, a linear range for the biosensing of anthracene could be obtained for the laccase/ABTS and the laccase/MWCNT systems. Furthermore, we also took advantage of the engineered laccase-hydrophobin chimera to modify commercial magnetic beads. This strategy was employed to underline the versatility of this type of PAH biosensors and to demonstrate the possibility to integrate this sensing strategy in future magnetic-bead-based biosensing platform. The immobilization procedure was easy and fast, since no derivatization procedure was necessary, and allowed to obtain 70% immobilization yield. The immobilized laccase showed high stability, retaining almost total activity after 28 days of storage at both 4° and 25 °C. These biofunctionalized magnetic beads were also used with ABTS to provide anthracene biosensing in solution. Fig. 6 displays the linear region for all three configurations towards anthracene concentrations. The performances of the three configurations are given in Table 2.

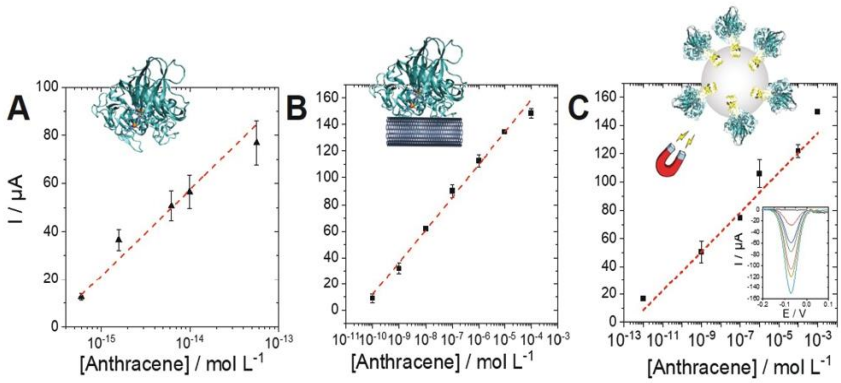

Fig. 6 Linear part of the logarithmic plot of the SWV peak current against anthracene concentration for the detection of anthracene at MWCNT electrode from (A) a solution of 1 U mL^{-1} of laccase and 20 mM ABTS left to react for 1 h at 25 °C min, (B) from a POXA1b-modified MWCNT electrode in a solution of anthracene left to react for 2 h at 40 °C and (C) a solution of 20 mU mL^{-1} of biofunctionaized microbeads and 50 mM ABTS left to react for 1 h at 25 °C min (inset: corresponding SWV performed in a 0.1 M phosphate/citrate buffer solution pH 5).

Table 2 Electrochemical parameters for anthracene biosensing

	Sensitivity	Linear range	R^2
Laccase/ABTS	36(±4)	0.6 fM–0.1 pM	0.966
Laccase/MWCNT	24.4(±0.6)	0.1 nM–0.1 mM	0.997
MB-laccase/ABTS	14(±2)	1 pM–1 mM	0.960

As expected, the best sensitivity and LOD (0.6 fM) is obtained for the laccase/ABTS system in solution with excellent repeatability (performed on three electrodes). This originates for the high concentration of enzyme (1 U mL^{-1}) and the efficiency of the laccase/ABTS system towards anthracene oxidation. The laccase/MWCNT system (without the use of ABTS) exhibits a higher LOD of 0.1 nM but a wider linear range between 0.1 nM and 0.1 mM. The chimera-modified magnetic beads exhibit a lower sensitivity of 14 μA per log unit as compared to the laccase/ABTS system. This is caused by the lower activity of the biofunctionalized beads (10 mU L^{-1}), as compared to laccase in solution (1 U mL^{-1}). However, this lower activity affords a lower production of 1,4-anthraquinone and a higher linear range between 1 pM and 1 mM. These results underline the fact that a wide linear range and an extremely low LOD can be obtained depending on the biosensing conditions. These conditions can be easily adapted depending on the concentration range of the starting anthracene solution.

Owing to the high sensitivity of the laccase mediator system based on laccase and ABTS in solution and the ability of MWCNT electrodes to sensibly detect anthraquinone, the biosensing of different PAHs were studied using this strategy. Fig. S1† shows the oxidation of pyrene and benzo(a)pyrene, two well-known PAHs. By performing a logarithmic fit, calibration curves were obtained for all PAHs. Table 3 summarizes the analytical performances of the biosensors.

It is noteworthy that a one—order-of-magnitude difference is observed compared to anthracene biosensing, arising from the lower efficiency of the oxidation process for both pyrene and benzo(a)pyrene by the laccase/ABTS system.

This is the first example of a PAH biosensor based on an enzymatic process. For comparison, few electrochemical biosensors for PAH have been developed, only based on affinity-type receptors such as antibody/antigen interaction. A biosensor based on the interaction of PAH with DNA was able to detect PAH by DPV at high potential (1 V) with a LOD of 10 nM.[45] Other type of electrochemical sensor are mostly based on the high potential oxidation of PAH on different electrode materials.[1] Polyaniline-based nanostructured electrodes exhibit LOD of 4.4 nM and 0.1 fM for anthracene and phenanthrene respectively[46–48] Direct electrochemical detection of monohydroxylated PAHs by conjugated polyelectrolyte/graphene-based electrodes exhibits LOD of 1.4 nM.[49] Imprinted polymers have also been used, showing LOD of 0.5 fM and sensitivity of 80 μA per log unit.[50] Cadmium/aluminum layered double hydroxide-based electrodes[51] are able to interact with anthracene and its electrochemical sensing was achieved at −0.92 V in 1 M KOH by DPV with a sensitivity of 1.9 μA per log unit, a linear range of 0.1 to 100 pM and a LOD of 0.5 fM.

Table 3 Electrochemical parameters for pyrene and benzo(a)pyrene biosensing

	Sensitivity	Linear range	R^2
Pyrene	3.6(±0.1)	1 fM–10 pM	0.998
Benzo(a)pyrene	3.5(±0.4)	1 fM–10 pM	0.979

Conclusions

In this work we developed a novel strategy for oxidation and detection of PAH using a combination of laccase and MWCNT electrodes. Owing to the high sensitivity of MWCNT electrodes towards quinones, the products of the oxidation of PAHs can be adsorbed and detected at MWCNT electrodes using SWV. The study of anthracene oxidation by the thermophilic POXA1b shows that MWCNTs can play the role of a redox mediator towards oxidation of anthracene into 9,10-anthraquinone, as confirmed by SWV experiments and DFT calculations. Using ABTS, 1,4- and/or 1,2-anthraquinone are preferably formed and provide the most efficient way of anthracene oxidation and detection. A highly sensitive biosensor of anthracene was designed with extremely low LOD of 0.6 fM and a linear range which can be easily adapted depending on the biosensing conditions. Owing to the flexibility of laccase and its hydrophobin chimera, laccase-modified magnetic beads can also be employed in combination with MWCNT electrodes for anthracene detection. Furthermore, this biosensor can be extended to other PAH such as pyrene or benzo(a)-pyrene. This study paves the way for the use of laccase and laccase-modified nanomaterials for the design of highly efficient PAH oxidation and detection systems.

Author contributions

Project administration, funding acquisition, conceptualization: P. G. and A. L. G. writing, review and editing: A. P., H. J., P. G. and A. L. G., investigation, methodology, formal analysis: I. S., M. C., H. J. and A. P.

Conflicts of interest

There are no conflicts to declare.

Acknowledgements

This project is funded by Italian Education, University and Research Ministry (MIUR), French National Research Agency (ANR) and co-funded by European Union's Horizon 2020 research and innovation program under the framework of ERA-NET Cofund MarTERA (Maritime and Marine

Technologies for a new Era). This work was supported by the Agence Nationale de la Recherche through the LabEx ARCANE programe (ANR-11-LABX-0003-01) and the Graduate School on Chemistry, Biology and Health of Univ Grenoble Alpes CBH-EUR-GS (ANR-17-EURE-0003). The authors acknowledge support from the plateforme de Chimie NanoBio ICMG FR 2607 (PCN-ICMG).

Notes and references

1 S. A. Nsibande, H. Montaseri and P. B. C. Forbes, *TrAC, Trends Anal. Chem.*, 2019, **115**, 52–69.
2 A. Le Goff, M. Holzinger and S. Cosnier, *Analyst*, 2011, 1279–1287.
3 M. Holzinger, A. Le Goff and S. Cosnier, *Sensors*, 2017, **17**, 1010.
4 M. Holzinger, A. Le Goff and S. Cosnier, *Front. Chem.*, 2014, **2**, 63.
5 H. Ju, *Appl. Mater. Today*, 2018, **10**, 51–71.
6 A. Le Goff and M. Holzinger, *Sustainable Energy Fuels*, 2018, **2**, 2555–2566.
7 J. B. Haun, T.-J. Yoon, H. Lee and R. Weissleder, *WIREs Nanomed. Nanobiotechnol.*, 2010, **2**, 291–304.
8 X. He, H. Huo, K. Wang, W. Tan, P. Gong and J. Ge, *Talanta*, 2007, **73**, 764–769.
9 C. Sun, J. S. H. Lee and M. Zhang, *Adv. Drug Delivery Rev.*, 2008, **60**, 1252–1265.
10 T. Konry, S. S. Bale, A. Bhushan, K. Shen, E. Seker, B. Polyak and M. Yarmush, *Microchim. Acta*, 2012, **176**, 251–269.
11 C. Pezzella, L. Guarino and A. Piscitelli, *Cell. Mol. Life Sci.*, 2015, **72**, 923–940.
12 A. Le Goff, M. Holzinger and S. Cosnier, *Cell. Mol. Life Sci.*, 2015, **72**, 941–952.
13 N. Mano and A. de Poulpiquet, *Chem. Rev.*, 2017, **118**, 2392–2468.
14 C. Pezzella, V. G. Giacobelli, V. Lettera, G. Olivieri, P. Cicatiello, G. Sannia and A. Piscitelli, *J. Biotechnol.*, 2017, **259**, 175–181.
15 A. M. Garzillo, M. C. Colao, V. Buonocore, R. Oliva, L. Falcigno, M. Saviano, A. M. Santoro, R. Zappala, R. P. Bonomo, C. Bianco, P. Giardina, G. Palmieri and G. Sannia, *J. Protein Chem.*, 2001, **20**, 191–201.
16 I. Sorrentino, I. Stanzione, Y. Nedellec, A. Piscitelli, P. Giardina and A. Le Goff, *Int. J. Mol. Sci.*, 2020, **21**, 3741.
17 M. M. Rodríguez-Delgado, G. S. Alemán-Nava, J. M. Rodríguez-Delgado, G. Dieck-Assad, S. O. Martínez-Chapa, D. Barceló and R. Parra, *TrAC, Trends Anal. Chem.*, 2015, **74**, 21–45.
18 I. Sorrentino, P. Giardina and A. Piscitelli, *Appl. Microbiol. Biotechnol.*, 2019, **103**, 3061–3071.
19 S. Palanisamy, S. K. Ramaraj, S.-M. Chen, T. C. K. Yang, P. Yi-Fan, T.-W. Chen, V. Velusamy and S. Selvam, *Sci. Rep.*, 2017, **7**, 1–12.
20 I. Sorrentino, I. Stanzione, A. Piscitelli, P. Giardina and A. Le Goff, *Biosens. Bioelectron.: X*, 2021, 100074.
21 O. V. Morozova, G. P. Shumakovich, S. V. Shleev and Ya. I. Yaropolov, *Appl. Biochem. Microbiol.*, 2007, **43**, 523–535.
22 D. E. Dodor, H.-M. Hwang and S. I. N. Ekunwe, *Enzyme Microb. Technol.*, 2004, **35**, 210–217.
23 C. Johannes, A. Majcherczyk and A. Hüttermann, *Appl. Microbiol. Biotechnol.*, 1996, **46**, 313–317.
24 N. N. Pozdnyakova, J. Rodakiewicz-Nowak, O. V. Turkovskaya and J. Haber, *Enzyme Microb. Technol.*, 2006, **39**, 1242–1249.
25 T. G. Hedderman, S. M. Keogh, G. Chambers and H. J. Byrne, *J. Phys. Chem. B*, 2006, **110**, 3895–3901.
26 S. Gotovac, H. Honda, Y. Hattori, K. Takahashi, H. Kanoh and K. Kaneko, *Nano Lett.*, 2007, **7**, 583–587.
27 Y. Kusumoto, *Chem. Phys. Lett.*, 1987, **136**, 535–538.
28 A. Le Goff, K. Gorgy, M. Holzinger, R. Haddad, M. Zimmerman and S. Cosnier, *Chem. – Eur. J.*, 2011, **17**, 10216–10221.
29 B. Reuillard, A. Le Goff, M. Holzinger and S. Cosnier, *J. Mater. Chem. B*, 2014, **2**, 2228–2232.
30 N. Lalaoui, B. Reuillard, C. Philouze, M. Holzinger, S. Cosnier and A. Le Goff, *Organometallics*, 2016, **35**, 2987–2992.
31 A. Le Goff, B. Reuillard and S. Cosnier, *Langmuir*, 2013, **29**, 8736–8742.
32 J. A. Mann, J. Rodríguez-López, H. D. Abruña and W. R. Dichtel, *J. Am. Chem. Soc.*, 2011, **133**, 17614–17617.
33 A. Bruckner and M. Baerns, *Appl. Catal., A*, 1997, **157**, 311–334.
34 L. Bezalel, Y. Hadar, P. P. Fu, J. P. Freeman and C. E. Cerniglia, *Appl. Environ. Microbiol.*, 1996, **62**, 2554–2559.
35 M. Sosna, J.-M. Chrétien, J. D. Kilburn and P. N. Bartlett, *Phys. Chem. Chem. Phys.*, 2010, **12**, 10018–10026.
36 N. Lalaoui, A. Le Goff, M. Holzinger, M. Mermoux and S. Cosnier, *Chem. – Eur. J.*, 2015, **21**, 3198–3201.
37 S. Gentil, S. M. Che Mansor, H. Jamet, S. Cosnier, C. Cavazza and A. Le Goff, *ACS Catal.*, 2018, 3957–3964.
38 S. Sharma and G. P. Agarwal, *Anal. Biochem.*, 2001, **288**, 126–140.
39 R. Puopolo, I. Sorrentino, G. Gallo, A. Piscitelli, P. Giardina, A. Le Goff and G. Fiorentino, *Sci. Rep.*, 2021, **11**, 2991.
40 B. Reuillard, A. Le Goff and S. Cosnier, *Chem. Commun.*, 2014, **50**, 11731–11734.
41 K. Yang, X. Wang, L. Zhu and B. Xing, *Environ. Sci. Technol.*, 2006, **40**, 5804–5810.
42 C. Pezzella, S. Giacobbe, V. G. Giacobelli, L. Guarino, S. Kylic, M. Sener, G. Sannia and A. Piscitelli, *J. Mol. Catal. B: Enzym.*, 2016, **134**, 274–279.
43 F. Haddache, A. Le Goff, B. Reuillard, K. Gorgy, C. Gondran, N. Spinelli, E. Defrancq and S. Cosnier, *Chem. – Eur. J.*, 2014, **20**, 15555–15560.

44 P. Barathi and A. S. Kumar, *Chem. – Eur. J.*, 2013, **19**, 2236–2241.
45 Y. Ni, P. Wang, H. Song, X. Lin and S. Kokot, *Anal. Chim. Acta*, 2014, **821**, 34–40.
46 O. Tovide, N. Jaheed, N. Mohamed, E. Nxusani, C. E. Sunday, A. Tsegaye, R. F. Ajayi, N. Njomo, H. Makelane, M. Bilibana, P. G. Baker, A. Williams, S. Vilakazi, R. Tshikhudo and E. I. Iwuoha, *Electrochim. Acta*, 2014, **128**, 138–148.
47 O. E. Fayemi, A. S. Adekunle and E. E. Ebenso, *J. Nanomater.*, 2016, **2016**, e9614897.
48 O. Tovide, N. Jahed, C. E. Sunday, K. Pokpas, R. F. Ajayi, H. R. Makelane, K. M. Molapo, S. V. John, P. G. Baker and E. I. Iwuoha, *Sens. Actuators, B*, 2014, **205**, 184–192.
49 Y. Pang, Y. Huang, W. Li, L. Feng and X. Shen, *ACS Appl. Nano Mater.*, 2019, **2**, 7785–7794.
50 H. Munawar, J. S. Mankar, M. D. Sharma, A. Garcia-Cruz, L. A. L. Fernandes, M. Peacock and R. J. Krupadam, *Talanta*, 2020, **219**, 121273.
51 X. Qiao, M. Wei, D. Tian, F. Xia, P. Chen and C. Zhou, *J. Electroanal. Chem.*, 2018, **808**, 35–40.

Chapter 6

6. Conclusions

The predicted outcomes of the present PhD project, *i.e.* the identification of new fungal protein biosurfactants and their exploitation in diagnostic and biosensing fields, were successfully achieved.
In the research of new protein biosurfactants produced by filamentous fungi, three different marine fungal strains have been investigated. *Penicillium chrysogenum* produces a protein named *SAP-Pc*, annotated as hypothetical protein, able to stabilize emulsions rather than to reduce surface tension, thus defined as bioemulsifier. Moreover, proteins isolated from *Paradendryphiela salina* and *Talaromyces pinophilus*, have been identified as protein biosurfactants belonging to the hydrophobins and ceratoplatanins classes.
The employment of these kind of proteins in different application fields has been demonstrated using the most characterized protein biosurfactant produced by the fungus *Pleurotus ostreatus*. Indeed, Vmh2, having the capability to form amphiphilic layers on several surfaces allowing the adhesion of other biomolecules in their active form, has been exploited both in diagnosis of cultural heritage and in biosensing fields.
The sampling invasiveness of the cultural heritage object represent the main issue that our developed system allows to overcome. The functionalization of cellulose acetate sheets with Vmh2 and the following immobilization of proteolytic enzymes, trypsin and PNGaseF, permitted the proteomic analysis of ancient objects through a contact of only few minutes between the functionalized sheet and the sample. Indeed, the functionalized surface not only allows the hydrolysis of the proteins but also the adhesion of the hydrolysed peptides on it to be later recovered and analysed by mass spectrometry techniques.
The genetic fusion between the hydrophobin Vmh2 and different target proteins of biotechnological interest, is a successful strategy exploitable for the development of several kind of biosensors. This approach, in fact, allowed a one-step immobilization of the fusion proteins on several surfaces avoiding their chemical derivatization. In this context, the recombinant production of the chimeric proteins Vmh2-ScFvs was employed for the development of optical and electrochemical biosensors, to measure concentrations of the two algal neurotoxins saxitoxin and domoic acid, with a low limit of detection. Furthermore, the chimeric protein Vmh2-Laccase was exploited for the detection of different aromatic and phenolic compounds. Indeed, this protein has been immobilized on nanomaterials, such as graphene and carbon nanotubes, and electrochemical biosensors to detect cathecol, dopamine and anthracene were developed. Finally, an innovative, cheap and easy-to use electroanalytical biosystem was developed during the period spent at the University of Oviedo. The laccase chimera was

immobilized, for the first time, into common polypropylene tips and coupled with a screen-printed electrode to detect caffeic acid into a real matrix, tea samples.

References

1. Spatafora, J.W.; Aime, M.C.; Gregoriev, I. V.; Martin, F.; Stajich, J.E.; Blackwell, M. The fungal tree of life: From molecular systematics to genome-scale phylogenies. *The Fungal Kingdom* **2017**, 3–34, doi:10.1128/9781555819583.ch1.
2. Lange, L. Fungal Enzymes and Yeasts for Conversion of Plant Biomass to Bioenergy and High-Value Products. *Microbiol. Spectr.* **2017**, *5*, doi:10.1128/microbiolspec.FUNK-0007-2016.
3. Sunde, M.; Pham, C.L.L.; Kwan, A.H. Molecular characteristics and biological functions of surface-active and surfactant proteins. *Annu. Rev. Biochem.* **2017**, *86*, 585–608, doi:10.1146/annurev-biochem-061516-044847.
4. Luft, L.; Confortin, T.C.; Todero, I.; Zabot, G.L.; Mazutti, M.A. An overview of fungal biopolymers: bioemulsifiers and biosurfactants compounds production. *Crit. Rev. Biotechnol.* **2020**, *40*, 1059–1080, doi:10.1080/07388551.2020.1805405.
5. Kee, S.H.; Chiongson, J.B. V.; Saludes, J.P.; Vigneswari, S.; Ramakrishna, S.; Bhubalan, K. Bioconversion of agro-industry sourced biowaste into biomaterials via microbial factories – A viable domain of circular economy. *Environ. Pollut.* **2021**, *271*, doi:10.1016/j.envpol.2020.116311.
6. Sena, H.H.; Sanches, M.A.; Rocha, D.F.S.; Segundo, W.O.P.F.; De Souza, É.S.; De Souza, J.V.B. Erratum to: Production of biosurfactants by soil fungi isolated from the Amazon forest (International Journal of Microbiology (2018) 2018 (5684261) DOI: 10.1155/2018/5684261). *Int. J. Microbiol.* **2018**, *2018*, doi:10.1155/2018/1586859.
7. Sałek, K.; Euston, S.R. Sustainable microbial biosurfactants and bioemulsifiers for commercial exploitation. *Process Biochem.* **2019**, *85*, 143–155, doi:https://doi.org/10.1016/j.procbio.2019.06.027.
8. Rane, A.N.; Baikar, V. V.; Ravi Kumar, D. V.; Deopurkar, R.L. Agro-industrial wastes for production of biosurfactant by Bacillus subtilis ANR 88 and its application in synthesis of silver and gold nanoparticles. *Front. Microbiol.* **2017**, *8*, 1–12, doi:10.3389/fmicb.2017.00492.
9. Landeta-Salgado, C.; Cicatiello, P.; Stanzione, I.; Medina, D.; Berlanga Mora, I.; Gomez, C.; Lienqueo, M.E. The growth of marine fungi on seaweed polysaccharides produces cerato-platanin and hydrophobin self-assembling proteins. *Microbiol. Res.* **2021**, *251*, 126835, doi:10.1016/j.micres.2021.126835.
10. Uzoigwe, C.; Burgess, J.G.; Ennis, C.J.; Rahman, P.K.S.M. Bioemulsifiers are not biosurfactants and require different screening approaches. *Front. Microbiol.* **2015**, *6*, 1–6, doi:10.3389/fmicb.2015.00245.
11. Jiménez-Peñalver, P.; Rodríguez, A.; Daverey, A.; Font, X.; Gea, T. Use of wastes for sophorolipids production as a transition to circular economy: state of the art and perspectives. *Rev. Environ. Sci. Biotechnol.* **2019**, *18*, 413–435, doi:10.1007/s11157-019-09502-3.
12. Drakontis, C.E.; Amin, S. Biosurfactants: Formulations, properties, and applications. *Curr. Opin. Colloid Interface Sci.* **2020**, *48*, 77–90, doi:10.1016/j.cocis.2020.03.013.
13. Nitschke, M.; Silva, S.S.E. Recent food applications of microbial surfactants. *Crit. Rev. Food Sci. Nutr.* **2018**, *58*, 631–638, doi:10.1080/10408398.2016.1208635.
14. Mnif, I.; Ellouz-Chaabouni, S.; Ghribi, D. Glycolipid Biosurfactants, Main Classes, Functional Properties and Related Potential Applications in Environmental Biotechnology. *J. Polym. Environ.* **2018**, *26*, 2192–2206, doi:10.1007/s10924-017-1076-4.
15. Talbot, N.J. Aerial morphogenesis: Enter the chaplins. *Curr. Biol.* **2003**, *13*, 696–698, doi:10.1016/j.cub.2003.08.040.
16. Wösten, H.A.B. Hydrophobins: Multipurpose proteins. *Annu. Rev. Microbiol.* **2001**, *55*, 625–646, doi:10.1146/annurev.micro.55.1.625.
17. Lo, V.; I-Chun Lai, J.; Sunde, M. Fungal Hydrophobins and Their Self-Assembly into Functional Nanomaterials. *Adv. Exp. Med. Biol.* **2019**, *1174*, 161–185, doi:10.1007/978-981-13-9791-2_5.
18. Wessels, J.G.; de Vries, O.M.; Asgeirsdóttir, S.A.; Springer, J. The thn mutation of Schizophyllum commune, which suppresses formation of aerial hyphae, affects expression of the Sc3 hydrophobin gene. *J. Gen. Microbiol.* **1991**, *137*, 2439–2445, doi:10.1099/00221287-137-10-2439.
19. Wösten, H.A.B.; Willey, J.M. Surface-active proteins enable microbial aerial hyphae to grow into the air. *Microbiology* **2000**, *146*, 767–773, doi:10.1099/00221287-146-4-767.
20. Heddergott, C.; Bruns, S.; Nietzsche, S.; Leonhardt, I.; Kurzai, O.; Kniemeyer, O.; Brakhage, A.A. The arthroderma benhamiae hydrophobin HypA mediates hydrophobicity and influences recognition by human immune effector cells. *Eukaryot. Cell* **2012**, *11*, 673–682, doi:10.1128/EC.00037-12.
21. Kono, M.; Kon, Y.; Ohmura, Y.; Satta, Y.; Terai, Y. In vitro resynthesis of lichenization reveals the genetic background of symbiosis-specific fungal-algal interaction in Usnea hakonensis. *BMC Genomics* **2020**, *21*, 1–16, doi:10.1186/s12864-020-07086-9.
22. Gandier, J.A.; Langelaan, D.N.; Won, A.; O'Donnell, K.; Grondin, J.L.; Spencer, H.L.; Wong, P.; Tillier, E.; Yip, C.; Smith, S.P.; et al. Characterization of a Basidiomycota hydrophobin reveals the structural basis for a high-similarity Class i subdivision. *Sci. Rep.* **2017**, *7*, 1–9, doi:10.1038/srep45863.
23. De Vocht, M.L.; Reviakine, I.; Ulrich, W.-P.; Bergsma-Schutter, W.; Wösten, H.A.B.; Vogel, H.; Brisson, A.; Wessels, J.G.H.; Robillard, G.T. Self-assembly of the hydrophobin SC3 proceeds via two structural intermediates. *Protein Sci.* **2002**, *11*, 1199–1205, doi:10.1110/ps.4540102.
24. Linder, M.B. Hydrophobins: Proteins that self assemble at interfaces. *Curr. Opin. Colloid Interface Sci.*

2009, *14*, 356–363, doi:10.1016/j.cocis.2009.04.001.
25. Bayry, J.; Aimanianda, V.; Guijarro, J.I.; Sunde, M.; Latgé, J.P. Hydrophobins-unique fungal proteins. *PLoS Pathog.* **2012**, *8*, 6–9, doi:10.1371/journal.ppat.1002700.
26. Winandy, L.; Hilpert, F.; Schlebusch, O.; Fischer, R. Comparative analysis of surface coating properties of five hydrophobins from Aspergillus nidulans and Trichoderma reseei. *Sci. Rep.* **2018**, *8*, 1–11, doi:10.1038/s41598-018-29749-0.
27. Jensen, B.G.; Andersen, M.R.; Pedersen, M.H.; Frisvad, J.C.; Søndergaard, I. Hydrophobins from Aspergillus species cannot be clearly divided into two classes. *BMC Res. Notes* **2010**, *3*, 1–6, doi:10.1186/1756-0500-3-344.
28. Kwan, A.H.Y.; Winefield, R.D.; Sunde, M.; Matthews, J.M.; Haverkamp, R.G.; Templeton, M.D.; Mackay, J.P. Structural basis for rodlet assembly in fungal hydrophobins. *Proc. Natl. Acad. Sci. U. S. A.* **2006**, *103*, 3621–3626, doi:10.1073/pnas.0505704103.
29. Morris, V.K.; Kwan, A.H.; Mackay, J.P.; Sunde, M. Backbone and sidechain ^{1}H, ^{13}C and ^{15}N chemical shift assignments of the hydrophobin DewA from Aspergillus nidulans. *Biomol. NMR Assign.* **2012**, *6*, 83–86, doi:10.1007/s12104-011-9330-5.
30. Rey, A.A.; Hocher, A.; Kwan, A.H.; Sunde, M. Backbone and sidechain 1H, 13C and 15N chemical shift assignments of the hydrophobin MPG1 from the rice blast fungus Magnaporthe oryzae. *Biomol. NMR Assign.* **2013**, *7*, 109–112, doi:10.1007/s12104-012-9394-x.
31. Pille, A.; Kwan, A.H.; Cheung, I.; Hampsey, M.; Aimanianda, V.; Delepierre, M.; Latgé, J.P.; Sunde, M.; Guijarro, J.I. 1H, 13C and 15N resonance assignments of the RodA hydrophobin from the opportunistic pathogen Aspergillus fumigatus. *Biomol. NMR Assign.* **2015**, *9*, 113–118, doi:10.1007/s12104-014-9555-1.
32. Kallio, J.M.; Linder, M.B.; Rouvinen, J. Crystal structures of hydrophobin HFBII in the presence of detergent implicate the formation of fibrils and monolayer films. *J. Biol. Chem.* **2007**, *282*, 28733–28739, doi:10.1074/jbc.M704238200.
33. Chang, H.J.; Choi, H.; Na, S. Predicting the self-assembly film structure of class II hydrophobin NC2 and estimating its structural characteristics. *Colloids Surfaces B Biointerfaces* **2020**, *195*, doi:10.1016/j.colsurfb.2020.111269.
34. Wösten, H.A.B.; Scholtmeijer, K. Applications of hydrophobins: current state and perspectives. *Appl. Microbiol. Biotechnol.* **2015**, *99*, 1587–1597, doi:10.1007/s00253-014-6319-x.
35. Pennacchio, A.; Cicatiello, P.; Notomista, E.; Giardina, P.; Piscitelli, A. New clues into the self-assembly of Vmh2, a basidiomycota class i hydrophobin. *Biol. Chem.* **2018**, *399*, 895–901, doi:10.1515/hsz-2018-0124.
36. Cox, A.; Aldred, D.; Russell, A. Exceptional stability of food foams using class II hydrophobin HFBII. *Food Hydrocoll.* **2009**, *23*, 366–376, doi:10.1016/j.foodhyd.2008.03.001.
37. Niu, B.; Wang, D.; Yang, Y.; Xu, H.; Qiao, M. Heterologous expression and characterization of the hydrophobin HFBI in Pichia pastoris and evaluation of its contribution to the food industry. *Amino Acids* **2012**, *43*, 763–771, doi:10.1007/s00726-011-1126-5.
38. Wu, Y.; Li, J.; Yang, H.; Shin, H.-J. Fungal and mushroom hydrophobins: A review. *J. Mushroom* **2017**, *15*, 1–7, doi:10.14480/jm.2017.15.1.1.
39. Sánchez, C. Fungal potential for the degradation of petroleum-based polymers: An overview of macro- and microplastics biodegradation. *Biotechnol. Adv.* **2020**, *40*, 107501, doi:10.1016/j.biotechadv.2019.107501.
40. Qin, M.; Wang, L.K.; Feng, X.Z.; Yang, Y.L.; Wang, R.; Wang, C.; Yu, L.; Shao, B.; Qiao, M.Q. Bioactive surface modification of mica and poly(dimethylsiloxane) with hydrophobins for protein immobilization. *Langmuir* **2007**, *23*, 4465–4471, doi:10.1021/la062744h.
41. Longobardi, S.; Gravagnuolo, A.M.; Funari, R.; Della Ventura, B.; Pane, F.; Galano, E.; Amoresano, A.; Marino, G.; Giardina, P. A simple MALDI plate functionalization by Vmh2 hydrophobin for serial multi-enzymatic protein digestions. *Anal. Bioanal. Chem.* **2015**, *407*, 487–496, doi:10.1007/s00216-014-8309-3.
42. Zhang, M.; Wang, Z.; Wang, Z.; Feng, S.; Xu, H.; Zhao, Q.; Wang, S.; Fang, J.; Qiao, M.; Kong, D. Immobilization of anti-CD31 antibody on electrospun poly(e{open}-caprolactone) scaffolds through hydrophobins for specific adhesion of endothelial cells. *Colloids Surfaces B Biointerfaces* **2011**, *85*, 32–39, doi:10.1016/j.colsurfb.2010.10.042.
43. Palomo, J.M.; Peñas, M.M.; Fernández-Lorente, G.; Mateo, C.; Pisabarro, A.G.; Fernández-Lafuente, R.; Ramírez, L.; Guisán, J.M. Solid-phase handling of hydrophobins: Immobilized hydrophobins as a new tool to study lipases. *Biomacromolecules* **2003**, *4*, 204–210, doi:10.1021/bm020071l.
44. Soikkeli, M.; Kurppa, K.; Kainlauri, M.; Arpiainen, S.; Paananen, A.; Gunnarsson, D.; Joensuu, J.J.; Laaksonen, P.; Prunnila, M.; Linder, M.B.; et al. Graphene Biosensor Programming with Genetically Engineered Fusion Protein Monolayers. *ACS Appl. Mater. Interfaces* **2016**, *8*, 8257–8264, doi:10.1021/acsami.6b00123.
45. Zhao, Z.X.; Wang, H.C.; Qin, X.; Wang, X.S.; Qiao, M.Q.; Anzai, J. ichi; Chen, Q. Self-assembled film of hydrophobins on gold surfaces and its application to electrochemical biosensing. *Colloids Surfaces B Biointerfaces* **2009**, *71*, 102–106, doi:10.1016/j.colsurfb.2009.01.011.
46. Duan, S.; Wang, B.; Qiao, M.; Zhang, X.; Liu, B.; Zhang, H.; Song, B. Hydrophobin HGFI – based fibre-optic biosensor for detection of antigen – antibody interaction. **2020**, *9*, 177–186.

47. Wang, X.; Wang, H.; Huang, Y.; Zhao, Z.; Qin, X.; Wang, Y.; Miao, Z.; Chen, Q.; Qiao, M. Noncovalently functionalized multi-wall carbon nanotubes in aqueous solution using the hydrophobin HFBI and their electroanalytical application. *Biosens. Bioelectron.* **2010**, *26*, 1104–1108, doi:10.1016/j.bios.2010.08.024.
48. Khalesi, M.; Gebruers, K.; Derdelinckx, G. Recent Advances in Fungal Hydrophobin Towards Using in Industry. *Protein J.* **2015**, *34*, 243–255, doi:10.1007/s10930-015-9621-2.
49. Kulkarni, S.; Nene, S.; Joshi, K. Production of Hydrophobins from fungi. *Process Biochem.* **2017**, *61*, 1–11, doi:https://doi.org/10.1016/j.procbio.2017.06.012.
50. Pedersen, M.H.; Borodina, I.; Moresco, J.L.; Svendsen, W.E.; Frisvad, J.C.; Søndergaard, I. High-yield production of hydrophobins RodA and RodB from Aspergillus fumigatus in Pichia pastoris. *Appl. Microbiol. Biotechnol.* **2011**, *90*, 1923–1932, doi:10.1007/s00253-011-3235-1.
51. Longobardi, S.; Picone, D.; Ercole, C.; Spadaccini, R.; Stefano, L. De; Rea, I.; Giardina, P. Environmental conditions modulate the switch among different states of the hydrophobin Vmh2 from Pleurotus ostreatus. *Biomacromolecules* **2012**, *13*, 743–750, doi:10.1021/bm201663f.
52. De Stefano, L.; Rea, I.; De Tommasi, E.; Rendina, I.; Rotiroti, L.; Giocondo, M.; Longobardi, S.; Armenante, A.; Giardina, P. Bioactive modification of silicon surface using self-assembled hydrophobins from Pleurotus ostreatus. *Eur. Phys. J. E* **2009**, *30*, 181–185, doi:10.1140/epje/i2009-10481-y.
53. Longobardi, S.; Gravagnuolo, A.M.; Rea, I.; De Stefano, L.; Marino, G.; Giardina, P. Hydrophobin-coated plates as matrix-assisted laser desorption/ionization sample support for peptide/protein analysis. *Anal. Biochem.* **2014**, *449*, 9–16, doi:10.1016/j.ab.2013.11.021.
54. Cicatiello, P.; Ntasi, G.; Rossi, M.; Marino, G.; Giardina, P.; Birolo, L. Minimally Invasive and Portable Method for the Identification of Proteins in Ancient Paintings. *Anal. Chem.* **2018**, *90*, 10128–10133, doi:10.1021/acs.analchem.8b01718.
55. Gravagnuolo, A.M.; Morales-Narváez, E.; Longobardi, S.; Da Silva, E.T.; Giardina, P.; Merkoçi, A. In situ production of biofunctionalized few-layer defect-free microsheets of graphene. *Adv. Funct. Mater.* **2015**, *25*, 2771–2779, doi:10.1002/adfm.201500016.
56. Politi, J.; De Stefano, L.; Longobardi, S.; Giardina, P.; Rea, I.; Methivier, C.; Pradier, C.M.; Casale, S.; Spadavecchia, J. The amphiphilic hydrophobin Vmh2 plays a key role in one step synthesis of hybrid protein-gold nanoparticles. *Colloids Surfaces B Biointerfaces* **2015**, *136*, 214–221, doi:10.1016/j.colsurfb.2015.09.021.
57. Politi, J.; De Stefano, L.; Rea, I.; Gravagnuolo, A.M.; Giardina, P.; Methivier, C.; Casale, S.; Spadavecchia, J. One-pot synthesis of a gold nanoparticle-Vmh2 hydrophobin nanobiocomplex for glucose monitoring. *Nanotechnology* **2016**, *27*, 0, doi:10.1088/0957-4484/27/19/195701.
58. Artini, M.; Cicatiello, P.; Ricciardelli, A.; Papa, R.; Selan, L.; Dardano, P.; Tilotta, M.; Vrenna, G.; Tutino, M.L.; Giardina, P.; et al. Hydrophobin coating prevents Staphylococcus epidermidis biofilm formation on different surfaces. *Biofouling* **2017**, *33*, 601–611, doi:10.1080/08927014.2017.1338690.
59. Sorrentino, I.; Gargano, M.; Ricciardelli, A.; Parrilli, E.; Buonocore, C.; de Pascale, D.; Giardina, P.; Piscitelli, A. Development of anti-bacterial surfaces using a hydrophobin chimeric protein. *Int. J. Biol. Macromol.* **2020**, *164*, 2293–2300, doi:10.1016/j.ijbiomac.2020.07.301.
60. Della Ventura, B.; Rea, I.; Caliò, A.; Giardina, P.; Gravagnuolo, A.M.; Funari, R.; Altucci, C.; Velotta, R.; De Stefano, L. Vmh2 hydrophobin layer entraps glucose: A quantitative characterization by label-free optical and gravimetric methods. *Appl. Surf. Sci.* **2016**, *364*, 201–207, doi:10.1016/j.apsusc.2015.12.080.
61. Piscitelli, A.; Pennacchio, A.; Longobardi, S.; Velotta, R.; Giardina, P. Vmh2 hydrophobin as a tool for the development of “self-immobilizing” enzymes for biosensing. *Biotechnol. Bioeng.* **2017**, *114*, 46–52, doi:10.1002/bit.26049.
62. Piscitelli, A.; Pennacchio, A.; Cicatiello, P.; Politi, J.; De Stefano, L.; Giardina, P. Rapid and ultrasensitive detection of active thrombin based on the Vmh2 hydrophobin fused to a Green Fluorescent Protein. *Biosens. Bioelectron.* **2017**, *87*, 816–822, doi:10.1016/j.bios.2016.09.052.
63. Sorrentino, I.; Giardina, P.; Piscitelli, A. Development of a biosensing platform based on a laccase-hydrophobin chimera. *Appl. Microbiol. Biotechnol.* **2019**, *103*, 3061–3071, doi:10.1007/s00253-019-09678-2.
64. Puopolo, R.; Sorrentino, I.; Gallo, G.; Piscitelli, A.; Giardina, P.; Le Goff, A.; Fiorentino, G. Self-assembling thermostable chimeras as new platform for arsenic biosensing. *Sci. Rep.* **2021**, *11*, 1–12, doi:10.1038/s41598-021-82648-9.
65. Pennacchio, A.; Giampaolo, F.; Piccialli, F.; Cuomo, S.; Notomista, E.; Spinelli, M.; Amoresano, A.; Piscitelli, A.; Giardina, P. A machine learning-enhanced biosensor for mercury detection based on an hydrophobin chimera. *Biosens. Bioelectron.* **2022**, *196*, 113696, doi:10.1016/j.bios.2021.113696.
66. Djonović, S.; Vargas, W.A.; Kolomiets, M. V.; Horndeski, M.; Wiest, A.; Kenerley, C.M. A proteinaceous elicitor Sm1 from the beneficial fungus Trichoderma virens is required for induced systemic resistance in Maize. *Plant Physiol.* **2007**, *145*, 875–889, doi:10.1104/pp.107.103689.
67. Gaderer, R.; Bonazza, K.; Seidl-Seiboth, V. Cerato-platanins: a fungal protein family with intriguing properties and application potential. *Appl. Microbiol. Biotechnol.* **2014**, *98*, 4795–4803, doi:10.1007/s00253-014-5690-y.
68. Frischmann, A.; Neudl, S.; Gaderer, R.; Bonazza, K.; Zach, S.; Gruber, S.; Spadiut, O.; Friedbacher, G.; Grothe, H.; Seidl-Seiboth, V. Self-assembly at air/water interfaces and carbohydrate binding properties of the small secreted protein EPL1 from the fungus Trichoderma atroviride. *J. Biol. Chem.* **2013**, *288*,

4278–4287, doi:10.1074/jbc.M112.427633.
69. Pitocchi, R.; Cicatiello, P.; Birolo, L.; Piscitelli, A.; Bovio, E.; Cristina Varese, G.; Giardina, P. Cerato-platanins from marine fungi as effective protein biosurfactants and bioemulsifiers. *Int. J. Mol. Sci.* **2020**, *21*, doi:10.3390/ijms21082913.
70. Pazzagli, L.; Zoppi, C.; Carresi, L.; Tiribilli, B.; Sbrana, F.; Schiff, S.; Pertinhez, T.A.; Scala, A.; Cappugi, G. Characterization of ordered aggregates of cerato-platanin and their involvement in fungus-host interactions. *Biochim. Biophys. Acta - Gen. Subj.* **2009**, *1790*, 1334–1344, doi:10.1016/j.bbagen.2009.07.014.
71. De Oliveira, A.L.; Gallo, M.; Pazzagli, L.; Benedetti, C.E.; Cappugi, G.; Scala, A.; Pantera, B.; Spisni, A.; Pertinhez, T.A.; Cicero, D.O. The structure of the elicitor cerato-platanin (CP), the first member of the CP fungal protein family, reveals a double ψβ-barrel fold and carbohydrate binding. *J. Biol. Chem.* **2011**, *286*, 17560–17568, doi:10.1074/jbc.M111.223644.
72. Quarantin, A.; Castiglioni, C.; Schäfer, W.; Favaron, F.; Sella, L. The Fusarium graminearum cerato-platanins loosen cellulose substrates enhancing fungal cellulase activity as expansin-like proteins. *Plant Physiol. Biochem. PPB* **2019**, *139*, 229–238, doi:10.1016/j.plaphy.2019.03.025.
73. Pennacchio, A.; Pitocchi, R.; Varese, G.C.; Giardina, P.; Piscitelli, A. Trichoderma harzianum cerato-platanin enhances hydrolysis of lignocellulosic materials. *Microb. Biotechnol.* **2021**, *14*, 1699–1706, doi:10.1111/1751-7915.13836.
74. Amend, A.; Burgaud, G.; Cunliffe, M.; Edgcomb, V.P.; Ettinger, C.L.; Gutiérrez, M.H.; Heitman, J.; Hom, E.F.Y.; Ianiri, G.; Jones, A.C.; et al. Fungi in the marine environment: Open questions and unsolved problems. *MBio* **2019**, *10*, 1–15, doi:10.1128/mBio.01189-18.
75. Ferreira, J.A.; Varjani, S.; Taherzadeh, M.J. A Critical Review on the Ubiquitous Role of Filamentous Fungi in Pollution Mitigation. *Curr. Pollut. Reports* **2020**, *6*, 295–309, doi:10.1007/s40726-020-00156-2.
76. Kües, U. Fungal enzymes for environmental management. *Curr. Opin. Biotechnol.* **2015**, *33*, 268–278, doi:10.1016/j.copbio.2015.03.006.
77. Aranda, E. Promising approaches towards biotransformation of polycyclic aromatic hydrocarbons with Ascomycota fungi. *Curr. Opin. Biotechnol.* **2016**, *38*, 1–8, doi:10.1016/j.copbio.2015.12.002.
78. Theerachat, M.; Guieysse, D.; Morel, S.; Remaud-Siméon, M.; Chulalaksananukul, W. Laccases from Marine Organisms and Their Applications in the Biodegradation of Toxic and Environmental Pollutants: a Review. *Appl. Biochem. Biotechnol.* **2019**, *187*, 583–611, doi:10.1007/s12010-018-2829-9.
79. Graminha, E.B.N.; Gonçalves, A.Z.L.; Pirota, R.D.P.B.; Balsalobre, M.A.A.; Da Silva, R.; Gomes, E. Enzyme production by solid-state fermentation: Application to animal nutrition. *Anim. Feed Sci. Technol.* **2008**, *144*, 1–22, doi:10.1016/j.anifeedsci.2007.09.029.
80. Wan, C.; Li, Y. Fungal pretreatment of lignocellulosic biomass. *Biotechnol. Adv.* **2012**, *30*, 1447–1457, doi:10.1016/j.biotechadv.2012.03.003.
81. Cicatiello, P.; Gravagnuolo, A.M.; Gnavi, G.; Varese, G.C.; Giardina, P. Marine fungi as source of new hydrophobins. *Int. J. Biol. Macromol.* **2016**, *92*, 1229–1233, doi:10.1016/j.ijbiomac.2016.08.037.
82. Winandy, L.; Schlebusch, O.; Fischer, R. Fungal hydrophobins render stones impermeable for water but keep them permeable for vapor. *Sci. Rep.* **2019**, *9*, 1–8, doi:10.1038/s41598-019-42705-w.
83. Hong, H.; Chen, N.; Wang, D. River-estuary-coast continuum: Biogeochemistry and ecological response to increasing human and climatic changes – Editorial overview. *Estuar. Coast. Shelf Sci.* **2015**, *166*, 144–145, doi:10.1016/j.ecss.2015.10.036.
84. Mills, G.; Fones, G. A review of in situ/IT methods and sensors for monitoring the marine environment. *Sens. Rev.* **2012**, *32*, 17–28, doi:10.1108/02602281211197116.
85. Rodríguez-Delgado, M.M.; Alemán-Nava, G.S.; Rodríguez-Delgado, J.M.; Dieck-Assad, G.; Martínez-Chapa, S.O.; Barceló, D.; Parra, R. Laccase-based biosensors for detection of phenolic compounds. *TrAC - Trends Anal. Chem.* **2015**, *74*, 21–45, doi:10.1016/j.trac.2015.05.008.

Communications

Poster

- “Fungal proteic biosurfactants for the development of biosensing and biomedical platform” (**I. Stanzione**, P. Cicatiello, R. Pitocchi, A. Piscitelli, P. Giardina), 2nd Workshop BIO/10 Napoli, Italy, 17 May 2019.
- “Electrochemical detection of environmental contaminants based on Laccase/nanomaterial-based sensor” (I. Sorrentino, **I. Stanzione**, A. Piscitelli, P. Giardina, A. Le Goff) FrenchBIC Meeting. October 12-14, 2020.

Oral presentation

- “Self-immobilizing laccase through genetic fusion with hydrophobin” (A. Piscitelli, I. Sorrentino, **I. Stanzione**, P. Giardina) 9th OxiZymes Meeting, Belfast, Ireland 8-10 July 2018.
- “Bio-functionalization of graphene with a laccase hydrophobin chimera” (I. Sorrentino, **I. Stanzione**, A. Piscitelli, A. Le Goff, P. Giardina) 7th International Symposium on Sensor Science. Napoli, Italy, 09- 11 May 2019.
- “Straightforward immobilization of chimeric proteins” (A. Piscitelli, I. Stanzione, R. Puopolo, **I. Sorrentino**, G. Fiorentino, P. Giardina) SIB 2019, Lecce, Italy, September 18–20, 2019.
- “Sensor-bioinspired based on laccase for contaminants biosensing” (I. Sorrentino, **I. Stanzione**, A. Piscitelli, P. Giardina, A. Le Goff) BIO-INSPIRATION - GDR 2088 BIOMIM Nice, France, October 13-14, 2020.
- “”In”-equalities in sciences:a mirror of the society. An environmental pollution overview.” (**I. Stanzione**, D. Liberti, R. Puopolo, N. Curci, M. Abdalrazeq, F. Mirpoor) Web edition of National meeting 'A. Castellani' of PhD students in biochemical sciences. December 18, 2020
- “Immobilization of fungal adhesive proteins and their chimeric variants” (A. Piscitelli, **I. Stanzione**, A. Pennacchio, P. Giardina) ICBBA Conference. February 18-19, 2021.
- “Development of immuno-sensors based on a hydrophobin-Protein A chimera” (**I. Stanzione**, A. Piscitelli, P. Giardina) Workshop SCI. July 14, 2021.

Publications

- Cicatiello P., **Stanzione I.**, Dardano P., De Stefano L., Birolo L., De Chiaro A., Monti D.M., Petruk G., D’Errico G. and Giardina P. “Characterization of a

surface-active protein extracted from a marine strain of Penicillium chrysogenum" Int. J. Mol, Sci., 2019; 20(13); DOI: 10.3390/ijms20133242.

- **Stanzione I.***, Pezzella C.*, Giardina P., Sannia G., Piscitelli A. “Beyond natural laccases: extension of their potential applications by protein engineering” Appl. Microbiol. Biotechnol 2020, 104: 915–924 DOI: 10.1007/s00253-019-10147-z.
- Sorrentino I.*, **Stanzione I.***, Nedellec Y., Piscitelli A., Giardina P., Le Goff A. “From graphite to laccase biofunctionalized few-layer graphene: a “one pot” approach using a chimeric enzyme” Int. J. Mol. Sci. 2020, 21, 3741; doi:10.3390/ijms21113741.
- Sorrentino I., **Stanzione I.**, Piscitelli A., Giardina P., Le Goff A. “Carbon-nanotube-supported POXA1b laccase and its hydrophobin chimera for oxygen reduction and picomolar phenol biosensing” Biosens. Bioelectron.: X 2021, 8, 100074 DOI: 10.1016/j.biosx.2021.100074.
- Ntasi G., Kirby D.P., **Stanzione I.**, Carpentieri A., Somma A., Cicatiello P., Marino G., Giardina P., Birolo L. “A versatile and user-friendly approach for the analysis of proteins in ancient and historical objects.” J. Proteom 2021, 231, 104039 DOI: 10.1016/j.jprot.2020.104039.
- Landeta-Salgado C., Cicatiello P., **Stanzione I.**, Medina D., Berlanga Mora I., Gomez C., Lienqueo M.E., “The growth of marine fungi on seaweed polysaccharides produces cerato-platanin and hydrophobin self-assembling proteins” Microbiol. Res. 2021, 251, 126835 DOI: 10.1016/j.micres.2021.126835.
- **Stanzione I.**, Izquierdo-Bote D., González García M.B., Giardina P., Piscitelli A., “Immobilization of Antibodies by Genetic Fusion to a Fungal Self-Assembling Adhesive Protein” Front. Mol. Biosci. 2021, 8, 725697. DOI: 10.3389/fmolb.2021.725697.
- Sorrentino I., Carrière M., Jamet H., **Stanzione I.**, Piscitelli A., Giardina P., Le Goff A. “The Laccase mediator system at carbon nanotubes for anthracene oxidation and femtomolar electrochemical biosensing” Submitted to Analyst November 2021
- **Stanzione I.**, Pennacchio A., Piscitelli A., Giardina P., Costa-Rama E., Fernández Abedul M.T. “Functionalization of micropipette tips with hydrophobin-laccase chimera and application to the electrochemical determination of caffeic acid in tea samples” Manuscript in preparation.

Experience in foreign laboratory

June 2020- September 2020: Visiting PhD student in the laboratory of Professor Maria Teresa Fernàndez Abedul, at Department of Analytical Chemistry, University of Oviedo, Asturia, Spain. The stage was focused on the development of an electrochemical biosystem based on laccase chimera.

APPENDIX

Supplementary materials

Characterization of a surface-active protein extracted by a marine strain of *Penicillium chrysogenum*

Paola Cicatiello[1], Ilaria Stanzione[1], Principia Dardano[2], Luca De Stefano[2], Leila Birolo[1], Addolorata De Chiaro[1],Daria Maria Monti[1], Ganna Petruk[1],Gerardino D'Errico[1], Paola Giardina[1]*

[1] Department of Chemical Sciences, University of Naples «Federico II», Via Cinthia, 80126 Naples, Italy; giardina@unina.com
[2] Institute for Microelectronics and Microsystems, Unit of Naples-National Research Council, Via P. Castellino 111, 80127, Italy; e-mail@e-mail.com
* Correspondence: giardina@unina.it; Tel.: +39 081 674319

Thin-layer chromatography (TLC)

Silica gel on TLC aluminium foil was used as stationary phase for TLC realization, and a mixture of toluene-chloroform-acetone (7:2:1) was utilized as the mobile phase. The samples were dissolved in chloroform. Ten percent phosphomolybdic acid in ethanol was used as colour developer through dipping.

Fourier-transform infrared spectroscopy (FTIR)

20 µL of the sample in 60% ethanol was deposited on a hydrophilic polytetrafluoroethylene (PTFE) membrane and FTIR quantitation was performed by the Direct Detect® spectrometer, an infrared (IR)-based biomolecular quantitation system. This instrument enabled simultaneous protein quantitation and lipid analysis in the same sample.

Table S1: Mascot search results of LC-MS/MS data against NCBInr database showing identified proteins' score, number of peptides, and sequence coverage.

ID NCBInr (gi number)	Protein name	Score	Peptides Sequence	Score	Sequence coverage (%)
255936199	Pc13g06930	102	R. QIIW PAYTDK.Q	45	31
			K. QVAGGEVVKPDQSYSPAALP. -	27	
			K.SMM ADSPQWTLQDTK.R + Oxidation M	44	
			K.SMM ADSPQWTLQDTKR.V + 2Oxidation M	33	
			R.QIIWPAYTDKQVAGGEVVKPDQSYSPAALP.- + Gln->pyro-Glu (N-term Q)	20	

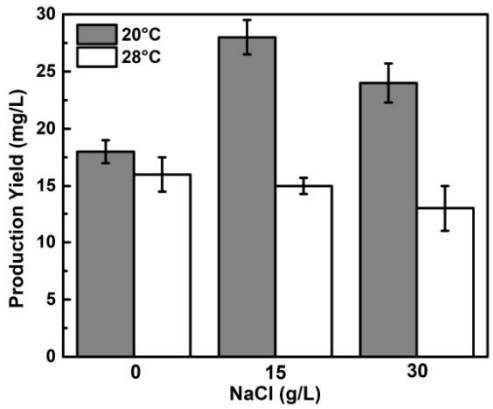

Figure S1: Protein production yield from *Penicilliumchrysogenum*at different temperatures and salt concentrations

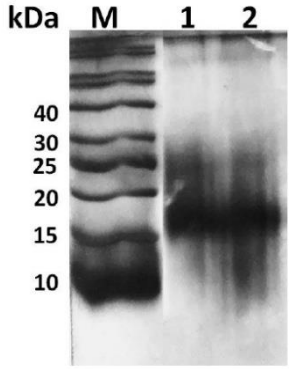

Figure S2: SDS-PAGE of filtrated culture broth **(1)** and air-bubbled culture broth **(2)**

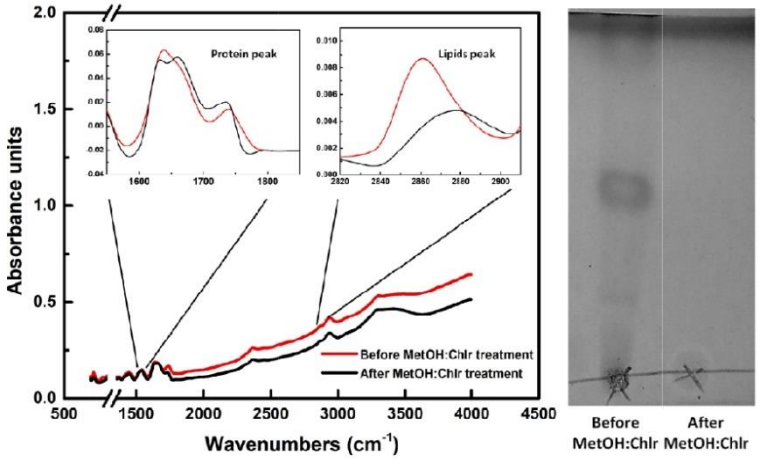

Figure S3:FTIR and TLC analysis of samples before and after the Methanol:Chloroform treatment to remove lipid contaminants. In the FTIR graph (left),the insets reported the main peaksrelated to proteinsandthe lipid peaks. The former remains unaltered after the treatment, while the lattersignificantly decreased.The TLC analysis (right)showed that thephosphomolybdic acid-stainedspot(related to lipids) was absentafter the treatment.

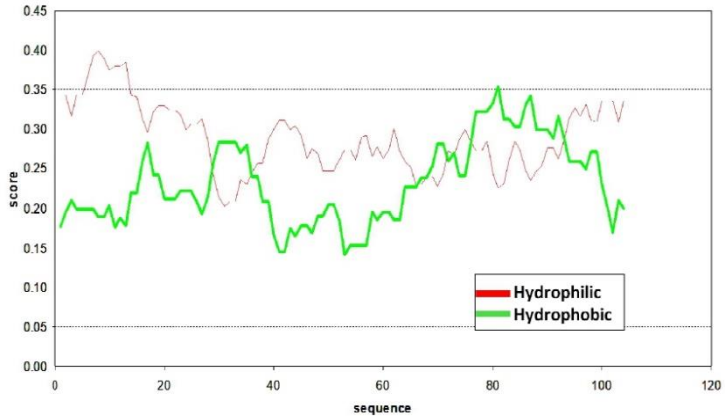

Figure S4: Hydrophobicity plot of Pc13g06930

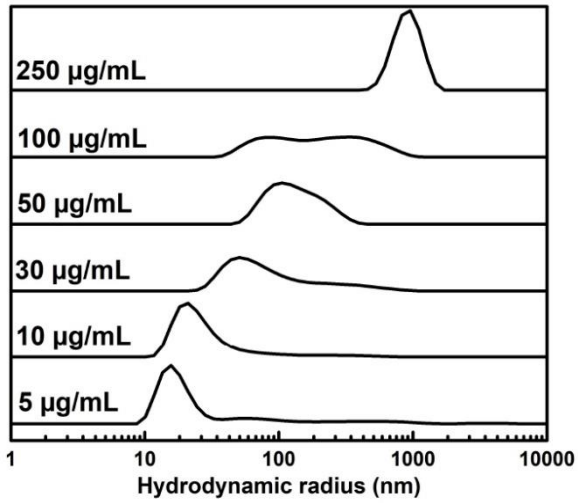

Figure S5:DLS analysis of Sap *Pc* at 100 µg/mL, in phosphate buffer pH 7, shown as volume-averaged size distribution.

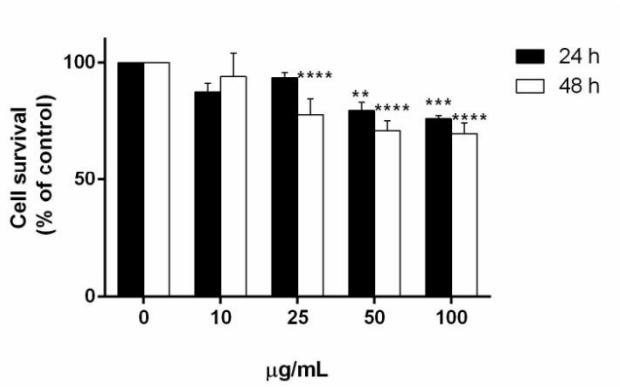

Figure S6: Effect of SAP-*Pc* on human immortalized keratinocytes. Dose-response plot of cells after 24-48 h incubation with increasing concentrations (10-100 µg mL^{-1}) of SAP-*Pc*. Cell viability was assessed by the MTT assay and expressed as described in Materials and Methods section. Values are given as means ± S.D. ($n \geq 3$);** indicates $p < 0.01$, *** indicates $p < 0.005$, **** indicates $p < 0.001$, with respect to control cells.

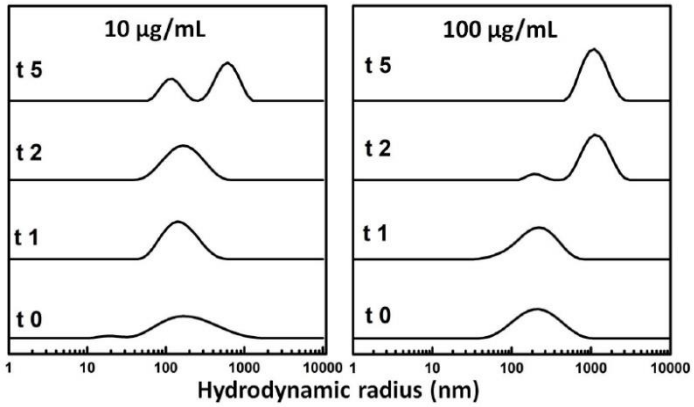

Figure S7: DLS analysis of Sap *Pc* at 10 and 100 µg/mL, in phosphate buffer pH 7, during time.

Title : The growth of marine fungi on seaweed polysaccharides produces cerato-platanin and hydrophobin self-assembling proteins

Authors: Catalina Landeta Salgado[1,2], Paola Cicatiello[3], Ilaria Stanzione[3], David Medina[1,2], Isadora Berlanga Mora[1], Carlos Gomez[4], María Elena Lienqueo[1,2]

Author affiliations:

[1] Department of Chemical Engineering, Biotechnology, and Materials, Faculty of Physical and Mathematical Sciences, University of Chile, Santiago, Beauchef 851-8370456 Chile

[2] Center for Biotechnology and Bioengineering (CeBiB), Santiago, Beauchef 851-8370456 Chile

[3]Department of Chemical Sciences, University of Naples Federico II, via Cintia 4, I-80126 Naples, Italy

[4] Chemistry Department, University of Valle-Yumbo, Valle del Cauca, 760501, Colombia

Corresponding author:

Prof. María Elena Lienqueo

E-mail: *mlienque@ing.uchile.cl; mlienque@cebib.cl*

Tel.: +56 9 97126991

Supplementary data

Table S1.

Protein sequences classified as class I hydrophobins and cerato-platanin for *P. salina* and *T. pinophilus* organisms.

ID-Sequence	Fungi marine	Sequence	Classification
g581.t1 Named: PsCP	*P. salina*	MKCSAAVSAAVLGLASMASAITVS YDTGYDDANRALTALACSDGDNG LITKYKWQTQGQIARFPHIGGYMG VAGWNSPQCGTCYGITYNGKTIYV LAVDHTANGFNLAKSAMDELTNG QAAAQGRVDAQYAQVAVSNCGL	Cerato-Platanin
CH3 Seq790 Named: TpHYD1	*T. pinophilus*	MQFTTALLALAATAVALPNIGPAPG KGSEVGGQQTFWPVSDDVTVEEAK AACGTDNQIACCDDTTFTGDQVEV VSGPLAGALSDLLGGKNGAKGLGL FDKCSKLNIDIIIGISDLINSQCKQNI ACCQGNTADSEGDLIGLNVPCIALG SLL	Hydrophobin Class I
CH7 Seq966 Named: TpHYD2	*T. pinophilus*	MHFNFACITACVFAAAALAVPVEV ERKVVVVRADVCPAPAPVTTTAPA PSPPAEYYSPPPAAPPVTTTVSNPPP	Hydrophobin Class I

		APQSTSVDNKQCSAGTSVHCCDTV DSTDNSNVLNALNAAGLDHGDATQ KGQVGLTCTPITTSLVDALNGNVCQ GAVTACCENTNQVGLVNLNLGCTII PVNL	

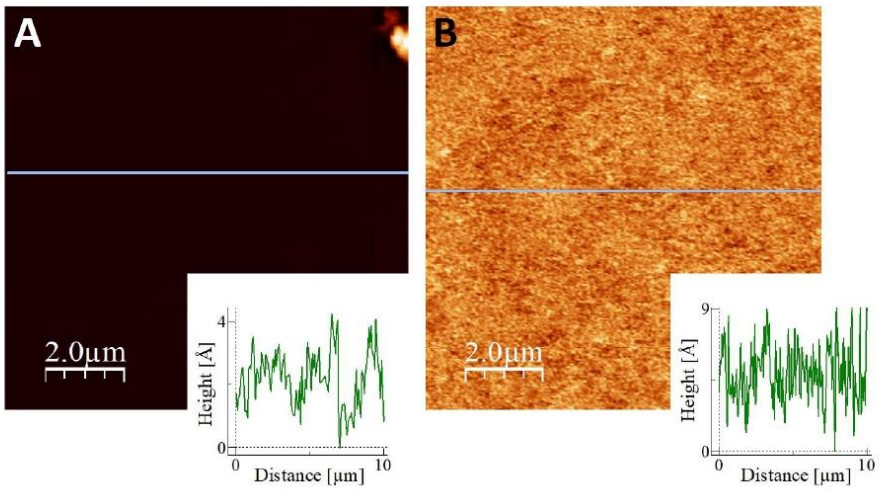

Figure S1. AFM analysis data of control experiments obtained for (A) buffer 50 mM Tris HCl pH7 and (B) ethanol solution with their corresponding profile of a cross-section.

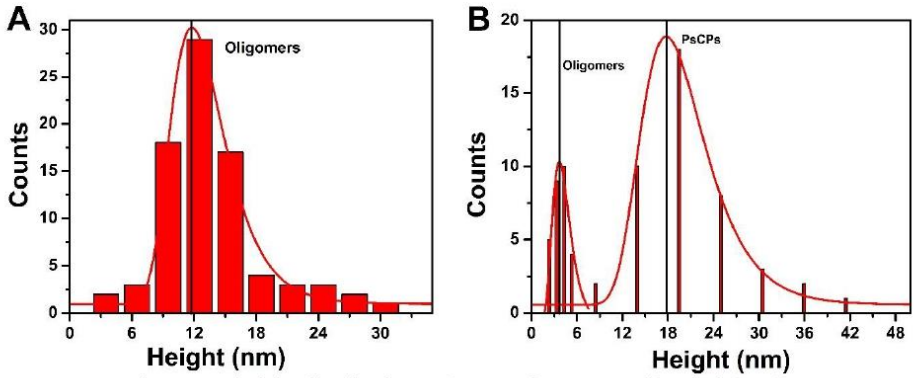

Figure S2. Histogram height distributions of PsCPs from SW with a height of (11.8 ± 1.3) nm (A), and alginate with heights of (3.7 ± 0.6) nm and (17.8 ± 2.1) nm (B) measured by AFM.

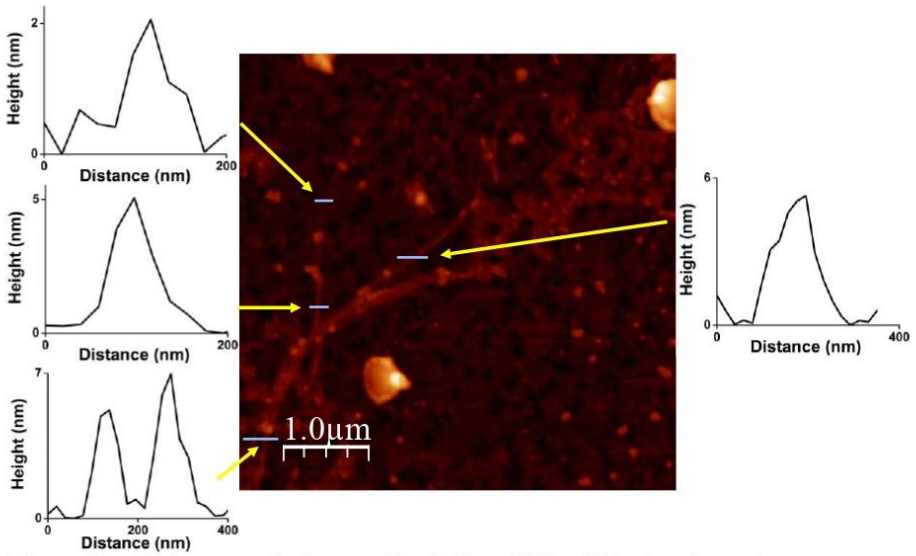

Figure S3. AFM topography image of PsCP from SW in 60% ethanol together with height profiles.

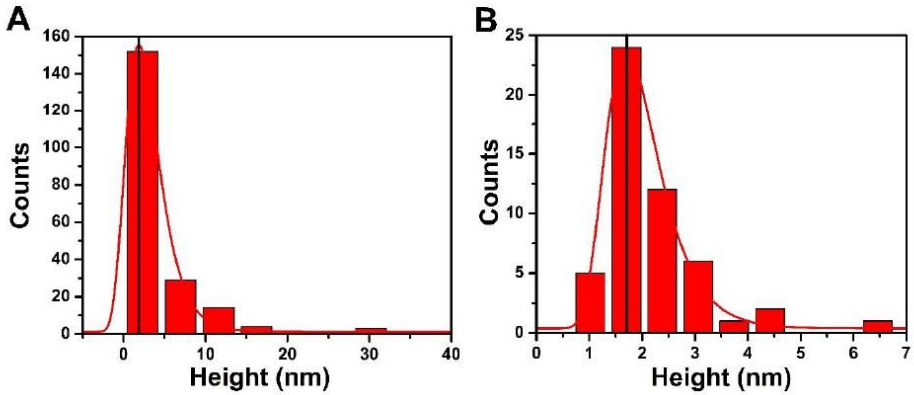

Figure S4. Histogram height distributions of TpHYD from SW with a height of (1.9 ± 1) nm (A), and alginate with a height of (1.7 ± 0.3) nm (B) measured by AFM.

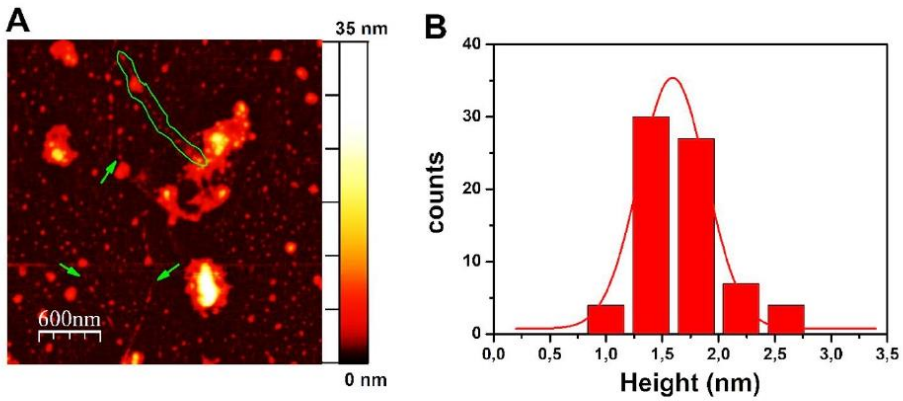

Figure S5. AFM topography image of TpHYD aggregates formed fibrillar structures (marked in yellow arrows). Aggregates of oligomers tend to cluster in the proximity of the early fibers (marked in green line) (A). Histogram height

distributions of TpHYD from SW with a height of (1.6 ± 0.3) nm measured by AFM (B).

Supplementary material

A versatile and user-friendly approach for the analysis of ancient proteins.

Georgia Ntasi[1], Daniel Kirby[2], Ilaria Stanzione[1], Andrea Carpentieri[1,3], Patrizia Somma[3], Paola Cicatiello[1], Gennaro Marino[1,3], Paola Giardina[1], Leila Birolo[1,*].

1-Department of Chemical Sciences, University of Naples Federico II, Naples, Italy

2-Private Practice, Milton, MA, USA

3-University Suor Orsola Benincasa, Naples, Italy

* corresponding author E-mail birolo@unina.it

Table of contents

Samples description

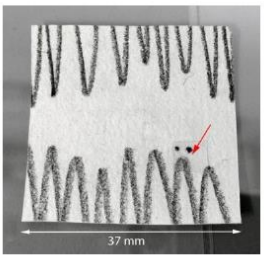

Fig S1. Casein-fixed paper with 25mm^2 functionalized film.

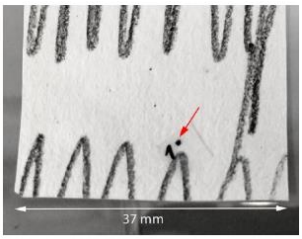

Fig S2. Isinglass-fixed paper with 25mm^2 functionalized film.

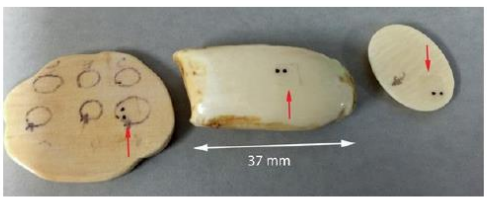

Fig S3. Mammoth, walrus and elephant ivory samples with 25mm^2 functionalized film.

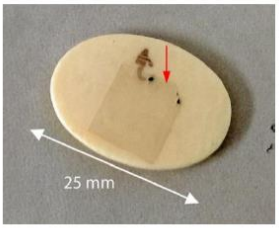

Fig S4. Elephant ivory sample with 100mm^2 film.

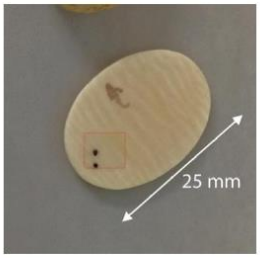

Fig. S5. Elephant ivory sample with 25mm^2 film.

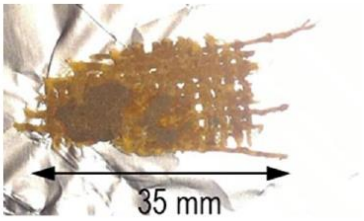

Fig. S6. Historical sample from the Lining of Canvas "The Virgin and Child, Saints and Cherubins".

Application of the micro-invasive trypsin functionalized film to different artistic/historical samples.

Table S1. Markers Ions for MALDI-TOF Peptide Mass Fingerprint (PMF)

Egg Yolk	Egg White	Animal Glue	Casein	Fish	Keratin
1048.6*	1345.7*	1095.6*	830.5	1083.5	1179.7*
1077.6*	1428.6	1105.6*	1195.7	1262.7	1235.6
1085.7*	1555.7	1241.8	1251.7	1278.7	1300.6
1164.5*	1687.8*	1267.8*	1267.7	1411.7	1475.8*
1324.7	1773.9	1427.7*	1337.7	1443.8	1493.8
1401.7*	1859.9*	1435.8*	1384.7	1551.9	1707.8
1406.6*	1913.0	1459.7*	1580.8	1598.9	1765.8
1445.7	2009.0*	1473.7	1759.9	1906.0	1791.8
1560.7		1586.9	1872.0	2139.0	2384.0*
1561.7*		1648.8*	2186.2		2705.2
1591.7		1655.9	2202.2		
1891.0		1923.0	2235.2		
1892.0		1963.0	2332.1		
1893.0*		1976.0			
2236.1		2705.3*			

* Usually most intense

Table S1. Markers used to identify materials found in artworks and objects of cultural heritage. Markers are collected and validated from several sources including published research data and protein sequences, LC-MS/MS data from known samples, and analysis of known reference samples. If the majority of the expected markers is observed in the MALDI spectrum, the indicate protein or material is considered to be positively identified. Egg yolk and white markers were derived from database searching of PMF spectra of authentic samples with Mascot, (www.Matrixscience.com) as well as LC-MS/MS data from known references. Keratin markers were also derived from database searching of PMF spectra with Mascot. The keratin markers noted here are a truncated list of the most intense and persistent ions (attributed to the Uniprot IDs: P35527, P13645 and P04264). Casein markers were verified through "in silico" digestion of published sequences [2-4]. Animal glue markers are comprised of highly conserved peptides derived from published sequences [2-4] and indicate the presence of mammalian collagen but not its source. Fish markers are derived from PMF spectra of known reference materials and indicated the presence of fish-derived material but not the specific source.

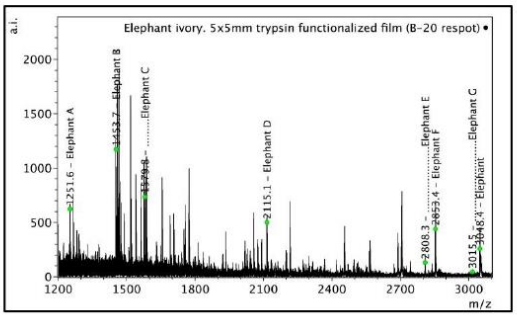

Figure S7. MALDI spectrum from elephant ivory sampled with a 25mm^2 film. Elephant marker ions are indicated. Unlabeled ions are all collagen-related.

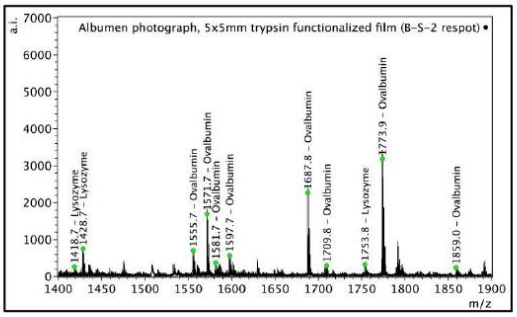

Figure S8. MALDI spectrum from the albumen photograph sampled with a 25 mm^2 film with albumen markers indicated. Note that both ovalbumin and lysozyme-related ions are used in the identification.

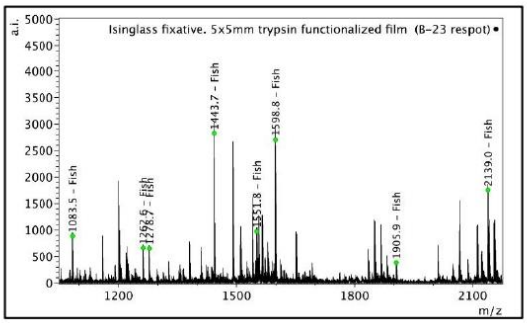

5

Figure S9. MALDI spectrum from the isinglass fixed paper sampled with a 25mm^2 film with fish-related ions indicated. This set of markers is used to indicate fish in general and not to indicate a particular species of fish

Table S2. Identification of proteins in the lining of the canvas "The Virgin and Child, Saints and Cherubins" by LC-MS/MS upon digestion with the trypsin functionalized film. The sample was subjected to *in-situ* digestion with the trypsin functionalized film and the peptide mixture was analysed by LC-MS/MS. Raw data were searched by Mascot MS/MS Ion search using the homemade COLLE database. No fixed chemical modification was inserted, and deamidation on Gln and Asn, hydroxylation at Pro and Lys, oxidation on Met, were considered as variable modifications. Individual ion score threshold provided by Mascot software (>15) to evaluate the quality of matches in MS/MS data was used for confidence threshold in protein identification. (**U**) Indicates unique peptides.

Protein	*m/z*	Ion Score	Charge	Peptide
Collagen 1(I) *Ovis aries* (W5P481)	322.6706	20	2	R.GLPGER.G + Hydroxylation (P)
	339.6628	19	2	R.GFPGER.G + Hydroxylation (P)
	419.2127	57	2	R.GPAGPQGPR.G + Deamidated (NQ)
	434.7166	42	2	K.GEAGPQGPR.G **(U)**
	444.2138	42	2	R.GSEGPQGVR.G + Deamidated (NQ)
	450.2497	38	2	R.GVVGLPGQR.G + Deamidated (NQ); Hydroxylation (P)
	365.8593	39	3	R.GRPGAPGPAGAR.G + 2 Hydroxylation (P)
	367.1873	23	3	K.GADGAPGKDGVR.G
	552.7679	45	2	R.GFPGSDGVAGPK.G + Hydroxylation (P) **(U)**
	553.7812	69	2	R.GVQGPPGPAGPR.G + Deamidated (NQ); Hydroxylation (P)
	629.7976	64	2	K.GLTGSPGSPGPDGK.T + 2 Hydroxylation (P)
	656.3175	45	2	K.GETGPSGPAGPTGAR.G
	667.3240	54	2	R.GPSGPQGPSGPPGPK.G + Deamidated (NQ); Hydroxylation (P)
	672.8239	40	2	R.GFPGLPGPSGEPGK.Q + Hydroxylation (K) (K); 2 Hydroxylation (P)
	718.3417	55	2	R.GEPGPAGLPGPPGER.G + 3 Hydroxylation (P)
	724.8524	83	2	R.AGEVGPPGPPGPAGEK.G + 2 Hydroxylation (P) **(U)**
	780.9075	63	2	R.GETGPAGPAGPIGPVGAR.G
	781.8953	42	2	K.DGLNGLPGPIGPPGPR.G + Deamidated (NQ); 3 Hydroxylation (P)
	795.9072	17	2	R.GLTGPIGPPGPAGAPGDK.G + 2 Hydroxylation (P)
	543.5807	34	3	K.NGDDGEAGKPGRPGER.G + Deamidated (NQ); Hydroxylation (P)
	854.3815	71	2	K.DGEAGAQGPPGPAGPAGER.G + Deamidated (NQ); Hydroxylation (P)
	880.3607	96	2	K.GEPGSPGENGAPGQMGPR.G + Deamidated (NQ); Oxidation (M); 3 Hydroxylation (P)
	924.9283	65	2	R.GPPGPMGPPGLAGPPGESGR.E + Oxidation (M); 3 Hydroxylation (P)
	686.6569	20	3	K.TGPPGPAGQDGRPGPPGPPGAR.G + Deamidated (NQ); 4 Hydroxylation (P)
	1037.9888	25	2	K.GAPGADGPAGAPGTPGPQGIAGQR.G + 2 Deamidated (NQ); Hydroxylation (P) **(U)**
	1146.5629	42	2	K.GDAGPPGPAGPAGPPGPIGNVGAPGPK.G + Deamidated (NQ); Hydroxylation (K) (K); Hydroxylation (P)
Collagen 2(I) *Ovis aries* (W5NTT7)	322.6706	20	2	R.GLPGER.G + Hydroxylation (P)
	379.6921	37	2	R.GLPGADGR.A + Hydroxylation (P)
	393.6901	24	2	R.GDQGPVGR.T + Deamidated (NQ)
	421.2290	33	2	R.GVVGPQGAR.G + Deamidated (NQ)
	451.2243	20	2	R.GPSGPQGIR.G + Deamidated (NQ); 2 Hydroxylation (P)
	459.7255	31	2	R.AGVMGPAGSR.G + Oxidation (M)
	540.7501	32	2	R.GPSGPPGPDGNK.G + Deamidated (NQ)
	631.3157	61	2	R.GEAGPAGPAGPAGPR.G
	751.8619	20	2	R.TGEPGAAGPPGPVGEK.G + 2 Hydroxylation (P) **(U)**
	762.8562	55	2	R.GAPGAVGAPGPAGANGDR.G + Deamidated (NQ); 2 Hydroxylation (P)
	790.8851	58	2	R.GPPGESGAAGPTGPIGSR.G + Hydroxylation (P) **(U)**
	808.9031	60	2	K.GELGPVGNPGPAGPAGPR.G + Deamidated (NQ); Hydroxylation (P)

Table S3. Identification of Proteins in in the lining of the canvas "The Virgin and Child, Saints and Cherubins" by LC-MS/MS upon digestion in heterogeneous phase. The sample was subjected to overnight digestion with trypsin in heterogeneous phase and the peptide mixture was analysed by LC-MS/MS. Raw data were analysed as those of Table S2.

Protein	*m/z*	Ion Score	Charge	Peptide
	988.5033	73	2	K.SGDRGETGPAGPAGPIGPVGAR.G
	961.1275	37	3	R.GVPGPPGAVGPAGKDGEAGAQGPPGPAGPAGER.G + Deamidated (NQ); 3 Hydroxylation (P)
	932.9335	41	2	K.GEPGPTGIQGPPGPAGEEGK.R + Deamidated (NQ); 2 Hydroxylation (P)
	916.9332	99	2	R.GPPGPMGPPGLAGPPGESGR.E + Oxidation (M); 2 Hydroxylation (P)
	907.4111	32	2	R.GAPGDRGEPGPPGPAGFAGPPGADGQPGAK.G + Deamidated (NQ); 5 Hydroxylation (P)
	880.8567	57	2	K.GEPGSPGENGAPGQMGPR.G + 2 Deamidated (NQ); Oxidation (M); 3 Hydroxylation (P)
	853.8911	71	2	K.DGEAGAQGPPGPAGPAGER.G + Hydroxylation (P)
	837.6944	58	3	K.GDAGPAGPKGEPGSPGENGAPGQMGPR.G + 2 Deamidated (NQ); Oxidation (M); 3 Hydroxylation (P)
	833.0728	37	3	K.GDRGETGPAGPPGAPGAPGAPGPVGPAGK.S + 3 Hydroxylation (P)
	828.4073	35	2	K.GSPGEAGRPGEAGLPGAK.G + 3 Hydroxylation (P)
	807.3688	32	3	R.GPSGPQGPSGPPGPKGNSGEPGAPGSK.G + Deamidated (NQ); 2 Hydroxylation (P); 2 Hydroxylation (K) (K)
	793.8822	62	2	K.GANGAPGIAGAPGFPGAR.G + Deamidated (NQ); 3 Hydroxylation (P)
	781.8940	48	2	K.DGLNGLPGPIGPPGPR.G + Deamidated (NQ); 3 Hydroxylation (P)
	780.9088	64	2	R.GETGPAGPAGPIGPVGAR.G
	730.3492	111	2	R.GSAGPPGATGFPGAAGR.V + 2 Hydroxylation (P)
	724.8536	90	2	R.AGEVGPPGPPGPAGEK.G + 2 Hydroxylation (P) **(U)**
Collagen 1(I) *Ovis aries* (W5P481)	718.3442	74	2	R.GEPGPAGLPGPPGER.G + 3 Hydroxylation (P)
	695.3134	35	3	R.GPAGPQGPRGDKGETGEQGDR.G + 2 Deamidated (NQ); Hydroxylation (K) (K)
	681.3276	36	3	K.TGPPGPAGQDGRPGPPGPPGAR.G + Deamidated (NQ); 3 Hydroxylation (P)
	674.3259	43	3	K.GEPGPTGIQGPPGPAGEEGKR.G + Deamidated (NQ); 2 Hydroxylation (P)
	672.8245	65	2	R.GFPGLPGPSGEPGK.Q + 3 Hydroxylation (P)
	666.8298	60	2	R.GPSGPQGPSGPPGPK.G + Hydroxylation (P)
	656.3192	63	2	K.GETGPSGPAGPTGAR.G
	621.8008	65	2	K.GLTGSPGSPGPDGK.T + Hydroxylation (P)
	621.3325	17	2	R.GVVGLPGQRGER.G + Deamidated (NQ); Hydroxylation (P)
	596.8188	63	2	R.GVPGPPGAVGPAGK.D + 2 Hydroxylation (P)
	591.7759	23	4	R.GPPGPPGKNGDDGEAGKPGRPGER.G + Deamidated (NQ); 4 Hydroxylation (P)
	589.7787	66	2	R.GQAGVMGFPGPK.G + Deamidated (NQ); Oxidation (M); Hydroxylation (P)
	558.7490	35	2	R.EGAPGAEGSPGR.D + 2 Hydroxylation (P)
	553.7829	62	2	R.GVQGPPGPAGPR.G + Deamidated (NQ); Hydroxylation (P)
	552.7681	51	2	R.GFPGSDGVAGPK.G + Hydroxylation (P)
	473.2219	24	2	K.QGPSGASGER.G
	450.2501	31	2	R.GVVGLPGQR.G + Deamidated (NQ); Hydroxylation (P)
	426.7188	31	2	R.GPPGPQGAR.G + Hydroxylation (P)
	426.2160	33	2	R.GFSGLDGAK.G
	392.2210	34	2	R.GAAGLPGPK.G + Hydroxylation (P)

Search for chemical modifications with the digestion with the trypsin functionalized film

Table S4. Identification of spontaneous hydrolysis sites in the lining of the historical canvas "The Virgin and Child, Saints and Cherubins" by LC-MS/MS upon digestion with the trypsin functionalized film. LC-MS/MS raw data from *in situ* digestion with the trypsin functionalized film were searched by Mascot MS/MS Ion search, using COLLE database, considering semitrypsin as the enzyme, deamidation on Gln and Asn, oxidation on Met, hydroxylation at Pro and Lys as variable modifications. Individual ion score threshold provided by Mascot software (>15) to evaluate the quality of matches in MS/MS data was used for confidence threshold in protein identification. (**U**) Indicates unique peptides.

Protein	*m/z*	Ion Score	Charge	Peptide
Collagen 1(I) *Ovis aries* (W5P481)	323.1808	33	2	Q.IENIR.S + Deamidated (NQ)
	362.6896	30	2	R.GRPGAPGP.A + Hydroxylation (P)
	363.2004	24	2	P.IGPPGPR.G + 2 Hydroxylation (P)
	367.1849	31	3	A.PGFPGAR.G + 2 Hydroxylation (P)
	372.2048	19	2	V.VGLPGQR.G + Deamidated (NQ); Hydroxylation (P)
	379.6921	19	2	L.PGPKGDR.G + 2 Hydroxylation (P)
	402.7019	45	2	G.APGFPGAR.G + 2 Hydroxylation (P)
	405.6827	40	2	R.GEPGPPGPA.G + 2 Hydroxylation (P)
	419.2135	21	2	P.GPPGPPGAR.G + 2 Hydroxylation (P)
	431.2133	33	2	A.GAPGFPGAR.G + 2 Hydroxylation (P)
	434.1933	18	2	R.GEPGPPGPAG.A + 2 Hydroxylation (P)
	440.2359	28	2	P.GPIGPPGPR.G + 2 Hydroxylation (P)
	456.2315	33	2	A.GLPGPPGER.G + 2 Hydroxylation (P)
	463.7494	50	2	P.IGNVGAPGPK.G + Deamidated (NQ); Hydroxylation (P)
	468.7415	49	2	R.GVPGPPGAVGP.A + 2 Hydroxylation (P)
	469.7120	53	2	R.GEPGPPGPAGA.A + 2 Hydroxylation (P)
	475.7302	42	2	R.GVQGPPGPAGP.R + Deamidated (NQ); Hydroxylation (P)
	482.2472	38	2	A.GPPGPPGPAGK.E + 2 Hydroxylation (P)
	482.7385	75	2	R.GLPGPPGAPGP.Q + 3 Hydroxylation (P)
	483.7288	37	2	R.AGEVGPPGPPG.P + 2 Hydroxylation (P) **(U)**
	490.2251	29	2	K.GDAGPPGPAGPA.G + Hydroxylation (P)
	504.2595	51	2	R.GVPGPPGAVGPA.G + 2 Hydroxylation (P)
	505.2314	50	2	R.GEPGPPGPAGAA.G + 2 Hydroxylation (P)
	507.2522	33	2	P.GLAGPPGESGR.E + Hydroxylation (P)
	514.2358	35	2	K.GETGPSGPAGPT.G
	517.7666	45	2	N.AGPPGPPGPAGK.E + 2 Hydroxylation (P)
	524.2577	34	2	G.FPGSDGVAGPK.G + Hydroxylation (P)
	524.7974	31	2	A.GPAGPIGPVGAR.G

	525.2713	47	2	G.VQGPPGPAGPR.G + Deamidated (NQ); Hydroxylation (P)
	531.7686	37	2	Q.GPPGPAGPAGER.G
	532.2551	61	2	R.AGEVGPPGPPGP.A + 2 Hydroxylation (P) **(U)**
	537.7463	21	2	A.PGLQGMPGER.G + Deamidated (NQ); Oxidation (M); Hydroxylation (P)
	542.2640	26	2	S.VPGPMGPSGPR.G + Oxidation (M); Hydroxylation (P)
	546.7674	50	2	R.GLPGPPGAPGPQ.G + 3 Hydroxylation (P)
	367.1873	23	3	K.GADGAPGKDGVR.G
	570.2688	54	2	F.AGPPGADGQPGAK.G + Deamidated (NQ); Hydroxylation (P)
	574.7446	24	2	R.GEQGPAGSPGFQ.G + Deamidated (NQ); Hydroxylation (P)
	575.2790	28	2	G.NAGPPGPPGPAGK.E + Deamidated (NQ); 2 Hydroxylation (P)
	575.7703	44	2	R.GLPGPPGAPGPQG.F + Deamidated (NQ); 3 Hydroxylation (P)
	581.2621	50	2	G.APGLQGMPGER.G + Deamidated (NQ); Oxidation (M); 2 Hydroxylation (P)
	581.8124	46	2	N.GLPGPIGPPGPR.G + 3 Hydroxylation (P)
	388.5354	34	3	D.GRPGPPGPPGAR.G + 3 Hydroxylation (P)
	589.7916	23	2	P.SGPQGPSGPPGPK.G + Hydroxylation (P)
	596.3007	15	2	E.VGPPGPPGPAGEK.G + 2 Hydroxylation (P)
	602.7802	41	2	R.GPSGPQGPSGPPGP.K + Hydroxylation (P)
	603.7897	59	2	S.GNAGPPGPPGPAGK.E + Deamidated (NQ); 2 Hydroxylation (P)
	604.2872	32	2	A.QGPPGPAGPAGER.G + Deamidated (NQ); Hydroxylation (P)
	609.7728	32	2	Q.GAPGLQGMPGER.G + Deamidated (NQ); Oxidation (M); 2 Hydroxylation (P)
	639.3260	40	2	L.NGLPGPIGPPGPR.G + Deamidated (NQ); 3 Hydroxylation (P)

10

	639.8086	45	2	G.AQGPPGPAGPAGER.G + Deamidated (NQ); Hydroxylation (P)
	640.8127	44	2	M.GPPGLAGPPGESGR.E + 2 Hydroxylation (P)
	647.3088	57	2	P.SGNAGPPGPPGPAGK.E + Deamidated (NQ); 2 Hydroxylation (P)
	652.3030	15	2	K.GDAGPPGPAGPAGPPG.P + 2 Hydroxylation (P)
	655.8130	63	2	T.GIQGPPGPAGEEGK.R + Deamidated (NQ); Hydroxylation (P)
	656.2939	75	2	A.GPAGNPGADGQPGAK.G + 2 Deamidated (NQ); Hydroxylation (P)
	656.3394	49	2	T.GPAGPPGFPGAVGAK.G + 2 Hydroxylation (P)
	660.2859	18	2	R.GEQGPAGSPGFQGL.P + 2 Deamidated (NQ); Hydroxylation (P)
	660.3304	57	2	T.GPIGPPGPAGAPGDK.G + 2 Hydroxylation (P)
	660.8233	31	2	G.EVGPPGPPGPAGEK.G + 2 Hydroxylation (P)
	662.8356	16	2	T.GISVPGPMGPSGPR.G + Hydroxylation (P)
	667.3240	54	2	R.GPSGPQGPSGPPGPK.G + Deamidated (NQ); Hydroxylation (P)
	672.8239	40	2	R.GFPGLPGPSGEPGK.Q + Hydroxylation (K); 2 Hydroxylation (P)
	689.3347	59	2	A.GEVGPPGPPGPAGEK.G + 2 Hydroxylation (P)
	691.3382	24	2	A.GAPGTPGPQGIAGQR.G + 2 Deamidated (NQ); Hydroxylation (P)
	691.8105	58	2	A.AGPAGNPGADGQPGAK.G + 2 Deamidated (NQ); Hydroxylation (P)
	702.8567	41	2	R.GETGPAGPAGPIGPVGA.R
	706.3320	70	2	P.MGPPGLAGPPGESGR.E + Oxidation (M); Hydroxylation (P)
	706.8591	17	2	P.TGPAGPPGFPGAVGAK.G + 2 Hydroxylation (P)
	724.8524	83	2	R.AGEVGPPGPPGPAGEK.G + 2 Hydroxylation (P) **(U)**
	729.3282	18	2	R.GEQGPAGSPGFQGLPG.P + 2 Deamidated (NQ)

11

	488.8980	21	3	A.GQDGRPGPPGPPGAR.G + Deamidated (NQ); 3 Hydroxylation (P)
	745.8454	21	2	K.GAPGADGPAGAPGTPGPQ.G + Hydroxylation (P)
	755.8419	40	2	A.GAAGPAGNPGADGQPGAK.G + 2 Deamidated (NQ); Hydroxylation (P)
	786.9016	44	2	A.GPAGPPGPIGNVGAPGPK.G + Deamidated (NQ); 2 Hydroxylation (P)
	788.8991	16	2	F.PGERGVQGPPGPAGPR.G + 3 Hydroxylation (P)
	543.5807	34	3	K.NGDDGEAGKPGRPGER.G + Deamidated (NQ); Hydroxylation (P)
	855.8718	29	2	Q.GPPGEPGEPGASGPMGPR.G + Oxidation (M); 3 Hydroxylation (P)
	857.9028	44	2	V.GPPGPSGNAGPPGPPGPAGK.E + Deamidated (NQ); Hydroxylation (K); 2 Hydroxylation (P)
	880.3607	96	2	K.GEPGSPGENGAPGQMGPR.G + Deamidated (NQ); Oxidation (M); 3 Hydroxylation (P)
	920.3948	69	2	F.QGPPGEPGEPGASGPMGPR.G + Deamidated (NQ); Oxidation (M); 3 Hydroxylation (P)
	952.9722	62	2	A.AGPPGPTGPAGPPGFPGAVGAK.G + 3 Hydroxylation (P)
	976.4869	23	2	R.GETGPAGPPGAPGAPGAPGPVGPA.G + Hydroxylation (P)
	1014.4406	68	2	Q.GFQGPPGEPGEPGASGPMGPR.G + Deamidated (NQ); 3 Hydroxylation (P)
	686.6569	20	3	K.TGPPGPAGQDGRPGPPGPPGAR.G + Deamidated (NQ); 4 Hydroxylation (P)
	1217.9469	19	3	P.PGPAGPAGPPGPIGNVGAPGPKGARGSAGPPGATGFPGAAGR.V + Deamidated (NQ); Hydroxylation (K); 5 Hydroxylation (P)
	1461.9896	17	3	K.GETGPSGPAGPTGARGAPGDRGEPGPPGPAGFAGPPGADGQPGAKGEPG.D + Hydroxylation (K); 6 Hydroxylation (P)
	1489.6873	15	3	R.GSEGPQGVRGEPGPPGPAGAAGPAGNPGADGQPGAKGANGAPGIAGAPGFP.G + Deamidated (NQ); Hydroxylation (K); 6 Hydroxylation (P)

12

	1563.1168	15	3	P.PGPAGFAGPPGADGQPGAKGEPGDAGAKGDAGPPGPAGPAGPPGPIGNVGAPGPK.G + Hydroxylation (P)
	1577.7714	22	3	P.PGPPVSMLSPSPAPSPASSLQGPPGSAGTPGKDGLNGLPGPIGPPGPRGR.T + Deamidated (NQ); Oxidation (M); Hydroxylation (K); 5 Hydroxylation (P) **(U)**
	1600.3743	18	3	A.PGPQGFQGPPGEPGEPGASGPMGPRGPPGPPGKNGDDGEAGKPGRPGER.G + Deamidated (NQ); Oxidation (M); Hydroxylation (K); 8 Hydroxylation (P) (P
Collagen 2(I) *Ovis aries* (W5NTT7)	314.6735	19	2	S.GPQGIR.G + Deamidated (NQ)
	355.2024	21	2	P.PGPPGLR.G + Hydroxylation (P)
	358.1891	43	2	P.SGPQGIR.G + Deamidated (NQ)
	363.2004	24	2	A.PGLPGPR.G + 2 Hydroxylation (P)
	390.2101	37	2	P.GPAGPAGPR.G
	398.7177	39	2	G.APGLPGPR.G + 2 Hydroxylation (P)
	406.2231	33	2	L.GIAGPPGAR.G + Hydroxylation (P)
	406.2234	27	2	F.GLPGPAGAR.G + Hydroxylation (P)
	427.2282	22	2	A.GAPGLPGPR.G + 2 Hydroxylation (P)
	435.2258	16	2	S.GPSGLPGER.G
	446.7336	29	2	N.PGPAGPAGPR.G + Hydroxylation (P)
	452.2306	29	2	A.GPPGFVGEK.G + Hydroxylation (P)
	456.2315	30	2	A.GPPGPPGLR.G + 4 Hydroxylation (P)
	456.7484	31	2	A.AGPTGPIGSR.G
	477.2359	23	2	R.GAPGAVGAPGPA.G + 2 Hydroxylation (P)
	482.2472	38	2	S.GPPGPPGPAGK.E + 2 Hydroxylation (P)
	492.2644	24	2	G.AAGPTGPIGSR.G
	511.7702	40	2	Q.GAPGAVGPAGPR.G + Hydroxylation (P)
	512.2572	27	2	R.GEPGPVGAVGPA.G + Hydroxylation (P) **(U)**
	516.7353	19	2	R.GFPGSPGNIGP.A + Deamidated (NQ); 2 Hydroxylation (P)
	520.7753	39	2	S.GAAGPTGPIGSR.G

13

	524.2375	38	2	R.GYPGNAGPVGAA.G + Deamidated (NQ); Hydroxylation (P)
	532.7578	69	2	V.GNPGPAGPAGPR.G + Deamidated (NQ); Hydroxylation (P)
	537.7407	18	2	R.GEPGNIGFPGP.K + Deamidated (NQ); 2 Hydroxylation (P)
	563.7763	42	2	A.GPSGPSGLPGER.G + Hydroxylation (P)
	563.7776	20	2	A.GPPGFPGAPGPK.G + Hydroxylation (K); 2 Hydroxylation (P)
	582.2912	64	2	P.VGNPGPAGPAGPR.G + Deamidated (NQ); Hydroxylation (P)
	584.2744	35	2	P.SGPNGPPGPAGSR.G + Deamidated (NQ); Hydroxylation (P)
	599.2953	21	2	T.AGPSGPSGLPGER.G + Hydroxylation (P)
	609.3346	24	2	E.IGPAGPPGPPGLR.G + 2 Hydroxylation (P)
	610.8140	88	2	A.GISGPPGPPGPAGK.E + 2 Hydroxylation (P)
	631.3157	61	2	R.GEAGPAGPAGPAGPR.G
	659.3292	21	2	L.GPVGNPGPAGPAGPR.G + Deamidated (NQ); Hydroxylation (P)
	660.8188	48	2	A.GPSGPNGPPGPAGSR.G + Hydroxylation (P)
	663.7932	52	2	V.GQPGPPGPSGEEGK.R + Deamidated (NQ); 2 Hydroxylation (P)
	673.8547	16	2	G.EIGPAGPPGPPGLR.G + 2 Hydroxylation (P)
	696.8281	43	2	A.AGPSGPNGPPGPAGSR.G + Deamidated (NQ); Hydroxylation (P)
	701.3353	23	2	T.GEPGAAGPPGFVGEK.G + 2 Hydroxylation (P) **(U)**
	702.3653	31	2	T.GEIGPAGPPGPPGLR.G + 2 Hydroxylation (P)
	711.3636	36	2	R.GEVGLPGLSGPVGPPG.N + 2 Hydroxylation (P)
	745.3113	52	2	R.GPNGDSGRPGEPGLM.G + Deamidated (NQ); Oxidation (M); 2 Hydroxylation (P)
	746.8675	18	2	R.GSTGEIGPAGPPGPPGL.R + 2 Hydroxylation (P)

14

	780.3972	48	2	G.ELGPVGNPGPAGPAGPR.G + Deamidated (NQ); Hydroxylation (P)
	790.8827	31	2	V.GAPGTAGPSGPSGLPGER.G + Hydroxylation (P)
	803.8872	38	2	S.GPVGPPGNPGANGLPGAK.G + 2 Deamidated (NQ); Hydroxylation (K); 2 Hydroxylation (P)
	825.8833	19	2	R.GPSGPPGPDGNKGEPGVV.G + Deamidated (NQ); 2 Hydroxylation (P)
	600.6022	20	2	R.GPNGDSGRPGEPGLMGPR.G + Deamidated (NQ); Oxidation (M); 2 Hydroxylation (P)
	904.9019	49	2	F.QGPPGEPGEPGQTGPAGAR.G + Deamidated (NQ); 3 Hydroxylation (P)
	912.4074	45	2	R.GPPGNVGNPGVNGAPGEAGR.D + 2 Deamidated (NQ); 3 Hydroxylation (P)
	946.4536	61	2	R.GEVGLPGLSGPVGPPGNPGAN.G + Deamidated (NQ); 3 Hydroxylation (P)
	1006.9481	42	2	Q.GFQGPPGEPGEPGQTGPAGAR.G + Deamidated (NQ); 3 Hydroxylation (P)
	1078.9707	50	2	R.GSQGSQGPAGPPGPPGPPGPPG PSG.G + 2 Deamidated (NQ); 4 Hydroxylation (P)
	1107.4874	18	2	R.GSQGSQGPAGPPGPPGPPGPPG PSGG.G + 2 Deamidated (NQ); 4 Hydroxylation (P)
	1485.7643	16	2	R.GLPGERGRVGAPGPAGARGSDG SVGPVGPAGPI.G + 3 Hydroxylation (P)
	1126.1639	22	3	K.GPKGENGPVGPTGPVGAAGPSG PNGPPGPAGSRGDGGP.P + 2 Deamidated (NQ); Hydroxylation (K); 8 Hydroxylation (P)
	1247.2050	22	3	R.GSQGSQGPAGPPGPPGPPGPPG PSGGGYDFGFDGDFYRA.D + Deamidated (NQ); 5 Hydroxylation (P) **(U)**
	1359.2848	15	3	G.DDGIPGPPGPPGPPGPPGLGGN FAAQFDGKGGGPGPMGLMGPR.G + Oxidation (M); 7 Hydroxylation (P) **(U)**
Collagen 1(III) *Ovis aries* (W5Q4S0)	363.2004	24	2	P.IGPPGPR.G + 2 Hydroxylation (P)
	396.6979	22	2	G.FPGSPGAK.G + Hydroxylation (K); Hydroxylation (P)

15

	405.6827	40	2	R.GEPGPPGPA.G + 2 Hydroxylation (P)
	419.2135	19	2	P.GPPGSPGPR.G + Hydroxylation (P)
	434.1933	18	2	R.GEPGPPGPAG.F + 2 Hydroxylation (P)
	455.7413	16	2	A.VGSPGPAGPR.G + Hydroxylation (P)
	456.2315	30	2	P.GPIGPPGPR.G + 4 Hydroxylation (P)
	465.7284	18	2	P.AGANGLPGEK.G + Deamidated (NQ); Hydroxylation (K)
	485.7492	34	2	R.DGLPGGPGLR.G + 2 Hydroxylation (P)
	490.2251	31	2	K.GEGGPPGAAGPP.G + Hydroxylation (P)
	491.2567	32	2	G.AVGSPGPAGPR.G + Hydroxylation (P)
	519.7687	20	2	Q.GAVGSPGPAGPR.G + Hydroxylation (P)
	537.7463	21	2	T.PGLQGMPGER.G + Deamidated (NQ); Oxidation (M); Hydroxylation (P)
	375.8592	28	3	S.GVDGAPGKDGPR.G
	563.7763	19	2	S.GPAGPPGPQGVK.G + Deamidated (NQ); Hydroxylation (K); 3 Hydroxylation (P)
	388.5354	29	3	T.GRPGPPGSPGPR.G + 2 Hydroxylation (P)
	603.2717	17	2	R.GAPGPQGPPGAPGPP.L + Deamidated (NQ); 3 Hydroxylation (P)
	624.7780	32	2	A.GTPGLQGMPGER.G + Deamidated (NQ); Oxidation (M); 2 Hydroxylation (P)
	629.7973	19	2	G.SNGAPGSPGISGPK.G + Deamidated (NQ); 2 Hydroxylation (P)
	655.3199	17	2	R.GPVGPSGPPGKDGTS.G
	667.3212	24	2	R.GAPGPQGPPGAPGPL.G + 4 Hydroxylation (P)
	454.5556	34	3	A.GHQGAVGSPGPAGPR.G + Deamidated (NQ); Hydroxylation (P)
	716.8172	35	2	A.GFPGAPGQNGEPGAK.G + Deamidated (NQ); 3 Hydroxylation (P)
	723.3727	22	2	A.GPPGPPGAIGPSGPAGK.D + 2 Hydroxylation (P)
	494.9131	25	3	A.GEPGRDGLPGGPGLR.G + 3 Hydroxylation (P)

16

	773.8771	66	2	A.GPPGGSGPAGPPGPQGVK.G + Deamidated (NQ); 2 Hydroxylation (P)
	832.3967	17	2	R.GPPGPQGLPGLAGAAGEPG.R + 4 Hydroxylation (P)
	1048.4703	16	2	R.GENGSPGAPGAPGHPGPPGPVG PA.G + Deamidated (NQ); 4 Hydroxylation (P)
	1516.7301	17	2	G.EMGPAGIPGAPGLLGARGPPGP PGTNGAPGQR.G + 8 Hydroxylation (P)
	1126.1639	27	3	K.GNDGAPGKNGERGGPGGPGPQ GPAGKNGETGPQGPPG.P + 3 Deamidated (NQ); Hydroxylation (K); 5 Hydroxylation (P)
	1163.8682	16	3	R.GPPGPQGLPGLAGAAGEPGRDG NPGSDGLPGRDGAPGT.K + Deamidated (NQ); 7 Hydroxylation (P) **(U)**
	1288.6129	17	3	K.GHRGFPGNPGPPGSPGPAGHQG AVGSPGPAGPRGPVGPSGPPG.K + 5 Hydroxylation (P) **(U)**
	1407.6699	18	3	Q.RGEPGPQGHAGAPGPPGPPGS NGSPGGKGEMGPAGIPGAPGLLGA R.G + Deamidated (NQ); Oxidation (M); 8 Hydroxylation (P)
	1418.3666	16	3	P.KGDAGQPGERGAPGPQGPPGAP GPLGIAGLTGARGLAGPPGMPGAR. G + 2 Deamidated (NQ); 8 Hydroxylation (P)
	1471.1599	15	4	R.GNDGARGSDGQPGPPGPPGTA GFPGSPGAKGEVGPAGSPGSSGAP GQRGEPGPQGHAGAPGPPGPP.G + 3 Deamidated (NQ); Hydroxylation (K); 6 Hydroxylation (P)

Table S5. Identification of spontaneous hydrolysis sites in the lining of the historical canvas "The Virgin and Child, Saints and Cherubins" by LC-MS/MS upon overnight digestion with trypsin in heterogeneous phase. LC-MS/MS raw data from overnight digestion with trypsin in heterogeneous phase were analysed as those of Table S4.

Protein	*m/z*	Ion Score	Charge	Peptide
Collagen 1(I) *Ovis aries* (W5P481)	301.6486	17	2	R.GARGEP.G + Hydroxylation (P)
	321.1720	26	2	A.PGPAGAR.G + Hydroxylation (P)
	335.2051	26	2	P.IGPVGAR.G
	367.1848	42	2	A.PGFPGAR.G + 2 Hydroxylation (P)
	372.2057	34	2	V.VGLPGQR.G + Deamidated (NQ); Hydroxylation (P)
	374.6900	22	2	T.GFPGAAGR.V + Hydroxylation (P)
	383.7318	16	2	G.PIGPVGAR.G
	450.7226	60	2	F.PGSDGVAGPK.G + Hydroxylation (P)
	466.7321	19	2	I.AGAPGFPGAR.G + 2 Hydroxylation (P)
	475.7372	31	2	V.QGPPGPAGPR.G + Deamidated (NQ); Hydroxylation (P)
	480.7663	59	2	L.PGPIGPPGPR.G + Hydroxylation (P)
	491.7509	44	2	T.PGPQGIAGQR.G + 2 Deamidated (NQ)
	496.2864	34	2	G.PAGPIGPVGAR.G
	518.7715	29	2	V.PGPPGAVGPAGK.D + 2 Hydroxylation (P)
	524.7997	39	2	A.GPAGPIGPVGAR.G
	534.2697	51	2	S.VPGPMGPSGPR.G + Oxidation (M)
	537.7467	25	2	A.PGLQGMPGER.G + Deamidated (NQ); 2 Hydroxylation (P)
	543.2884	15	2	V.VGLPGQRGER.G + Deamidated (NQ); Hydroxylation (P)
	582.2949	30	2	R.GVQGPPGPAGPRG.A + Deamidated (NQ); Hydroxylation (P)
	388.5352	22	3	D.GRPGPPGPPGAR.G + 3 Hydroxylation (P)
	594.2932	55	2	G.PPGATGFPGAAGR.V + 2 Hydroxylation (P)
	596.8188	63	2	R.GVPGPPGAVGPAGK.D + 2 Hydroxylation (P)
	404.8826	30	3	E.AGRPGEAGLPGAK.G + Hydroxylation (P); Hydroxylation (K)
	608.3107	21	2	A.PGIAGAPGFPGAR.G + 3 Hydroxylation (P)
	619.8224	19	2	M.PGERGAAGLPGPK.G + 2 Hydroxylation (P)
	625.3102	33	2	E.PGPAGLPGPPGER.G + 3 Hydroxylation (P)
	643.8029	42	2	K.GSPGEAGRPGEAGL.P + 2 Hydroxylation (P)
	654.3328	23	2	R.GVPGPPGAVGPAGKD.G + 2 Hydroxylation (P)
	670.8038	16	2	R.GSEGPQGVRGEPGP.P + Deamidated (NQ); Hydroxylation (P)
	695.8298	38	2	R.GPSGPQGPSGPPGPKG.N + Deamidated (NQ); Hydroxylation (P)
	469.8907	26	3	G.QDGRPGPPGPPGAR.G + Deamidated (NQ); 3 Hydroxylation (P)
	718.8248	25	2	R.GAPGDRGEPGPPGPAG.F + 3 Hydroxylation (P)
	719.3354	15	2	K.GEPGPTGIQGPPGPAG.E + Deamidated (NQ); 3 Hydroxylation (P)
	728.8376	18	2	K.GSPGEAGRPGEAGLPG.A + 3 Hydroxylation (P)
	753.3429	45	2	R.GPSGPQGPSGPPGPKGN.S + 2 Deamidated (NQ); Hydroxylation (P)
	753.3646	62	2	R.AGEVGPPGPPGPAGEKG.A + 2 Hydroxylation (P) **(U)**
	755.8391	36	2	R.GSEGPQGVRGEPGPPG.P + Deamidated (NQ); 2 Hydroxylation (P)
	756.3759	46	2	S.PGEAGRPGEAGLPGAK.G + 3 Hydroxylation (P)
	512.5780	34	3	P.AGQDGRPGPPGPPGAR.G + Deamidated (NQ); 3 Hydroxylation (P)
	782.3550	16	2	K.TGPPGPAGQDGRPGPPG.P + Deamidated (NQ); 3 Hydroxylation (P)
	533.5989	21	3	G.SPGEAGRPGEAGLPGAK.G + 2 Hydroxylation (P); Hydroxylation (K)

Table S6. Glycation products in the lining of the historical canvas "The Virgin and Child, Saints and Cherubins" upon digestion with the trypsin

functionalized film. LC-MS/MS raw data from *in situ* digestion with trypsin functionalized film were searched by Mascot MS/MS Ion search using COLLE database considering semitrypsin as the enzyme, deamidation on Gln and Asn, hydroxylation at Pro, carboxyethyl(K), carboxymethyl(K), Glyoxal(R) (reported as G-H1) and methylglyoxal (R) (reported as MG-H1) as variable modifications. Individual ion score threshold provided by Mascot software (>15) to evaluate the quality of matches in MS/MS data was used for confidence threshold in protein identification. (**U**) Indicates the unique peptides. Only peptides modified with glycation products are herein reported.

Protein	*m/z*	Ion Score	Charge	Peptide
Collagen 1(I) *Ovis aries* (W5P481)	363.1856	23	2	P.PGPRGR.T 2 Hydroxylation (P); MG-H1 (R)
	435.2077	15	2	P.GPPGPPGAR.G + 2 Hydroxylation (P) (P); G-H1 (R)
	385.2021	25	3	D.GVAGPKGPAGER.G Carboxymethyl (K)
	485.7496	17	2	A.GLPGPKGDR.G Hydroxylation (P); Carboxymethyl (K)
	532.7563	21	2	G.KPGRPGER.G Hydroxylation (P); Carboxymethyl (K); G-H1 (R); MG-H1 (R)
	599.2724	34	2	F.AGPPGADGQPGAK.G Deamidated (NQ); Hydroxylation (P); Carboxymethyl (K)
	891.0864	21	3	A.RGPSGPQGPSGPPGPKGNSGEPG APGSK.G 3 Hydroxylation (P); Carboxymethyl (K); MG-H1 (R)
	973.9772	19	2	A.AGPPGPTGPAGPPGFPGAVGAK. G 2 Hydroxylation (P); Carboxymethyl (K)
	1294.5898	31	3	A.GPQGPRGSEGPQGVRGEPGPPG PAGAAGPAGNPGADGQPGAK.G 2 Deamidated (NQ); Hydroxylation (P); Carboxymethyl (K); G-H1 (R); MG-H1 (R)
	1333.2559	15	3	R.GVQGPPGPAGPRGANGAPGND GAKGDAGAPGAPGSQGAPGLQGM P.G 5 Deamidated (NQ); 3 Hydroxylation (P); Carboxyethyl (K)
	1347.6487	17	3	D.VICDELKDCPNAKVPTPPRPVSPH PPPPPPPPTTTK.Q Deamidated (NQ); 4 Hydroxylation (P); 2 Carboxymethyl (K); G-H1 (R) **(U)**
	1453.6953	15	2	G.RVGPPGPSGNAGPPGPPGPAGK EGSKGPR.G 4 Hydroxylation (P); 2

				Carboxymethyl (K); G-H1 (R); MG-H1 (R)
	1721.8243	19	3	G.LTGSPGSPGPDGKTGPPGPAGQDGRPGPPGPPGARGQAGVMGFPGPKGAAGEPGK.A 2 Deamidated (NQ); 5 Hydroxylation (P); 2 Carboxyethyl (K)
Collagen 2(I) *Ovis aries* (W5NTT7)	476.2131	21	2	R.GERGPPGPP.G 3 Hydroxylation (P); G-H1 (R)
	532.7563	21	2	G.KPGRPGER.G Hydroxylation (P); Carboxymethyl (K); G-H1 (R); MG-H1 (R)
	578.6300	16	3	A.GISGPPGPPGPAGKEGLR.G 2 Hydroxylation (P); Carboxymethyl (K)
	923.4585	15	3	P.GKAGEDGHPGKPGRPGERGVVGPQGAR.G Deamidated (NQ); 2 Hydroxylation (P); Carboxyethyl (K); G-H1 (R)
	1139.2302	17	3	D.GHPGKPGRPGERGVVGPQGARGFPGTPGLPGFK.G 6 Hydroxylation (P); Carboxymethyl (K); G-H1 (R)
	1259.0591	20	2	G.ANGDRGEAGPAGPAGPAGPRGSPGER.G Deamidated (NQ); 4 Hydroxylation (P); G-H1 (R); MG-H1 (R)
	1412.3319	26	3	P.GQTGPAGARGPPGPPGKAGEDGHPGKPGRPGERGVVGPQGAR.G 2 Deamidated (NQ); 3 Hydroxylation (P); 2 Carboxymethyl (K); G-H1 (R); 2 MG-H1 (R)
	1443.7001	19	2	G.PAGARGPPGPPGKAGEDGHPGKPGRPGER.G 2 Hydroxylation (P); Carboxymethyl (K); G-H1 (R)
	1488.3948	15	3	G.PAGLPGIDGRPGPIGPAGARGEPGNIGFPGPKGPTGDPGKAGEK.G 6 Hydroxylation (P); 3 Carboxyethyl (K); 2 G-H1 (R) **(U)**
	1537.1033	15	3	R.GFPGSPGNIGPAGKEGPAGLPGIDGRPGPIGPAGARGEPGNIGFPGPKG.P Deamidated (NQ); 5 Hydroxylation (P); Carboxyethyl (K) **(U)**
	1721.8243	19	3	P.GSPGNIGPAGKEGPAGLPGIDGRPGPIGPAGARGEPGNIGFPGPKGPTGDPGK.A 2 Deamidated (NQ); 7 Hydroxylation (P); 2 Carboxyethyl (K); Carboxymethyl (K); G-H1 (R)
Collagen 1(III) *Ovis aries* (W5Q4S0)	532.8502	16	5	K.DGSPGEPGANGLPGAAGERGVPGFRGPA.G Deamidated (NQ); 2 Hydroxylation (P); 2 G-H1 (R)

20

	572.7723	25	2	P.GIAGPKGEDGK.D 2 Carboxymethyl (K)
	652.3187	20	2	K.DGPRGPTGPIGPP.G 2 Hydroxylation (P); MG-H1 (R)
	669.3250	17	2	E.RGGPGGPGPKGDK.G 2 Hydroxylation (P); Carboxyethyl (K); MG-H1 (R)
	671.2975	27	2	R.GAPGEKGEGGPPGAA.G 2 Hydroxylation (P); Carboxymethyl (K)
	798.0392	16	3	G.RDGNPGSDGLPGRDGAPGTKGD R.G 2 Hydroxylation (P); 2 MG-H1 (R)
	928.8966	25	2	K.GEDGKDGSPGEPGANGLPGA.A Deamidated (NQ); Hydroxylation (P); Carboxymethyl (K)
	1226.7600	17	5	L.PGGPGLRGIPGSPGGPGSDGKPG PPGSQGETGRPGPPGSPGPRGQPG VMGFPGPKGNDGAPGK.N 2 Deamidated (NQ); 10 Hydroxylation (P); 2 Carboxyethyl (K); Carboxymethyl (K); 2 G-H1 (R)
	1454.7354	15	3	G.ERGAPGPQGPPGAPGPLGIAGLT GARGLAGPPGMPGARGSPGPQGIK .G 3 Hydroxylation (P); 2 G-H1 (R)
	1469.3512	25	3	R.GSPGPQGIKGENGKPGPSGQNGE RGPPGPQGLPGLAGAAGEPGRDG. N 2 Deamidated (NQ); 6 Hydroxylation (P); G-H1 (R); MG-H1 (R)
	1579.4224	19	3	L.RGIPGSPGGPGSDGKPGPPGSQG ETGRPGPPGSPGPRGQPGVMGFPG PK.G Deamidated (NQ); 2 Hydroxylation (P); Carboxymethyl (K); 2 G-H1 (R); MG-H1 (R)
	1689.8057	20	3	R.GAPGPQGPPGAPGPLGIAGLTGA RGLAGPPGMPGARGSPGPQGIKGE NGKPGPSG.Q 2 Deamidated (NQ); 5 Hydroxylation (P); 2 Carboxymethyl (K); G-H1 (R)

Table S7. Glycation products identified in the lining of the historical canvas "The Virgin and Child, Saints and Cherubins" upon overnight trypsin digestion in heterogeneous phase. LC-MS/MS raw data from overnight digestion with trypsin in heterogeneous phase were searched by Mascot MS/MS Ion search were analysed as those of Table S6.

Protein	*m/z*	Ion Score	Charge	Peptide
Collagen 1(I) *Ovis aries* (W5P481)	482.0243	15	5	R.GPPGPPGKNGDDGEAGKPGRPGER.G + Deamidated (NQ); 3 Hydroxylation (P); Carboxymethyl (K)
	535.9902	21	4	R.GPAGPQGPRGDKGETGEQGDR.G Deamidated (NQ); Hydroxylation (P); Carboxymethyl (K)
	561.6094	22	3	R.GDAGPKGADGAPGKDGVR.G Carboxymethyl (K)
	589.7694	16	4	G.KTGPPGPAGQDGRPGPPGPPGAR.G Deamidated (NQ); 6 Hydroxylation (P); Carboxymethyl (K); 2 G-H1 (R)
	610.7836	21	2	R.GQAGVMGFPGPK.G Deamidated (NQ); Hydroxylation (P); Carboxymethyl (K)
	703.3604	16	2	A.PGQMGPRGLPGER.G MG-H1 (R)
	758.3607	36	3	R.VGPPGPSGNAGPPGPPGPAGKEGSK.G Deamidated (NQ); 3 Hydroxylation (P); Carboxymethyl (K)
	802.7028	27	3	R.GPPGPPGKNGDDGEAGKPGRPGER.G Deamidated (NQ); 3 Hydroxylation (P); Carboxymethyl (K)
	821.6967	31	3	R.GPSGPQGPSGPPGPKGNSGEPGAPGSK.G 2 Deamidated (NQ); 3 Hydroxylation (P); Carboxymethyl (K)
	857.0328	16	3	K.GDAGPAGPKGEPGSPGENGAPGQMGPR.G 2 Deamidated (NQ); 4 Hydroxylation (P); Carboxymethyl (K)
	865.4083	19	2	R.GFPGSDGVAGPKGPAGER.G Hydroxylation (P); Carboxymethyl (K)
	981.1467	44	3	R.GLTGPIGPPGPAGAPGDKGETGPSGPAGPTGAR.G 2 Hydroxylation (P); Carboxymethyl (K)
	1039.9747	27	2	K.GEPGPTGIQGPPGPAGEEGKR.G Deamidated (NQ); 2 Hydroxylation (P); Carboxymethyl (K)
Collagen 2(I) *Ovis aries* (W5NTT7)	379.2027	38	3	R.GRVGAPGPAGAR.G Hydroxylation (P); MG-H1 (R)
	839.8946	17	4	R.GLPGADGRAGVMGPAGSRGATGPAGVRGPNGDSGRP.G

				Deamidated (NQ); 2 Hydroxylation (P); MG-H1 (R); G-H1 (R)
	980.4880	20	3	G.RTGPPGPAGISGPPGPPGPAGKEGLRGPR.G 2 Hydroxylation (P); Carboxyethyl (K); 2 MG-H1 (R); G-H1 (R)
Collagen 1(III) *Ovis aries* (W5Q4S0)	584.6108	36	3	R.GPAGANGLPGEKGPPGER.G Deamidated (NQ); 2 Hydroxylation (P); Carboxymethyl (K)
	657.6464	21	3	G.DKGEPGTSGVDGAPGKDGPR.G Hydroxylation (P); Carboxymethyl (K)
	662.3361	15	2	E.PGAKGERGAPGEK.G Hydroxylation (P); MG-H1 (R)
	748.9938	23	3	G.EDGKDGSPGEPGANGLPGAAGER.G Deamidated (NQ); 3 Hydroxylation (P); Carboxymethyl (K)
	1018.4827	16	2	G.QRGAAGEPGKNGAKGDPGPR.G 2 Deamidated (NQ); Hydroxylation (P); Carboxymethyl (K); G-H1 (R)
	1153.5731	18	2	G.HQGAVGSPGPAGPRGPVGPSGPPGK.D 3 Hydroxylation (P); G-H1 (R)
	1502.1821	22	2	K.GENGKPGPSGQNGERGPPGPQGLPGLAGAAG.E 6 Hydroxylation (P); Carboxyethyl (K); MG-H1 (R)

Fig. S10: MS/MS spectra of the doubly charged ions at *m/z* 532.7563 (A) of the peptide K(Carboxymethyl)P(Hydroxylation)GR(G-H1)PGER(MG-H1) identified in the analysis by LC-MS/MS of the lining of the historical canvas "The Virgin and Child, Saints and Cherubins" upon digestion with the trypsin functionalized The product ions are indicated with the observed masses reported in the table below.

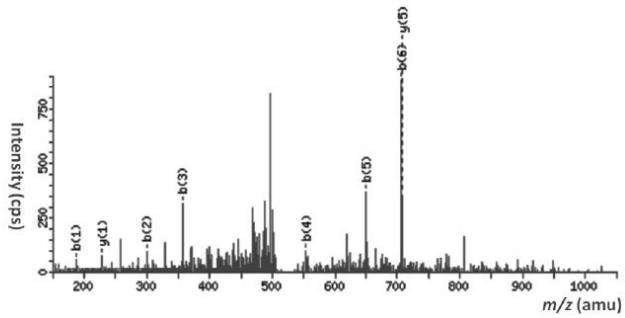

	b	Sequence	y	
1	**187.1077**	**K (Carboxymethyl)**		8
2	**300.1554**	**P (Hydroxylation)**	878.4115	7
3	**357.1769**	**G**	765.3638	6
4	**553.2729**	**R (G-H1)**	**708.3424**	5
5	**650.3257**	**P**	512.2463	4
6	**707.3471**	**G**	415.1936	3
7	**836.3897**	**E**	358.1721	2
8		**R (MG-H1)**	**229.1295**	1

Implementation with the integration of the PNGase functionalized film.

24

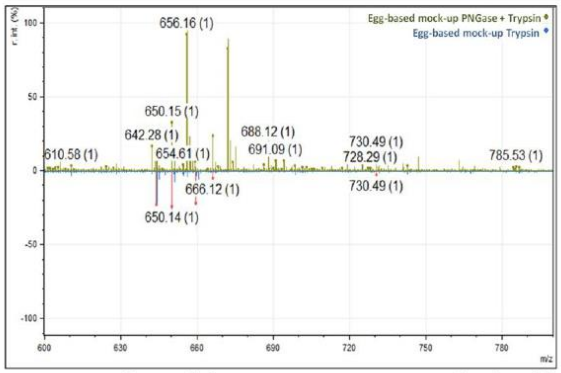

Figure S11. Comparison of the MALDI-TOF spectra obtained from the digestion of the egg-based painting mock-up either with the combined use of PNGaseF and trypsin functionalized films (top spectrum) and with the use of trypsin functionalized film alone (lower spectrum). Identification of *Gallus gallus* ovalbumin was performed by manual MALDI-TOF Peptide mass fingerprint (see table S8 below). Moreover, identifications were then confirmed by LC-MS/MS analysis of the peptides mixtures with the results are reported in tables S9-S10. Data analysis was done using the mMass freeware program [1].

Table S8: Peptide mass fingerprinting in the egg-based painting mock-up with the combined use of PNGase and trypsin functionalized films. MALDI-TOF data from the lower spectrum of Figure S11 were inserted in Mascot Peptide mass fingerprint to search the SwissProt database with taxonomic restriction to *Gallus gallus*.

Protein	*m/z* expected	*m/z* observed	Start	End	Sequence
Ribosomal protein L19 *Gallus gallus* (Q5ZKK8_CHICK)	642.33	642.28	75	80	
	656.38	656.16	39	43	R.QQIRK.L +Gln->pyro-Glu + deamidation(NQ)
	659.39	659.15	168	172	K.EARKR.R
	672.41	672.14	39	43	R.QQIRK.L
	688.41	688.12	147	152	K.ADKARK.K
	703.42	703.1	65	70	R.KNTLAR.R + deamidation(NQ)

25

	717.4	717.28	82	88	R.KGTANAR.M
	730.43	730.48	66	71	K.NTLARR.K
Ubiquitin-60S ribosomal protein *Gallus gallus* (L40RL40_CHICK)	650.34	650.13	35	39	K.MICRK.C
	666.34	666.12	35	39	K.MICRK.C + oxidation(M)
Uncharacterized protein *Gallus gallus* (A0A1D5NZA9_CHICK)	624.27	624.28	23	27	K.HNPQK.V + 2Deamidated (NQ)

Table S9. Identification of proteins in the egg-based painting mock-up upon digestion with the trypsin functionalized film after pretreatment with the PNGaseF functionalized film and analysis by LC-MS/MS. The sample was subjected to *in-situ* digestion with the trypsin functionalized film after *in-situ* deglycosylation with PNGaseF functionalized film as described in the main text, and the peptide mixture was analysed by LC-MS/MS. Raw data were searched by Mascot MS/MS Ion search using Chordata as the taxonomic restriction in the SwissProt protein database, with deamidation on Gln and Asn, and oxidation on Met, as variable modifications, Individual ion score threshold provided by Mascot software (>12) to evaluate the quality of matches in MS/MS data was used for confidence threshold in protein identification. (**U**) Indicates unique peptides.

Protein[a]	***m/z***	**Ion Score**	**Charge**	**Peptide**
Ovalbumin *Gallus gallus* (P01012)	324.2003	36	2	K.VYLPR.M
	390.7010	31	2	R.LYAEER.Y **(U)**
	319.8692	23	3	R.TQINKVVR.F
	339.5619	28	3	R.KIKVYLPR.M **(U)**
	605.2692	26	2	K.DEDTQAMPFR.V **(U)**
	472.9377	12	3	K.DSTRTQINKVVR.F
	778.3686	34	2	K.AFKDEDTQAMPFR.V **(U)**
	799.3682	23	2	K.LTEWTSSNVMEER.K + Oxidation (M) **(U)**
	563.2890	56	3	R.GGLEPINFQTAADQAR.E **(U)**

	592.3030	22	3	K.ISQAVHAAHAEINEAGR.E + Deamidated (NQ) **(U)**
	620.3307	42	3	R.ELINSWVESQTNGIIR.N **(U)**
	761.0714	55	3	R.DILNQITKPNDVYSFSLASR.L
	762.0603	19	3	R.VTEQESKPVQMMYQIGLFR.V **(U)**
	820.7767	27	3	R.NVLQPSSVDSQTAMVLVNAIVFK.G
	630.0922	12	4	R.ADHPFLFCIKHIATNAVLFFGR.C **(U)**
Ovotransferrin *Gallus gallus* (P02789)	389.2159	13	2	K.DSAIMLK.R
	419.7037	16	2	R.FGVNGSEK.S + Deamidated (NQ) **(U)**
	445.2254	38	2	R.DLTQQER.I **(U)**
	457.2447	10	2	K.DQLTPSPR.E **(U)**
	602.2954	18	2	K.DSNVNWNNLK.G **(U)**
	654.8288	35	2	K.GTEFTVNDLQGK.T **(U)**
	512.2919	33	3	R.SAGWNIPIGTLLHR.G **(U)**
	551.6204	12	3	K.TDERPASYFAVAVAR.K **(U)**
	565.9504	12	3	R.DDNKVEDIWSFLSK.A **(U)**
Ovalbumin-related protein Y *Gallus gallus* (P01014)	324.2003	36	2	K.VYLPR.M
	336.1966	27	3	K.TINFDKLR.E **(U)**
	374.5580	19	3	K.KSMKVYLPR.M **(U)**
	569.7678	19	2	R.EWTSTNAMAK.K **(U)**
	580.2936	20	2	K.HSLELEEFR.A **(U)**
	344.9553	25	4	R.IEKTINFDKLR.E **(U)**
	706.8721	23	2	R.YNPTNAILFFGR.Y **(U)**
Elongation factor 1-alpha 1 *Gallus gallus* (Q90895)	447.7538	12	2	R.TIEKFEK.E **(U)**
	457.791	28	2	R.QTVAVGVIK.A **(U)**
	488.2799	12	2	R.LPLQDVYK.I **(U)**
	513.3124	23	2	K.IGGIGTVPVGR.V **(U)**

Ubiquitin *Gallus gallus* (P79781)	324.7063	23	2	R.LIFAGK.Q **(U)**
	356.5478	27	3	K.ESTLHLVLR.L **(U)**

Table S10. Identification of proteins in the egg-based painting mock-up sample upon digestion with the trypsin functionalized film and analysis by LC-MS/MS. The sample was subjected to *in-situ* digestion with the trypsin functionalized film and the peptide mixture was analysed by LC-MS/MS. Raw data were analysed by Mascot MS/MS Ion search as those of Table S9

Protein	*m/z*	Ion Score	Charge	Peptide
Ovalbumin *Gallus gallus* (P01012)	324.1944	42	2	K.VYLPR.M
	411.7059	23	2	R.VASMASEK.M **(U)**
	519.2429	21	3	K.AFKDEDTQAMPFR.V **(U)**
	799.3591	20	2	K.LTEWTSSNVMEER.K + Oxidation (M) **(U)**
	844.4206	33	2	R.GGLEPINFQTAADQAR.E **(U)**
	591.9677	47	3	K.ISQAVHAAHAEINEAGR.E + Deamidated (NQ) **(U)**
	620.3287	31	3	R.ELINSWVESQTNGIIR.N **(U)**
	767.3778	21	3	R.VTEQESKPVQMMYQIGLFR.V + Oxidation (M) **(U)**
	826.1115	23	3	R.NVLQPSSVDSQTAMVLVNAIVFK.G + Oxidation (M) **(U)**
Ovotransferrin *Gallus gallus* (P02789)	318.1891	18	2	K.DLLFK.D
	445.22	14	2	R.DLTQQER.I **(U)**
	457.2366	16	2	K.DQLTPSPR.E **(U)**
	305.5172	18	2	K.IRDLLER.Q **(U)**
	534.2508	18	2	K.AQSDFGVDTK.S **(U)**
	512.2878	36	3	R.SAGWNIPIGTLLHR.G **(U)**
Elongation factor 1-alpha 1 *Gallus gallus* (Q90895)	457.7843	28	2	R.QTVAVGVIK.A **(U)**
	513.3049	29	2	K.IGGIGTVPVGR.V **(U)**

Table S11. Identification of proteins in the decoration of a XXIInd dynasty wooden Sarcophagus (yellow coffin) by LC-MS/MS upon digestion with the trypsin functionalized film after pretreatment with the PNGaseF functionalized film. The sample was subjected to *in-situ* digestion with the trypsin functionalized film after *in-situ* deglycosylation with PNGaseF functionalized film as described in the main text, and the peptide mixture was analysed by LC-MS/MS. Raw data were searched by Mascot MS/MS Ion search in the SwissProt protein database with Chordata as taxonomic restriction, with deamidation on Gln and Asn, and oxidation on Met, as variable modifications. Since collagen was detected, a further search was carried out using the homemade COLLE database considering hydroxylation at Pro and Lys as additional variable modifications. Individual ion score threshold provided by Mascot software (>10) to evaluate the quality of matches in MS/MS data was used for confidence threshold in protein identification. (**U**) Indicates the unique peptides.

Protein[a]	*m/z*	Ion Score	Charge	Peptide
Ovalbumin *Gallus gallus* (P01012)	324.1994	27	2	K.VYLPR.M
	799.3674	18	2	K.LTEWTSSNVMEER.K Oxidation (M) **(U)**
	844.4276	27	2	R.GGLEPINFQTAADQAR.E Deamidation(NQ) **(U)**
	591.9747	40	3	K.ISQAVHAAHAEINEAGR.E Deamidation(NQ)
Ubiquitin *Gallus gallus* (P79781)	647.3985	13	2	R.LIFAGK.Q **(U)**
	1066.6194	45	3	K.ESTLHLVLR.L **(U)**
ATP synthase subunit beta, mitochondrial *Gallus gallus* (Q5ZLC5)	720.3991	20	2	R.VALTGLTVAEYFR. **(U)**
	718.3829	34	2	R.FTQAGSEVSALLGR.I **(U)**
Vitellogenin 2 *Gallus gallus* (P02845)	717.8885	21	2	R.LSQLLESTMQIR.S Oxidation (M) **(U)**
	543.3208	20	2	R.QQLTLVEVR.S **(U)**
	723.3912	15	2	R.VGATGEIFVVNSPR.T **(U)**
	516.2744	10	2	R.EETEIVVGR.H **(U)**
Collagen, type I, alpha 1 *Bos taurus* (P02453)	898.4923	25	2	R.GVVGLPGQR.G Deamidated (NQ); Hydroxylation (P)

29

	1104.5677	33	2	R.GVQGPPGPAGPR.G Hydroxylation (P)
	1327.6476	13	2	R.GFPGLPGPSGEPGK.Q 2 Hydroxylation (P)
	1559.8133	27	2	R.GETGPAGPAGPIGPVGAR.G
	2852.4204	10	3	R.GLTGPIGPPGPAGAPGDKGEAGPSGPAGPTGAR.G Hydroxylation (K); Hydroxylation (P)
Collagen, type I, alpha 2 *Bos taurus* (P02465)	421.2303	24	2	R.GVVGPQGAR.G Deamidated (NQ)
	824.9182	19	2	R.GSTGEIGPAGPPGPPGLR.G 2 Hydroxylation (P)
	714.3698	13	2	R.GIPGEFGLPGPAGAR.G 2 Hydroxylation (P)
	1066.0687	15	2	R.GLPGVAGSVGEPGPLGIAGPPGAR.G 3 Hydroxylation (P)
	597.3342	10	2	R.IGQPGAVGPAGIR.G Deamidated (NQ)
Collagen, type I, alpha 1 *Gallus gallus* (P02457)	450.2534	25	2	R.GVVGLPGQR.G Deamidated (NQ); Hydroxylation (P)
	764.0599	10	3	R.GAAGLPGAKGDRGDPGPKGADGAPGK.D Hydroxylation (P) **(U)**
Collagen, type I, alpha 2 *Gallus gallus* (P02460)	721.6944	12	3	R.GSNGEPGSAGPPGPAGLRGVPGSR.G 2 Hydroxylation (P)
	1214.8793	10	3	R.GPPGPPGRDGEDGPPGPPGPPGPPGLGGNFAAQYDPSK.A 2 Deamidated (NQ); Hydroxylation (K); 4 Hydroxylation (P) **(U)**
Collagen, type III, alpha 1 *Gallus gallus* (P12105)	638.9733	11	3	R.GQPGVMGFPGPKGNEGAPGK.N Deamidated (NQ); Oxidation (M); Hydroxylation (P) **(U)**
	787.603	10	3	K.LMSSVETDIKAEGNSKYMYAVLEDGCTK.H Deamidated (NQ); Oxidation (M); 3 Hydroxylation (K) **(U)**

[a] Egg proteins are from the search in the SwissProt protein database with Chordata as taxonomic restriction, while results for collagen proteins were from the search in the homemade COLLE database.

30

Table S12. Identification of proteins in the decoration of a XXIInd dynasty wooden Sarcophagus (yellow coffin) by LC-MS/MS upon digestion with the trypsin functionalized film. The sample was subjected to *in-situ* digestion with the trypsin functionalized film and the peptide mixture was analysed by LC-MS/MS. Raw data were searched by Mascot MS/MS Ion search analysed by Mascot MS/MS Ion search as those of Table S9.

Protein[a]	*m/z*	Ion Score	Charge	Peptide
Ovalbumin *Gallus gallus* (P01012)	324.1994	21	2	K.VYLPR.M **(U)**
	390.6992	18	2	R.LYAEER.Y **(U)**
	844.4276	11	2	R.GGLEPINFQTAADQAR.E + Deamidation(NQ) **(U)**
Collagen, type I, alpha 2 *Bos taurus* (P02465)	714.3739	40	2	R.GIPGEFGLPGPAGAR.G + 2 Hydroxylation (P)
	549.5093	10	4	R.GAPGPDGNNGAQGPPGLQG VQGGK.G + Deamidated (NQ); 4 Hydroxylation (P)
	824.9257	10	2	R.GSTGEIGPAGPPGPPGLR.G + 2 Hydroxylation (P)
	604.8174	11	2	R.GAPGPQGPVGPVGK.H + Hydroxylation (K); 2 Hydroxylation (P)

[a] Egg proteins are from the search in the SwissProt protein database with Chordata as taxonomic restriction, while collagen proteins were from the search in the homemade COLLE database.

References

[1] M. Strohalm, M. Hassman, B. Kosata, M. Kodicek, mMass data miner: an open source alternative for mass spectrometric data analysis., Rapid Commun. Mass Spectrom. 22 (2008) 905–908. https://doi.org/10.1002/rcm.3444.

[2] M. Buckley, M.J. Collins, Collagen survival and its use for species identification in Holocene-lower Pleistocene bone fragments from British archaeological and paleontological sites, Antiqua. 1 (2011) 1–7. https://doi.org/10.4081/antiqua.2011.e1.

[3] D.P. Kirby, N. Khandekar, J. Arslanoglu, K. Sutherland, Protein identification in artworks by peptide mass fingerprinting, in: Prepr. ICOM Comm. Conserv. 16th Trienn. Conf. Lisbon, 2011.

[4] D.P. Kirby, M. Buckley, E. Promise, S.A. Trauger, T.R. Holdcraft, Identification of collagen-based materials in cultural heritage. Analyst. 138 (2013) 4849–4858. https://doi.org/10.1039/c3an00925d.

International Journal of Molecular Sciences

MDPI

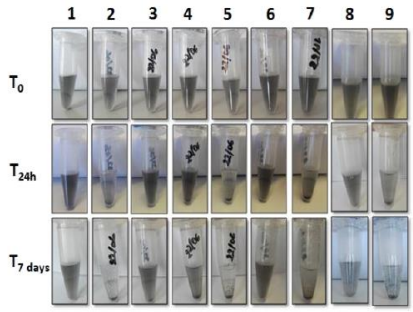

Figure S1- Stability of graphene dispersion in different solvents: lane 1, 60% EtOH; lane 2 40% EtOH; lane 3, 40% EtOH+ Vmh2; lane 4 40% EtOH + Vmh2 + 10mM Tris-HCl pH 8; lane 5 50% EtOH; lane 6, 50% EtOH + Vmh2; lane 7 50% EtOH + Vmh2 + 10mM Tris-HCl pH 8; lane 8, 20% EtOH + Vmh2; lane 9 20% EtOH + Vmh2 + 10mM Tris-HCl pH 8.

Table S1 – $t_{1/2}$ of laccases in different buffers measured by enzyme activity assays over days for native laccase and the chimera laccase **Lac-Vmh2.**

	t ½	
	PoxA1b	Lac-Vmh2
10 mM Tris-HCl pH 8	6 days	8 days
20% EtOH	4 days	5 days
40% EtOH	4 days	4 days
50% EtOH	2 days	1 days
60% EtOH	12 hours	13 hours

Table S2. Summary of the performed experiments: 1

	PoxA1b			Lac-Vmh2		
Tests	Immobilized (U_{tot})	Immobilization yield (%)	Graphene [µg/mL]	Immobilized (U_{tot})	Immobilization yield (%)	Graphene [µg/mL]
Route A	nd	nd	85	nd	nd	85
Route B	nd	nd	na	nd	nd	na
Route C	0.22±0.07	5	70	0.44±0.07	11	100

*nd: not detected; na: not analyzed

Supplementary informations for

Carbon-nanotube-supported POXA1b laccase and its hydrophobin chimera for oxygen reduction and picomolar phenol biosensing

Ilaria Sorrentino [1], Ilaria Stanzione[2], Alessandra Piscitelli [2], Paola Giardina[2]* and Alan Le Goff [1]*

[1] Department of Molecular Chemistry, University Grenoble Alpes, CNRS, 38000 Grenoble, France

[2]Department of Chemical Sciences, University Federico II, 80126 Naples, Italy

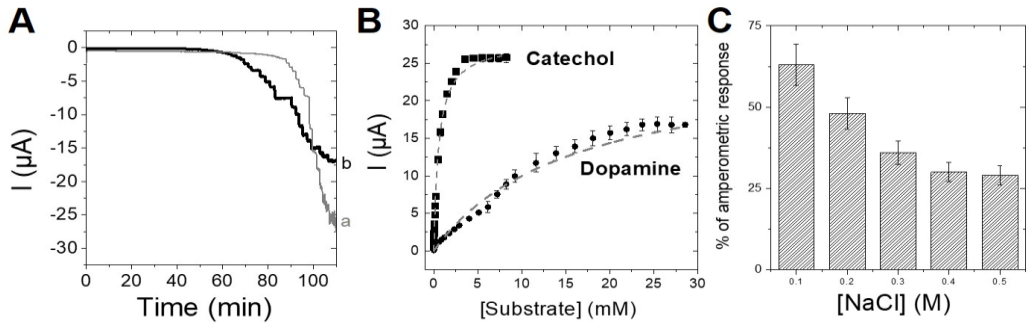

Figure S1. (A) Chronoamperometry measurements after successive additions of (a, gray) catechol and (b, black) dopamine between 0 and 0.03M for concentrated POXA1b immobilized on AQ-MWCNT electrodes; (B) Corresponding plot of the catalytic current towards increasing concentrations of (■) catechol and (●) dopamine (Measurements performed by chronoamperometry at E=-0.2 V vs. SCE, 0.1 M phosphate/citrate buffer, pH 5, 25 °C**)** Fitting curves were obtained using Origin PRO 9.0 software.**; (C)** Percentage of the amperometric response performed at 5 mM catechol and increasing concentrations of NaCl in the electrolyte (Measurements performed at E= -0.2 V vs. SCE, 0.1 M phosphate/citrate buffer, pH 5, 25 °C**)**

Supporting informations

The Laccase mediator system at carbon nanotubes for anthracene oxidation and femtomolar electrochemical biosensing

Ilaria Sorrentino,[a] Marie Carrière, [a] Hélène Jamet,[a] Ilaria Stanzione,[b] Alessandra Piscitelli[b], Paola Giardina,[b]* Alan Le Goff [a]*

alan.le-goff@univ-grenoble-alpes.fr

giardina@unina.it

[a] Univ. Grenoble Alpes, CNRS, DCM, 38000 Grenoble, France

[b] Department of Chemical Sciences, University of Naples Federico II, 80126 Naples, Italy

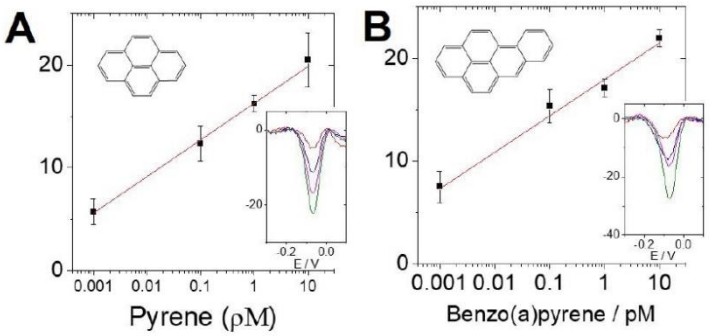

Figure S1. Linear part of the logarithmic plot of the SWV peak current towards (A) pyrene and (B) benzo(a)pyrene concentration at a MWCNT electrode soaked (10 min) in a solution of 1 U mL^{-1} of laccase and 20 mM ABTS left to react for 1 h at 25 °C min with the corresponding PAH.

Methods

Reagents

All reagents were purchased from Sigma-Aldrich (Saint Louis, Missouri, USA) and were used without further purification. All chemicals employed were of analytical grade. Distilled water was passed through a Milli-Q water purification system to obtain 18.2 MΩ cm−1 ultrapure water. Phosphate/citrate (McIlvaine) and Tris-HCl buffer solutions were prepared from Milli-Q water. The

PAH stock solutions (10mM) and their serial dilutions are prepared in acetone. The addition of PAHs, during calibration curves, is carried out in order to maintain the final concentration of acetone in the reaction solution constant.

Electrochemical Measurements

The electrochemical experiments were carried out in a three-electrode electrochemical cell using a Biologic VMP3 Multi Potentiostat. The saturated calomel electrode (SCE) served as the reference electrode, a Pt wire was used as the counter electrode and MWCNT bioelectrodes were used as working electrodes. All experiments were conducted at room temperature. All simulated curves were obtained via Origin Pro 9.0. Error bars were estimated from three measurements recorded per sample.

Preparation of the glassy carbon- modified MWCNT electrode

The working electrodes were glassy carbon electrodes (3 mm diameter). 5 mg/mL NMP dispersions of MWCNTs (Multi-Walled Carbon Nanotube, purity > 99% Sigma-Aldrich) were prepared by 30 min in ultrasonic bath (Fisher scientific FB 15050) until homogeneous black suspension was obtained. Then 20 µL of the MWCNTs solution were drop-casted on a GCE and NMP was removed under vacuum obtaining a 5-µm-thick film.

Laccase Enzymes

POXA1b laccase was produced in *Pichia pastoris* as described in Pezzella et al., 2017[1]. Hydrophobin chimera-laccase was produced in *Pichia pastoris* as described in Sorrentino et al., 2019[2].

The laccase activity was assayed at room temperature, monitoring the oxidation of ABTS (2,2′-azino-bis(3-ethylbenzothiazoline-6-sulphonic acid)) at 420 nm (ε_{420} nm = 3.6 × 10 4 M^{-1} cm^{-1})—the assay mixture contained 2 mM ABTS and 50 mM phosphate/citrate buffer, pH 3.0.

100 µL of pristine magnetic beads (MBs) (Absolute Mag™ Magnetic Particles, 3.0-3.9 µm, Creative Diagnostics) were washed once with 500 µL of water and three times with 500 µL of 50 mM Tris HCl pH8. Then, MBs were incubated with 500 µL of laccase chimera (0.2 U/mL) on a rotary tube mixer overnight at 4°C. The functionalized MBs were precipitated by using a magnet and, after three washes with buffer, the immobilization yield was calculated as a difference between the incubated laccase units and those measured in the supernatant and in the washes.

PAH biosensing

Two different strategies have been set up:

- 40°C/ no ABTS, immobilized enzyme

The modified MWCNT electrodes were incubated in 20 µL of laccase (100 U mL^{-1}) for 2h at room temperature. Electrodes were then rinsed with 50mM Tris-HCl buffer solution at pH = 8 and stored at 4°C. The modified bioelectrodes were immersed in a phosphate/citrate buffer solution (2 mL at pH= 5) at increasing concentrations of Anthracene (from 0 to 1 mM) and incubated at 40°C for 2h.

Then, the detection of as-produced and adsorbed oxidized products were measured by SWV in a phosphate/citrate buffer solution pH 5.

- Laccase in solution

In the second developed assay to detect HAPs, a reaction solution was prepared with 2 U of laccase, 0.01 mM ABTS as a redox mediator in phosphate/citrate (2mL at pH = 5) at increasing anthracene concentrations (from 0 to 1mM) and incubated at room temperature for 1 hour. MWCNT electrodes were immersed in the reaction solution for 10 minutes, and the detection of as-produced and adsorbed oxidized products were measured by SWV in a phosphate/citrate buffer solution pH 5.

DFT calculations:

All calculations were performed using the Gaussian16 package[3] at the WB97XD/6-311G(d,p) level in gaz phase. The MWCNT electrodes were modelized using a graphene ribbon of 18*12 $Å^2$. Benchmarks were done at the B3LYP/6-311G(d,p) level, but a perpendicular orientation of the anthracene was obtained on the graphene. Vibrational frequency calculations were performed to ensure that each geometry optimization converged to a real minimum. Orbitals were computed using the cubegen of Gaussian16 and their representations done using the software VMD.[4]

References

1 C. Pezzella, V. G. Giacobelli, V. Lettera, G. Olivieri, P. Cicatiello, G. Sannia and A. Piscitelli, *Journal of Biotechnology*, 2017, **259**, 175–181.

2 I. Sorrentino, P. Giardina and A. Piscitelli, *Appl Microbiol Biotechnol*, 2019, **103**, 3061–3071.

3 *Gaussian09 : Gaussian 09, Revision D.01, M. J. Frisch, G. W. Trucks, H. B. Schlegel, G. E. Scuseria, M. A. Robb, J. R. Cheeseman, G. Scalmani, V. Barone, B. Mennucci, G. A. Petersson, H. Nakatsuji, M. Caricato, X. Li, H. P. Hratchian, A. F. Izmaylov, J. Bloino, G. Zheng, J. L. Sonnenberg, M. Hada, M. Ehara, K. Toyota, R. Fukuda, J. Hasegawa, M. Ishida, T. Nakajima, Y. Honda, O. Kitao, H. Nakai, T. Vreven, J. A. Montgomery, Jr., J. E. Peralta, F. Ogliaro, M. Bearpark, J. J. Heyd, E. Brothers, K. N. Kudin, V. N. Staroverov, R. Kobayashi, J. Normand, K. Raghavachari, A. Rendell, J. C. Burant, S. S. Iyengar, J. Tomasi, M. Cossi, N. Rega, J. M. Millam, M. Klene, J. E. Knox, J. B. Cross, V. Bakken, C. Adamo, J. Jaramillo, R. Gomperts, R. E. Stratmann, O. Yazyev, A. J. Austin, R. Cammi, C. Pomelli, J. W. Ochterski, R. L. Martin, K. Morokuma, V. G. Zakrzewski, G. A. Voth, P. Salvador, J. J. Dannenberg, S. Dapprich, A. D. Daniels, Ö. Farkas, J. B. Foresman, J. V. Ortiz, J. Cioslowski, and D. J. Fox, Gaussian, Inc., Wallingford CT, 2009.*

4 W. Humphrey, A. Dalke and K. Schulten, *Journal of Molecular Graphics*, 1996, **14**, 33–38.